universität wien

DISSERTATION/ DOCTORAL THESIS

Titel der Dissertation/ Title of the Doctoral Thesis

"Predictive *in vitro* methods in experimental nuclear medicine:

Blood Brain Barrier Penetration"

verfasst von / submitted by

Chrysoula Vraka, Bakk. MSc

angestrebter akademischer Grad/ in partial fulfilment of the requirements for the degree of

Doktorin der Naturwissenschaften (Dr.rer.nat.)

Wien, 2017/ Vienna 2017

Studienkennzahl lt. Studienblatt/ degree programme code as it appears on the student record sheet:	A 796 610 474
Dissertationsgebiet lt. Studienblatt/ field of study as it appears on the studen record sheet:	Doktoratsstudium; NAWI aus d. Bereich Lebenswissenschaften; UG2002 (Dissertationsgebiet: Ernährungswissenschaften)
Betreuer/ Supervisor:	Univ.-Prof. Mag. Dr. Karl-Heinz Wagner Mag. Dr. Markus Mitterhauser

“Prediction is very difficult, especially if it's about the future”

- Niels Bohr

Acknowledgements

Firstly, I would like to express my sincere gratitude to my mentors Prof. Karl-Heinz Wagner and Prof. Markus Mitterhauser, who give me the opportunity to work in a multidisciplinary area and support my personal and scientific development in radiopharmaceutical sciences.

Thank you, Markus, for driving my ambition and creativity.

I would also like to thank Prof. Wolfgang Wadsak, for his positive attitude and support.

A very special gratitude goes out to my colleges of the division of nuclear medicine. For all the hours we spend together working, discussing, motivating each other and laughing.

I also want to thank my colleges at the department of nutrional sciences, for inviting me as an “exotic bird” still to the working group retreats, I always benefited from the discussions.

At least, I would like to thank my many friends and family, you should know that your support, advice and encouragement were worth more than I can express on paper.

Thank you!

Index

Abstract

The incidence of neurological diseases increases perpetually, on the one hand, due to the rising incidence of psychiatric diseases in young people and on the other hand due to an increase in the elderly population, resulting from the enhanced overall life expectancy coming along with pathologies of the brain. However, the pathways of these disorders are unclear. These circumstances impede the diagnosis and therapy of patients. The development of new cerebral radiotracers for the positron emission tomography (PET) could be essential for the evaluation of these diseases and may lead to new therapeutic treatments. Therefore, the demand of brain PET tracers is expanding rapidly. However, their preclinical evaluation is costly and time-consuming. Several radiotracers failed in later stages of drug development caused to poor BBB penetration or interactions to efflux transporters, thus predictive DMPK (drug metabolism and pharmacokinetics) assessments gain in value to determine the most promising radiotracers before conducting animal experiments.

Hence, the aim of this thesis was the evaluation and discussion of the most crucial physicochemical properties in PET tracer development namely the lipophilicity ($HPLClogP_{ow}^{pH7.4}$), plasma protein binding (PPB), the fluid membrane coefficient (K_m) and the permeability (Pm) of a drug using high throughput methods. The influence on BBB penetration of these drug properties shall be discussed in this thesis. Additional aims of this thesis were the focus on drugs interacting with diverse efflux transporters concerning their physio chemical properties and the development of an assay, which predict the interactions towards P-gp (ABCB1 or MDR1 protein).

In total 191 compounds were experimentally tested using high throughput HPLC methods. 121 compounds were correlated regarding their properties to penetrate the BBB as well as to widely accepted logP ranges and thresholds, which are supposed to be optimal for brain entry. For 113 compounds $HPLClogP_{ow}^{pH7.4}$, PPB, Pm and K_m measurements were performed and the drugs were split to three different groups: the most commonly used PET/SPECT tracers, drugs showing no brain uptake or CNS side effects, and drugs interacting with efflux transporters. To this end, a centralized and comprehensive database was complied. Moreover, selected results of PPB and HPLC logP measurements were compared to traditional shake-flask and ultrafiltration methods as well as to the calculated logP value. Additionally, a new *in vitro* method predicting the

interactions at the efflux transporter P-gp was developed and compared to standard uptake assays.

For all experimental values the comparison between the groups shows a broad overlapping range of the single values. Accordingly, a classification into the CNS positive, CNS negative or drugs with interactions to efflux transporter is virtually impossible. However, significant differences were found for the $HPLClogP_{ow}^{pH7.4}$ means between CNS positive and CNS negative drugs as well as between the CNS negative drug group and the group interacting with efflux transporters. These findings indicate that experimental values have an influence on predicting BBB penetration. However, an interpretation or classification with a single parameter as solely with the $HPLClogP_{ow}^{pH7.4}$ is intricate. Therefore, the widely accepted thresholds or ranges for the lipophilicity of a tracer illustrating optimal brain uptake are inadequate, especially when different methods are used for determination of the lipophilicity.

The developed cell based real-time kinetic model could successfully identify the two PET tracers, [^{18}F]FE@SNAP and [^{11}C]SNAP-7941, as high potent P-gp substrates.

Zusammenfassung

Der Bedarf an Radiotracern für die zentrale Bildgebung mittels Positronen-Emission-Tomographie steigt. Ein Grund dafür ist der zunehmende Anteil der älteren Bevölkerung mit spezifischen neurologischen Erkrankungen, aber auch der Anstieg von neurologischen und psychiatrischen Erkrankungen in jungen Jahren. Bis dato sind viele der Zusammenhänge und Stoffwechselwege dieser Erkrankungen nicht gänzlich aufgeklärt. Somit wird eine erfolgreiche medikamentöse Therapie erschwert. Die Entwicklung neuer PET-Tracer kann der Aufklärung dienen und neue Therapieansätze aufzeigen. Daher steigt der Bedarf an PET-Tracern für die zerebrale Anwendung. Die Entwicklung von Biomarkern ist zeit- und kostenintensiv, da es noch in späteren Phasen der präklinischen Evaluierung eine hohe Anzahl an Kandidatentracern ausgeschlossen wird. Ein Hauptgrund des Ausschlusses ist die mangelnde Aufnahme ins zentrale Nervensystem (ZNS). Daher sind prädiktive *in vitro* Methoden mit hohem Probendurchsatz, sogenannte „high-throughput Methoden“, von großem Interesse, die bereits vor Tierversuchen zum Einsatz kommen können.

Ziel dieser Dissertation war es bedeutende physikochemischen Eigenschaften, nämlich die Lipophilie (logP), Plasmaproteinbindung (PPB), den Membranverteilungskoeffizienten (K_m) und die Permeabilität (Pm) eines Moleküls, zu evaluieren und im Hinblick auf ihre Fähigkeit die BHS Penetration vorherzusagen zu diskutieren. Zusätzlich lag ein weiterer Fokus auf den besagten physikochemischen Eigenschaften und der Entwicklung einer zellbasierten Methode von Substanzen die Wechselwirkungen mit diversen Effluxtansportern aufweisen.

In Summe wurden für 191 Substanzen HPLC $logP_{ow}^{pH7.4}$ Werte ermittelt. 121 dieser Substanzen wurden im Hinblick auf ihre Eigenschaft passiv ins ZNS zu diffundieren sowie unter Betrachtung von allgemein akzeptierten optimalen logP Bereichen und Grenzwerten diskutiert. Für 112 Substanzen wurden HPLC $logP_{ow}^{pH7.4}$, PPB, K_m und Pm Messergebnisse ermittelt und die Substanzen nach Klassen eingeteilt: kommerziell erhältliche Standards von PET-Tracern, die die BHS passiv überwinden, Pharmaka die keine Aufnahme oder Nebenwirkungen im ZNS aufzeigen und Substanzen die Wechselwirkungen zu Effluxtransportern aufweisen. Somit entstand eine umfassende Datenbank an experimentellen Werten. Zusätzlich wurden ausgewählte Ergebnisse des

HPLC $logP_{ow}^{pH7.4}$ und der PPB mit Ergebnissen der klassischen Shake-Flask und Ultrazentrifugation Methode verglichen.

Beim Vergleich der experimentellen logP Werte mit allgemein bekannten logP Bereichen und Grenzwerten, die als optimal für eine BHS Penetration vorausgesetzt werden, zeigte sich eine hohe und unterschiedliche Anzahl an falsch negativen Klassifikationen. Vergleicht man das Gruppenmittel der einzelnen Parameter zeigen sich signifikante Unterschiede für den HPLC $logP_{ow}^{pH7.4}$, allerdings bewegen sich die Einzelresultate in einem sehr weiten Bereich, sodass es zu einer großen Bandbreite an Werten kommt, die sich überschneiden. Experimentelle Werte haben durchaus einen Stellenwert in der Präklinik, allerdings ist es nicht möglich Substanzklassen zu bestimmen oder eine BHS Penetration prädiktiv basierend auf einem einzigen dieser Werte zu ermitteln.

Die neue zellbasierte Echtzeit-Methode ermöglichte es die die PET-Tracer [^{18}F]FE@SNAP und [^{11}C]SNAP-7941 als hochpotente P-gp Substrate zu identifizieren.

1 Introduction

Out of 7000 licensed drugs on the market worldwide, only 5% (350 drugs) have clinical relevance for the treatment of neurological or psychiatric diseases. Drugs developed for neurological disorders are less successful than for example cardiovascular medications (1). A primary cause might be that the blood brain barrier (BBB) penetration is still a challenging factor in drug development.

It is well known that ~98% of all developed small molecules do not penetrate the BBB (2). Indeed, there are only a few scientists, scientific programs and industry branches covering the scientific gap of knowledge concerning the BBB and its penetration (less than 1%) (1,2). However, the incidence of neurological disorders is rising, not only caused by the increasing number of elderly but also due to the higher prevalence of depression and burnout at all ages. According to the World Health Organization, there is an incident rate of ~1:4 to suffer from mental or neurological disorders once in a lifetime. Currently, more than 450 million people worldwide are affected (3).

Hence, the worldwide market for drugs of the central nervous system (CNS) is a multi-billion-dollar market. In 2005 a net worth of 50 billion dollars was estimated, with a tendency to further rise. In 2010, the estimation was already raised to $78 billion. Recorded sales for depression treatment were almost $16 billion in the same year (4). In 2013, statistics stated that CNS drugs maintain a leading position among small molecules (5). Positron emission tomography (PET), a non-invasive technique, may be used to support drug development, diagnosis and therapy of neurological and mental disorders.

Molecular imaging of the brain using PET enables clinical investigations of the pathways of these diseases. Therapy outcomes (success or no effect) can be visualized and thus assist in therapeutic drug development. Therefore, the demand of new PET tracers for brain imaging is continuously increasing.

1.1 Brain imaging using positron emission tomography

The physical principle of PET is described elsewhere (6–9). In short, radionuclides, which decay by emission of a neutrino and a positron (β + -decay) are PET nuclides (e.g. carbon-11, fluorine-18, nitrogen-13 and gallium-68). The accrued positron collides with

results in a simultaneous ejection of two photons at an angle of approximately 180° and energy of two times 511keV. These two annihilation photons are detected during the scan with circularly arranged detectors. Signals of coincidentally detected photon pairs on the scintillator are detected as light flashes at the photomultiplier and converted to electrical signals. The capability of detecting the tracer distribution by means of radioactive decay is the physical principal of PET. Hence, this non-invasive technique enables the visualization of biochemical processes and is therefore of high interest in brain research. It is a molecular imaging technique and provides dynamic information about the metabolism (e.g. sugar pathways using [^{18}F]FDG), changes in expression or function of receptors, transporters or enzymes (PET tracers as [^{11}C]-(+)-PHNO targeting the dopamine transporter D3/D2, [^{11}C]DASB targeting serotonin transporters (SERT) and [^{11}C]Harmine imaging monoamino oxidase A (MAO A)). Additionally, PET image fusion with computed tomography (CT) or magnetic resonance images (MRI) provides anatomical and functional information simultaneously.

Depending on the tracer properties and the required information, different quantification models are used. In general, the tissue compartment model (TCM) is a mathematical description following the tracer's pathway in the human or animal body. The definition of compartments in a model is necessary to distinguish between the various superimposed signals derived from a PET image. So, it is used to describe the changes over time (not in space). Accordingly, for each defined compartment the tracer concentration is represented as function of time. The resulting differential equations describe the equilibrium of a tracer. To quantify a model it needs a start, the input function. The input function is the direct measured radiotracer concentration in blood over time. Even though, the blood pool is mostly illustrated as a box (as the compartments are illustrated) and of course a compartment in physiological point of view, the input function is not a mathematical compartment in the TCM (10).

The simplest approach is the single tissue compartment model, describing the distribution of a tracer between the blood pool and tissue. This modeling method is applied for perfusion tracers such as [^{15}O]H_2O. Hence, this is only feasible, if the tracer is freely diffusible. (Figure 1 B). Two or three tissue compartment models are much more complex and require more than one differential equation to fit the tracer behavior. (Figure 1 A + C)

These models describe different pharmacokinetic and –dynamic properties of a drug: free ligand concentration in plasma that is corrected for the percentage of radioactive

metabolites, free ligand in the target area (e.g. brain), amount of tracer which is specifically bound to the target (Figure 1 A) and non-specific binding in the target region (Figure 1 C) (10–12). For such complex kinetic modeling approaches, *ex vivo* blood sampling for the determination of the plasma free fraction, whole blood to plasma ratio and the amount of metabolites over time are required.

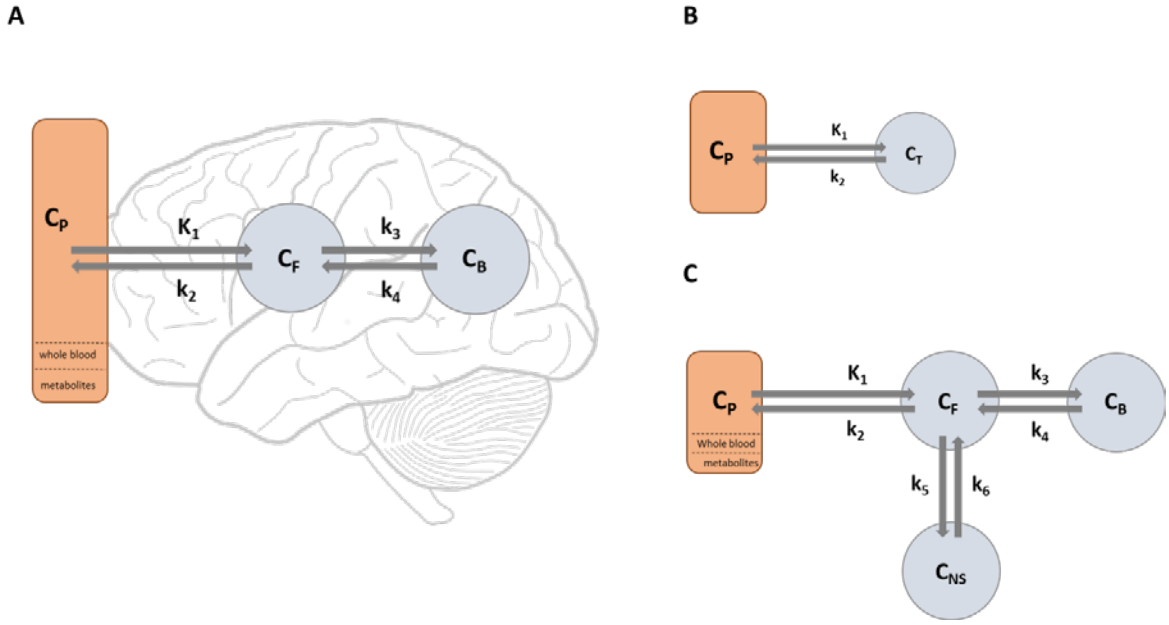

Figure 1 illustrates different tissue compartment models (TCM): (A) two-TCM, (B) one-TCM and (C) three-TCM. CP: tracer concentration in plasma, K1: influx rate from blood to tissue [mL/min/g], k2: constant representing the efflux from tissue to blood, CT: tracer concentration in tissue, CF: free tracer concentration in target organ, k3: kon constant to target, k4: koff constant of target, CB: bound tracer concentration in target area. Adapted from Morris et al. (10).

In cases were the target (e.g. receptor) is located at the vascular system, it might be necessary to adapt the TCM for a supplementary compartment, which represent the binding at the endothelial cells. Thus, an additional rate constant from blood pool to vascular compartment is created (13).

The quality of the PET image modeling strongly depends on the tracer properties. To this end, an operative PET brain tracer should fulfill the following criteria (14,15):

I. High affinity to the target (K_D in nanomolar range)
II. High selectivity against other targets
III. Reliable radiosynthesis with high molar radioactivity
IV. Metabolic stability or free of interfering radio-metabolites in the target
V. Low non-specific binding
VI. Ability to penetrate the BBB
VII. No interactions with efflux transporters
VIII. Suitable pharmacokinetics in relation to radiolabel half-life

For the evaluation of the tracer's affinity and selectivity to the target (e.g. receptors) different well-established methods are available. These include, for example, cell-based assays overexpressing the target, membrane assays (e.g. vacuum filtration methods) or tissue samples (e.g. autoradiography). Furthermore, blocking and competition experiments are performed as well as the repetition of the assay with other subtypes of the target-receptor (selectivity) (I. &II.). In small-scale reactions, the optimum synthesis conditions are determined. Subsequently, these conditions are transferred to a fully automated process on commercially available synthesis modules, which are directly connected to a generator or cyclotron (III.). After a successful implementation of the radiosynthesis, the metabolic stability and potentially interfering radio-metabolites can be determined. For this purpose, different assays are available: most commonly the tracer is spiked to pooled plasma or serum and the amount of the parent compound is determined over time. Additionally, stability assessment against certain enzymes (e.g. carboxylesterase) or enzyme complexes (CYP P 450 complexes) can be conducted. In a later phase of tracer development, also *ex vivo* metabolite analyses via blood sampling or tissue harvesting are performed (IV.). Non-specific binding can be assessed during the experiments and by evaluation of the lipophilicity. However, a method for a reliable prediction of *in vivo* non-specific binding does not exist (V.). Therefore, animal experiments are conducted and the target-to-background ratio, describing the uptake in non-target areas and biodistribution experiments (e.g. fatty tissue) are interpreted. Similar difficulties can be stated for the last three points (VI., VII. and VIII.). Therefore, the

validation of these tracer properties (e.g. observable brain uptake and washout kinetics) is regularly conducted using animal experiments (imaging and *ex vivo* biodistribution). However, a translation to the human application is not always assured. Particularly, the BBB penetration is the bottleneck for suitable newly developed brain radiotracers.

1.2 Blood Brain Barrier

The BBB is a dynamic interface that separates the brain from the circulatory system and protects the central nervous system from potentially harmful compounds while regulating the transport of essential molecules and maintaining a stable environment. In detail, the BBB consists of astrocytes, pericytes and endothelia cells, which are connected by tight junctions (TJ). The human brain has more than 100 billion capillaries with a distance of 50µm to each other. Meaning, every neuron is perfused by its own capillary with a maximum diffusion distance of 25µm in brain parenchyma (transvascular diffusion). The volume of intraendothelial space is 5mL for the human brain. Therefore, the efficiency of a drug, which is delivered to the brain, will be enormous (depending on the affinity to the target) since it will reach all parts of the brain (1,16,17). However, the permeation of compounds into the brain is limited in a broad range (exception areas are the pituitary glands and the ventricular system). The distinct active transport systems allow only the penetration of certain molecules (e.g. glucose & amino acids). Therefore, scientists in tracer development are focusing on the passive diffusion. Passive diffusion can be either a paracellular transport or a transcellular transport through the endothelial membrane. In case of the BBB, paracellular transport is restricted, because of the TJ creating a strong cell connection between the endothelial cells and thus the vascular wall. Therefore, the transcellular lipophilic pathway is used as a synonym for the passive diffusion at the BBB (Figure 2, pathway A). As the name implies, examining the lipophilicity (logP) of a molecule has become a measure of passive diffusion, although it is still a matter of debate (14,18–22). Besides the limited active and paracellular transport, an additional security system for non-endogens and potentially harmful molecules has to be mentioned: efflux transporters. After transcellular transport through the endothelial cells, an active efflux system can be found (Figure 2, pathway B) for certain compounds, returning them to the luminal side of the vessel. Responsible for this additional barrier, are the efflux transporters which belong to the ABC transporter group, indicating an ATP depended

process. They are located at the luminal side of the endothelial cells and show affinities for a considerable number of chemically different molecules (cf. chapter efflux transporter).

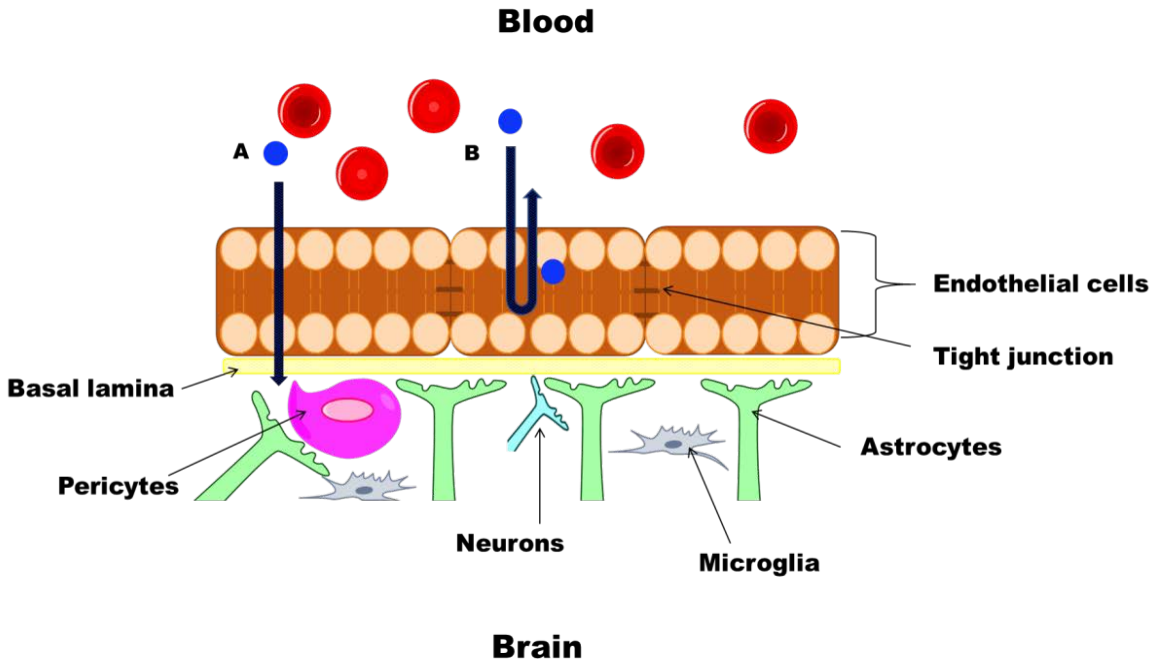

Figure 2 shows the blood brain barrier, which is composed of endothelial cells connected through tight junctions (TJ) and surrounded by the basal lamina, pericytes, neurons, microglia, and astrocytes at the abluminal side. Pathway (A) illustrates the passive diffusion through the endothelial cells via transcellular transport. The high density of TJ prohibits the drug to penetrate through the paracellular way. Pathway (B) represents the active efflux of a drug via a transporter from the ABC transporter family (e.g. MDR1, BCRP or MRP1). Graphic updated from Abbott et al. (84).

Designing tracers that can successfully overcome the BBB is still a formidable challenge in CNS drug development. Modifications of the widely accepted rule of 5 (Ro5) in the design of oral drugs, required for optimal brain uptake, have therefore been extensively reported and attempt to define properties of successful CNS drug candidates, cf. table 1 (17,23–27).

1.3 Rule of Five (Ro5)

Pioneering work was done by Christopher A. Lipinski when he proposed his Ro5. The original Ro5 deals with oral medication and defines four simple physicochemical parameters, which are related to the number five or to a multiple of five:

- molecular weight > 500 Da
- LogP ≥ 5 (or MlogP. ≥4.15)
- HBD ≥5
- HBA≥ 10

These physiochemical parameters are associated with unacceptable aqueous solubility and poor intestinal permeability. The rule was constructed using the United States Adopted Name (USAN) or International Non-proprietary Name (INN) and World Drug Index (WDI) drug database. According to the available datasets, a hit probability of approximately 90% of the compounds was achieved (28). The aim was the computational identification of lead compounds in early stages of drug development when thousands of candidates were produced. With regard to the prediction of BBB permeability, Lipinski adapted his rule of five after evaluation of 150 CNS drugs according to the following properties for optimal BBB permeability (29–31):

- molecular weight ≤ 400
- ClogP ≤ 5
- HBD≤ 2
- HBA ≤ 6

Later, the equation logP minus HBA has stated: a positive integer predicated a CNS drug, while negative numbers described BBB non-penetrating compounds (31–33). During the last decades, a variety of adaptions of the Ro5 has been stated by different authors (17,24–27,29,31,34,35) concerning the prediction of BBB penetration (Table 1). In these rules, the parameter ranges or cutoffs were altered, some of the original parameters were eliminated and or new parameters were added (e.g. polar surface area (PSA)). The results are based on mostly calculated, but also experimental values. Additionally, databases were constructed and plenty of manuscripts are available reviewing the different rules while creating new ones.

Table 1 Proposed rules, which increase the chance to penetrate the BBB

author	Conclusion and recommendation	Used Data set
1968, Hansch et al. (36)	LogP is critical for in vivo activity. Found drug *in vivo* efficacy in a parabolic dependence on LogP. **Suggested optimal LogP = 2**	201 barbiturates with preclinical in vivo efficacy data
1988, Young et al. (37)	LogBB[b] can be increased by **↑ lipophilicity (LogP) or/and ↓ hydrogen-bonding capacity**	20 CNS penetrating histamine H2-antagonists
1998, Van der Waterbeemd et al. (38)	Improved chance of CNS uptake: **MW <450; PSA <90 Å^2 and LogD 1−4**	125 CNS and non-CNS drugs
1999, Kelder et al. (39)	Upper PSA limit for the most CNS drugs: **<60 − 70 Å^2** oral drugs do not exceed PSA of 120 Å^2	776 CNS and 1590 non-CNS oral drugs that reached at least Phase II
2000, Lipinski (29)	**MW ≤ 400** **ClogP ≤ 5** **HBD≤ 2** **HBA ≤ 6**	Pfizer data, United States Adopted Name (USAN) or International Non-proprietary Name (INN) and World Drug Index (WDI) drug database
2002, Doan et al. (40)	Difference between non-CNS active drugs versus CNS drugs: **↓ cLogP** (CNSpos mean 2.08) **↓ HBD** (CNSpos mean 0.67) **↓ PSA** (CNSpos mean 40.5 Å^2) *in vitro* **Pm >150 nm/s**	*In vitro* permeability and efflux ratio using MDCKII cells of 48 CNS and 45 non-CNS drugs
2002, Norinder and Haeberlein (32)	Rule of thumb for brain uptake: **HBA[c] < 5 (~ 70 Å^2)**, or **ClogP − (HBA[c]) > 0** [b]	Literature review
2003, Clarke (33)	More likely to penetrate BBB: **logP 1-3** **PSA<90 (60-70)** **MW <450** **ClogP- (N+O) >0**	Review
2003, Didziapetris et al.(41)	Likely to be no P-gp-substrates (vs. substrates) **MW < 400** (MW> 400) **N + O ≤4** (N+O ≥8) **pKa < 8** (pKa <4)	Calculated & measured values of 1000 P-gp measurements (data of different *in vivo* and *in vitro* methods)

2004, **Leeson and Davis** **(42)**	CNS drug properties changed (median): **MW (307)** **HBA[c] (4)** **HBA[d] (2)** **RNB (4.5)** **PSA, ClogP & HBD (no differences)**	Comparison of oral drugs prior 1983 "old" (864 drugs) taken from Vieth's compilation between oral drugs of the period 1983 – 2002 (329 drugs) taken from Annual Reports in Medicinal Chemistry. Drugs were subdivided into six therapeutic classes. Means were reduced for CNS drugs.
2004, Lipinski	**ClogP- (N+O) >0 (CNS positive drugs)** **ClogP- (N+O) <0 (CNS negative drugs)**	Review and data based on previous works of Lipinski
2005, **Pajouhesh and Lenz** **(27)**	Attributes of a successful CNS drug candidate: **MW < 450** **cLogP <5** **HBD < 3** **HBA < 7** **RNB < 8** **H-bonds < 8** **PSA < 60 − 70 Å^2** (upper limit 90 Å^2) pK a 7.5 − 10.5 (avoid acids) Metabolic stability (>80% after 1h) P450 enzyme CYP inhibition (<50% at 30μM), no significant CYP2D6 metabolism, not a potent CYP3A4 inducer Not a P-gp substrate (*in vivo*) Not a high affinity serum albumin ligand (K_d <10μM) Aqueous solubility >60 μg/mL	Marketed CNS drugs
2006, **Hitchcock and Pennington** **(35)**	Suggested physicochemical property ranges for increasing the potential for BBB penetration: **PSA < 90 Å²** **HBD < 3** **ClogP 2 – 5** **ClogD (pH 7.4) 2 – 5** **MW < 500** preferred ranges: **PSA<70 Å²** **HBD 0-1** **ClogP 2-4** **ClogD (pH 7.4) 2 –4** **MW<450**	Medicinal chemistry literature review

2006, Reichel (17)	CNS-likeness: **logP <3** **HBD <4** **HBA <10** **MW <450**	Review
2008, Gleeson (43)	Increasing brain uptake: Suggested optimal **ClogP is <3** **↑ MW leads to ↓ P_{app}, ↑ ER and ↓ LogBB[b]** **and ↑ brain tissue binding** **MW <300 and corresponding ↓ PSA** MW and logP are the two key characteristics to determine ADME probabilities (PPB, permeability, solubility, oral bioavailability, volume of distribution, P-gp efflux, brain tissue binding, in vivo clearance, metabolism, excretion and toxicity)	Structure-activity relationship for 15 different ADMET assays conducting *in vivo* (rat) and *in vitro* assays and 12 calculated parameters using ACD database. 3059 compounds with CNS penetration data
2009, Waring (44)	[f]AZLogD limits required for a high permeability (≥100 nm/s) **for MW <300 → [f]AZLogD > 0.5** **for MW 300 – 350 → [f]AZLogD > 1.1** **for MW 350-400 → [f]AZLogD >1.7** **for MW 400-450 → [f]AZLogD > 3.1;** **for MW 450 – 500 → [f]AZLogD > 3.4** **for MW >500 → [f]AZLogD > 4.5**	Permeability assay with 9571 compounds using Caco-2 cells and ([g]PAMP (n=1922), AZLogD data not shown for these results)
2010, Wager et al. (45,46)	Median values for marketed CNS drugs: **ClogP = 2.8** **CLogD = 1.7** **MW = 305.3** **PSA = 44.8 Å^2** **HBD = 1** **pKa = 8.4**	119 marketed CNS drugs and 108 Pfizer CNS clinical candidates. *In vitro* ADME attributes, binding efficiencies and *in vitro* safety assay data
2012, Ghose et al. (24)	Properties for designed high-quality guidelines during lead optimization: **tPSA < 76 Å^2(25 − 60 Å^2)** **At least 1 (1 or 2, including 1 aliphatic amine) nitrogen** **<7 (2 − 4) linear chains outside of rings** **<3 (0 − 1) polar hydrogen** **volume of 740 − 970 Å^3** **solvent accessible surface of 460 − 580 Å^2** Positive [g]QikProp for CNS parameter One violation of these rules is acceptable (~10%)	317 CNS and 626 non-CNS oral drugs (Schrodinger/QikProp software: http://www.schrodinger.com/ products/14/17/)

	Additional values can be added (table1 Ghose et al.)	
2012, Hitchcock (47)	General guidelines for minimizing P-gp recognition include: **HBD < 2** **tPSA < 90 Å^2 (preferably <70 Å^2)**	Medicinal chemistry literature review
2012 & 2015, Pardridge (2,26)	Exceeding of these thresholds minimize brain uptake: **MW 400 (average molecular mass 357 Da)** **HB (HBD+HBA) < 8**	Review
2013, Desai et al (48)	Compounds with are less likely to be P-gp substrates, if **tPSA < 60 Å^2** **pKa < 8**	P-gp ER for 2000 compounds from Eli Lilly collection. Comparison of transport assay with QSAR

Table 1 modified and supplemented from Rankovic (34) [a]Based on drug unbound (free) blood/brain concentrations. [b]Based on drug total blood/brain concentrations; [c]Sum of O+N according to Lipinski; [d]overall H-bond acceptors; [e]Sum of OH+NH according to Lipinski ; [f]AZLogD calculation according to Brueau and McElroy (AstraZeneca) MW: molecular weight; (t)PSA: (topological) polar surface area; TPSA: topological polar surface area; HBD: hydrogen-bond donors; HBA: hydrogen-bond acceptors; RNB: rotatable bonds; ER: efflux ratio; ↑: increased; ↓: decreased, =: no changes; [g](QikProp, http://www.schrodinger.com/products/14/17/)

However, most authors propose that more than one value is needed for the prediction of BBB penetration, nevertheless, the lipophilicity has become the most famous and most important predictive value. Yet, the logP, which is the measure of lipophilicity, received much criticism (34).

1.3.1 Lipophilicity

The logP describes the partition-coefficient of an un-ionized compound in two immiscible phases (n-octanol and water/buffer) at equilibrium, whereas logD is defined as the distribution of all species (un-ionized and ionized solutes) at equilibrium. Therefore, under physiological pH (7.4), the terms logP and logD can be used synonymously (49). Different methods are available for the calculation or experimental measurement of the logP value: the simplest and most authentic approach is by using the shake-flask or shake-tube method. This method directly measures the coefficient in two immiscible phases (e.g. aqueous phase and octanol) based on the definition. However, these methods are prone to operating mistakes and vulnerable to already small amounts of impurities (50).

The International Union of Pure and Applied Chemistry (IUPAC) extended the definition of lipophilicity and describes it as “distribution behavior in a biphasic system, either liquid-liquid or solid–liquid. Therefore, different HPLC methods measuring the logP are known” (51). Although experimental measurements of the logP are easy, these days lipophilicity values are rather calculated. For that purpose, different calculation models, as well as software packages, are available. An important fact, to keep in mind about these different methods is that the resulting logP value (for the same compound) is not necessarily equivalent. Concerning the BBB penetration, a wide range of utterly different conclusions can be found in literature. The opinions diverge from assertions that the logP is the most crucial predictive factor for the BBB penetration, up to statements that no valid prediction of membrane penetration can be achieved based on the logP value (14,18–22).

1.3.2 Calculated and structure-based values

Molecular Weight

In contrast to the logP, which can be calculated and experimentally testes, all other parameters, which are included in the Ro5, are structure based or calculated values, respectively. The simplest included value is probably the molecular weight (MW) of a molecule. Smaller compounds penetrate faster across the BBB than larger molecules. However, these correlations are massively depending on other properties of compounds examined (lipophilicity). Thus, if lipid-soluble compounds are included, the strong correlation between BBB permeability and molecular weight was decreased (52). Indeed, 100% of all large molecules will not enter the BBB, while ~98% of all small molecules will not reach the brain (2).

Hydrogen bond donors and acceptors

More complex is the number of hydrogen bond donors (HBD) and – acceptors (HBA). Hydrogen bonds are a type of dipole-dipole attraction and can be formed between hydrogen atoms that are bonded to large electronegative atoms such as oxygen, nitrogen or sulfur. The greater the number of potentially formed hydrogen bonds of a molecule, the

greater will be its overall electrostatic attraction for water molecules and the lower the solubility in non-polar solvents. To describe the hydrogen bonding capacity, most researchers count the number of HBD and HBA existing in a molecule. According to Lipinski, HBD is expressed as the sum of hydroxyl and amino groups and HBA is expressed as the sum of nitrogens and oxygens. Almost all Ro5 use the definition according to Lipinski. If not, there is a big difference of these values between the different calculation methods (e.g. counting HB with fluorine) (24). CNS drugs show significantly lower numbers of HBD and HBA in comparison to non-penetrating compounds. Additionally, it is described that efflux transporter substrates show a higher number of HBD and HBA. To this end, a reduction of HBD and or HBA may be a successful strategy to optimize BBB penetration (27,34).

Number of rotatable bonds

Additionally, parameters were introduced later and further modified in different rules. The first parameter is the number of rotatable bonds (RNB). RNB was defined as any single bond bound to a nonterminal heavy atom (i.e., non-hydrogen, not in a ring). Excluded from the count were amide C-N bonds, because of their high rotational energy barrier. The RNB is further defined as molecular flexibility of a compound (34,53).CNS drugs show reduced RNB values in comparison to non-CNS drugs (27,42). Furthermore, it is stated that molecular flexibility, meaning RNB and PSA, are more important than the MW (42).

Polar Surface Area

Finally, the molecular polar surface area (PSA) must be mentioned: PSA is defined as the sum of the surface contributions of polar atoms (usually oxygen and nitrogen and attached hydrogens) in a molecule, and it has been shown to correlate well with drug transport properties, such as intestinal absorption or blood brain barrier penetration (33). For the calculation of the PSA, different methods can be used. The first one is based on a three-dimensional model of the molecule and its polar surfaces. Indeed, this needs high-performance computing. The alternative calculation is based on two-dimensional structures using fragments of the molecule and totalizes the single fragments thereafter

according to Ertl et al. (54). The PSA value counts also to the parameters that influence the molecular flexibility and it is stated that CNS drugs show lower PSA values (55).

Summarizing, these intermolecular forces, represented in the HBD, HBA, PSA, and RNB, between the drug and the cell membranes, play an important role in the transport by passive diffusion (14,56,57). Indeed, the single influence of each of these forces should be reconsidered since e.g. HBD are used to calculate the PSA and thus correlate strongly. Therefore, the PSA can also be used as a drugs H-bond capacity descriptor (38).

135 substances were categorized according to their BBB behavior and classified (physiochemical parameters are taken from ChemBioDraw software and ACD database) to different rules.

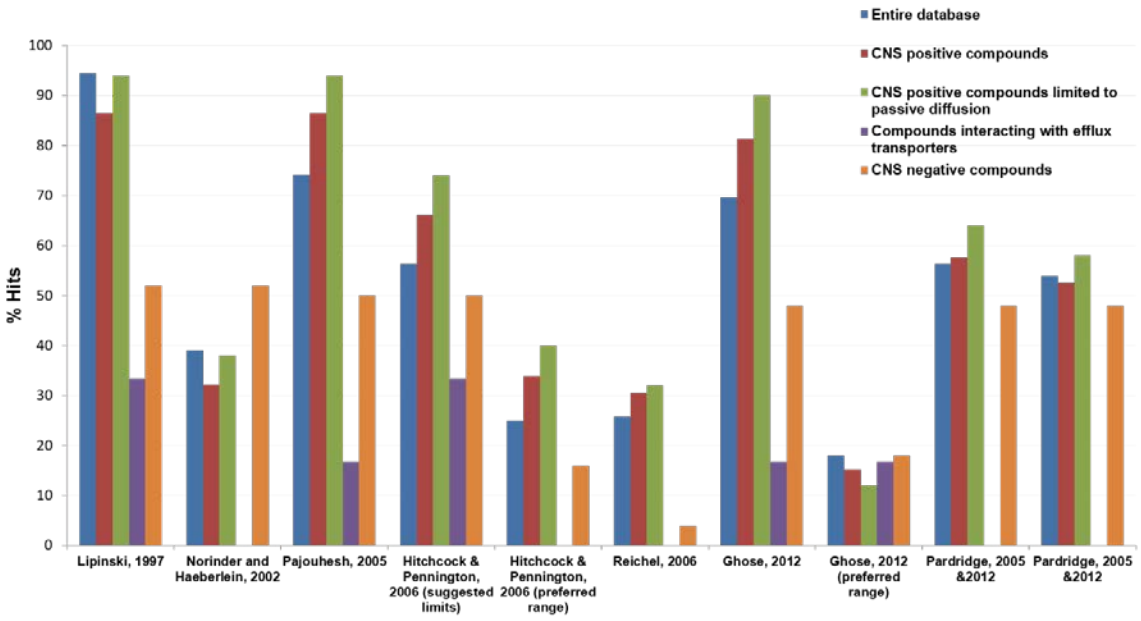

Figure 3 illustrates the percent of hits per rule. Included are false positive hits and false negative hits depending on the used dataset (cf. colored bars). The blue bars include the whole investigated dataset of 135 substances: BBB penetrating compounds (active transport or passive diffusion), BBB non-penetrating compounds and compounds with interactions towards efflux transporters as well as compounds with unknown behavior at the BBB. The red bars include all CNS positive compounds whereas the green bars include solely the compounds with passive diffusion. The hits of the violet bars include only compounds showing interactions with efflux transporters and the orange bars comprise the CNS negative compounds. (Unpublished data, presented at the 24th AGRR conference, 2016, Switzerland).

Thereby, a high number of false positive, as well as false negative outcomes, were found. Accordingly, lead drug selection based solely on calculated physicochemical parameters is intricate, since:

I. A plurality of rules is available

II. Variation of the resulting parameter is high when using different software, definitions, and databases

III. Classification into CNS penetrating and non-penetrating groups is often problematic

IV. The calculations using software are limited to known or simple structures

1.4 Plasma Protein Binding

A plenty of chemistry-based drug delivery strategies or rules for CNS drug candidates include and discuss the influence of plasma protein binding (PPB) (16). There is common sense that PPB is a crucial value explaining the pharmacokinetics of a drug. Therefore, PPB was evaluated in DMPK (drug metabolism and pharmacokinetics) studies through all therapeutic areas. In this mathematical model, the PPB provides information about the distribution of free (unbound) drug concentration in plasma (Cu_{PLASMA}) and tissue. The brain plasma ratio is commonly used in CNS drug development and gives a simple ratio of the distribution of a drug between brain and plasma. However, this approach does not take the drug concentration in the brain vessels into account.

Historically, free drug concentration in plasma is evaluated, since it has been believed that drugs bound to plasma proteins are not available in the target regions ("**free drug hypothesi**s"). Considering the "free drug hypothesis", the plainest approach is to assume that under freely diffusible conditions (with the absence of transporters), the unbound drug concentration in plasma is equal to the unbound concentration in the brain (Cu_{Brain}) (58,59). Although this has been confirmed to be valid for several drugs, such as propranolol, plasma bound drugs are transported into the brain. Nowadays, it is known that almost all CNS drugs show high plasma protein binding (~90%PPB) (60). However, especially in PET brain tracer development, the free drug hypothesis has been persisting for a long time and can still be found until nowadays in publications and is still reported on scientific conferences (12,14). The main reason may be that the Cu_{PLASMA} is considered for kinetic modeling approaches (Figure 1). However, in the last decades, the free drug hypothesis was subsequently replaced by the "**equilibrium theory**". This concept suggests that plasma protein binding is reversible and follows equilibrium conditions. Therefore, free drug concentration is continuously available for the target

region during steady-state (Cu_{Brain}= Cu_{Brain}/ Cu_{PLASMA}) x Cu_{PLASMA}). Important to note is that the drug delivery efficiency does not take parameters as affinity or binding to the target into account (60). This means in practice that increasing the free drug concentration during drug development is obsolete. Indeed, there is no correlation between brain tissue binding and the drug delivery efficiency (ratio between Cu_{Brain} and $Cu_{PLASMA)}$ and therefore it is not useful to determine the free fraction (60).

A different and less known theory is the "**enhanced dissociation hypothesis**". This theory explains the drug uptake into the target by conformational changes of the albumin-ligand complex during the contact with endothelial cells. Such conformational changes may be induced by non-specific adsorption at tissue surfaces (61,62).

Nevertheless, it is in general questionable whether *in vitro* measurements can reflect the *in vivo* situation.

However, measurements of the %PPB can be performed using different methods starting from equilibrium dialysis, through ultrafiltration or ultracentrifugation methods up to HPLC methods. The most commonly used methods, especially in PET tracer studies, are filtration/centrifugation methods. Therefore, whole blood of the study participant or patient is drawn, plasma is extracted via a centrifugation step and plasma is spiked with the radiolabeled biomarker. Only the unbound drug fraction will be left in the filtrate. Correction for non-specific binding to the centrifugation tubes is performed by repetition of the experiment in PBS (63–65).

It is known and widely approved that serum albumin (HSA) and alpha-glycoprotein (α-gp or AGP) are the two major proteins in plasma and responsible for the PPB (57). Therefore, HPLC columns have been introduced using immobilized human serum albumin (HSA-column) (56,66,67) for rapid PPB measurements. This HPLC method can provide relative information about PPB, the binding constants, characterization of binding sites, examination of drug-drug interactions and drug-protein dissociation rates (68). Advantages in contrast to the gold standard ultrafiltration methods are the high number of compounds that can be measured, the cost efficiency and the suitability for compounds with high affinity towards HSA. The stationary phase consists of a silica matrix in which HSA is immobilized (Figure 4).

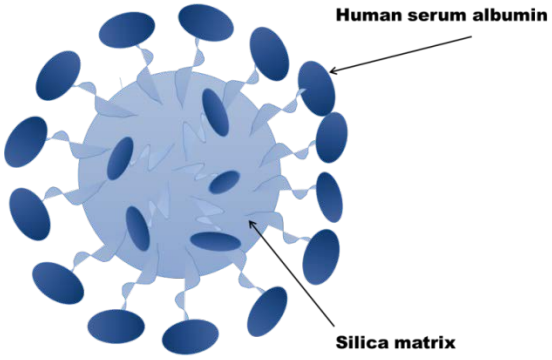

Figure 4 schematically shows the column matrix of the high-performance bioaffinity chromatography immobilized with human serum albumin. The protein is immobilized on spherical 5 µm particles.

The disadvantage of this method is that the %PPB outcome is limited to one single protein whereas in plasma many others such as AGP, globulins or lipids are involved. To this end, this can lead to underestimation of the degree of PPB. However, the %PPB values are taken from literature and calculated with a regression analysis of reference standards using the method according to Valko et al (56). Therefore, it was shown that the results using conventional methods with new HPLC approaches correlate strongly (56,69). The discussion about the impact of PPB on DMPK and especially BBB penetration persists since decades. Fact is that an interpretation of DMPK behavior solely with PPB data is not enough to predict the distribution and therefore penetration through biomembranes. Accordingly, permeability models and transport assay have been presented and grow in attractiveness.

1.5 Permeability

Permeability measurements can be carried out in different models. Basically, two types of models can be distinguished: assays using artificial phospholipids and cell-based assays.

The artificial assay can further be divided in the PAMPA (parallel artificial membrane permeability assay) and immobilized artificial membrane chromatography (IAM). Both methods are so called “high-throughput approaches” in comparison to cell based assays. However, comparing the artificial methods with each other, IAM exceeds in terms of time and cost efficiency the PAMPA model.

IAM chromatography was developed in 1989 by Pidgeon and Venkataram (70). Initially, the IAM has been introduced to measure drug adsorption from the gut passage (71).

Nowadays, diverse columns are commercially available for different applications. For drug discovery applications (drug permeation), the stationary material consists of a diacylated or double chain ester PC ligand denoted as ester IAM.PC.DD2, and is end-capped with C10/C3 alkyl chains.

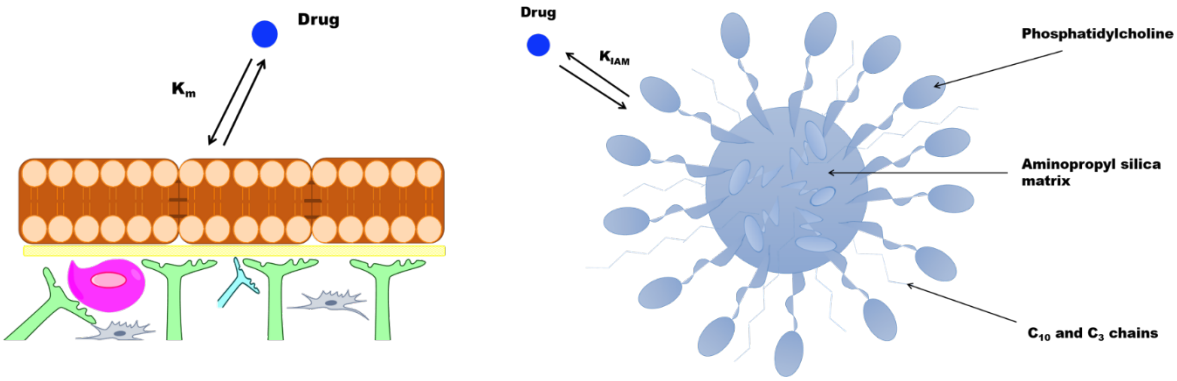

Figure 5 illustrates the fluid membrane coefficient (Km) with the biomembrane and the KIAM with the IAM column matrix. The column consists of phosphatidylcholines, which are covalently bound to the aminopropyl silica matrix. Additionally, the stationary phase contains C10 and C3 chains. All possible interactions (↔), drug (blue circle). Graphic adapted from Pidgeon et al. (70) and Ong et al. (72).

IAM chromatography provides data for passive diffusion by measuring the solute interaction with the artificial phospholipids (K_{IAM}) in an HPLC system. The membrane coefficient, K_{IAM}, is directly proportional to the permeability (P_m) (19,71–75).

In 2012, IAM chromatography has been used for the first time to evaluate PET brain tracers. Tavares and co-workers showed by evaluation of ten tracers that the Pm values correlate stronger with percent injected doses (%ID) of the whole brain uptake than the PPB or logP measurements did (20). The main difference between the IAM and the PAMPA model (figure 5 A) is that IAM indirectly measures permeability based on the membrane coefficient and the molecular weight, whereas PAMPA belongs to the transport assays and generate an apparent permeability (P_{app}) (59,76).

Other transport assays, which directly generate the P_{app}, are cell-based (illustration cf. figure 5 B-D). These P_{app} measurements can be performed with different cell lines in a monolayer or co-culture model. Advantages are depending on the used cell lines, but in general, the positive aspects are the use of biological material, formation of tight junctions and expression of transporters.

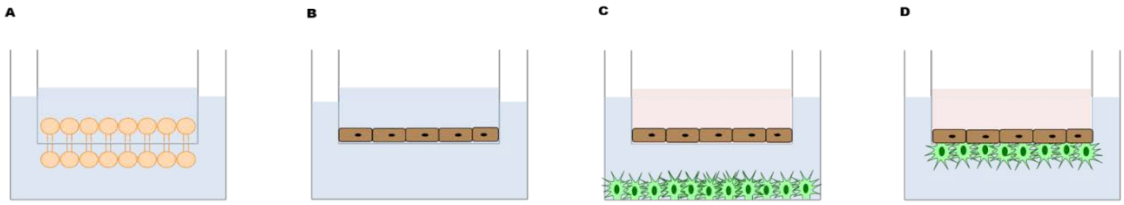

Figure 6 shows artificial and cell-based models of permeability measurements. 5A illustrates the PAMPA model, whereas B, C and D are cells based assay. C and D are examples for co-culture models using two different cell lines in one assay.

Hence, transporter assays using cells are not limited to passive diffusion. Moreover, they are used to predict interactions with efflux transporters.

Typical permeability assays are performed using human endothelial cells (hCMEC/D3), Caco-2 cells or MDCKII cells. The cells can differentiate into a columnar epithelium and form tight junctions (TJ). Due to this narrow grow pattern, the transcellular transport is assumed to be restricted, just as it is at the BBB. In this respect, the significantly increased growth of MDCKII cells (seven-fold higher) is more favorable than the growth rate of human endothelial cells and Caco-2 cells (77). Additionally, when MDCKII cells are infected with the MDR1 virus (MDCKII-MDR1) P-gp is expressed in a polarized manner on the upper surface of the cells. MDCKII-MDR1 cells are commercially available and used to investigate potential interactions of newly developed tracers with the P-gp. Furthermore, the assay can be simplified by performing cell uptake assays in well plates. For this purpose, the tracer uptake of the wildtype cell line (MDCKII) is compared to the uptake in the transfected cell line (MDCKII-MDR1).

Another possibility is to use a co-culture model (78–83). It is assumed that astrocytes are required to induce the formation of TJ in endothelial cells (bovine, porcine or human), which is likely to result in a native BBB model (84). Hence, a co-culture model with BBMEC (Bovine brain endothelial cells) and human astrocytes has been introduced to better mimic the BBB and enhance the quality of prediction, due to the of higher efflux transporter expression (85).

However, very low transendothelial electrical resistance (TEER) was observed for the hCMEC/D3 cell line (30-50 Ω cm²) compared to the *in vivo* situation (1,000 Ω cm²) (83). On the other hand, cultivation of a co-culture model is a long process. For models as illustrated in figure 5 C, durations of 34 days are described (78,86). For the model illustrated in figure 5 D even more extensive working steps and time frames are needed

(unpublished data). Furthermore, integrity and functionality of the endothelial monolayer have to be quantified by performing TEER measurements, immunohistological staining or western blot (for e.g. occluding, JAM or P-gp), the lucifer yellow assay or pre-experiments with [^{14}C]-sucrose to establish the model. Occasionally, this has to be repeated before conducting experiments (78,81,86).

Thus, there are different methods available with individual pros and cons. Transport assays as illustrated in 5 B, C and D may better mimic BBB conditions as they express, for example, efflux transporters, however, they require extensive workflows. In the early stage of drug development, when the variety of candidate ligands is large, IAM chromatography or simplified methods are advisable.

1.6 Efflux transporter

Even if the physicochemical properties are presumed to be “optimal” to penetrate the BBB, there still might not a detectable tracer uptake in the brain. One plausible reason might be that the brain is protected from compounds which are predominately affine to efflux transporters. Permeability-glycoprotein (P-gp, ABCB1 or MDR1) binding is one main cause of tracer candidate exclusion (78,87). Therefore, identification of efflux transporter substrates is one of the mentioned criteria a successful PET brain tracer in drug development should fulfill, cf. chapter “Brain imaging using positron emission tomography” criteria of operative PET tracer, point VII (14,88). Furthermore, the identification of P-gp substrates and inhibitors is of high interest, because the expression of efflux transporters can lead to drug resistance. They significant changes in the bioavailability and they are discussed to be involved in the etiology of diverse neurological and metabolic disorders like Alzheimer’s Disease or Diabetes (89–92).

The human **ABC (ATP-binding cassette) transporters** are a large group (48 members) of membrane proteins and classified in seven subfamilies categorized (A-G) after gene homology. Structurally, all of the 48 members have two nucleotide-binding domains (NBD) and two transmembrane domains (TMD) (93). The most potent efflux transporter is P-gp, which is encoded by the MDR1 gene (ABCB1 gene) (94). P-gp is a large, 170 kDa, and glycosylated membrane protein and associated with a multi-drug resistance in

mammalian cells. Besides at the BBB, P-gp is expressed on the luminal surface of various mammalian tissues (e.g. intestinal epithelia, kidney, liver, placenta) (95,96).

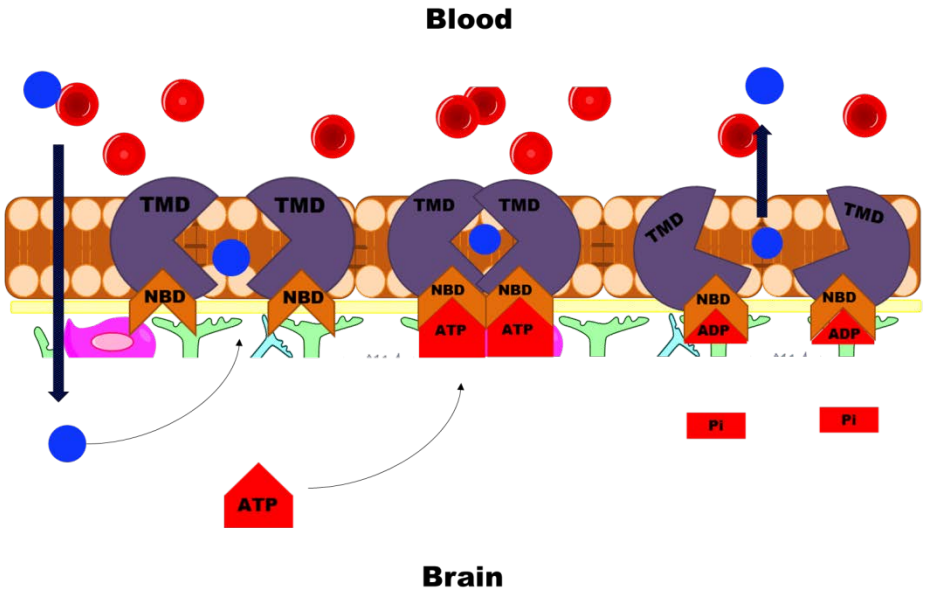

Figure 7: Function of ABC transporters at the BBB. Conformational changes of the transporter are illustrated due to the binding of a substrate and due to ATP hydrolysis. TMD (transmembrane binding site); NBD (nucleotide binding side); ATP (adenosine triphosphate); ADP (adenosine diphosphate); Pi (inorganic phosphate). Adapted graphic form Chen et al. (93).

The biological tasks of P-gp are to exclude drugs from cells with a broad affinity for several and diverse lipophilic substrates. Accordingly, P-gp substrates can have completely different chemical structures and pharmacological functions. Selected substrates of P-gp are members of antibiotics (e.g. doxycycline, erythromycin), anticancer drugs (e.g. 5-fluorouracil, actinomycin D, bisantrene), HIV-protease inhibitors (like amprenavir, indinavir) and immunosuppressive agents (e.g. cyclosporine A and D and FK506) (93,97). Therefore, a prediction of P-gp substrates using the structure or other chemical properties (e.g. logD) at the early stage of drug development is virtually impossible (93). Many authors contributed to P-gp substrate recognition and suggested *in silico* rules (cf. Table 1). These rules include the number of HBD or HBA and thresholds for the tPSA and the molecular weight (41,47,48,91,93,98). However, the prediction of interactions towards P-gp is based on experimental transport assays (Figure 5B), cell uptake assays (e.g. Rhodamine-123, digoxin) or based on animal experiments (blocking studies with P-gp inhibitors, e.g. Tariquidar). None of these *in vitro* assays routinely use PET tracers; instead, the experiments are performed with tritium-labeled ligands.

1.7 In vivo Imaging of Efflux Transporters

In literature, different interactions of compounds with the efflux transporters are described. A compound, which is transported (being subject of an active efflux) by an efflux transporter (e.g. P-gp) is called a substrate. Compounds which modulate the function of efflux transporters can either be inhibitors or modulators. Inhibitors restrict ATP hydrolysis, whereas modulators can increase the potential of the respective transporters. Some authors do not distinguish between inhibitors and modulators and use the term “modulator” for any kind of interaction. Furthermore, the term competitive inhibitor is used: many substrates are supposed to exhibit a concentration depending interaction, being a substrate at low concentration and an inhibitor at high concentrations (verapamil is such an example).

However, the definition of the terms is a minor challenge in contrast to the challenges which occur in *in vi*vo studies. Different concepts have been reported to image efflux transporter function or density (99):

I. The “blood efflux index” method, measures the efflux rate from brain to the blood pool for intracranial applied drugs. This is the most direct imaging technique, but not applicable as a human application.

II. The “metabolite extrusion” method uses a PET tracer, which penetrates the BBB by passive diffusion but is highly metabolized in brain tissue. The formed metabolite is a highly potent substrate, which subsequently is excluded from brain tissue and transported into the blood pool. However, this sophisticated principle is limited due to the lack of specific PET tracers which realize these properties.

III. Imaging using substrates (TCM). Therefore, the substrate (PET tracer) is given in a baseline scan and the administration is repeated under inhibition of the respective transporters. The difference in the uptake levels represents the potency of the efflux transporter and should be shown by an increased K1 (influx rate, cf. figure 1).

IV. Second option for TCM is the administration of a PET tracer that belongs to the group of inhibitors. This generates information about the density of the respective transporter.

However, in order to a visualize 50% increase in substrate uptake (III.), more than 80% of the respective transporters must be blocked. This could lead to toxicological effects of the administrated inhibitor (99). Furthermore, pharmacokinetic changes cannot be excluded since the transporters are blocked in peripheral tissue (e.g. emunctories) as well.

The most commonly used PET tracers imaging human P-gp have foibles. The main weaknesses are poor selectivity, degradation of the parent compound to interfering radiometabolites, low brain uptake or concentration dependent changes in the characteristics of the radiotracer.

((R)-[^{11}C]verapamil is, indeed, selective for the P-gp transporter, but in nanomolar concentrations transported and in higher concentration an inhibitor. Furthermore, it degrades quickly into radiometabolites (97,99,100). [^{11}C]dLop shows an acceptable brain signal (increased ratio between the baseline and blocking scan) and no interfering metabolites. However, the selectivity for P-gp was not yet proven. Some authors state that [^{11}C]dLop is selective, but shows a limited brain uptake ratio when comparing P-gp knockout mice to wildtype mice (4-fold) (101). Studies of third generation inhibitors [^{11}C]tariquidar, [^{11}C]elacridar and [^{11}C]laniquidar show controversial results (90,99–107). Especially, tariquidar is still debated controversially in the radiopharmaceutical community. On the one hand, tariquidar is discussed to be non-selective for P-gp as it is supposed to also interact with BCRP (108). On the other hand, tariquidar is also supposed to be a P-pg substrate *in vivo* (97), although the K_D of 5.1 nM is described in literature for the tariquidar as inhibitor (97,107,109). The reasons for these discrepancies might be species differences. Unfortunately, different experimental models (cell based assays, animal experiments (rats or mice, knockout, human studies) generate inconsistent results. Another hypothesis is a mutation of the human P-gp (“Cys-less”-form), which results in different outcomes (107). Elacridar is also described to be a potent non-competitive P-gp inhibitor (105). However, in *in vivo* studies it was shown that there is evidence that [^{11}C]elacridar acts as a substrate for P-gp and BCRP (97). Laniquidar is reported to have a 10-fold lower affinity towards P-gp in comparison to tariquidar and elacridar. Indeed, high selectivity is described towards P-gp. Again also for [^{11}C]laniquidar it has not been validated in an *in vivo* evaluation.

1.8 Methods for the Verification of Brain Uptake

The most relevant and most direct proof of brain uptake in general is achieved by *in vivo* approaches. Thereby, the tracer is injected intravenously to an animal and brain images are assessed. Alternatively, after the accumulation time an *ex vivo* biodistribution or *ex vivo* autoradiography can be conducted. For this purpose, the animal has to be sacrificed. Thus, the organs of interest (e.g. brain) are harvested and the amount of radioactivity in the brain tissue is counted using a gamma-counter or (frozen) brain slices are exposed to a phosphor screen, which is read out with a Phosphor Imager. Accordingly, the injected dose per gram tissue (%ID/g) is calculated using cross-calibration factors and regression analysis (converting regression) (110). To evaluate whether a PET tracer interacts with efflux transporters, an inhibitor (e.g. tariquidar) can be applied before the tracer administration (blocking study). The resulting difference in uptake between the baseline (vehicle) and blocking condition depicts the interaction with efflux transporters. *Ex vivo* biodistribution studies neither consider the tracer in the capillary brain bed, nor interfering radiometabolites. Another option to assess the potential brain distribution of a PET tracer and the efflux rate from brain to periphery is the intracranial injection or implantation of an intracranial catheter (port). This method does not reflect BBB penetration per se but can examine the efflux rate from brain to peripheral tissue while avoiding first-pass metabolism effects (cf. In vivo Imaging of Efflux Transporters, point I). In PET tracer development, animal experiments are still the gold standard in order to evaluate DMPK properties. However, the number of animals, which are sacrificed, is smaller than in the development of therapeutic drugs.

2 Aim of the thesis

Aim of this thesis was the systematic evaluation of the most important physicochemical and pharmacokinetic parameters (lipophilicity and plasma protein binding) regarding their effect on brain uptake. For this purpose, a special focus was put on the evaluation of three experimental high throughput methods to systematically measure drug lipophilicity (logP), plasma protein binding (PPB) and permeability (Pm)/fluid membrane coefficient (K_m) based on HPLC methods.

First aim of the thesis was the comprehensive assessment of the lipophilicity with regard to the comparability from results using different methods and the influence on BBB penetration by following "optimal" ranges of logP values, which are supposed to predict brain uptake and are stated in literature. Herewith, the logP of the most commonly used PET brain tracers were evaluated (**manuscripts 1 and 2**).

Second part of the present work aimed to evaluate two different high performance bioaffnity chromatography (HPBAC) methods measuring the K_m, Pm and the PPB. Based on these data, I aimed to critically discuss the influence of these parameters on BBB penetration (**manuscript 3**).

Third objective of this thesis was the development of a method to predict potential interactions of newly developed PET tracers with the most potent efflux transporter at the BBB, the P-gp protein. This method should be able to directly examine the PET tracer's interaction with P-gp using concentrations in nanomolar range **(manuscript 4)**.

3 Scientific Part

3.1 Authors contribution

I herewith affirm that I contributed significantly to all peer-reviewed articles comprised in this thesis. All included publications are in the format as submitted to the journal or printed and the references follow the citation style of the respective journals. Following responsibilities were taken for each publication:

In the first manuscript, I designed the study, performed the measurements, carried out the interpretation and wrote the manuscript:

Vraka C, Nics L, Wagner KH., Hacker M, Wadsak W, Mitterhauser M. LogP, a yesterday's value? Nucl Med Biol. 2017, Mar 20; 50:1-10

In the respond letter to the editor, I conceived the response and took significant part of the writing:

Vraka C and Mitterhauser M "Reconsider LogP!" Nucl Med Biol 2017;54:p42

Concerning the third publication, I designed the study, performed or supervised the experimental part as well as I carried out the data analysis and interpretation of the results. Additionally, I wrote the manuscript draft:

Vraka C, Mijailovic S, Fröhlich V, Wadsak W, Wagner KH, Hacker M, Mitterhauser M. Expanding LogP: Present Possibilities. Submitted, 2017 September 22nd, Journal of Nuclear Medicine and Biology, (NUCMEDBIO_2017_232).

Regarding the fourth manuscript, I designed the study, establish the in vitro assay and supervised the in vitro experiments. Additionally, I significantly performed the interpretation of the data and drafting of the manuscript:

Vraka C, Dumanic M, Racz T, Pichler F, Philippe C, Balber T, Klebermass EM, Wagner KH, Hacker M, Wadsak W, Mitterhauser M. A New Model for the Prediction of the Interaction of Radiotracers with the P-glycoprotein (P-gp) transporter.

Submitted, 2017 November 13th, Journal of Nuclear Medicine and Biology (NUCMEDBIO_2017_285).

In the following manuscript, I performed the lipophilicity and permeability measurements using IAM Chromatography and contributed to the metabolic stability testing:

Rami-Mark C, Bornatowicz B, Fink C, Otter P, Ungersboeck J, **Vraka C**, Haeusler D, Nics L, Spreitzer H, Hacker M, Mitterhauser M, Wadsak W. Synthesis, radiosynthesis and first in vitro evaluation of novel PET-tracers for the dopamine transporter: [(11)C]IPCIT and [(18)F]FE@IPCIT. Bioorg Med Chem. 2013 Dec 15;21(24):7562-9.

Regarding the following publication, I performed the lipophilicity and permeability measurements using IAM chromatography. Additionally, I performed the plasma protein binding using an ultrafiltration method:

Rami-Mark C, Berroterán-Infante N, Philippe C, Foltin S, **Vraka C**, Hoepping A, Lanzenberger R, Hacker M, Mitterhauser M, Wadsak W. Radiosynthesis and first preclinical evaluation of the novel norepinephrine transporter pet-ligand [(11)C]ME@HAPTHI. EJNMMI Res. 2015 Dec;5(1):113.

Concerning the last manuscript, I performed all lipophilicity and permeability measurement, took significantly part of drafting method part of the performed experiments, as well as the interpretation of these results:

Wenzel B, Mollitor J, Deuther-Conrad W, Dukic-Stefanovic S, Kranz M, **Vraka C**, Teodoro R, Günther R, Donat C, Ludwig F-A, Fischer S, Smits R, Wadsak W, Mitterhauser M, Steinbach J, Hoepping A, Brust P. On the development of a novel non-peptidic 18F-labeled radiotracer for in vivo imaging of oxytocin receptors with positron emission tomography. J Med Chem. 2016 Mar 10;59(5):1800-17.

3.1.1 Manuscript I

Vraka C, Nics L, Wagner KH., Hacker M, Wadsak W, Mitterhauser M. LogP, a yesterday's value? Nucl Med Biol. 2017, Mar 20; 50:1-10

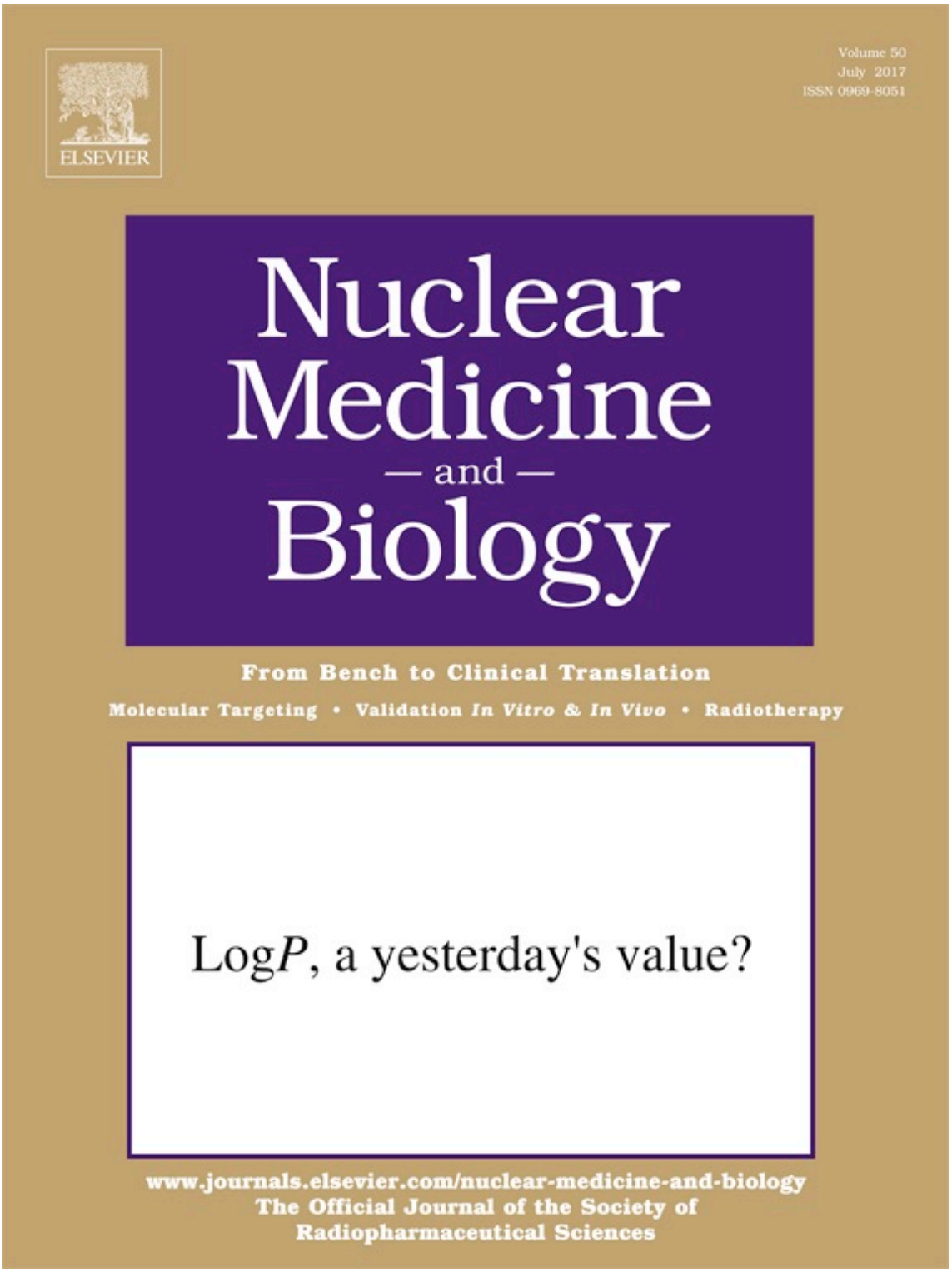

Nuclear Medicine and Biology 50 (2017) 1–10

Contents lists available at ScienceDirect

Nuclear Medicine and Biology

journal homepage: www.elsevier.com/locate/nucmedbio

Log*P*, a yesterday's value?

Chrysoula Vraka [a,b], Lukas Nics [a,b], Karl-Heinz Wagner [b], Marcus Hacker [a], Wolfgang Wadsak [a,c,d], Markus Mitterhauser [a,e,f,*]

[a] Department of Biomedical Imaging and Image-guided Therapy, Division of Nuclear Medicine, Medical University of Vienna, Vienna, Austria
[b] Department for Nutritional Science, University of Vienna, Vienna, Austria
[c] Department of Inorganic Chemistry, University of Vienna, Vienna, Austria
[d] CBmed, Graz, Austria
[e] Department of (PTB) Pharmaceutical Technology and Biopharmaceuticals, University of Vienna, Vienna, Austria
[f] Ludwig Boltzmann Institute Applied Diagnostics, Vienna, Austria

ARTICLE INFO

Article history:
Received 15 February 2017
Received in revised form 16 March 2017
Accepted 16 March 2017
Available online xxxx

Keywords:
Radioligand &-tracer
Lipophilicity
HPLC log*P*
Database
Blood brain barrier

ABSTRACT

Introduction: There is an increasing demand for high throughput methods at early stages of preclinical radioligand development, in order to predict pharmacokinetic properties (e.g., biodistribution) and blood brain barrier (BBB) penetration. One of the most important physicochemical properties is the lipophilicity, measured by means of shake-flask (log*P*) or HPLC methods. Yet, a plethora of experimental methods are described in the literature for the determination of logP values. These varying methods often lead to different results for one identical compound, which complicates any comparison or prediction for subsequent preclinical studies. However, a standardized and internationally applied and accepted database with log*P* values for a reliable comparison of the lipophilic character of radiotracers is still missing.
Method: Lipophilicity measurements were performed with 121 molecules using a high throughput HPLC method and Clog*P* values were calculated using ChemBioDraw®. Furthermore, log*P* measurements for six representative radiotracers were performed with the conventional shake-flask method and the results were statistically compared to the Clog*P* and HPLC log*P* results. Different log*P* thresholds, suggesting optimal BBB penetration according to literature, were selected and put into relation with the acquired HPLC log*P* and Clog*P* values of cerebral tracers.
Results: The results of the tested compounds ranged from −2.1 to 5.4 with the applied HPLC method. The acquired database comprises Clog*P* values of the whole set of compounds ranging from −4.11 to 6.12. Log*P* data from different methods were not comparable. The correlation of the obtained log*P* data to thresholds suggesting an optimal brain uptake resulted in a high number of false positive classifications.
Conclusion: The log*P* determination for prediction of BBB penetration is obsolete. The extensive database, including clinical relevant radiotracers, can be used as comparative set of values for preclinical studies, and serves as a basis for further critical discussions concerning the eligibility of log*P*.

1. Introduction

The term lipophilicity describes the extent of solubility of a compound in lipids, oil or non-polar solvents like hexane or 1-octanol. The lipophilicity is defined as the partition-coefficient of an un-ionized compound in two immiscible phases (*n*-octanol and water/buffer) at equilibrium, whereas log*D* describes the distribution of all species (un-ionized and ionized solutes) at equilibrium. Therefore, the logarithm of the ratio is the log*P* or log*D*. At physiological pH (7.4), the terms log*P* and log*D* can be used synonymously. Based on this definition, the shake-flask or shake-tube method is currently the "gold standard" for the determination log*P* or log*D* values [1–4]. A plethora of shake flask or shake tube methods with differences in shaking time, number of distribution repetitions and detection of the distribution between the phases have been proposed. Measuring the partition coefficient in two phases appears very simple, especially with radiolabeled compounds. Since the sensitivity of radiodetectors is very high, the use of very small quantities of the tested compounds suffices. However, for highly lipophilic or hydrophilic compounds, the application of very high concentrations or radioactivity is necessary to achieve the limit of detection in the respective phase where the tracer is weakly distributed. Therefore, OECD (Organization for Economic Co-operation and Development) guidelines recommend a log*P* range of −2.0 to 4.0 [5]; measurements above or below are inaccurate.

A modern definition of lipophilicity according to the International Union for Pure and Applied Chemistry (IUPAC) states that the

* Corresponding author at: Ludwig Boltzmann Institute Applied Diagnostics, General Hospital of Vienna, Waehringer Guertel 18-20, A-1090 Vienna, Austria. Tel.: +43 1 40400 55340; fax: +43 1 40400 15590
E-mail address: markus.mitterhauser@meduniwien.ac.at (M. Mitterhauser).

http://dx.doi.org/10.1016/j.nucmedbio.2017.03.003
0969-8051/

$$\frac{(\log P_{\text{toluene}} - \log P_{\text{triphenylene}}) * \text{measuredRt}_{\text{analyte}} + \text{measuredRttoluene} * \log P_{\text{triphenylene}} - \text{measuredRt}_{\text{triphenylene}} * \log P_{\text{toluene}}}{\text{measuredRt}_{\text{toluene}} - \text{measuredRt}_{\text{triphenylene}}} = \text{HPLC log}P_{\text{ow}}\text{pH}^{7.4}{}_{\text{analyte}}$$

Equation 1. Calculation of HPLC $\log P_{ow}^{pH7.4}$ measurements. The equation describes the calculation of the log*P* value ($HPLClogP_{ow}{}^{pH7.4}{}_{analyte}$), whereby the unknown log*P* value of the analyte is derived from the measured retention times and the known log*P* values of the internal standards toluene and triphenylene. The measured retention times of the internal standards and the log*P* values of the internal standards are set in relation to the measured retention time of the tested reference standard or radiotracer (measured $Rt_{analyte}$) to obtain the log*P* value of the analyte. According to the different literature sources of the log*P* of toluene and triphenylene, three log*P* values were obtained ($_1HPLClogP_{ow}^{pH7.4}$, $_2HPLClogP_{ow}^{pH7.4}$ and $_3HPLClogP_{ow}^{pH7.4}$) and a mean log*P* value ($_\mu HPLC\ logP_{ow}^{pH7.4}$) calculated (see results, Table 1).

"lipophilicity represents the affinity of a molecule or a moiety for a lipophilic environment". Further, the method is also described as the "distribution behavior in a biphasic system, either liquid–liquid (e.g., partition coefficient in 1-octanol/water) or solid–liquid (retention on reversed-phase high-performance liquid chromatography (RP-HPLC) or thin-layer chromatography (TLC) system)" [6]. The extension of the lipophilicity definition and the facilitated handling of HPLC systems compared to the conventional shake flask method led to the development of a variety of HPLC methods. General benefits of HPLC methods are speed, simplicity, direct partitioning and stability against impurities or solvent residues in the sample solution. The fifteenth addendum of the OECD (Organization for Economic Co-operation and Development) guidelines for testing chemicals describes an HPLC method using reverse phase (C8 or C18 chains bound to a silica matrix) and as mobile phase a methanol–water mixture (3:1 v/v). The accurate range is given as log*P* 0 to 6. Due to the free Si–OH and Al–OH groups, this method "is not applicable to strong acids and bases, metal complexes, substances which react with the eluent, or surface-active agents" [5].

In recent years, lipophilicity measurements are increasingly calculated, with computational methods assuming that experimental methods are cost intensive and time consuming. Common in silico methods calculate log*P*- or Clog*P*-values using state-of-the-art software (e.g., Chemdraw®) or quantitative structure–activity relationships (QSAR) from databases. These calculations are straightforward and provide the log*P* or Clog*P* for a large number of molecules. However, there are significant deviations between the calculated and measured log*P* values. Especially, if the pattern of connectivity and non-bonded intramolecular interactions are not listed in the applied database [7–9]. In drug development, especially for central applications, the lipophilicity is a pivotal and early indicator of the potential in vivo pharmacokinetic and dynamic behavior. Lipophilicity measurements, as it is widely known, provide information about unspecific binding, metabolic stability, plasma protein binding, the distribution and excretion of drugs. Hence, an adapted version of Lipinski's rule of five postulated that a lipophilicity range of 2.0 to 3.5 is a fundamental predictive factor for the blood brain barrier (BBB) penetration probability via passive diffusion [10–12]. This manifoldness of the lipophilicity is the reason why it is one of the most crucial physicochemical properties and one of the most frequently analyzed and published parameters [4,11].

As there are a high number of techniques available for log*P* measurements and the evidence that shake-flask or -tube methods are prone to operational mistakes and errors caused by radiochemical impurities, the comparability of the data should be questioned.

Thus, a centralized database, collecting log*P* data of the most common radiotracers for primarily cerebral application, is necessary to improve the comparability and validity of log*P* values of newly developed tracers in the preclinical stage.

Accordingly, the present work used a modern HPLC technique for the measurement and the subsequent evaluation and comparison of log*P* values of 121 reference compounds.

The aim of this work was

(I) the provision of a conclusive database of the most commonly used radiotracers in clinical routine and clinical studies, (II) the comparative evaluation of lipophilicity values based on calculation, shake flask and HPLC measurements, and (III) the assessment of the eligibility to use log*P* thresholds as general predictive parameters at all.

2. Materials and methods

2.1. General information and materials

The used Agilent HPLC (Agilent technologies, Santa Clara, USA) system consists of an auto-injector (1100 series), a pump (1200 series), a diode array detector (1100 series) and a radio-detector (Ramona, Elysia-Raytest, Straubenhardt, GER).

2.1.1. Internal standard mixture

Methanol (CAS 67-56-1), triphenylene (CAS 217-59-4), both from Sigma-Aldrich, St. Louis, USA and toluene (for liquid chromatography, CAS 108-88, MERCK, Darmstadt, GER).

2.1.2. Stationary phase

ODP(octadecyl-poly(vinyl alcohol)-50 column (20 × 4 mm, 5 μm, Shodex, Showa Denko Europe GmbH, Munich, GER) and apHERA (10 × 6 mm, 5 μm, Supelco, Sigma-Aldrich, St Louis, USA).

2.1.3. Mobile phase

Methanol (CAS 67–56-1) and sodium phosphate dibasic dehydrate (CAS 10028–24-7), sodium phosphate monobasic monohydrate (CAS 10049-21-5), all from Sigma-Aldrich, St Louis, USA, water from Milli-Q® Integral Water Purification System (Merck Millipore, Billerica, USA) and weighing scales (Mettler PJ 300, Mettler Toledo GmBH, Vienna, Austria).

2.1.4. Calculated logP

ChemBioDraw (CBD) Software Version 12.0.2, Level Ultra © 1986–2010 CambridgeSoft, PerkinElmer, Waltham, USA.

2.1.5. Shake-tube

1-Octanol (extra pure, CAS 111v87-5, Merck, Darmstadt, GER), and 3 mL phosphate buffered saline pH 7.4 (PBS buffer pH 7.4 10× stock solution, REF 11237.00500, MORPHISTO, Frankfurt a. Main, GER), 12 mL tube (Greiner centrifuge tube 12 mL, No. 188271, Sigma-Aldrich, St. Luis, USA), gamma-counter (Wizard2 3″ detector, type 2480, PerkinElmer, Waltham, USA), cycling plate shaker device (GFL 3017, Burgwedel, GER), centrifuge (Hettich Rotana 460 RC, Tuttlingen, GER), 5 mL-tubes (REF 55.526, Sarstedt, Nuernbrecht, GER) and weighing scales (Sartorius BP 210 D, Goettingen, GER).

2.2. Reference standards and radiolabeled compounds

The non-radiolabeled standards were purchased from ABX (Advanced Biochemical Compounds, Radeberg, GER), PharmaSynth AS (Tartu, EST), Hayuan Chemexpress (Shanghai, CHN) and Sigma-Aldrich (St. Louis, USA). Some of the compounds were tested, synthesized or kindly provided in cooperation with the scientific partners ABX, the Department of Drug and Natural Product Synthesis (University of Vienna, AUT), the Department of Clinical Pharmacology (Medical University of Vienna, AUT) and the Institute of Organic Chemistry (University of Vienna, AUT). All radiolabeled tracers are in-house productions of the Department of Biomedical Imaging and Image-guided Therapy, Division of Nuclear Medicine, General Hospital of Vienna,

Table 1
Results of ClogP and HPLC $\log P_{ow}^{pH7.4}$.

IUPAC	Trivial name	ClogP	Mean ± SD $_1$HPLC $\log P_{ow}^{pH7.4}$	Mean ± SD $_2$HPLC $\log P_{ow}^{pH7.4}$	Mean ± SD $_3$HPLC $\log P_{ow}^{pH7.4}$	Mean ± SD $_\mu$HPLC $\log P_{ow}^{pH7.4}$
(*E*)-3-((6-methylpyridin-2-yl)ethynyl)cyclohex-3-enone *O*-methyl oxime	ABP688	2.29 2.29	2.89 ± 0.02 3.07 ± 0.06	2.87 ± 0.02 3.05 ± 0.06	2.8 ± 0.02 3.05 ± 0.06	2.86 ± 0.04 3.06 ± 0.06
3-(2-(4-(4-Fluorobenzoyl)piperidin-1-yl)ethyl)-2-thioxo-2,3-dihydroquinazolin-4(1*H*)-one	Altanserin	2.58	4.13 ± 0.03	4.12 ± 0.03	4.46 ± 0.04	4.24 ± 0.17
1-(3-Amino-1-phenylpropyl)-3-phenyl-1*H*-benzo[d]imidazol-2(3*H*)-one	APPI:0	4.49	3.09 ± 0.01	3.08 ± 0.01	3.08 ± 0.02	3.08 ± 0.01
Ethyl 8-azido-5-methyl-6-oxo-3a,4,5,6-tetrahydro-3*H*-benzo[f]imidazo[1,5-*a*] [1, 4]diazepine-3-carboxylate	Azidomazenil	2.16	1.88 ± 0.02	1.85 ± 0.02	1.46 ± 0.03	1.73 ± 0.2
(1*R*,2*S*,3*S*,5*S*)-methyl 3-(4-fluorophenyl)-8-((*E*)-3-iodoallyl)-8-azabicyclo[3.2.1]octane-2-carboxylate	(−)-2-beta-Carbomethoxy-3-beta-(4-fluorophenyl) tropane (beta-CFT)	4.51	0.11 ± 0.01	0.07 ± 0.01	−0.89 ± 0.01	−0.23 ± 0.49
(1*R*,2*S*,3*S*,5*S*)-methyl 3-(4-iodophenyl)-8-methyl-8-azabicyclo[3.2.1]octane-2-carboxylate	(−)-2-beta-Carbomethoxy-3-beta-(4-iodophenyl) tropane (beta-CIT)	3.94	2.24 ± 0.2	2.21 ± 0.2	1.94 ± 0.26	2.13 ± 0.25
(1*R*,2*S*,3*S*,5*S*)-3-(4-iodophenyl)-8-methyl-8-azabicyclo[3.2.1]octane-2-carboxylic acid	beta-CIT acid	1.34	0.06 ± 0.03	0.02 ± 0.03	−0.96 ± 0.04	−0.3 ± 0.48
1-((9*H*-carbazol-4-yl)oxy)-3-(isopropylamino)propan-2-ol	(R,S)-Carazolol	3.06	3.21 ± 0.09	3.2 ± 0.09	3.24 ± 0.12	3.22 ± 0.10
Methyl 1-phenethyl-4-(*N*-phenylpropionamido) piperidine-4-carboxylate	Carfentanil oxalate	3.69	3.28 ± 0.1	3.27 ± 0.1	3.33 ± 0.13	3.29 ± 0.11
(1*R*,2*S*,3*S*,5*S*)-methyl 8-(2-fluoroethyl)-3-(4-iodophenyl)-8-azabicyclo[3.2.1]octane-2-carboxylate	CITFE	4.20	4.08 ± 0.02	4.07 ± 0.02	4.39 ± 0.03	4.18 ± 0.16
(1*R*,2*S*,3*S*,5*S*)-8-(2-fluoroethyl)-3-(4-iodophenyl)-8-azabicyclo[3.2.1]octane-2-carboxylic acid	CITFES	1.46	0.16 ± 0.04	0.12 ± 0.04	−0.82 ± 0.05	−0.18 ± 0.46
(1*R*,2*S*,3*S*,5*S*)-methyl 8-(3-fluoropropyl)-3-(4-iodophenyl)-8-azabicyclo[3.2.1]octane-2-carboxylate	CITFP	4.42	4.31 ± 0.01	4.3 ± 0.01	4.7 ± 0.01	4.44 ± 0.19
8-Cyclopentyl-3-(3-fluoropropyl)-1-propyl-1*H*-purine-2,6(3*H*,7*H*)-dione	CPFPX	3.19	2.86 ± 0.04	2.84 ± 0.04	2.77 ± 0.05	2.83 ± 0.06
3-Amino-4-((2-((dimethylamino)methyl)phenyl)thio)benzonitrile	DASB	3.21	3.77 ± 0.01	3.76 ± 0.01	3.99 ± 0.02	3.84 ± 0.11
4,6-Diethyl-5-((ethylthio)carbonyl)-2-phenylnicotinic acid	DFE@SUPPY	4.24	0.92 ± 0.05	0.89 ± 0.06	0.19 ± 0.07	0.67 ± 0.35
5-(Ethoxycarbonyl)-2,4-diethyl-6-phenylpyridine-3-carbothioic *S*-acid	DFE@SUPPY:2	3.83	4.67 ± 0.6	4.67 ± 0.6	5.18 ± 0.8	4.84 ± 0.73
2-(1-(6-((2-Fluoroethyl)(methyl)amino)naphthalen-2-yl)ethylidene)malononitrile	DMFEAN or FDDNP	3.42	4.4 ± 0.34	4.39 ± 0.34	4.82 ± 0.45	4.54 ± 0.42
2-Fluor-5-hydroxy-L-tyrosin	DOPA	−2.29	n.m.			<−2.5
N-(4-(2-(6,7-dimethoxy-3,4-dihydroisoquinolin-2(1*H*)-yl)ethyl)phenyl)-5-methoxy-9-oxo-9,10-dihydroacridine-4-carboxamide	Elacridar	4.21	4.66 ± 0.02	4.65 ± 0.02	5.16 ± 0.03	4.82 ± 0.24
(*S*)-*N*-((1-ethylpyrrolidin-2-yl)methyl)-5-iodo-2,3-dimethoxybenzamide	Epidepride	3.46	2.78 ± 0.03	2.76 ± 0.03	2.66 ± 0.04	2.73 ± 0.06
	Erlotinib	3.20	3.18 ± 0.03	3.16 ± 0.03	3.19 ± 0.04	3.17 ± 0
(*R*)-ethyl 1-(1-phenylethyl)-1*H*-imidazole-5-carboxylate	(*R*)-Etomidate	2.67	2.62 ± 0.22	2.6 ± 0.22	2.46 ± 0.29	2.56 ± 0.03
(*S*)-*N*-((1-allylpyrrolidin-2-yl)methyl)-1-(5-(3-fluoropropyl)-2,3-dimethoxyphenyl)ethenamine	Fallypride	3.89	3.01 ± 0.08	2.99 ± 0.08	2.96 ± 0.11	2.99 ± 0.1
1-(1-(4-Fluorophenyl)-3-(methylamino)propyl)-3-phenyl-1*H*-benzo[d]imidazol-2(3*H*)-one	FAPPI:1	4.87	3.44 ± 0.06	3.42 ± 0.06	3.54 ± 0.08	3.5 ± 0.07
1-(4-Fluorophenyl)-3-(3-(methylamino)-1-phenylpropyl)-1*H*-benzo[d]imidazol-2(3*H*)-one	FAPPI:2	4.90	3.4 ± 0.05	3.38 ± 0.05	3.48 ± 0.07	3.16 ± 0.07
1-(2-Fluorophenyl)-3-(3-(methylamino)-1-phenylpropyl)-1*H*-benzo[d]imidazol-2(3*H*)-one	FAPPI:3	4.90	3.12 ± 0.07	3.1 ± 0.07	3.12 ± 0.1	3.11 ± 0.07
(1*R*,2*S*,3*S*,5*S*)-2-fluoroethyl 3-(4-iodophenyl)-8-methyl-8-azabicyclo[3.2.1]octane-2-carboxylate	2-FE-beta-CIT	4.33	3.23 ± 0	3.21 ± 0	3.26 ± 0	3.23 ± 0.02
1-(3-((2-Fluoroethyl)amino)-1-phenylpropyl)-3-phenyl-1*H*-benzo[d]imidazol-2(3*H*)-one	FE@APPI	4.98	3.4 ± 0.01	3.39 ± 0.01	3.49 ± 0.01	3.43 ± 0.05
(1*R*,2*S*,3*S*,5*S*)-2-fluoroethyl 8-((*E*)-3-iodoallyl)-3-(4-iodophenyl)-8-azabicyclo[3.2.1]octane-2-carboxylate	FE@IPCIT	5.74	4.83 ± 0.01	4.82 ± 0.01	5.39 ± 0.01	5.01 ± 0.28
2-Fluoroethyl 4-(1-acetyl-5-(anthracen-9-yl)-4,5-dihydro-1*H*-pyrazol-3-yl)benzoate	FE@MAOBI:1	5.73	4.77 ± 0.02	4.77 ± 0.02	5.32 ± 0.03	4.95 ± 0.27
2-fluoroethyl 5-(1-acetyl-5-(anthracen-9-yl)-4,5-dihydro-1*H*-pyrazol-3-yl)thiophene-2-carboxylate	FE@MAOBI:2	5.45	4.71 ± 0.01	4.7 ± 0.01	5.23 ± 0.01	4.88 ± 0.3
2-fluoroethyl 5-(1-acetyl-5-(anthracen-9-yl)-4,5-dihydro-1*H*-pyrazol-3-yl)furan-2-carboxylate	FE@MAOBI:4	4.90	4.28 ± 0.01	4.27 ± 0.01	4.66 ± 0.01	4.4 ± 0.22
2-Fluoroethyl 6-(1-acetyl-5-(anthracen-9-yl)-4,5-dihydro-1*H*-pyrazol-3-yl)nicotinate	FE@MAOBI:5	4.38	4.15 ± 0.01	4.14 ± 0.01	4.49 ± 0.02	4.26 ± 0.2
2-Fluoroethyl 4,6-diethyl-5-((methylthio)carbonyl)-2-phenylnicotinate	FEMe@SUPPY	5.58	3.83 ± 0.01	3.82 ± 0.01	4.06 ± 0.02	3.9 ± 0.12
Methyl 4,6-diethyl-5-(((2-fluoroethyl)thio)carbonyl)-2-phenylnicotinate	FEMe@SUPPY:2	5.58	3.89 ± 0.04	3.88 ± 0.04	4.14 ± 0.05	3.97 ± 0.13
2-Fluoro-*N*-methyl-*N*-(((3*S*,4*S*)-4-(*o*-tolyloxy)isochroman-3-yl)methyl)ethanamine	FE@PHOXI:1	4.06	3.6 ± 0.05	3.59 ± 0.05	3.75 ± 0.06	3.65 ± 0.09
2-Fluoro-*N*-methyl-*N*-(((3*S*,4*S*)-4-(2-(trifluoromethyl)phenoxy) isochroman-3-yl)methyl)ethanamine	FE@PHOX:2	4.69	3.57 ± 0	3.56 ± 0	3.72 ± 0	3.62 ± 0.09
2-Fluoroethyl 3-((3-(4-(3-acetamidophenyl)piperidin-1-yl)propyl) carbamoyl)-4-(3,4-difluorophenyl)-6-(methoxymethyl)-2-oxo-1,2,3,4-tetrahydropyrimidine-5-carboxylate	FE@SNAP	5.17	3.66 ± 0.04	3.64 ± 0.04	3.81 ± 0.04	3.71 ± 0.09
2-Fluoroethyl 4,6-diethyl-5-((ethylthio)carbonyl)-2-	FE@SUPPY	6.11	4.02 ± 0.01	4.01 ± 0.01	4.31 ± 0.02	4.12 ± 0.14

(continued on next page)

Table 1 *(continued)*

IUPAC	Trivial name	Clog*P*	Mean ± SD $_1$HPLC log$P_{ow}^{pH7.4}$	Mean ± SD $_2$HPLC log$P_{ow}^{pH7.4}$	Mean ± SD $_3$HPLC log$P_{ow}^{pH7.4}$	Mean ± SD $_\mu$HPLC log$P_{ow}^{pH7.4}$
phenylnicotinate						
2-Fluoroethyl 4,6-diethyl-5-(((fluoromethyl)thio)carbonyl)-2-phenylnicotinate	FE^2@SUPPY	5.25	3.98 ± 0.03	3.97 ± 0.03	4.26 ± 0.04	4.07 ± 0.14
Ethyl 4,6-diethyl-5-(((2-fluoroethyl)thio)carbonyl)-2-phenylnicotinate	FE@SUPPY:2	6.11	4.03 ± 0.03	4.02 ± 0.03	4.32 ± 0.04	4.1 ± 0.15
2,4-Diethyl-5-((2-fluoroethoxy)carbonyl)-6-phenylpyridine-3-carbothioic *S*-acid	FE@SUPPY:11	3.55	5.18 ± 0.03	5.18 ± 0.03	5.86 ± 0.03	5.41 ± 0.33
4,6-Diethyl-5-(((2-fluoroethyl)thio)carbonyl)-2-phenylnicotinic acid	FE@SUPPY:21	3.96	0.56 ± 0.1	0.53 ± 0.1	−0.29 ± 0.14	0.27 ± 0.41
(*S*)-2-Amino-3-(4-(2-fluoroethoxy)phenyl)propanoic acid	FET hydrochloride	−1.39	−1.56 ± 0.13	− 1.61 ± 0.13	−3.12 ± 0.17	−2.1 ± 0.75
(*S*)-5-Bromo-*N*-((1-ethylpyrrolidin-2-yl)methyl)-2,3-dimethoxybenzamide	FLB 457	3.20	2.46 ± 0.04	2.43 ± 0.04	2.23 ± 0.06	2.370.11
Ethyl 8-fluoro-5-methyl-6-oxo-5,6-dihydro-4*H*-benzo[f]imidazo[1,5-*a*][1, 4]diazepine-3-carboxylate	Flumazenil or Ro 15-1788	1.29	1.16 ± 0.03	1.12 ± 0.04	0.5 ± 0.05	0.93 ± 0.31
2-fluoroethyl 1-phenethyl-4-(*N*-phenylpropionamido)piperidine-4-carboxylate	Fluoroethyl-Carfentanil hydrochloride	3.94	3.38 ± 0.03	3.36 ± 0.03	3.46 ± 0.04	3.4 ± 0.05
2-Fluoro-*N*-(2-hydroxyethyl)-*N*,*N*-dimethylethanaminium chloride	Fluoroethylcholine (FEC)	-4.11	−1.5 ± 0.04	−1.55 ± 0.04	−3.03 ± 0.06	−2.03 ± 0.76
(*R*)-2-fluoroethyl 1-(1-phenylethyl)-1*H*-imidazole-5-carboxylate	(*R*)-Fluoroethyl-Etomidate (FETO)	2.39	2.29 ± 0.31	2.26 ± 0.32	2 ± 0.42	2.18 ± 0.36
2-Fluoroethyl 8-fluoro-5-methyl-6-oxo-5,6-dihydro-4*H*-benzo[f]imidazo[1,5-*a*] [1, 4]diazepine-3-carboxylate	Fluoroethylflumazenil (FFMZ)	1.01	1.16 ± 0.04	1.13 ± 0.04	0.51 ± 0.05	0.93 ± 0.31
3-(2-Fluoroethyl)-8-(4-(4-fluorophenyl)-4-oxobutyl)-1-phenyl-1,3,8-triazaspiro[4.5]decan-4-one	Fluoroethyl-spiperone (FESP)	3.64	3.89 ± 0.07	3.88 ± 0.07	4.14 ± 0.09	3.97 ± 0.14
(6*S*,10*bR*)-6-(4-((fluoromethyl)thio)phenyl)-1,2,3,5,6,10*b*-hexahydropyrrolo[2,1-*a*]isoquinoline	(+)-Fluoromethyl-McN 5652	4.33	4.23 ± 0.04	4.22 ± 0.04	4.59 ± 0.05	4.35 ± 0.18
1-Fluoro-3-(2-nitro-1*H*-imidazol-1-yl)propan-2-ol	Fluoromisonidazole (FMISO)	-0.54	−1.06 ± 0.06	−1.11 ± 0.06	−2.45 ± 0.08	−1.54 ± 0.66
1-((2*R*,4*R*,5*R*)-4-fluoro-5-(hydroxymethyl)tetrahydrofuran-2-yl)-5-methylpyrimidine-2,4(1*H*,3*H*)-dione	3′-Fluoro-thymidine (FLT)	-0.74	−0.89 ± 0.08	−0.94 ± 0.08	−2.22 ± 0.11	−1.35 ± 0.63
2-((*S*)-(2-(dideuterofluoromethoxy)phenoxy)(phenyl)methyl)morpholine	FMeNER-D2	1.62				2.73 ± 0.01
1-(1-(4-(4-Fluorophenyl)-4-oxobutyl)piperidin-4-yl)-3-methyl-1*H*-benzo[d]imidazol-2(3*H*)-one	FNMB	3.50	3.51 ± 0.02	3.5 ± 0.02	3.64 ± 0.03	3.55 ± 0.07
3-Fluoro-5-(pyridin-2-ylethynyl)benzonitrile	FPEB Standard	2.86	3.15 ± 0.04	3.13 ± 0.04	3.16 ± 0.05	3.15 ± 0.04
(*R*)-methyl 4-(2-(3,4-dichlorophenyl)acetyl)-3-(pyrrolidin-1-ylmethyl)piperazine-1-carboxylate	GR89696 fumarate	4.17	3.04 ± 0.03	3.02 ± 0.03	3.01 ± 0.04	3.02 ± 0.04
7-Methoxy-1-methyl-9*H*-pyrido[3,4-b]indole	Harmine	3.13	3 ± 0.01	2.99 ± 0.01	2.96 ± 0.02	2.98 ± 0.02
1-methyl-9*H*-pyrido[3,4-b]indol-7-ol	Harmol	2.63	2.18 ± 0.05	2.16 ± 0.05	1.86 ± 0.07	2.07 ± 0.16
(1*R*,2*S*,3*S*,5*S*)-methyl 8-((*E*)-3-iodoallyl)-3-(4-iodophenyl)-8-azabicyclo[3.2.1]octane-2-carboxylate	IPCIT	5.49	4.76 ± 0.01	4.75 ± 0.01	5.29 ± 0.01	4.93 ± 0.27
(1*R*,2*S*,3*S*,5*S*)-8-((*E*)-3-iodoallyl)-3-(4-iodophenyl)-8-azabicyclo[3.2.1]octane-2-carboxylic acid	IPCIT acid	2.76	1.43 ± 0.04	1.41 ± 0.04	0.87 ± 0.05	1.24 ± 0.28
4-(1-Acetyl-5-(anthracen-9-yl)-4,5-dihydro-1*H*-pyrazol-3-yl)benzoic acid	MAOBI:1 acid	5.25	2.32 ± 0.01	2.3 ± 0.01	2.05 ± 0.01	2.22 ± 0.15
5-(1-Acetyl-5-(anthracen-9-yl)-4,5-dihydro-1*H*-pyrazol-3-yl)thiophene-2-carboxylic acid	MAOBI:2 acid	5.01	2.34 ± 0	2.32 ± 0	2.08 ± 0.01	2.24 ± 0.15
3-(1-Acetyl-5-(anthracen-9-yl)-4,5-dihydro-1*H*-pyrazol-3-yl)pyrazine-2-carboxylic acid	MAOBI:3 acid	3.46	1.94 ± 0	1.91 ± 0	1.54 ± 0	1.8 ± 0.22
5-(1-Acetyl-5-(anthracen-9-yl)-4,5-dihydro-1*H*-pyrazol-3-yl)furan-2-carboxylic acid	MAOBI:4 acid	4.42	1.99 ± 0.01	1.97 ± 0.01	1.62 ± 0.01	1.86 ± 0.19
6-(1-Acetyl-5-(anthracen-9-yl)-4,5-dihydro-1*H*-pyrazol-3-yl)nicotinic acid	MAOBI:5 acid	4.16	1.84 ± 0.01	1.81 ± 0.01	1.41 ± 0.01	1.69 ± 0.24
3-Amino-4-((2-((methylamino)methyl)phenyl)thio)benzonitrile	MASB	2.74	3.25 ± 0.22	3.24 ± 0.22	3.29 ± 0.29	3.26 ± 0.25
(6*S*,10*bR*)-6-(4-(methylthio)phenyl)-1,2,3,5,6,10*b*-hexahydropyrrolo[2,1-*a*]isoquinoline	(+)-McN 5652	4.16	4.22 ± 0	4.21 ± 0	4.57 ± 0.01	4.33 ± 0.17
2,3-Dimethoxyphenyl)(1-(4-fluorophenethyl)piperidin-4-yl)methanol	MDL100151	3.29	3.14 ± 0.04	3.12 ± 0.04	3.14 ± 0.05	3.13 ± 0.05
(*R*)-(2,3-dimethoxyphenyl)(1-(4-fluorophenethyl)piperidin-4-yl)methanol	MDL100907	3.29	3.11 ± 0.04	3.1 ± 0.04	3.11 ± 0.05	3.11 ± 0.04
1-(3-(Methylamino)-1-phenylpropyl)-3-phenyl-1*H*-benzo[d]imidazol-2(3*H*)-one	Me@APPI	4.73	3.14 ± 0.01	3.12 ± 0.01	3.14 ± 0.01	3.13 ± 0.01
Methyl 4-(5-(anthracen-9-yl)-1-carbamothioyl-4,5-dihydro-1*H*-pyrazol-3-yl)benzoate	Me@CarbomoiethylMAOBI:1	5.03	5.04 ± 0.02	5.04 ± 0.02	5.66 ± 0.02	5.24 ± 0.3
(*S*)-1-(3-hydroxy-4-(methylamino)butyl)-3-phenyl-1,3-dihydrobenzo[c] [1, 2, 5]thiadiazole 2,2-dioxide	Me@HAPTHI (VieNET 21)	0.73	2.62 ± 0.16	2.59 ± 0.16	2.44 ± 0.22	2.55 ± 0.19
Methyl 4-(1-acetyl-5-(anthracen-9-yl)-4,5-dihydro-1*H*-pyrazol-3-yl)benzoate	Me@MAOBI:1	5.47	4.73 ± 0	4.73 ± 0	5.26 ± 0	4.91 ± 0.31
Methyl 5-(1-acetyl-5-(anthracen-9-yl)-4,5-dihydro-1*H*-pyrazol-3-yl)thiophene-2-carboxylate	Me@MAOBI:2	5.20	4.69 ± 0	4.72 ± 0.06	5.2 ± 0	4.87 ± 0.27

Table 1 *(continued)*

IUPAC	Trivial name	ClogP	Mean ± SD $_1$HPLC log$P_{ow}^{pH7.4}$	Mean ± SD $_2$HPLC log$P_{ow}^{pH7.4}$	Mean ± SD $_3$HPLC log$P_{ow}^{pH7.4}$	Mean ± SD $_\mu$HPLC log$P_{ow}^{pH7.4}$
Methyl 3-(1-acetyl-5-(anthracen-9-yl)-4,5-dihydro-1*H*-pyrazol-3-yl)pyrazine-2-carboxylate	Me@MAOBI:3	2.69	4.08 ± 0	4.07 ± 0	4.4 ± 0.01	4.18 ± 0.15
Methyl 5-(1-acetyl-5-(anthracen-9-yl)-4,5-dihydro-1*H*-pyrazol-3-yl)furan-2-carboxylate	Me@MAOBI:4	4.65	4.15 ± 0.02	4.14 ± 0.02	4.49 ± 0.02	4.26 ± 0.18
Methyl 6-(1-acetyl-5-(anthracen-9-yl)-4,5-dihydro-1*H*-pyrazol-3-yl)nicotinate	Me@MAOBI:5	4.13	4.05 ± 0.01	4.04 ± 0.01	4.35 ± 0.01	4.15 ± 0.18
2-((*S*)-(2-methoxyphenoxy)(phenyl)methyl)morpholine	MeNER	2.73	1.74 ± 0.11	1.71 ± 0.11	1.28 ± 0.14	1.57 ± 0.24
4-(6-Methoxybenzo[d]thiazol-2-yl)aniline	6-MeO-BTA-0	3.44	4.12 ± 0.02	4.15 ± 0.08	4.5 ± 0.11	4.25 ± 0.19
N,*N*-dimethyl-1-((3*S*,4*S*)-4-(*o*-tolyloxy)isochroman-3-yl)methanamine	Me@PHOXI:1	3.81	3.16 ± 0.01	3.14 ± 0.01	3.16 ± 0.01	3.16 ± 0.013
N,*N*-dimethyl-1-((3*S*,4*S*)-4-(2-(trifluoromethyl)phenoxy) isochroman-3-yl)methanamine	Me@PHOXI:2	4.44	3.25 ± 0.01	3.23 ± 0.01	3.29 ± 0.01	3.26 ± 0.03
1-((3*S*,4*S*)-4-(2-fluoro-6-(trifluoromethyl)phenoxy) isochroman-3-yl)-*N*,*N*-dimethylmethanamine	ME@PHOXI:3	4.43	3.13 ± 0.02	3.12 ± 0.02	3.14 ± 0.02	3.13 ± 0.01
2,4-Diethyl-5-(methoxycarbonyl)-6-phenylpyridine-3-carbothioic *S*-acid	Me@SUPPY:11	3.30	5.20 ± 0.04	5.20 ± 0.04	5.89 ± 0.05	5.43 ± 0.33
4,6-Diethyl-5-((methylthio)carbonyl)-2-phenylnicotinic acid	Me@SUPPY:21	3.71	0.25 ± 0.07	0.21 ± 0.07	−0.70 ± 0.09	−0.08 ± 0.45
Methyl 4,6-diethyl-5-((methylthio)carbonyl)-2-phenylnicotinate	$(Me)^2$@SUPPY	5.33	3.71 ± 0.03	3.70 ± 0.03	3.90 ± 0.04	3.77 ± 0.10
3-((1*R*,2*S*)-2-amino-1-hydroxypropyl)phenol	Metaraminol (free base)	−0.08	n.m.			< −2.5
fff(*S*)-2-amino-4-(methylthio)butanoic acid	Methionine	−1.73	n.m.			< −2.5
(*R*)-methyl 1-(1-phenylethyl)-1*H*-imidazole-5-carboxylate	(*R*)-Metomidate hydrochloride	2.14	2.19 ± 0.04	2.16 ± 0.04	1.87 ± 0.05	2.07 ± 0.15
3-((1*R*,2*S*)-1-hydroxy-2-(methylamino)propyl)phenol	MHED hydrochloride	0.22	−1.61 ± 0.01	−1.67 ± 0.01	−3.19 ± 0.01	−2.16 ± 0.77
4-Fluoro-*N*-(2-(4-(2-methoxyphenyl)piperazin-1-yl)ethyl)-*N*-(pyridin-2-yl)benzamide	MPPF	3.49	2.86 ± 0.04	2.84 ± 0.05	2.77 ± 0.06	2.83 ± 0.06
2-((1*S*)-morpholin-2-yl(phenyl)methoxy)phenol	NER	2.26	2.05 ± 0.13	2.02 ± 0.13	1.69 ± 0.18	1.92 ± 0.22
3-(2-(1-(4-Nitrobenzoyl)piperidin-4-yl)ethyl)-2-thioxo-2,3-dihydroquinazolin-4(1*H*)-one	Nitro-Altanserin	2.42	4.51 ± 0.02	4.5 ± 0.02	4.96 ± 0.02	4.66 ± 0.23
(8*aS*,14*bR*)-7-(cyclopropylmethyl)-14-methyl-5,6,7,8,8*a*,9,14,14*b*-octahydro-4,8-methanobenzofuro[2,3-*a*]pyrido[4,3-b]carbazole-1,8*a*-diol	*N*-Methylnaltrindole	2.42	4.16 ± 0.02	4.15 ± 0.02	4.51 ± 0.02	4.28 ± 0.17
2-(4-(Methylamino)phenyl)benzo[*d*]thiazol-6-ol	6-OH-BTA-1 (free base) (PiB)	3.71	3.86 ± 0.11	3.88 ± 0.21	4.1 ± 0.14	3.94 ± 0.19
(1*R*,2*S*,3*S*,5*S*)-methyl 8-((*E*)-3-iodoallyl)-3-(p-tolyl)-8-azabicyclo[3.2.1]octane-2-carboxylate	PE2I	4.87	4.41 ± 0.07	4.4 ± 0.07	4.83 ± 0.09	4.55 ± 0.22
(1*R*,2*S*,3*S*,5*S*)-8-((*E*)-3-iodoallyl)-3-(p-tolyl)-8-azabicyclo[3.2.1]octane-2-carboxylic acid	PE2I acid	2.13	0.58 ± 0.05	0.54 ± 0.05	−0.27 ± 0.07	0.28 ± 0.4
(4*R*,4*aR*,10*bR*)-9-hydroxy-4-propyl-3,4,4*a*,5,6,10*b*-hexahydro-2*H*-naphtho[1,2-*b*] [1, 4]oxazin-4-ium	(+)-PHNO hydrochloride	2.79	2.14 ± 0.03	2.12 ± 0.03	1.81 ± 0.04	2.02 ± 0.16
N-methyl-1-((3*S*,4*S*)-4-(2-(trifluoromethyl)phenoxy) isochroman-3-yl)methanamine	PHOXI:2	3.85	2.99 ± 0	2.97 ± 0	2.94 ± 0	2.97 ± 0.02
N-(sec-butyl)-1-(2-chlorophenyl)-*N*-methylisoquinoline-3-carboxamide	(R,S)-PK11195	5.58	3.240 ± 0.010	3.23 ± 0.010	3.280 ± 0.020	3.250 ± 0.030
(*S*)-3,5-dichloro-*N*-((1-ethylpyrrolidin-2-yl)methyl)-2-hydroxy-6-methoxybenzamide	Raclopride	4.06	1.65 ± 0.03	1.62 ± 0.03	1.15 ± 0.04	1.47 ± 0.23
4-(3-(Cyclopentyloxy)-4-methoxyphenyl)pyrrolidin-2-one	Rolipram	1.72	1.84 ± 0.04	1.82 ± 0.04	1.42 ± 0.05	1.69 ± 0.2
(1-Methylpiperidin-4-yl)methyl 8-amino-7-chloro-2,3-dihydrobenzo[b] [1, 4]dioxine-5-carboxylate	SB207145	2.79	1.78 ± 0.07	1.76 ± 0.07	1.34 ± 0.1	1.62 ± 0.22
(*S*)-8-Chloro-3-methyl-5-phenyl-2,3,4,5-tetrahydro-1*H*-benzo[d]azepin-7-ol	SCH-23388 hydrochloride	3.24	4.22 ± 0.61	4.21 ± 0.62	4.59 ± 0.81	4.3 ± 0.68
(*R*)-8-chloro-3-methyl-5-phenyl-2,3,4,5-tetrahydro-1*H*-benzo[d]azepin-7-ol	SCH-23390 hydrochloride	3.24	3.12 ± 0.03	3.1 ± 0.03	3.11 ± 0.04	3.11 ± 0.03
6-(2-(4-(4-Fluorobenzoyl)piperidin-1-yl)ethyl)-7-methyl-2*H*-thiazolo[3,2-*a*]pyrimidin-5(3*H*)-one	Setoperone	1.95	2.44 ± 0.09	2.42 ± 0.09	2.21 ± 0.13	2.36 ± 0.15
3-((3-(4-(3-Acetamidophenyl)piperidin-1-yl)propyl)carbamoyl)-4-(3,4-difluorophenyl)-6-(methoxymethyl)-2-oxo-1,2,3,4-tetrahydropyrimidine-5-carboxylic acid	SNAP-acid	2.06	1.73 ± 0.01	1.71 ± 0.01	1.27 ± 0.01	1.57 ± 0.22
Methyl 3-((3-(4-(3-acetamidophenyl)piperidin-1-yl)propyl)carbamoyl)-4-(3,4-difluorophenyl)-6-(methoxymethyl)-2-oxo-1,2,3,4-tetrahydropyrimidine-5-carboxylate	(+)-SNAP-7941	4.92	3.59 ± 0.03	3.58 ± 0.03	3.75 ± 0.04	3.64 ± 0.08
Methyl 3-((3-(4-(3-acetamidophenyl)piperidin-1-yl)propyl)carbamoyl)-4-(3,4-difluorophenyl)-6-(methoxymethyl)-2-oxo-1,2,3,4-tetrahydropyrimidine-5-carboxylate	SNAP-7941	4.92	3.58 ± 0.03	3.57 ± 0.04	3.73 ± 0.05	3.63 ± 0.08
4,6-Diethyl-2-phenyl-5-thiocarboxynicotinic acid	SUPPY:0	1.92	1.82 ± 0.02	1.79 ± 0.02	1.38 ± 0.03	1.66 ± 0.2
N-(2-((4-(2-(6,7-dimethoxy-3,4-dihydroisoquinolin-2(1*H*)-yl)ethyl) phenyl)carbamoyl)-4,5-dimethoxyphenyl)quinoline-3-carboxamide	Tariquidar	5.55	4.64 ± 0.01	4.65 ± 0.04	5.16 ± 0.05	4.81 ± 0.25
(*R*)-5-((3,4-dimethoxyphenethyl)(methyl)amino)-2-(3,4-dimethoxyphenyl)-2-isopropylpentanenitrile	(+)-Verapamil hydrochloride	4.47	3.31 ± 0.04	3.3 ± 0.04	3.37 ± 0.05	3.32 ± 0.06
(*S*)-1-(4-amino-3-hydroxybutyl)-3-phenyl-1,3-dihydrobenzo[*c*] [1, 2, 5]thiadiazole 2,2-dioxide	Vie-NET-20	0.32	2.51 ± 0	2.49 ± 0	2.3 ± 0.01	2.43 ± 0.1
N-(2-(4-(2-methoxyphenyl)piperazin-1-yl)ethyl)-*N*-(pyridin-2-yl)	carbonyl-WAY-100635	4.09	2.91 ± 0.01	2.89 ± 0.01	2.83 ± 0.01	2.88 ± 0.03

(continued on next page)

Table 1 *(continued)*

IUPAC	Trivial name	Clog*P*	Mean ± SD $_1$HPLC log$P_{ow}^{pH7.4}$	Mean ± SD $_2$HPLC log$P_{ow}^{pH7.4}$	Mean ± SD $_3$HPLC log$P_{ow}^{pH7.4}$	Mean ± SD $_\mu$HPLC log$P_{ow}^{pH7.4}$
cyclohexanecarboxamide						
N,*N*-bis(2-hydroxyethyl)-10-(2-methyl-2′-(trifluoromethyl)-[1,1′-biphenyl]-4-carbonyl)-10,11-dihydro-5*H*-benzo[e]pyrrolo[1,2-*a*][1, 4]diazepine-3-carboxamide	WAY-162720 (compound 6)	4.02	3.2 ± 0.01	3.19 ± 0.01	3.23 ± 0.01	3.21 ± 0.02
10-(5′-Fluoro-2-methyl-2′-(trifluoromethyl)-[1,1′-biphenyl]-4-carbonyl)-*N*,*N*-bis(2-hydroxyethyl)-10,11-dihydro-5*H*-benzo[e]pyrrolo[1,2-*a*][1, 4]diazepine-3-carboxamide	6a	5.32	3.3 ± 0.01	3.28 ± 0.01	3.35 ± 0.01	3.31 ± 0.04
10-(2′-(Fluoromethyl)-2-methyl-[1,1′-biphenyl]-4-carbonyl)-N,*N*-bis (2-hydroxyethyl)-10,11-dihydro-5H-benzo[e]pyrrolo[1,2-*a*][1, 4]diazepine-3-carboxamide	6b	2.94	3.15 ± 0	3.13 ± 0	3.15 ± 0.01	3.14 ± 0.001
N-(2-fluoroethyl)-*N*-(2-hydroxyethyl)-10-(2-methyl-2′-(trifluoromethyl)-[1,1′-biphenyl]-4-carbonyl)-10,11-dihydro-5*H*-benzo[e]pyrrolo[1,2-*a*][1, 4]diazepine-3-carboxamide	6c	4.57	4.72 ± 0	4.71 ± 0	5.24 ± 0	4.89 ± 0.3
N-(2-fluoroethyl)-10-(2-methyl-2′-(trifluoromethyl)-[1,1′-biphenyl]-4-carbonyl)-10,11-dihydro-5H-benzo[e]pyrrolo[1,2-*a*][1, 4]diazepine-3-carboxamide	6d	5.40	4.08 ± 0	4.07 ± 0	4.39 ± 0.01	4.18 ± 0.18
(5-Fluoro-4′-(3-((2-(methoxymethoxy)ethyl)((methoxymethoxy) methyl)carbamoyl)-10,11-dihydro-5*H*-benzo[e]pyrrolo[1,2-*a*] [1, 4] diazepine-10-carbonyl)-2′-methyl-[1,1′-biphenyl]-2-yl)methyl 4-methylbenzenesulfonate	6e	5.85	4.99 ± 0.43	4.99 ± 0.43	5.61 ± 0.57	5.20 ± 0.36
0-(2′-(Fluoromethyl)-2-methyl-[1,1′-biphenyl]-4-carbonyl)-*N*,*N*-bis (2-hydroxyethyl)-10,11-dihydro-5*H*-benzo[e]pyrrolo[1,2-*a*][1, 4]diazepine-3-carboxamide	6f	2.94	3.99 ± 0.00	3.98 ± 0.00	4.27 ± 0.00	4.08 ± 0.16

This table presents the Clog*P* values and the HPLC values of all tested molecules. In the first column, the nomenclature according to IUPAC and in column 2, the short name is given. The calculated log*P* values are given in column 3. The results of the HPLC log*P* measurements are illustrated in columns 4, 5 and 6 ($_{1,2\&\ 3}$HPLC log$P_{ow}^{pH7.4}$) according to different published log*P* values of the internal standards of toluene and triphenylene, which are used to calculate with Equation 1. The mean values, $_\mu$HPLC log$P_{ow}^{pH7.4}$, are given in column 7. Values represent mean ± standard deviation ($n \geq 3$).

Austria. Information of structure, target and product number is given in the supplementary data (cf. Supplementary material).

2.3. HPLC-log$P_{ow}^{pH7.4}$ measurements

The lipophilicity measurements were performed according to the method of Donovan and Pescatore [8]. The diode array detector was set to the optimum absorption maximum according to the analytes and standards absorbance spectrum. The injection volume was 3 μL for each reference of a 100–500 μg/mL standard dissolved in the internal standard mixture, containing 0.1 mg/mL triphenylene and 0.01 mg/mL toluene. The mobile phase consisted of a mixture of methanol and 0.01 M sodium phosphate buffer pH 7.4 using a gradient elution. The gradient program started with 10% methanol and 90% sodium phosphate buffer up to 100% methanol in 9.4 min with a flow rate of 1.5 mL/min and finished with initial conditions after 12 min. An equilibration time of 3 min restored the initial condition of the column. The log*P* values of the standards toluene and triphenylene were obtained from literature [8,13]. The HPLC log$P_{ow}^{pH7.4}$ was calculated based on Equation 1 by setting the measured retention time of the analyte in relation to the known log*P* values and the measured retention times of the internal standards toluene and triphenylene. The log*P* values for toluene and triphenylene were taken from a database, the average found in the literature and another HPLC method. This is resulting in three different log*P* values and a mean value (cf. Table 1). For radiolabeled compounds, a correction of time interval between UV-detector and the downstream connected radio-detector was calculated and corrected for each analyte.

$$\log\left(\frac{CPM\ octanolPhase}{CPM\ waterPhase}\right) = logP$$

Equation 2. Partition Coefficient of a compound in two immiscible phases. The calculation for the logarithmized partition coefficient of a compound in two immiscible phases (log*P*) is shown. Therefore, an aliquot of each phase is counted and CPMs (counts per minute) are corrected for volume and decay.

2.4. Calculated logP (ClogP)

Calculated log*P* (Clog*P*) values were derived from ChemBioDraw (CBD) Software Version 12.0.2, Level Ultra© 1986–2010 CambridgeSoft, PerkinElmer, Waltham, USA.

2.5. Shake-tube or -flask experiments

Shake-tube methods followed a slightly adapted standard protocol [4]. Determination of partition coefficient (P) of radiolabeled compounds [^{18}F]FE@SUPPY, [^{18}F]FET, [^{11}C]Harmine, [^{11}C]DASB, [carbonyl-^{11}C]WAY100635 and the precursor Harmol was performed in 3 mL 1-octanol and 3 mL phosphate buffered saline pH 7.4 in a 12 mL tube or in a 10 mL to 10 mL ratio in a separatory funnel. The two phases were pre-saturated and the tracers were added with respect to activity linearity range (limit of detection) of the used gamma-counter and automatically shaken on a cycling plate shaker device. After separation of the two phases (20 min resting time or centrifugation, 5 min and 3000 rpm), an additional number of distribution of the tracer was performed, in which either the 1-octanol phase was added to fresh PBS or fresh PBS was added to the separatory funnel after removing the first PBS phase. The shaking and separation procedure was repeated. From each phase, aliquots of 200 μL to 1000 μL were pipetted into preweighed tubes. The weighed tubes were counted and the CPM was corrected for volume and decay. The log*P* was calculated using Equation 2.

3. Results

3.1. HPLClog$P_{ow}^{pH7.4}$ and ClogP

Results of the HPLC log*P* measurements are presented in Table 1. The log*P* values range from −1.56 to 5.20 for $_1$HPLC log$P_{ow}^{pH7.4}$, −1.61 to 5.20 for $_2$HPLC log$P_{ow}^{pH7.4}$, and −3.13 to 5.89 for $_3$HPLC log$P_{ow}^{pH7.4}$. Mean values ranged from −2.1 to 5.43 ($_\mu$HPLC log$P_{ow}^{pH7.4}$)$_3$. ABP688 was the only

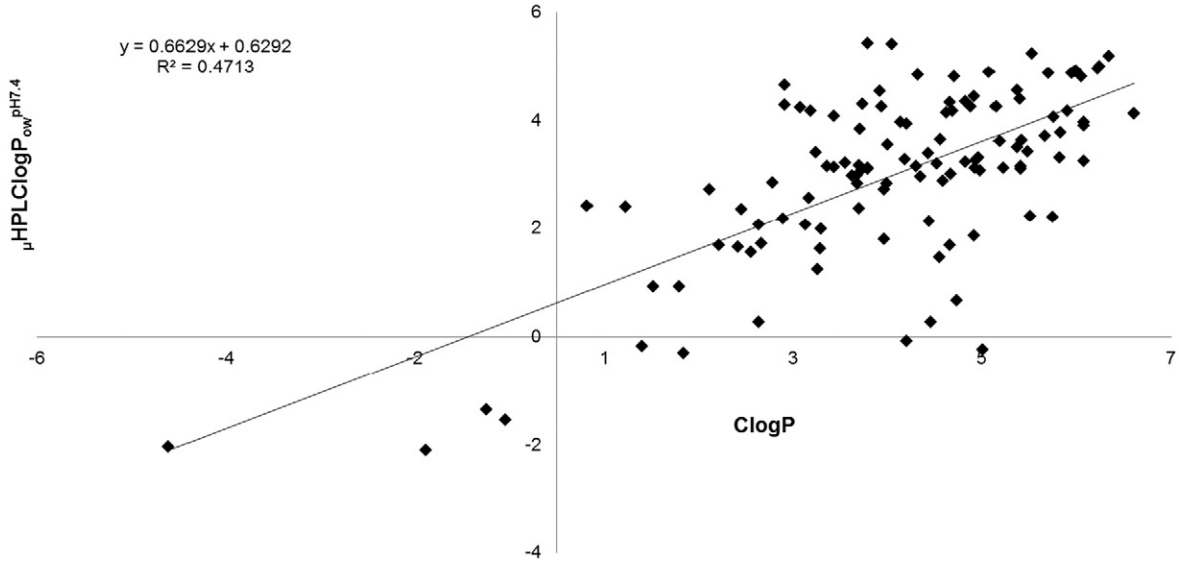

Fig. 1. Correlation between log*P* mean of HPLC measurements and the calculated log*P* value. This figure shows the poor correlation of the mean value of HPLC log*P* ($_{\mu}$HPLC $\log P_{ow}^{pH7.4}$) measurements and the calculated log*P* (Clog*P*) values of the results shown in Table 1. For illustrational reasons a trend line was set.

substance of the whole set showing a double peak. In the case of DOPA, metaraminol and methionine no retention was observed. Based on the fact that three different log*P* values are available in the literature for the internal standards (toluene and triphenylene), results are presented in four columns: $_1$HPLClog$P_{ow}^{pH7.4}$, $_2$HPLClog$P_{ow}^{pH7.4}$, $_3$HPLClog$P_{ow}^{pH7.4}$ and mean value of 1–3 presented as $_{\mu}$HPLC log$P_{ow}^{pH7.4}$. $_{\mu}$HPLC log$P_{ow}^{pH7.4}$ values of oxytocin receptor ligands, NET ligands, IPCIT derivatives and MCHR1 antagonist were previously published or equivalent results were found using the same HPLC method [14–18]. Additionally, the calculated log*P* (Clog) values for each compound are given. Clog*P* values ranged from −4.11 for FEC hydrochloride to 6.12 for FE@SUPPY and FE@SUPPY:2. Clog*P* values and HPLClog$P_{ow}^{pH7.4}$ values are correlated in Fig. 1.

There was no deviation between log*P* values of labeled and the same non-labeled analytes in the case of the radionuclides fluorine-18 and carbon-11 (Fig. 2).

3.2. Shake-flask and shake-tube logP

Results of the shake-flask measurements are presented in Fig. 3 and compared to results of HPLC log*P* measurements and the calculated log*P* values.

4. Discussion

4.1. General

Although lipophilicity and log*P* are well-established parameters for the physicochemical characterization of molecules, there is still controversy regarding the translational importance of this value. The first publication dates back more than 140 years [3]. In recent decades, log*P* received more recognition as a predictive value for pharmacodynamic

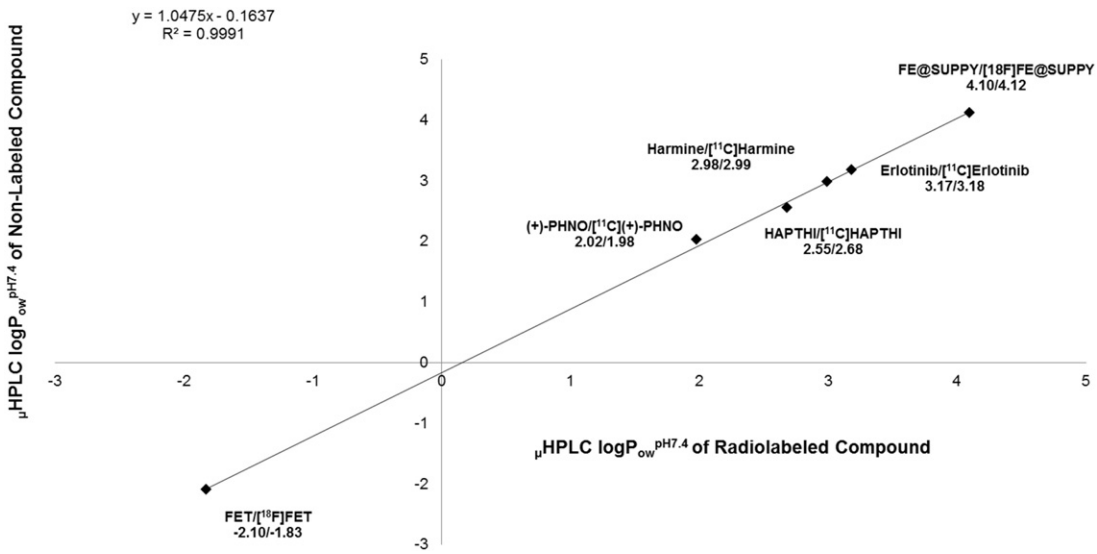

Fig. 2. Correlation between log*P* mean of HPLC measurements of the radiolabeled vs. non-radiolabeled compounds. The correlation between the same compound radiolabeled ([^{11}C] Erlotinib, [^{18}F]FET, [^{11}C]Me@HAPTHI, [^{11}C]Harmine, [^{18}F]FE@SUPPY and [^{11}C]PHNO) or non-radiolabeled (Erlotinib, FET, Me@HAPTHI, Harmine, FE@SUPPY and (+)PHNO) using the HPLC method shows no differences as illustrated with R^2 of almost 1. Individual $_{\mu}$HPLC log$P_{ow}^{pH7.4}$ results and the compound name are given beside the marks.

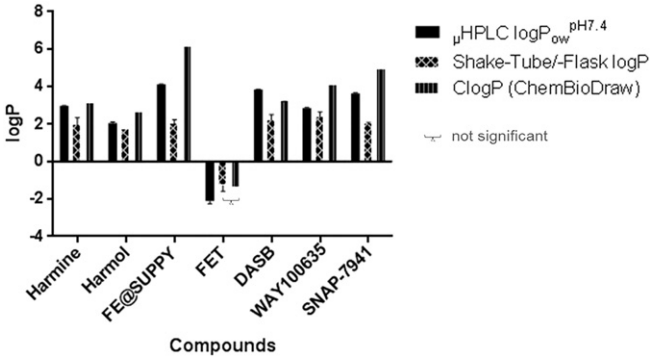

Fig. 3. Comparison of log*P* values from different methods. The graphic shows the log*P* values from different methods of the reference compounds Hamine, Harmol, FE@SUPPY, FET, DASB, WAY100635 and SNAP-7941. The multiple t-tests, corrected for multiple comparisons using the Holm–Sidak method, showed a significant difference between the log*P* values using the same compound with HPLC-, Shake-Tube/-Flask or calculated log*P* method ($\alpha < 0.05$). Significant differences in the log*P* values were found for Harmine, FE@SUPPY, DASB, WAY100635 and SNAP-7941 comparing HPLC $\log P_{ow}^{pH7.4}$, Shake-Tube/-Flask (pH 7.4) and Clog*P* with each other. For Harmol the log*P* values of the Clog*P* were significantly different from HPLC $\log P_{ow}^{pH7.4}$ as well as shake-flask to HPLC $\log P_{ow}^{pH7.4}$, but shake-flask (pH 7.4) versus Clog*P* could not be calculated. The HPLC $\log P_{ow}^{pH7.4}$ value of FET shows a significant difference from shake-flask (pH 7.4) log*P* and Clog*P*, but no significant difference was found comparing shake-tube/-flask (pH 7.4) log*P* and Clog*P* to each other.

properties, passive membrane diffusion and plasma protein binding. After "Lipinski's rule of five", the first milestone for early stratification of candidate molecules in drug development (n.b.: for peroral administration), various adoptions were published. For central applications, suggested log*P* thresholds differ significantly: 1 to 3.5, 2 to 3.5, 2 to 5, <5, <3 [10,11,19–23]. Although most of these authors predict blood brain barrier (BBB) permeation with a rule of five (Ro5), the log*P* value is considered to be the most crucial factor. Therefore, a huge number of publications, describing newly developed brain tracers or pharmaceuticals, base their prediction of BBB penetration exclusively on the log*P* (calculated or measured).

In the development process of radiopharmaceuticals, log*P* is also considered important, since high levels contribute to high unspecific binding. In contrast, low lipophilicity minimizes the ability of the tracer for free membrane diffusion. However, the question remains: what the appropriate threshold to predict BBB penetration a priori might be? A correct answer to this question is critical, since a large variety of methods with a wide range of log*P* outcomes is available. As an example, DASB, an established brain tracer for imaging the serotonin transporter, showed four different log*P* values: 1.9 [24], 2.4 [25], 3.0 [26], 1.9 and 3.2 [27]. We observed 3.84 ± 0.11 based on HPLC measurements, 1.7, and 2.1 in shake-flask experiments or 3.2 as calculated Clog*P*. This is a 145-fold range in lipophilicity.

As the poor correlations between the log*P* values of different methods show (cf. Fig. 3): log*P* data from different methods are not comparable. To this end, a classification into a threshold without precise reference to the used method is incorrect. Therefore, all log*P* or log*D* measurements are not indicative without a database to compare results of the same method.

4.2. LogP and blood brain barrier

The literature dealing with log*P* and BBB penetration is contradictory [11,19,28–31]. In total, 121 substances were tested. 57 are reference standards which are known to penetrate the BBB. Five of them are transported actively through the BBB and 52 via passive diffusion. Six of these 52 PET tracers interact with efflux transporters or are used to image the efflux transporter at the BBB. 54 of the tested compounds have unknown BBB penetration. Ten of the tested compounds do not show any clinically relevant brain uptake (unknown reason). The log*P* values of the actively transported reference standards FEC, FET and FLT had lower HPLC log*P* values (−2 to −1.4) than those diffusing passively. Methionine and DOPA, which are also transported actively, show no retention on the selected HPLC system at all (log*P* value of less than −2). FMISO (log*P* of −1.5) and beta-CFT (log*P* of −0.2) are exceptions to the widely accepted rule that only highly lipophilic compounds penetrate the BBB by passive diffusion. As mentioned earlier, a variety of log*P* ranges are given in the literature for the prediction of BBB penetration [11,19–21,23,32,33]. Based on our $_{\mu}$HPLC $\log P_{ow}^{pH7.4}$ data, the range would be −1.5 to 4.6. According to our Clog*P* results the threshold would range between −0.55 and 5.6. For example, for the log*P* threshold of 2–3.5, only 29 out of 53 compounds would classify as CNS positive (cf. Fig. 4A). In the case of the Clog*P*, only 23 compounds of the 52 would have been CNS penetrating (Fig. 4A and B). On the other hand, extending the prediction thresholds to our range of log*P* (−1.5 to 4.6), that would result in a high number of false positive decisions concerning the BBB penetration. Almost all CNS negative drugs would be classified as optimal for cerebral application as well as precursors and metabolites of compounds which are unlikely to penetrate.

4.3. HPLC logP

The HPLC log*P* measurements were performed with 57 well-established radioligands. In addition, we evaluated 54 experimental molecules: SUPPY-, Oxytocin-, MAOBI-, SNAP-, HAPTHI- and IPCIT derivatives, which are in different phases of preclinical evaluation at our department or cooperation partners. All details are given in Table 1. A total number of 121 compounds were tested with a wide panoply of chemical substance classes.

This robust HPLC method is suitable for a broad range from −2 (FET) to highly lipophilic compounds up to a log*P* of 6. The molecule with the highest lipophilicity was Me@SUPPY:11 (log*P* 5.4). This measured range is in line with the OECD (Organization for Economic Co-operation and Development) criteria and has no disadvantage against other methods (e.g., shake-flask or other HPLC methods) [5]. A limitation of the method is given for rather hydrophilic compounds (<−2.2), eluting with the front. The measurements can be performed both, with standards and radiolabeled substances (cf. Fig. 2). Compounds which could not be measured are labeled as not measurable in Table 1 (n.m.).

4.4. Calculated logP vs. HPLC $\log P_{ow}^{pH7.4}$

Lipophilicity measurements are frequently carried out using computational methods assuming that all experimental methods are cost and time consuming. However, there are significant deviations between the calculated and measured log*P* (Fig. 1). Furthermore, the Clog*P* is incalculable, when the structure of the molecule is complex (e.g., metal complexes, [5,7,9,34]). The calculated values range from −4.1 to 6.1, providing a broader range than HPLC log*P*.

4.5. Shake tube vs. HPLC $\log P_{ow}^{pH7.4}$

Seven radiolabeled tracers were tested using the "gold standard" shake-tube or shake-flask method. Comparing the measurable ranges of the HPLC method with shake-flask method, a broader range can be evaluated with the HPLC (−2 to 6) compared to −2 to 4; according to OECD (Organization for Economic Co-operation and Development) criteria [5]. Additionally, the traditional shake-flask method shows considerable inaccuracies: interactions of impurities (such as by-products from syntheses, instabilities or metabolites) of the measured compound are observed, pK_a differences can hamper analysis, highly hydrophilic compounds in the 1-octonal phase could be limiting (limit of detection). Wilson et al. [4] calculated, that 0.1% hydrophilic impurity results in a tenfold underestimation of the lipophilicity (e.g., log*P* of 3 instead of log*P* of 4).

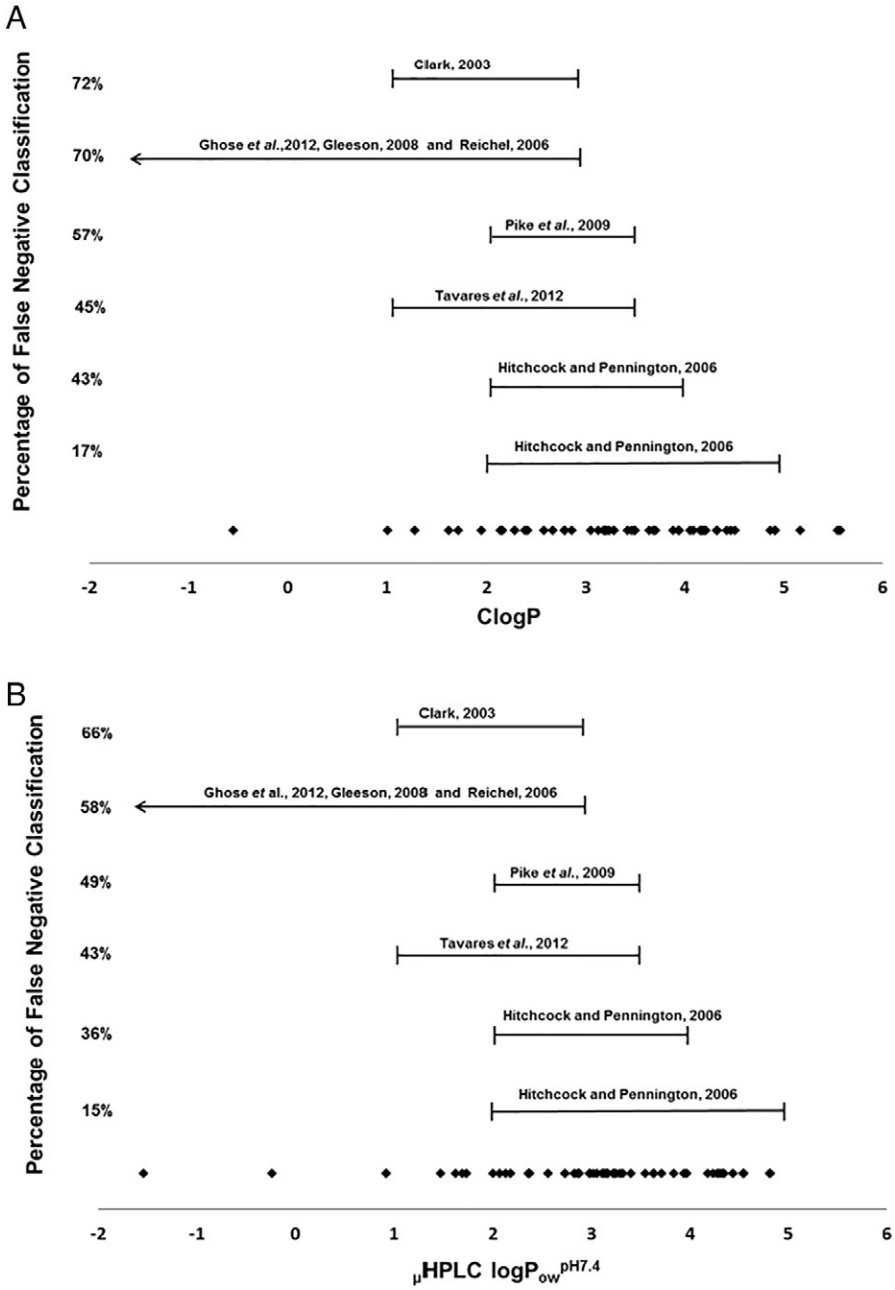

Fig. 4. (A and B) Suggested log*P* ranges for optimal blood brain barrier penetration and correlation to PET brain tracers. The figure shows the relation of the Clog*P* and $_{\mu}$HPLC $\log P_{ow}^{pH7.4}$ concerning their power to predict the blood brain barrier (BBB) penetration according to different thresholds from literature supposed to be optimal for passive diffusion through the BBB. The crossbars and arrows represent the suggested or preferred log*P* thresholds according to the literature: Clark et al. 1–3.5, Ghose et al. (2012), Gleeson (2008) and Reichel (2006) smaller than 3, Pike et al. (2009) 2–3.5, Tavares et al. (2012) 1–3.5, Hitchcock and Pennington (2006) preferred log*P* threshold 2–4 and suggested log*P* threshold 2–5. The marks represent the 52 tested compounds (PET tracers), which are known to penetrate the BBB by passive diffusion. The marks (compounds) are plotted against the $_{\mu}$HPLC $\log P_{ow}^{pH7.4}$ or the Clog*P*, respectively. The false negative classifications are given in percentage.

5. Conclusion

We provide a comprehensive database comprising several lipophilicity values for commonly used PET tracers (I). A simple, quick, versatile and inexpensive HPLC method for the optimal measurement of log*P* values of radiotracers was used and compared to Clog*P* and shake-flask methods, thereby showing a significant discrepancy between the different methods (II). Hence, based on the present evaluation, a prediction of BBB penetration relying solely on lipophilicity values is inappropriate (III).

Abbreviations

P	partition coefficient
D	distribution coefficient
Clog*P*	calculated log*P*
log*P*	partition-coefficient of an un-ionized compound in two immiscible phases (*n*-octanol and water/buffer) at equilibrium

log*D*	distribution of all species (un-ionized and ionized solutes) in two immiscible phases (*n*-octanol and water/buffer at equilibrium
MCHR1	melanin concentrating hormone receptor 1
NET	norepinephrine transporter
n.m.	not measurable
OECD	Organization for Economic Co-operation and Development
ODP	octadecyl-poly(vinyl alcohol)
PET	positron emission tomography
Rt	retention time
t_0	HPLC systems dead time

Supplementary data to this article can be found online at http://dx.doi.org/10.1016/j.nucmedbio.2017.03.003.

Acknowledgments

The authors thank Cecile Philippe, Theresa Balber and Neydher Berroteran for the production of radiolabeled compounds and their support. Eva-Maria Klebermass and Katharina Rebhan are acknowledged for their support in shake-tube experiments as well as Volker Weiss for his contribution in HPLC measurements. This work was supported by the Austrian Science Fund (FWF P26502-B24, M. Mitterhauser).

References

[1] Berthod A, Carda-Broch S. Determination of liquid-liquid partition coefficients by separation methods. J Chromatogr A 2004;1037:3–14.
[2] Rubas W, Cromwell M. The effect of chemical modifications on octanol/water partition (log *D*) and permeabilities across Caco-2 monolayers. Adv Drug Deliv Rev 1997; 23:157–62.
[3] Leo A, Hansch C, Elkins D. Partition coefficients and their uses. Chem Rev 1971;71:525–616.
[4] Wilson AA, Jin L, Garcia A, DaSilva JN, Houle S. An admonition when measuring the lipophilicity of radiotracers using counting techniques. Appl Radiat Isot 2001;54:203–8 [d].
[5] OECD. OECD guidelines for the testing of chemicals[Paris] ; 1993.
[6] Nic M, Jirat J, Kosata B. International Union of Pure and Applied Chemistry Compendium of Chemical Terminology Gold Book—version 2.3.3. Oxford: Blackwell Scientific Publications; 2014 849.
[7] Leo A, Jow PYC, Vittoria A, Hansch C. The fragment approach. J Med Chem 1975;18:865–8.
[8] Donovan SF, Pescatore MC. Method for measuring the logarithm of the octanol–water partition coefficient by using short octadecyl-poly(vinyl alcohol) high-performance liquid chromatography columns. J Chromatogr A 2002;952:47–61.
[9] Kowol CR, Miklos W, Pfaff S, Hager S, Kallus S, Pelivan K, et al. Impact of stepwise NH $_2$-methylation of triapine on the physicochemical properties, anticancer activity, and resistance circumvention. J Med Chem 2016;59:6739–52.
[10] Lipinski CA. Lead- and drug-like compounds: the rule-of-five revolution. Drug Discov Today Technol 2004;1:337–41.
[11] Pike VW. PET radiotracers: crossing the blood–brain barrier and surviving metabolism. Trends Pharmacol Sci 2009;30:431–40.
[12] Waterhouse RN. Determination of lipophilicity and its use as a predictor of blood–brain barrier penetration of molecular imaging agents. Mol Imaging Biol 2003;5: 376–89.
[13] Tomlin CDS, British Crop Protection Council. The pesticide manual: a world compendium. Farnham (Surrey): British Crop Protection Council; 2000.
[14] Rami-Mark C, Bornatowicz B, Fink C, Otter P, Ungersboeck J, Vraka C, et al. Synthesis, radiosynthesis and first in vitro evaluation of novel PET-tracers for the dopamine transporter: [11C]IPCIT and [18F]FE@IPCIT. Bioorg Med Chem 2013;21:7562–9.
[15] Rami-Mark C, Berroterán-Infante N, Philippe C, Foltin S, Vraka C, Hoepping A, et al. Radiosynthesis and first preclinical evaluation of the novel norepinephrine transporter PET-ligand [(11)C]ME@HAPTHI. EJNMMI Res 2015;5:34.
[16] Philippe C. Preparation and first preclinical evaluation of [18F]FE@SNAP: a potential PET tracer for the melanin concentrating hormone receptor 1 (MCHR1). Sci Pharm 2013;81:625–39. http://dx.doi.org/10.3797/scipharm.1306-02.
[17] Philippe C, Nics L, Zeilinger M, Kuntner C, Wanek T, Mairinger S, et al. Preclinical in vitro and in vivo evaluation of [11C]SNAP-7941—the first PET tracer for the melanin concentrating hormone receptor 1. Nucl Med Biol 2013;40:919–25.
[18] Wenzel B, Mollitor J, Deuther-Conrad W, Dukic-Stefanovic S, Kranz M, Vraka C, et al. Development of a novel nonpeptidic (18)F-labeled radiotracer for in vivo imaging of oxytocin receptors with positron emission tomography. J Med Chem 2016;59: 1800–17.
[19] Tavares AAS, Lewsey J, Dewar D, Pimlott SL. Radiotracer properties determined by high performance liquid chromatography: a potential tool for brain radiotracer discovery. Nucl Med Biol 2012;39:127–35.
[20] Reichel A. The role of blood–brain barrier studies in the pharmaceutical industry. Curr Drug Metab 2006;7:183–203.
[21] Hitchcock SA, Pennington LD. Structure—brain exposure relationships. J Med Chem 2006;49:7559–83.
[22] Pajouhesh H, Lenz GR. Medicinal chemical properties of successful central nervous system drugs. NeuroRx 2005;2:541–53.
[23] Ghose AK, Herbertz T, Hudkins RL, Dorsey BD, Mallamo JP. Knowledge-based, central nervous system (CNS) lead selection and lead optimization for CNS drug discovery. ACS Chem Nerosci 2012;3:50–68.
[24] Wilson AA, Ginovart N, Schmidt M, Meyer JH, Threlkeld PG, Houle S. Novel radiotracers for imaging the serotonin transporter by positron emission tomography: synthesis, radiosynthesis, and in vitro and ex vivo evaluation of ^{11} C-labeled 2-(phenylthio)araalkylamines. J Med Chem 2000;43:3103–10.
[25] Huang Y, Hwang D-R, Narendran R, Sudo Y, Chatterjee R, Bae S-A, et al. Comparative evaluation in nonhuman primates of five PET radiotracers for imaging the serotonin transporters: [11C]McN 5652, [11C]ADAM, [11C]DASB, [11C]DAPA, and [11C]AFM. J Cereb Blood Flow Metab 2002;22:1377–98.
[26] Small Animal Imaging Resource Programm. John Hopkins Medicine. http://pomper.sairp.rad.jhmi.edu/Private/Tracers/DASB/DASB.html. [accessed June 9, 2016].
[27] ChemSpider. Search and share chemistry. ACD properties. http://www.chemspider.com/Chemical-Structure.8621986.html. [accessed June 14, 2016].
[28] De Vrieze M, Lynen F, Chen K, Szucs R, Sandra P. Predicting drug penetration across the blood–brain barrier: comparison of micellar liquid chromatography and immobilized artificial membrane liquid chromatography. Anal Bioanal Chem 2013; 405:6029–41.
[29] Vrakas D, Giaginis C, Tsantili-Kakoulidou A. Different retention behavior of structurally diverse basic and neutral drugs in immobilized artificial membrane and reversed-phase high performance liquid chromatography: comparison with octanol–water partitioning. J Chromatogr A 2006:158–64.
[30] Giaginis C, Tsantili-Kakoulidou A. Alternative measures of lipophilicity: from octanol–water partitioning to IAM retention. J Pharm Sci 2008;97:2984–3004.
[31] Abraham MH, Acree WE, Fahr A, Liu X. Analysis of immobilized artificial membrane retention factors for both neutral and ionic species. J Chromatogr A 2013;1298:44–9.
[32] Gleeson MP. Generation of a set of simple, interpretable ADMET rules of thumb. J Med Chem 2008;51:817–34.
[33] Clark DE. In silico prediction of blood–brain barrier permeation. Drug Discov Today 2003;8:927–33.
[34] Rekker RF, de Kort HM. The hydrophobic fragment constant. Eur J Med Chem 1979; 14:479–88.

3.1.2 Manuscript II

Vraka C and Mitterhauser M “Reconsider LogP!” Nucl Med 2017;54:p42

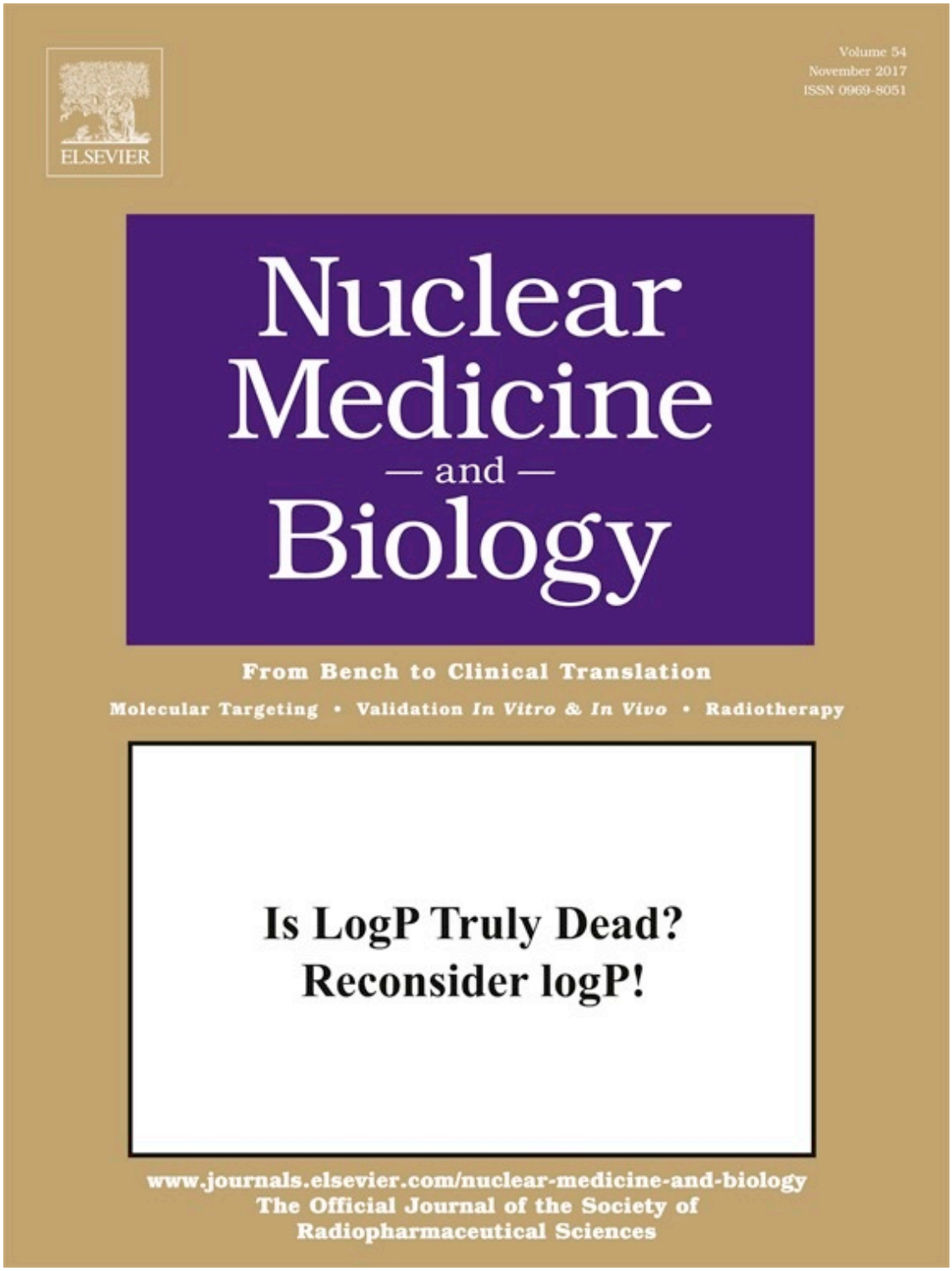

Nuclear Medicine and Biology 54 (2017) 41–42

Contents lists available at ScienceDirect

Nuclear Medicine and Biology

journal homepage: www.elsevier.com/locate/nucmedbio

Is logP truly dead?

More than 100 years ago, the importance of lipophilicity to the passive permeability of molecules through the blood brain barrier was recognized. In the intervening decades, various methods to measure the lipid nature of molecules were developed; with an ever-expanding database on molecule structures and measured physiochemical properties, computational methods for estimation of lipophilicity followed. Today, the simple estimate of lipophilicity known as the logP value (in its original definition, the logarithm of the distribution ratio for a molecule between immiscible organic and aqueous layers) is routinely used in drug design, including radiopharmaceuticals.

In a recent article in this journal entitled "LogP, a yesterday's value?" Vraka and coworkers [1] reported an extensive study comparing calculated and experimental logP values for 121 molecules identical to, or structurally related to, radiopharmaceuticals proposed for in vivo brain imaging studies. There was a poor correlation between cLogP values calculated by a widely available software program (ChemBioDraw) and experimental values they determined using multiple HPLC methods. That was a valid and not very surprising observation. The authors did not, however, actually determine the BBB permeability of any of the listed compounds. The conclusion of their paper that "The logP determination for prediction of BBB is obsolete" and "inappropriate" was a very bold assertion, particularly in view of the many years of use of logP values in CNS drug design and the many thousands of published papers reporting such values.

Are logP values "obsolete" and "inappropriate"? For uptake into the central nervous system, the role of other physiochemical factors (e.g., topological polar surface area (TPSA), number of hydrogen bond donors and acceptors, and molecular size and shape) and biochemical processes (e.g., plasma protein binding, active transport into or out of the CNS) has been recognized by many as important to the understanding of the passage of molecules from the plasma to the brain. It is highly likely that knowledgeable radiopharmaceutical chemists (and medicinal chemists) would not today base their selections of candidate compounds solely on calculated logP values, or for that matter on molecular polar surface area, a calculated value that has shown a very good inverse linear relationship with experimental brain penetration [3]. The development of radiotracers to study biochemistry of the brain remains challenging, with adequate BBB permeability one of many critical requirements. In our opinion, Vraka and coworkers miss the more important question: *are measures (or calculations) of molecular lipophilicity of use for predicting success of novel brain imaging radiotracers?*

The wide range of logP values for CNS radiotracers currently in human use (and a similar wide range for marketed drugs) supports the conclusion that lipophilicity is not the most crucial factor for defining BBB permeability. But are calculated or experimental estimates of lipophilicity (logP or logD) useful for predicting "success" of CNS radiopharmaceuticals? For brain imaging agents, we talk about "specific binding" and "nonspecific binding", or "bound" and "free + nonspecific" proportions of radiotracer distributions. As in vivo imaging methods such as PET are inherently incapable of differentiating between molecules in these two compartments, the goal of radiotracer design is often to maximize the ratio between the two conditions. So instead of asking if logP values are useful in predicting brain uptake, the more interesting question is whether estimates of lipophilicity are useful for predicting the in vivo ratio of specific to non-specific binding for CNS radiopharmaceuticals. The brain is a fatty tissue (10.7% fat, 7.9% protein, 79% water [2]) and in animal models, cLogP values are inversely proportional to drug free fraction in the brain [4,5]. From a simple perspective, one would expect that radiotracers with a high logP would exhibit higher non-specific binding, and every radiopharmaceutical chemist can likely find in their experience examples of poorly performing radiotracers with higher logP and good radiotracers with lower logP. Taking a retrospective look at our personal history with novel CNS radiotracers, we found poor human in vivo imaging results for [^{18}F]GBR12909 (cLogP = 5.3) and excellent performance with [^{11}C]dihydrotetrabenazine (cLogP = 2.1).

Several investigators have attempted to relate physiochemical characteristics to in vivo non-specific distribution of radiotracers, with the goal of better prediction of "successful" radiotracers in the future. Zhang et al [6] proposed a multiparameter optimization tool (CNS MPO) which included cLogP and clogD, and demonstrated they could correctly identify a set of "high-performing" PET radiotracers. Asmus et al [7] developed an in vitro assay suitable for measures of brain tissue/water distribution coefficients ($logD_{brain}$) and demonstrated, using several common PET radiotracers, a good correlation of those values with estimates of non-specific binding from PET studies. Finally, Friden et al [8] used a combination of in vitro estimates of non-specific binding (using a high-throughput brain slice assay), target concentration and binding affinities to predict the fraction of in vivo target-bound radiotracer (f_{tb}), and then used an arbitrary cut-off value to achieve a reasonable but not perfect discrimination between what they term as "functional" and "nonfunctional" PET radiotracers. However, for 34 "functional" radioligands there was a poor correlation ($R^2 = 0.06$) between their in vitro estimate of f_{tb} and values derived from human PET data (where $f_{tb} = (BP_{ND}/1 + BP_{ND})$). To be fair, there was also no correlation ($R^2 = 0.01$) between cLogP and PET-derived f_{tb} values.

These studies that attempt to identify necessary CNS radiotracer properties, together with the far larger literature in the field of therapeutic drug design [9,10], support a conclusion that lipophilicity can be considered a useful component but no single biological or physiochemical parameter will successfully predict a useful radiotracer for PET imaging in the human brain. Of course, defining radiotracers as "high-performing", "functional" or "successful" is in itself a controversial subject that won't be addressed here. Developing CNS radiotracers remains complex [11], and in our continuing efforts to construct molecules with the appropriate characteristics, we need to utilize all available "tools" in our toolbox. Brain uptake is important and lipophilicity is not the only physiochemical or biological descriptor that defines either BBB permeability or non-specific binding, but the study of Vraka et al [1] does not conclusively make logP values "obsolete" and "inappropriate" for inclusion in our radiotracer design efforts. Viva logP!

Michael R. Kilbourn*
Peter J.H. Scott
Department of Radiology, University of Michigan Medical School, Ann Arbor, MI 48109

*Corresponding author
E-mail address: mkilbour@umich.edu

http://dx.doi.org/10.1016/j.nucmedbio.2017.08.006

References

[1] Vraka C., Nics L., Wagner K.-H., Hacker M., Wadsak W., Mitterhauser M.. Log P, a yesterday's value? Nucl Med Biol 2017;50:1–10.
[2] Summerfield S.G., Dong K.C.. In vitro, in vivo and in silico models of drug distribution into the brain. J Pharmacokinet Pharmacodyn 2013;40:301–14.
[3] Kelder J., Grootenhuis P.D.J., Bayada D.M., Delbressine L.P., Ploemen J.P.. Polar molecular surface area as a dominating determinant for oral adsorption and brain penetration of drugs. Pharm Res 1999;16:1514–9.
[4] Summerfield S.G., Stevens A.J., Cutler L., del Carmen Osuna M., Hammond B., Tang S.P., et al. Improving the in vitro prediction of in vivo central nervous system penetration: integrating permeability, P-glycoprotein efflux, and free fractions in blood and brain. J Pharmacol Exp Ther 2006;316:1282–90.
[5] Wan H., Rehngren M., Giordanetto F., Bergstrom F., Tunek A., et al. High-throughput screening of drug-brain tissue binding and in silico prediction for assessment of central nervous system drug delivery. J Med Chem 2007;50:4606–15.
[6] Zhang L., Villalobos A., Beck E.M., Bocan T., Chappie T.A., Chen L., et al. Design and selection parameters to accelerate the discovery of novel central nervous system positron emission tomography (PET) ligands and their application in the development of a novel phosphodiesterase 2A PET ligand. J Med Chem 2013;56:4568–79.
[7] Asmus F., Seelig A., Gobbi L., Boroni E., Glaentzlin P., Fischer H.. Label-free assay for the assessment of nonspecific binding of positron emission tomography tracer candidates. Eur J Pharm Sci 2015;79:27–35.
[8] Friden M., Wennerberg M., Antonsson M., et al. Identification of positron emission tomography (PET) tracer candidates by prediction of target-bound fraction in the brain. Eur J Nucl Med Mol Imag 2014;4:50.
[9] Lipinsky C.A., Lombardo F., Dominy B.W., et al. Experimental and computational approaches to estimate solubility and permeability in drug discovery and development settings. Adv Drug Deliv Rev 1997;23:3–25.
[10] Lipinsky C.A.. Rule of five in 2015 and beyond: target and ligand structural limitations, ligand chemistry structure and drug discovery project decisions. Adv Drug Deliv Rev 2016;101:34–41.
[11] Van de Bittmer G.C., Ricq E.M., Hooker J.M.. A philosophy for CNS radiotracer design. Acc Chem Res 2014;47:3127–34.

Reconsider logP!

In our view, it is essential to start a general balanced but unprejudiced discussion on power and limitations of methods and predictive models in radiopharmacy. We fully agree that lipophilicity has a significant impact on the pharmacokinetic properties of radiopharmaceuticals, and we literally stated in our manuscript: "In drug development, especially for central applications, the lipophilicity is a pivotal and early indicator of the potential *in vivo* pharmacokinetic and dynamic behaviour. Lipophilicity measurements, as it is widely known, provide information about unspecific binding, metabolic stability, plasma protein binding, the distribution and excretion of drugs [1]." However, we do not want to rely on a single and simplified physicochemical value to predict complex biochemical processes *in vivo*.

The traditional method to measure logP is based on the distribution of the respective drug or tracer in octanol–water or octanol–buffer to mimic the situation *in vivo*. This method is severely intrigued, if the tested molecules are of low solubility (which is quite common for high lipophilicity) [2,3]. And the question is, why the distribution of a tracer in water and a fatty alcohol should reflect the distribution in the complex *in vivo* system with various lipid components in plasma, cell membrane or other fatty tissue at all. Therefore, we are convinced that logP alone, no matter if calculated or measured, is too general.

Above all, as pointed out as one of the main deliverables from our manuscript, logP values derived from different methods show a high discrepancy — leading to misinterpretations and bias. For that reason, it was one of our aims to provide a conclusive and comparative database for the most commonly used radiotracers.

Scott and Kilbourn stated from their own experience that they found "poor human *in vivo* imaging results for [^{18}F]GBR12909 (cLogP = 5.3) and excellent performance with [^{11}C]dihydrotetrabenazine (cLogP = 2.1)" [4]. These findings are not surprising, since – based on these calculations – [^{18}F]GBR12909 is 1584.9 times more lipophilic than [^{11}C]dihydrotetrabenazine (octanol–water ratios 199,526.23 to 125.89). This radical reduction of the lipophilicity influences e.g. metabolism, non-specific binding (if defined as physiologically non-displaceable non-target binding) or bioavailability for blood brain barrier penetration [5,6].

In our opinion, the general dogma of logP for the prediction of further *in vivo* efficacy of radiotracers has to be critically discussed. For that reason, based on a structured approach: reconsider logP!

Chrysoula Vraka
Department of Biomedical Imaging and Image-guided Therapy Division of Nuclear Medicine, Medical University of Vienna, Vienna, Austria
Department for Nutritional Science, University of Vienna, Vienna, Austria

Markus Mitterhauser*
Department of Biomedical Imaging and Image-guided Therapy Division of Nuclear Medicine, Medical University of Vienna, Vienna, Austria
Department of (PTB) Pharmaceutical Technology and Biopharmaceuticals University of Vienna, Vienna, Austria
Ludwig Boltzmann Institute Applied Diagnostics, Vienna, Austria

*Corresponding author at: Department of Biomedical Imaging and Image-guided Therapy, Division of Nuclear Medicine
Medical University of Vienna, Vienna, Austria
E-mail address: markus.mitterhauser@meduniwien.ac.at

http://dx.doi.org/10.1016/j.nucmedbio.2017.08.007

References

[1] Vraka C., Nics L., Wagner K.H., Hacker M., Wadsak W., Mitterhauser M.. LogP, a yesterday's value? Nucl Med Biol 2017;50:1–10.
[2] Young R.J., Green D.V., Luscombe C.N., Hill A.P.. Getting physical in drug discovery II: the impact of chromatographic hydrophobicity measurements and aromaticity. Drug Discov Today 2011;16:822–30.
[3] Hill A.P., Young R.J.. Getting physical in drug discovery: a contemporary perspective on solubility and hydrophobicity. Drug Discov Today 2010;15:648–55.
[4] Kilbourn M.R., Scott P.J.H.. Is LogP truly dead? Nucl Med Biol 2017;54:41–2.
[5] Pajouhesh H., Lenz R.G.. Medicinal chemical properties of successful central nervous system drugs. NeuroRx 2005;2:541–53.
[6] Chung T.D.Y., Terry D.B., Smith L.H.. In vitro and in vivo assessment of ADME and PK properties during lead selection and lead optimization — guidelines, benchmarks and rules of thumb. In: Sittampalam GS, Coussens NP, Brimacombe K, et al, editors. SciencesBethesda (MD): Eli Lilly & Company and the National Center for Advancing Translational; 2004 [Published September 9, 2015].

3.1.3 Manuscript III

Vraka C, Mijailovic S, Fröhlich V, Wadsak W, Wagner KH, Hacker M, Mitterhauser M. Expanding LogP: Present Possibilities. Submitted, 2017 September 22nd, Journal of Nuclear Medicine and Biology, (NUCMEDBIO_2017_232).

Expanding LogP: Present Possibilities.

Chrysoula Vraka[1,2], Sanja Mijailovic[1,3], Vanessa Fröhlich[1], Markus Zeilinger[1,4], Eva-Maria Klebermass[1], Wolfgang Wadsak[1,5,6], Karl-Heinz Wagner[2], Marcus Hacker[1], Markus Mitterhauser[1,3*]

Affiliation
[1]*Department of Biomedical Imaging and Image-guided Therapy, Division of Nuclear Medicine, Medical University of Vienna, Vienna, Austria*
[2]*Department for Nutritional Science, University of Vienna, Vienna, Austria*
[3]*Ludwig Boltzmann Institute Applied Diagnostics, Vienna, Austria*
[4]*Faculty of Engineering, University of Applied Sciences Wiener Neustadt, Wiener Neustadt, Austria*
[5]*Department of Inorganic Chemistry, University of Vienna, Vienna, Austria*
[6]*CBmed, Graz, Austria*

*Corresponding author:
Prof. Dr. Markus Mitterhauser
Ludwig Boltzmann Institute Applied Diagnostics, Vienna, Austria
General Hospital of Vienna
Waehringer Guertel 18-20
A-1090 Vienna / AUSTRIA
Email: markus.mitterhauser@meduniwien.ac.at
Telephone: +43 1 40400 55340
Fax: +43 1 40400 15590

Abstract

Introduction: Due to the high candidate exclusion rate during a drug development process, an early prediction of the pharmacokinetic behavior would be needed. Accordingly, high performance bioaffinity chromatography (HPBAC) approaches are growing in popularity, however, there is a lack of knowledge and no consensus about the relation between HPBAC measurements, *in vivo* distribution and blood brain barrier (BBB) penetration behavior. With respect to radiotracers, there is almost no reference data available for plasma protein binding (PPB), permeability (Pm) and the membrane coefficient (K_{IAM}). Thus, this study was aimed at exploring the relevance of measuring PPB, Pm and K_{IAM} for the prediction of BBB penetration.

Methods: Measurements of %PPB, Pm and K_{IAM} were performed using HPBAC. In total, 113 compounds were tested, 43 with brain uptake, 30 not showing brain uptake and 40 with known interactions with efflux transporters. Additionally, ClogP and HPLC $logP_{ow}^{pH7.4}$ data were collected.

Results: %PPB, K_{IAM}, Pm and ClogP values were in the same range for each of the three groups. A significant difference was observed for the HPLC $logP_{ow}^{pH7.4}$ between CNS penetrating drug group (CNS_{pos}) and the non-penetrating drug group (CNS_{neg}), as well as for the CNS_{neg} towards the drug group interacting with efflux transporters ($DRUG_{efflux}$). However, as the other experimental data, also the HPLC $logP_{ow}^{pH7.4}$ showed a broad overlapping of the single values between the groupings.

Conclusion: Experimental reference values (logP, Pm, K_{IAM} & PPB) of commonly used PET tracers and drugs showing different BBB penetration behavior are provided. The influence of the logP on brain uptake depends strongly on the selected method. However, using a single parameter (experimental or calculated) to predict BBB penetration or for the classification of drug groups is inexpedient.

Keywords: plasma protein binding (PPB), permeability (Pm), membrane coefficient (K_{IAM}), high performance bioaffinity chromatography (HPBAC), blood brain barrier (BBB)

1. Introduction

Chemistry-based drug delivery strategies to cross the blood brain barrier (BBB) focus on passive diffusion. Therefore, newly developed drugs and brain tracers should fulfil different physicochemical criteria, such as a certain molecular weight, number of hydrogen bonds and lipophilicity. Additionally, the plasma protein binding is part of these strategies [1,2]. Serum albumin is the major plasma protein (concentration of 0.53-0.75 mM) consisting of a mass of 66 kDa and three binding domains (I, II, and III), which are further divided into subdomains A and B [3]. It plays a pivotal role in the transport of drugs as well as in endogenous compounds and metabolites in the human body [4–6]. Plasma protein binding (PPB) and the plasma drug concentration (C_{PL}) characterize the pharmacokinetic profile of a drug [2,6–8]. However, the role of PPB of a drug and the effect on pharmacokinetics is not fully understood [7–9]. Therefore, different hypotheses and interpretations can be found in literature.

Considering the free drug hypothesis, the plainest approach is to assume that under freely diffusible conditions, the unbound drug concentration in plasma (Cu_{pl}) is equal to the unbound concentration in the brain (Cu_{br}) at equilibrium. Following that hypothesis, only the free drug concentration in plasma is available for binding at a target in the CNS (central nervous system) [5]. Accordingly, plasma protein binding of ligands is collected during radiopharmaceutical drug development and the quantity of the PPB, thus constitutes another criterion for the drug penetration of the BBB and biodistribution, respectively [1,10]. Since the distribution of a drug is rapid and reversible, changes in the plasma concentration of a drug reflect changes in the drug concentration in other tissues (equilibrium hypothesis). This approach is also considered for kinetic models in PET imaging, which also take the free

fraction in plasma into account. However, concepts in drug development focus on modifications of lead structures to optimize physiological parameters, such as PPB to e.g. prolong the circulation time of a tracer *in vivo*.

Besides PPB, the permeability (Pm) through biomembranes is crucial for the drug (*in vivo*). Different models have been presented such as cell based experiments using MDCKII cells or screening methods using phospholipids like immobilized artificial membrane chromatography (IAM) or parallel artificial membrane permeation assay (PAMPA). A study of Tavares and co-workers in 2012 showed a good correlation between the Pm value using IAM chromatography, %PPB using HSA chromatography and the percent injected dose (%ID whole brain peak), whereas the lipophilicity was not found to correlate with %ID [11]. However, since this correlation was endorsed by ten molecules, the overall validity still has to be proven.

Hence, *in vitro* high throughput methods (HSA and IAM chromatography) may be essential to identify biochemical properties and display changes of physiochemical values of newly developed PET tracers, even before conducting animal experiments [7]. The aim of this work was to elaborate reference values for the potential prediction of BBB. We used high performance bioaffinity chromatography (HPBAC) and classified three groups: (I) BBB penetrating drugs, (II) non-penetrating drugs and (III) compounds interacting with efflux transporters. To complete the picture, HPLC $\log P_{ow}^{pH7.4}$ measurements and ClogP values were additionally included.

2. Methods & Materials

2.1. General Information

For all measurements, a HPLC system of Agilent (Agilent technologies, Santa Clara, USA) was used. It consisted of an auto-injector (1100 series), a pump (1200 series), a diode array detector (1100 series) and a radioactivity-detector (Ramona, Elysia-Raytest, Straubenhardt, GER). Reference standards were mostly purchased from ABX (Radeberg, Germany) or Sigma Aldrich (St. Louis, Missouri, USA). Product information is provided in the results tables. Radiolabeled compounds were produced by the Department of Biomedical Imaging and Image-guided Therapy, Division of Nuclear Medicine at the Medical University of Vienna in Austria in accordance to published synthesis protocols [12–20]. In total, 113 compounds were experimentally tested and classified according to literature into three groups: I. BBB penetrating compounds (table 1), II. BBB non-penetrating drugs (table 2) and III. Compounds with known interactions towards various efflux transporters (table 3). Measurements which were not calculable or quantifiable are labeled as n.c. or n.q., respectively. All experiments were performed in triplicates or duplicate injection and repeated at least three times. Calculations were performed using Microsoft Excel Version 14.00©Microsoft Cooperation (WA, USA) and GraphPadPrism Version 6.01©1992-2012 GraphPad Software, Inc. (CA, USA). Differences among groups and multiple comparisons testing were proved using an ordinary one-way ANOVA with Tukey's correction. Values of $P < 0.05$ were considered as statistically significant.

2.2. Drug Protein Binding Studies

2.2.1. Measurement of Plasma Protein Binding using high performance bioaffinity chromatography (HPBAC)

The retention times of the analytes were measured by HPLC on the CHIRALPAK®HSA stationary phase (50x3 mm and 5 µm pore size, column-batch: H12B-2410 and H13L-2405

(Chiral Technologies, DAICEL Group, Europe SAS, France)) with a column oven (Kolonnenthermostat W.O. electronics, BFG-04 np, Ser.No. 941180-1, Langenzersdorf, Austria) set to a temperature of 30°C. The mobile phase A consisted of 50 mM aqueous ammonium acetate buffer (CAS 631-61-8, AmAc) (pH 7.4) and phase B of 2-propanol (MERCK EMSURE®ACS, ISO, Reag. PhEUR for analysis, CAS 67-63-0) according to Valko et al. [7]. The flow rate was reduced to 1 ml/min for prolonged column operation by using a linear gradient starting with 100% AmAc to 70% AmAc and 30% 2-propanol within 5.4 min and a constant composition of 30% B and 70% A for 2.5 minutes and back to 100% AmAc with an equilibrium time of another 2 minutes. Each chromatographic analysis was stopped after 14 min. The UV-detector was set to 230-280 nm depending on the absorption spectrum of the tested compound. The injection volume was 3 µl of 0.5 mg/mL standards. Retention capacity factors (k') were calculated by using DMSO or a substance with 0% HSA binding for systems' dead time (Rt_0). The system was calibrated by injecting the reference compounds: isoniazid CAS-54-85-3, metronidazole CAS-443-48-1, cimetidine CAS-51481-61-9, nizatidine CAS-76963-41-2, ciprofloxacin CAS-85721-33-1, trimethoprim CAS-738-70-5, acetylsalicylic acid CAS-69-72-7, betamethasone CAS-378-44-9, carbamazepine CAS-298-46-4, nicardipine CAS-55985-32-5, budesonide CAS-5133-22-3, warfarin CAS-81-81-2 and indomethacin CAS-53-86-1 obtained from Sigma Aldrich, flumazenil CAS-78755-81-4 ABX (Radeberg, Germany), ketoprofen CAS-22071-15-4 LKT LABS and diclofenac CAS-15307-86-5 EMD Chemicals Inc. The logarithmic capacity factors of the references' Rt (log(k')) on the HSA column were plotted against the %PPB values from literature. The slope and the intercept were used to convert the log(k') of the radiotracer to %PPB using the regression equation. For the sake of completeness, %PPB results were converted into the linear free energy related logK value, the logarithm of apparent affinity constant [7].

2.2.2. Plasma Protein Binding using Ultracentrifugation

Free fraction measurements were performed with 10 radiolabeled PET tracers using a conventional ultracentrifugation method [21]. To determine the free fraction or respectively the plasma bound fraction, 1 mL pooled normal human plasma (IPLA-N, Innovative Research, MI, USA) was spiked with radioactive labeled references with respect to the linearity range of the used Perkin Elmer Gamma-Counter (Waltham, Massachusetts, USA) calibrated for fluorine-18, and carbon-11. The identical amount of the radioactive labeled compound was added to 1 mL of PBS (PBS buffer pH 7.4 10× stock solution, REF 11237.00500, MORPHISTO, Frankfurt a. Main, GER). After an equilibration time of 20 min, aliquots of 200 µL were pipetted into Centrifree micropartition system units (Centrifree®Ultafiltration Devices, REF 4104, MERCK-Millipore) in triplicate and aliquots of 50 µL were measured in the gamma counter. The Centrifree units were centrifuged for 50 min and 37°C at 3950 n/min^{-1} in a fixed angle rotor centrifuge as recommended by the manufacturer. After centrifugation, the radioactivity concentrations in 50 µl of the ultrafiltrate was counted and corrected for the radioactive decay. The free fraction (FF) ratio was calculated according to Price et al.: $FF= X/Y * \omega$ (ω= 0.94 mL water/mL plasma; X= plasma ultrafiltrate/plasma standard and Y= PBS ultrafiltrate/ PBS standard [22].

2.2.3. Permeability Measurements using high performance bioaffinity chromatography (HPBAC)

The IAM (Immobilized Artificial Membrane) chromatography was slightly modified from previously published data [23–25]. The retention times of the analytes (reference tracer) on the IAM.PC.DD2 stationary phase (150x4.6mm, column-batch: 45873 and 49161, REGIS Technologies, USA) were measured by HPLC with an isocratic flow rate of 1 mL/min and wavelengths of 254 nm and 285m using four runs with different eluent ratios (50/50, 55/45, 60/40 and 65/35) of 0.01 M sodium phosphate buffer, pH 7.0 (sodium phosphate dibasic dehydrate CAS 10028–24-7 and sodium phosphate monobasic monohydrate (CAS10049-21-

5), all from Sigma-Aldrich, St Louis, USA, water from Milli-Q® Integral Water Purification System (Merck Millipore, Billerica, USA) and acetonitrile (LiChrosol®Reag. PhEur ACN, HPLC grade, CAS 75-05-08, MERCK). The capacity factors (k'_{IAM}) were calculated (cf. supplementary data where relative standard deviations (RSD%) of retention time shifts are listed) and linear extrapolated to 100% aqueous phase. After correcting the column conditions (total volume of solvent within column and volume of interphase, V_s and V_m) the membrane coefficient (K_{IAM}) was obtained [26]. Permeability (Pm) values were obtained by dividing the K_{IAM} through the molecular weight of the respective compound.

2.2.4. HPLC $logP_{ow}^{pH\ 7.4}$

The HPLC $logP_{ow}^{pH\ 7.4}$ measurements were performed as previously published [27].

2.2.5. Calculated logP

Calculated logP (ClogP) values were derived from ChemBioDraw (CBD) Software Version 12.0.2, Level Ultra© 1986-2010 CambridgeSoft, PerkinElmer, Waltham, USA.

3. Results

3.1. BBB penetrating compounds

The results of the BBB penetrating compounds are illustrated in table 1, which include only brain tracers with passive diffusion. The mean value of the membrane coefficient (K_{IAM}) over the whole dataset was 98 ±68. The lowest value was 4.6 for FMISO and the highest 249 for carazolol. The permeability (Pm) mean was 0.28 ±0.19, and ranged from 0.02 (FMISO, flumazenil, fluoroethylflumazenil) to 0.83 for carazolol. The plasma protein binding (%PPB) mean was 69 ±16%, whereas 0% (FMISO) was the lowest value and 89% the highest (FMcN5256). Since, FET, FEC and FMISO retain with the systems dead time, 0% plasma protein binding was specified for these three compounds. Variation coefficient of the single values were for all <10%, in one case higher (flumazenil). FET and FEC (active transport) are

not included in table 1 or group comparisons, but used for the comparison between ultrafiltration and HPBAC method. LogK values range from 2.00 to 0.88 (FMISO and FMcN5256) with a mean value of 0.34 ±0.43.

Table 1 Results of the HPLC $logP_{ow}^{pH7.4}$, ClogP, the membrane coefficient (K_{IAM}), the permeability (Pm), plasma protein binding (%PPB) and LogK value of BBB penetrating compounds.

In the first column of **table 1** the IUPAC name of the tested compounds is given, whereas in column 3 the trivial names in alphabetical order are listed. Column 2 is showing the product number of the compounds. From column four to nine the mean results of HPLC $logP_{ow}^{pH7.4}$, ClogP, K_{IAM}, Pm, %PPB and LogK of BBB penetrating compounds with standard deviation are shown. All measurements were performed at least in triplicate ($n \geq 3$). Total group means of the parameters are given in the last row. HPLC $logP_{ow}^{pH7.4}$ and the ClogP results were taken from a previously published manuscript [27].

3.2. BBB non-penetrating compounds

All experimental results of the BBB non-penetrating compounds are illustrated in table 2. HPLC $logP_{ow}^{pH7.4}$ measurements ranged between -2.1 (mHED) and 4.6 (miconazol) with a group mean value of 1.61 ±2.11. Variation coefficients were for single compound results less than < 2%. The calculated logP values ranged between -2.8 (neostigmine) and 7.3 (candesartan cilexetil), with an overall mean of 2.76 ±2.89. The ClogP of roxithromycin and teicoplanin were not calculable. The mean value of the membrane coefficient (K_{IAM}) over the whole dataset was 119 ±238. The lowest value was 0.67 for fulvestrant and the highest was 943 for terfenadine. The permeability (Pm) mean was 0.26 ±0.54, and it ranged from 0 (fulvestrant) to 2.2 (miconazol). Carbidopa and entacapone results for IAM were excluded since variation after extrapolation were higher than 100%. The plasma protein binding in percentage using HPBAC mean was 69 ±25%, whereas 26% (carbidopa) was the lowest measurable value and 93% the highest (miconazol). LogK values ranged from -0.5 to 1 (neostigmine and glibenclamide) with a mean value of 0.47 ±0.58. The variation coefficient of the single values of HSA chromatography are lower than 10% with exception of mHED 15% and sotalol 11% variation coefficient.

Table 2 Results of the HPLC $logP_{ow}^{pH7.4}$, ClogP, the membrane coefficient (K_{IAM}), the permeability (Pm), plasma protein binding (%PPB) and LogK value of BBB non-penetrating compounds using high performance chromatography.

In the first column of **table 2** the IUPAC names of the tested compounds are listed, whereas in column 3 the trivial name in alphabetical order is given. Column 2 is showing the product number of the compounds. From column four to nine the mean results of HPLC $logP_{ow}^{pH\ 7.4}$, ClogP, K_{IAM}, Pm, %PPB and LogK of BBB non-penetrating compounds with standard deviation are shown. All measurements were performed at least in triplicate (n≥3). The total group means of the parameters are illustrated in the last row.

3.3. Compounds with efflux transporter interactions

All experimental results of compounds showing interactions to diverse efflux transporter are illustrated in table 3. HPLC $logP_{ow}^{pH7.4}$ measurements ranged between -1.1 (ranitidine) and 4.9 (elacridar/GF120918) with a mean value of 2.6 ±1.4. The calculated logP values ranged between -0.9 (hydrocortisone) and 6.7 (quinacrine), with an overall mean of 2.9 ±2.3. The ClogP of actinomycin D, cyclosporine A, digoxin, vinblastine and vincristine were not calculable. The mean value of the membrane coefficient (K_{IAM}) over the whole dataset was 203 ±292. The lowest value was 4.8 for losartan and the highest was 1,254 for elacridar. The permeability (Pm) mean was 0.40±0.58 and values ranged from 0.01 (digoxin) to 2.53 (bisantrene). The plasma protein binding in percent using HPBAC mean was 71 ±21%, whereas 0% (digoxin) and 100% the highest (bisantrene). LogK values ranged from -0.9 to 2 (Ro 11-2933/ acetanilide and bisantrene) with a mean value of 0.5 ±0.5.

Table 3 Results of the HPLC $logP_{ow}^{pH7.4}$, ClogP, the membrane coefficient ($K_{IAM)}$, the permeability (Pm), plasma protein binding (%PPB) and LogK value of compounds showing interactions to various efflux transporters.

In the first column of **table 3** the IUPAC names of the tested compounds are given, whereas in column 3 the trivial names in alphabetical order are listed. Column 2 is showing the product number of the compounds. From column four to nine the mean values of HPLC $logP_{ow}^{pH\ 7.4}$, ClogP, K_{IAM}, Pm, %PPB, LogK of compounds which interact with efflux transporters with standard deviation are shown. All measurements were performed at least in triplicate (n≥3). The total group means of the parameters are illustrated in the last row.

3.4. Plasma Free Fraction

Plasma free fractions ranged from 5% [^{11}C]Harmine to 96% for [^{18}F]FMISO. Single results as well as the filter retention are illustrated in table 4.

Table 4 Results of the free fraction (FF%) using an ultrafiltration method (UF)

Table 4 shows the results of the plasma free fraction using ultrafiltration (UF). In the first column, the names of the tested tracers are listed. Plasma free fractions are given in percentage with standard deviations (column two). Last column represents the amount of the mean filter retention. All measurements were performed at least in triplicate ($n \geq 3$). FF data of [^{11}C]WAY-100635 are taken from literature [28]

Correlation of %PPB of the two different methods results in a strong relationship (figure 1).

Fig. 1.

3.5. Relation between the experimental logP and the HPBAC measurements

The correlation of the plasma protein binding using HPBAC and the HPLC $logP_{ow}^{pH7.4}$ is resulting in a moderate linear relationship (figure 2).

Fig. 2

Correlation of the K_{IAM} (figure 3) with the experimental logP and with the molecular weight (MW) shows weak relations.

Fig.3

3.6. Group comparison

For interpretation purposes, the values of each parameter (HPLC $logP_{ow}^{pH7.4}$, the membrane coefficient (K_{IAM}), permeability (Pm) and percent of plasma protein binding (%PPB)) for each of the three substance groups were illustrated as box plots and the results (cf "total mean" tables 1-3) compared to each other using a one-way ANOVA and multiple comparison (Tukey test). The results are shown in figure 4.

Fig.4.

4. Discussion

4.1. General

The so called “rules of five” are widely accepted in drug development for brain imaging [29–34]. However, there is a concomitant debate on the real predictive power and relevance. Within these “rules of five”, lipophilicity has become the major factor to predict the BBB penetration via passive diffusion. Another pronounced factor in brain drug development is plasma protein binding (PPB), as it plays a pivotal role in pharmacokinetic (PK) parameters like distribution and clearance [1,10]. Furthermore, especially in radiopharmaceutical sciences and for kinetic modelling, the free fraction (unbound concentration of tracer in plasma) is measured [35]. On the other hand, since it is known that most commercially available drugs with completely different PK properties have a high affinity to plasma proteins (greater than 90%PPB) [9], the “free drug hypothesis” is widely replaced by the “equilibrium theory” or “enhanced dissociation theory”. Nevertheless, considering the free drug hypothesis may lead to the exclusion of potential candidate tracers or trying to modify the degree of PPB [35]. Another parameter of increasing interest is the evaluation of the permeability on or binding to artificial membranes, mimicking the phospholipid bilayer of cell membranes. Both parameters are supposed to have influence on brain uptake and the potential to predict *in vivo* efficiency [11].

This manuscript provides a high number of reference values (%PPB, K_{IAM} and Pm) of various drug families using high performance bioaffinity chromatography (HPBAC) and compares the results concerning the drugs’ ability to penetrate the BBB.

4.2. HSA-HPBAC and Ultrafiltration

Human serum albumin (HSA) chromatography can be used for a high number of chemically different compounds. It is a stable and rapid method with high reproducibility, especially for high affinity compounds, as slightest changes in PPB can be measured. Further advantages include the easy application in every laboratory and low costs considering the long operational time of the column (500-1000 injections [36]). Substances which show very low %PPB are susceptible to higher variations of the retention time, since they retain shortly after or within the systems dead time (e.g. FLT, FMISO and FET). Beside measurements of %PPB, this method can also provide information about the binding constants, characterize binding sites, examine drug-drug interactions and drug-protein dissociation rates [36].

Furthermore, experimental logP values were correlated with the measured %PPB of all groups (figure 2), showing a relation between these values (correlation coefficient of 0.74 and coefficient of determination of 0.56, $P < 0.0001$), indicating, that lipophilicity is a main but not the only influencing factor. Within the groups only marginal differences concerning the influence of lipophilicity on PPB was calculated (coefficient of determination in the same range). Other working groups also reported a similar correlation with logP to %PPB respecting the charge of the molecules [4,5,7].

The conventional ultrafiltration method is the simplest approach for the evaluation of the plasma protein binding. The ratio of the compound bound to the unbound fraction in plasma is directly calculated. Ultrafiltration approaches are often used in clinical and preclinical imaging studies where kinetic modelling and corrections for radioactive metabolites are needed individually [28,37]. Disadvantages are the unsuitability for compounds with low PPB binding [37], or the high non-specific binding to the centrifugation tubes for highly lipophilic compounds. We found filter retentions of 0 up to 99% for the tested compounds (cf table 4). Of note, the high retention could be decreased by pre-saturation of the filter with the non-labelled reference compound, although, this leads to high consumption of the standard. %PPB

results using UF or HSA-chromatography correlate strongly (figure 1), which is in accordance with the findings described in literature [6,7,36]. HSA is the main protein responsible for PPB, however, results of the HPBAC might underestimate %PPB since alpha glycoprotein and lipids are missing (e.g. 84.30 versus 94.84 %PPB for altanserin). Concerning the BBB penetration (or brain uptake), no differences between the three groups were observed. We conclude, that slight modifications of the PPB might be useful for the pharmacokinetics in principle (e.g. prolongation of drug circulation), but do not influence the BBB penetration directly.

4.3. Permeability and Membrane coefficient using IAM-chromatography

IAM chromatography is a simple and high throughput approach to test the Pm and K_{IAM} of compounds. However, standard deviations of K_{IAM} higher than 10% are primarily caused by the extrapolation to 100% aqueous phase, although only minor changes of the retention time (Rt) are measured (cf. supplementary information relative standard deviation (RSD%) of retention time shifts, table S1-S3). Slight Rt shifts are caused due to column batch differences. In literature also column aging and inter-laboratory differences are described to be influencing factors for distinct variations in the results [26,38]. Results of K_{IAM} and consequently Pm are strongly depending on how calculations are performed (no extrapolation, extrapolation, the number of experimental data points (runs) and the amount organic solvent used for the extrapolation, cf. table S4 and S5). In this study, a consistent method using for runs with different acetonitrile contents was used and linear extrapolation was thus performed with four data points. While other authors apply different setups and compare non-extrapolated data to extrapolated data of varying organic solvent and different number of data points [11]. Compounds showing a huge variation in the K_{IAM} value are not listed in the result tables (listed as n.q.) and excluded from further correlations. Run durations vary extremely between the groups. For CNS negative and drugs interacting with efflux transporters ($DRUG_{efflux}$),

retention times up to 60 min per run were observed. This consequently led to higher K_{IAM} values. This issue raises the question, if IAM can be still entitled as a "high throughput method". Correlation of the molecular weight and the K_{IAM} (figure 3) shows a weak coefficient of determination and correlation coefficient, while comparing within the groups the correlation with MW of the CNS_{pos} drugs was stronger than the correlation solely for the CNS_{neg} drugs or the $DRUG_{efflux}$ group. Hence, the MW has a relatively small influence on the K_{IAM} value at least for penetrating compounds. However, more substances with molecular weights greater than 500 Da must be tested. Furthermore, the HPLC $logP_{ow}^{pH7.4}$ results were compared to the K_{IAM} (figure 3) values, showing a less strong correlation trend as it was shown for %PPB and lipophilicity (figure 2). In contrast to the correlation of the overall results the correlations within the groups were slightly stronger. This indicates that the experimental logP is by far not the only factor influencing interactions with biomembranes.

4.4. Comparison of group results & prediction of BBB penetration

In a previous work, HPLC $logP_{ow}^{pH7.4}$ and ClogP values of CNS positive brain tracers were compared with different logP ranges, which are considered optimal for BBB penetration. It was shown that there is a high number of false negative decisions using these simplified rules [27]. In the current study, logP data were expanded also by including a group of BBB non-penetrating compounds and a group of drugs which are known to have various interactions (inhibitors, modulators or substrates) with efflux transporters. These group datasets were compared.

No significant differences were found between the three groups for the calculated ClogP values. On the contrary, significant differences were found between the CNS_{pos} and CNS_{neg} drugs as well as between the $DRUG_{efflux}$ group and the CNS_{neg} compounds (see figure 4) for the $HPLClogP_{ow}^{pH7.4}$. This indicates that interpretations of logP results are strongly depending

on the used method. However, establishing of a new “optimal” range or threshold to predict BBB penetration is intricate since the overlap of the group results is broad.

For the %PPB no significant differences were found between the groups. Subsequently, a complete overlap of the group dataset is obvious. Conversely, this means determining the free fraction in plasma to predict *in vivo* pharmacokinetics might be questionable and is not useful in predicting brain uptake of a tracer. However, analysis of the unbound concentration in plasma using ultrafiltration methods is still important for kinetic modeling approaches.

K_{IAM} and Pm have been used together with the logP to predict BBB penetration in recent publications [23–25,39–41]. However, the emphasis was only the permeability value, but additional comprehensive reference values were missing. Moreover, reference values for non-penetrating compounds were neglected. Indeed, for the Pm and the K_{IAM} an increasing trend is observed between the groups CNS_{pos} < CNS_{neg} < $DRUG_{efflux}$). However, this observation is not significant and for these values also the datasets of the groups are overlapping in a broad range.

5. Conclusion

We provide a comprehensive database comprising several plasma protein binding, permeability and membrane coefficient values for commonly used brain tracers and well-established drugs using two simple, quick, versatile and inexpensive HPBAC (IAM & HSA chromatography) methods. Furthermore, the HPLC $logP_{ow}^{pH7.4}$ database of previous work was expanded and compared to the calculated logP value, thereby showing that influence on the BBB penetration depends on the selected method.

Hence, based on the present evaluation, a prediction of BBB penetration relying on HPLC $logP_{ow}^{pH7.4}$, ClogP, PPB, K_{IAM} or Pm using HPBAC is not successful due to broad overlap of the data sets, although significant differences between the drug groups (CNS_{pos}, CNS_{neg} and

$DRUG_{efflux}$) were observed for the HPLC $logP_{ow}^{pH7.4}$. The utility of experimental parameters on the prediction of BBB penetration must be further validated.

Acknowledgement

We gratefully acknowledge the support of Monika Dumanic, MSc for reviewing and improving the manuscript. Dr. Verena Pichler for support and inspiring discussions. Dr. Lukas Nics and Matthias Hendl are acknowledged for previous work on IAM chromatography. This work was supported by the Austrian Science Fund (FWF P26502-B24, M. Mitterhauser).

Abbreviations

BBB *blood brain barrier*
ClogP *calculated logP*
CNS central nerve system
CNS_{pos} *drugs penetrating the blood brain barrier*
CNS_{neg} *drugs showing no significant brain uptake or pharmacological effects or side effects in CNS*
$DRUG_{efflux}$ *drugs interacting with various efflux transporters (inhibitors and substrates)*
FF *free fraction*
HPBAC *high performance bioaffinity chromatography*
HSA *human serum albumin*
IAM *immobilized artificial membrane*
%ID *percent injected dose*
K_{IAM} *fluid membrane coefficient*
MW *molecular weight*
Pm *permeability*
PPB *plasma protein binding*
%RSD *relative standard deviation*
UF *ultrafiltration*

References

1. Pardridge WM. BLOOD-BRAIN BARRIER DRUG TARGETING: THE FUTURE OF BRAIN DRUG DEVELOPMENT. Mol. Interv. 2003;3:90–105.

2. Reichel A. The role of blood-brain barrier studies in the pharmaceutical industry. Curr. Drug Metab. 2006;7:183–203.

3. Yang F, Zhang Y, Liang H. Interactive Association of Drugs Binding to Human Serum Albumin. Int. J. Mol. Sci. 2014;15:3580–95.

4. Hollósy F, Valkó K, Hersey A, Nunhuck S, Kéri G, Bevan C. Estimation of Volume of Distribution in Humans from High Throughput HPLC-Based Measurements of Human Serum Albumin Binding and Immobilized Artificial Membrane Partitioning. J. Med. Chem. 2006;49:6958–71.

5. Kratochwil NA, Huber W, Müller F, Kansy M, Gerber PR. Predicting plasma protein binding of drugs: a new approach. Biochem. Pharmacol. 2002;64:1355–74.

6. Singh SS, Mehta J. Measurement of drug–protein binding by immobilized human serum albumin-HPLC and comparison with ultrafiltration. J. Chromatogr. B. 2006;834:108–16.

7. Valko K, Nunhuck S, Bevan C, Abraham MH, Reynolds DP. Fast gradient HPLC method to determine compounds binding to human serum albumin. Relationships with octanol/water and immobilized artificial membrane lipophilicity. J. Pharm. Sci. 2003;92:2236–2248.

8. Alavijeh MS, Chishty M, Qaiser MZ, Palmer AM. Drug metabolism and pharmacokinetics, the blood-brain barrier, and central nervous system drug discovery. NeuroRX. 2005;2:554–71.

9. Smith DA, Di L, Kerns EH. The effect of plasma protein binding on in vivo efficacy: misconceptions in drug discovery. Nat. Rev. Drug Discov. 2010;9:929–39.

10. Ametamey SM, Honer M, Schubiger PA. Molecular Imaging with PET. Chem. Rev. 2008;108:1501–16.

11. Tavares AAS, Lewsey J, Dewar D, Pimlott SL. Radiotracer properties determined by high performance liquid chromatography: a potential tool for brain radiotracer discovery. Nucl. Med. Biol. 2012;39:127–35.

12. Wadsak W, Mien L-K, Ettlinger DE, Lanzenberger RR, Haeusler D, Dudczak R, et al. Simple and fully automated preparation of [carbonyl-11C]WAY- 100635. Radiochim. Acta. 2007;95:417–22.

13. Philippe C, Zeilinger M, Mitterhauser M, Dumanic M, Lanzenberger R, Hacker M, et al. Parameter evaluation and fully-automated radiosynthesis of [11C]harmine for imaging of MAO-A for clinical trials. Appl. Radiat. Isot. 2015;97:182–7.

14. Philippe C, Haeusler D, Mitterhauser M, Ungersboeck J, Viernstein H, Dudczak R, et al. Optimization of the radiosynthesis of the Alzheimer tracer 2-(4-N-[11C]methylaminophenyl)-6-hydroxybenzothiazole ([11C]PIB). Appl. Radiat. Isot. 2011;69:1212–7.

15. Haeusler D, Mien L-K, Nics L, Ungersboeck J, Philippe C, Lanzenberger RR, et al. Simple and rapid preparation of [11C]DASB with high quality and reliability for routine applications. Appl. Radiat. Isot. 2009;67:1654–60.

16. Rami-Mark C, Ungersboeck J, Haeusler D, Nics L, Philippe C, Mitterhauser M, et al. Reliable set-up for in-loop 11C-carboxylations using Grignard reactions for the preparation of [carbonyl-11C]WAY-100635 and [11C]-(+)-PHNO. Appl. Radiat. Isot. 2013;82:75–80.

17. Zuhayra M, Alfteimi A, Papp L, Lützen U, Lützen A, Von Forstner C, et al. Simplified fast and high yielding automated synthesis of [18F]fluoroethylcholine for prostate cancer imaging. Bioorg. Med. Chem. 2008;16:9121–6.

18. Mitterhauser M, Wadsak W, Krcal A, Schmaljohann J, Eidherr H, Schmid A, et al. New aspects on the preparation of [11C]Methionine—a simple and fast online approach without preparative HPLC. Appl. Radiat. Isot. 2005;62:441–5.

19. Adamsen TCH, Grierson JR, Krohn KA. A new synthesis of the labeling precursor for [18F]-fluoromisonidazole. J. Label. Compd. Radiopharm. 2005;48:923–7.

20. Hamacher K, Coenen HH. Efficient routine production of the 18F-labelled amino acid O-(2-[18F]fluoroethyl)-l-tyrosine. Appl. Radiat. Isot. 2002;57:853–6.

21. Sadzot B, Price JC, Mayberg HS, Douglass KH, Dannals RF, Lever JR, et al. Quantification of human opiate receptor concentration and affinity using high and low specific activity [11C]diprenorphine and positron emission tomography. J. Cereb. Blood Flow Metab. Off. J. Int. Soc. Cereb. Blood Flow Metab. 1991;11:204–19.

22. Price JC, Mayberg HS, Dannals RF, Wilson AA, Ravert HT, Sadzot B, et al. Measurement of Benzodiazepine Receptor Number and Affinity in Humans Using Tracer Kinetic Modeling, Positron Emission Tomography, and [^{11} C]Flumazenil. J. Cereb. Blood Flow Metab. 1993;13:656–67.

23. Wenzel B, Mollitor J, Deuther-Conrad W, Dukic-Stefanovic S, Kranz M, Vraka C, et al. Development of a Novel Nonpeptidic (18)F-Labeled Radiotracer for in Vivo Imaging of Oxytocin Receptors with Positron Emission Tomography. J. Med. Chem. 2016;59:1800–17.

24. Rami-Mark C, Berroterán-Infante N, Philippe C, Foltin S, Vraka C, Hoepping A, et al. Radiosynthesis and first preclinical evaluation of the novel norepinephrine transporter pet-ligand [(11)C]ME@HAPTHI. EJNMMI Res. 2015;5:113.

25. Mark C, Bornatowicz B, Mitterhauser M, Hendl M, Nics L, Haeusler D, et al. Development and automation of a novel NET-PET tracer: [11C]Me@APPI. Nucl. Med. Biol. 2013;40:295–303.

26. Taillardat-Bertschinger A, Carrupt P-A, Barbato F, Testa B. Immobilized artificial membrane HPLC in drug research. J. Med. Chem. 2003;46:655–65.

27. Vraka C, Nics L, Wagner K-H, Hacker M, Wadsak W, Mitterhauser M. LogP, a yesterday's value? Nucl. Med. Biol. 2017;50:1–10.

28. Parsey RV, Slifstein M, Hwang D-R, Abi-Dargham A, Simpson N, Mawlawi O, et al. Validation and Reproducibility of Measurement of 5-HT $_{1A}$ Receptor Parameters with [

carbonyl - ^{11} C]WAY-100635 in Humans: Comparison of Arterial and Reference Tissue Input Functions. J. Cereb. Blood Flow Metab. 2000;20:1111–33.

29. Ghose AK, Herbertz T, Hudkins RL, Dorsey BD, Mallamo JP. Knowledge-Based, Central Nervous System (CNS) Lead Selection and Lead Optimization for CNS Drug Discovery. ACS Chem. Neurosci. 2012;3:50–68.

30. Rankovic Z. CNS Drug Design: Balancing Physicochemical Properties for Optimal Brain Exposure. J. Med. Chem. 2015;58:2584–608.

31. Clark DE. In silico prediction of blood–brain barrier permeation. Drug Discov. Today. 2003;8:927–33.

32. Pajouhesh H, Lenz GR. Medicinal Chemical Properties of Successful Central Nervous System Drugs. NeuroRx. 2005;2:541–53.

33. Hitchcock SA, Pennington LD. Structure-brain exposure relationships. J. Med. Chem. 2006;49:7559–83.

34. Lipinski CA. Lead- and drug-like compounds: the rule-of-five revolution. Drug Discov. Today Technol. 2004;1:337–41.

35. Laruelle M, Slifstein M, Huang Y. Relationships between radiotracer properties and image quality in molecular imaging of the brain with positron emission tomography. Mol. Imaging Biol. MIB Off. Publ. Acad. Mol. Imaging. 2003;5:363–75.

36. Hage DS, Anguizola J, Barnaby O, Jackson A, Yoo MJ, Papastavros E, et al. Characterization of drug interactions with serum proteins by using high-performance affinity chromatography. Curr. Drug Metab. 2011;12:313–28.

37. Huang Y, Hwang D-R, Narendran R, Sudo Y, Chatterjee R, Bae S-A, et al. Comparative Evaluation in Nonhuman Primates of Five PET Radiotracers for Imaging the Serotonin Transporters: [11C]McN 5652, [11C]ADAM, [11C]DASB, [11C]DAPA, and [11C]AFM. J. Cereb. Blood Flow Metab. 2002;22:1377–98.

38. Valko K, Du CM, Bevan CD, Reynolds DP, Abraham MH. Rapid- Gradient HPLC Method for Measuring Drug Interactions with Immobilized Artificial Membrane: Comparison with Other Lipophilicity Measures. J. Pharm. Sci. 2000;89:1085–96.

39. Rami-Mark C, Bornatowicz B, Fink C, Otter P, Ungersboeck J, Vraka C, et al. Synthesis, radiosynthesis and first in vitro evaluation of novel PET-tracers for the dopamine transporter: [(11)C]IPCIT and [(18)F]FE@IPCIT. Bioorg. Med. Chem. 2013;21:7562–9.

40. Philippe C, Nics L, Zeilinger M, Schirmer E, Spreitzer H, Karanikas G, et al. Preparation and First Preclinical Evaluation of [18F]FE@SNAP: A Potential PET Tracer for the Melanin-Concentrating Hormone Receptor-1 (MCHR1). Sci. Pharm. 2013;81:625–39.

41. Philippe C, Nics L, Zeilinger M, Kuntner C, Wanek T, Mairinger S, et al. Preclinical in vitro &in vivo evaluation of [(11)C]SNAP-7941 - the first PET tracer for the melanin concentrating hormone receptor 1. Nucl. Med. Biol. 2013;40:919–25.

Table 4

Results of free fraction (FF%) using an ultrafiltration method (UF).

Tracer Name	MEAN ±SD %Free Fraction UF	MEAN filter retention (%)
[^{18}F]Altanserin	5 ±3	75
[^{11}C]DASB	6 ±1	23
[^{11}C]Harmine	5 ±2	50
[^{11}C]PIB	40 ±7	99
[^{11}C](+)-PHNO hydrochloride	40 ±7	0
(±)-Verapamil hydrochloride	5 ±1	18
[^{11}C]WAY-100635	*6 ±3	n. described
[^{11}C]Methionine	91.27 ±17	0
[^{18}F]FET	83 ±18	59
[^{18}F]FEC	86 ±12	63
[^{18}F]FMISO	96 ±3	50

Table 4 shows the results of the plasma free fraction using ultrafiltration (UF). In the first column, the names of the tested tracers are listed. Plasma free fractions are given in percentage with standard deviation (column two). Last column represents the amount of the mean filter retention. All measurements were performed at least in a triplicate ($n \geq 3$). *FF data of [^{11}C]WAY-100635 are taken from literature [27]

Figure 1

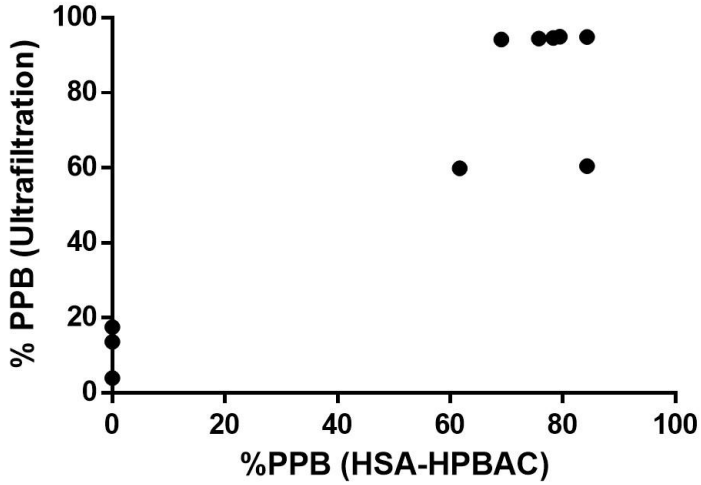

Fig. 1. shows the correlation of the plasma protein binding of the two methods (HPBAC and UF). Correlation coefficient is 0.93 (95% confidence interval, alpha= 0.05) and the coefficient of determination is 0.87, $P < 0.0001$.

Figure 2

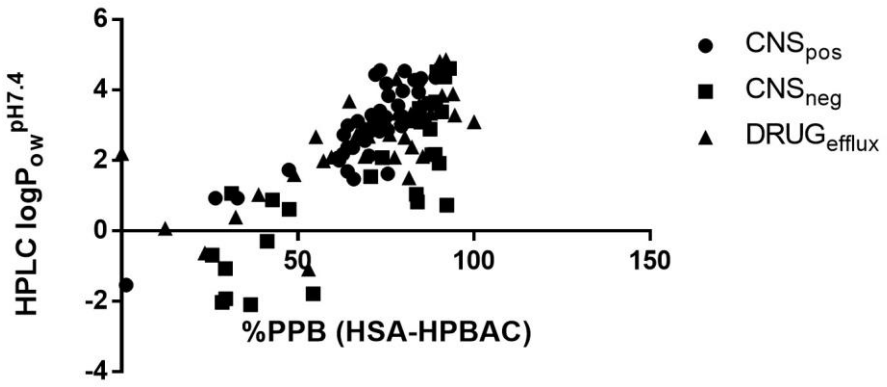

Fig. 2 shows the correlation between the HPLClogP$_{ow}^{pH7.4}$ and the plasma protein binding (%PPB) using HPBAC of all tested 112 compounds. HPLC logP$_{ow}^{pH7.4}$ values of blood brain barrier penetrating compounds are taken from literature. Correlation coefficient is 0.7429 with coefficient of determination of 0.55 (95% confidence interval, alpha= 0.05, $P < 0.0001$) for the whole dataset including all groups.

Figure 3

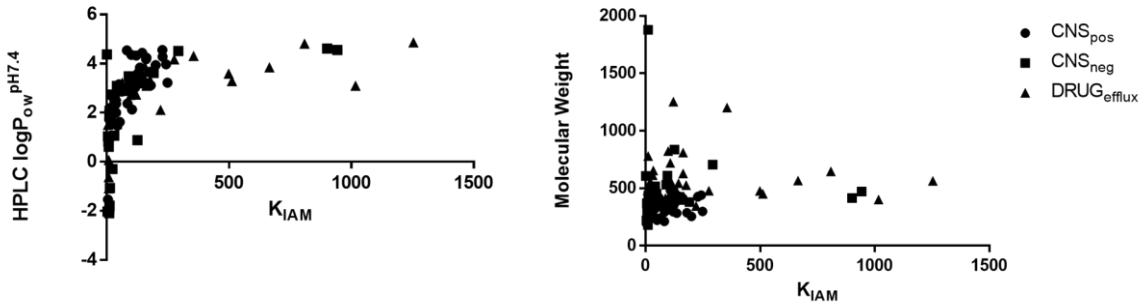

Fig. 3. shows the correlation of the HPLC $logP_{ow}^{pH7.4}$ and molecular weight (MW) with the membrane coefficient (K_{IAM}) of all tested 110 compounds.

Correlation of the experimental logP and K_{IAM} shows overall a weak correlation coefficient of 0.48 and coefficient of determination of 0.23 ($P < 0.0001$). Comparing within the groups, the correlations for the logP of the CNS positive drugs was the strongest with a correlation coefficient of 0.7 and a coefficient of determination of 0.5 ($P < 0.0001$). CNS_{neg} and the $DRUG_{efflux}$ group comparisons were in the same range (correlation coefficient of 0.5 and 0.6, coefficient of determination of 0.3 for both ($P= 0.005$ and $P =0.002$).

Correlation of the MW and K_{IAM} shows a weak correlation coefficient of 0.13 and a weak coefficient of determination of 0.02. Comparing within the groups the correlations for the MW of the CNS_{pos} drugs a coefficient of determination of 0.2 was calculated ($P = 0.005$). The $DRUG_{efflux}$ group and CNS_{neg} drugs show an even worse coefficient of determination of < 0.008.

Figure 4

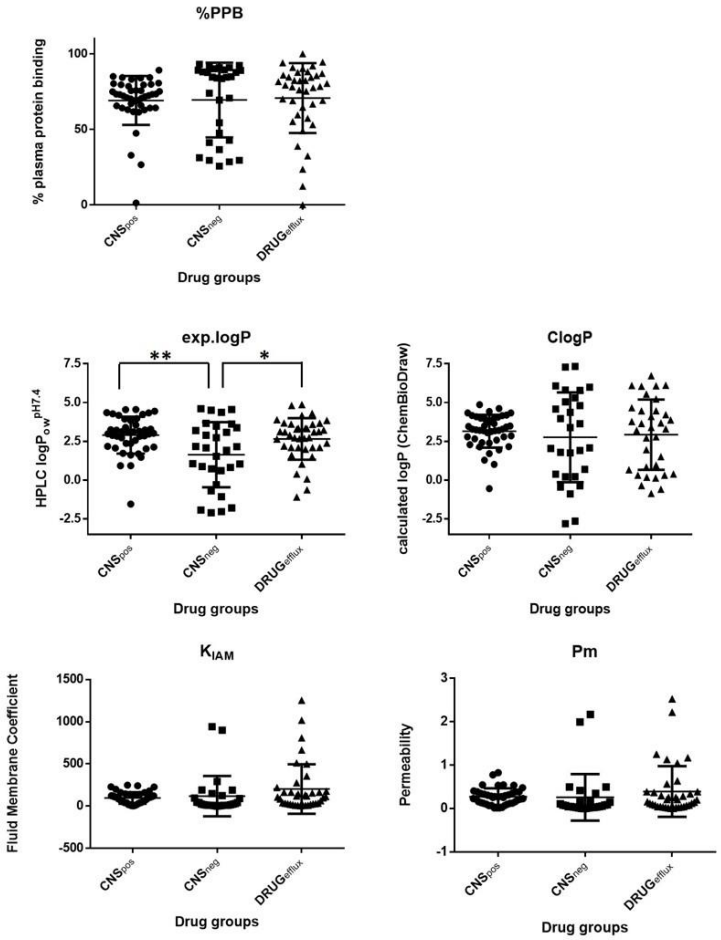

Fig.4. shows the comparison of the three groups (BBB penetrating compounds, not penetrating compounds and compounds interacting with efflux transporters by the mean values of the HPLC $logP_{ow}^{pH\ 7.4}$, ClogP, K_{IAM} and Pm using IAM-HPLC and %PPB using HSA-HPLC over the whole dataset:

The comparison of the group results of %PPB shows no significant difference between the groups (ordinary one-way ANOVA with Tukey correction, $P \leq 0.05$). Adjusted P values for multiple comparisons were greater than 0.9.

Statistical testing (ordinary one-way ANOVA with Tukey correction, $P \leq 0.05$) shows significance for the HPLC $logP_{ow}^{pH\ 7.4}$ value comparing BBB penetrating compounds versus non-penetrating compounds ($P = 0.002$) and non-penetrating drugs versus compounds interacting with efflux transporters ($P = 0.02$).

Whereas, there is no significant statistical difference between the groups for the ClogP (P values > 0.7).

Comparison of the K_{IAM} and the Pm results between the drug groups shows no significant difference (ordinary one-way ANOVA with Tukey correction, $P \leq 0.05$). Adjusted P values for multiple comparisons were greater than 0.09 for K_{IAM} and greater than 0.4 for Pm.

Table 1

Results of the HPLC $logP_{ow}^{pH7.4}$, the ClogP, the membrane coefficient (K_{IAM}), the permeability (Pm), plasma protein binding (%PPB) and LogK value of BBB penetrating compounds.

IUPAC	Product number	Trivial name	MEAN ±SD HPLC $logP_{ow}^{pH 7.4}$ [26]	ClogP [26]	MEAN ±SD K_{IAM} IAM-HPLC	MEAN ±SD Pm IAM-HPLC	MEAN ±SD %PPB HSA-HPLC	MEAN ±SD LogK HSA-HPLC
(E)-3-((6-methylpyridin-2-yl)ethynyl)cyclohex-3-enone O-methyl oxime	3570 ABX	**ABP688**	2.86 ±0.04 3.06 ±0.06	2.29	63 ±1	0.26 ±0.01	76 ±0.5 77 ± 1	0.47 ±0.01 0.51 ±0.02
3-(2-(4-(4-fluorobenzoyl)piperidin-1-yl)ethyl)-2-thioxo-2,3-dihydroquinazolin-4(1H)-one	1810 ABX	**Altanserin**	4.24 ±0.17	2.58	163 ±3	0.39 ±0.01	84 ±2	0.70 ±0.07
ethyl 8-azido-5-methyl-6-oxo-3a,4,5,6-tetrahydro-3H-benzo[f]imidazo[1,5-a][1,4]diazepine-3-carboxylate	1680 ABX	**Azidomazenil**	1.73 ±0.20	2.16	10 ±1	0.03 ±0.01	47 ±3	-0.05 ±0.05
(1R,2S,3S,5S)-methyl 3-(4-iodophenyl)-8-methyl-8-azabicyclo[3.2.1]octane-2-carboxylate	4030 ABX	**beta-CIT**	2.13 ±0.25	3.94	104 ±4	0.27 ±0.01	70 ±0.4	0.36 ±0.01
1-((9H-carbazol-4-yl)oxy)-3-(isopropylamino)propan-2-ol	2540 ABX	**(R,S)-Carazolol**	3.22 ±0.10	3.06	249 ±11	0.83 ±0.04	84 ±1	0.69 ±0.02
methyl 1-phenethyl-4-(N-phenylpropionamido)piperidine-4-carboxylate	2410 ABX	**Carfentanil oxalate**	3.29 ±0.11	3.73	141 ±1	0.29 ±0	71 ±1	0.37 ±0.02
(1R,2S,3S,5S)-methyl 8-(2-fluoroethyl)-3-(4-iodophenyl)-8-azabicyclo[3.2.1]octane-2-carboxylate	4110 ABX	**CITFE**	4.18 ±0.16	4.19	161 ±3	0.39 ±0.01	75 ±0.5	0.46 ±0.01
(1R,2S,3S,5S)-methyl 8-(3-fluoropropyl)-3-(4-iodophenyl)-8-azabicyclo[3.2.1]octane-2-carboxylate	4130 ABX	**CITFP**	4.44 ±0.19	4.42	145 ±5	0.35 ±0.01	72 ±1	0.40 ±0.01
(1R,2S,3S,5S)-methyl 8-(3-fluoropropyl)-3-(4-iodophenyl)-8-azabicyclo[3.2.1]octane-2-carboxylate	3751 ABX	**CPFPX**	2.83 ±0.06	3.19	40 ±1	0.12 ±0.00	73 ±0.4	0.42 ±0.01
3-amino-4-((2-((dimethylamino)methyl)phenyl)thio)benzonitrile	4310 ABX	**DASB**	3.84 ±0.11	3.21	136 ±4	0.48 ±0.01	76 ±0.5	0.48 ±0.01
2-(1-(6-((2-fluoroethyl)(methyl)amino)naphthalen-2-yl)ethylidene)malononitrile	5030 ABX	**DMFEAN**	4.54 ±0.42	3.42	83 ±2	0.28 ±0.01	80 ±2	0.59 ±0.02

IUPAC	Product number	Trivial name	MEAN ±SD HPLC $logP_{ow}^{pH\ 7.4}$ [26]	ClogP [26]	MEAN ±SD K_{IAM} IAM-HPLC	MEAN ±SD Pm IAM-HPLC	MEAN ±SD %PPB HSA-HPLC	MEAN ±SD LogK HSA-HPLC
(S)-N-((1-ethylpyrrolidin-2-yl)methyl)-5-iodo-2,3-dimethoxybenzamide	1522 ABX	**Epidepride**	2.73 ±0.06	3.46	109 ±4	0.23 ±0.01	63 ±3	0.31 ±0.06
(R)-ethyl 1-(1-phenylethyl)-1H-imidazole-5-carboxylate	1770 ABX	**(R)-Etomidate**	2.56 ±0.03	2.67	30 ±0.3	0.12 ±0	69 ±1	0.33 ±0.02
(S)-N-((1-allylpyrrolidin-2-yl)methyl)-1-(5-(3-fluoropropyl)-2,3-dimethoxyphenyl)ethenamine	1560 ABX	**Fallypride**	2.99 ±0.10	3.18	72 ±1	0.20 ±0	64 ±1	0.24 ±0.01
(1R,2S,3S,5S)-2-fluoroethyl 3-(4-iodophenyl)-8-methyl-8-azabicyclo[3.2.1]octane-2-carboxylate	4150 ABX	**2-FE-beta-CIT**	3.23 ±0.02	4.33	109 ±4	0.26 ±0.01	75 ±0.4	0.46 ±0.01
(S)-5-bromo-N-((1-ethylpyrrolidin-2-yl)methyl)-2,3-dimethoxybenzamide	1540 ABX	**FLB 457**	2.37 ±0.11	3.20	85 ±3	0.23 ±0.01	64 ±1	0.24 ±0.01
ethyl 8-fluoro-5-methyl-6-oxo-5,6-dihydro-4H-benzo[f]imidazo[1,5-a][1,4]diazepine-3-carboxylate	1710 ABX	**Flumazenil or Ro 15-1788**	0.93 ±0.31	1.29	7 ±0.5	0.02 ±0	33 ±8	-0.32 ±0.14
2-fluoroethyl 1-phenethyl-4-(N-phenylpropionamido)piperidine-4-carboxylate	2421 ABX	**Fluoroethyl-Carfentanil hydrochloride**	3.40 ±0.05	3.94	140 ±1	0.33 ±0	73 ±1	0.42 ±0.01
(R)-2-fluoroethyl 1-(1-phenylethyl)-1H-imidazole-5-carboxylate	1790 ABX	**(R)-Fluoroethyl-Etomidate (FETO)**	2.18 ±0.36	2.39	19 ±1	0.07 ±0	63 ±2	0.22 ±0.03
2-fluoroethyl 8-fluoro-5-methyl-6-oxo-5,6-dihydro-4H-benzo[f]imidazo[1,5-a][1,4]diazepine-3-carboxylate	1730 ABX	**Fluoroethylflumazenil (FFMZ)**	0.93 ±0.31	1.01	6 ±0.5	0.0 ±0	27 ±2	-0.45 ±0.04
3-(2-fluoroethyl)-8-(4-(4-fluorophenyl)-4-oxobutyl)-1-phenyl-1,3,8-triazaspiro[4.5]decan-4-one	1591 ABX	**Fluoroethyl-spiperone (FESP)**	3.97 ±0.14	3.64	243 ±5	0.55 ±0.01	80 ±0.3	0.58 ±0.01

IUPAC	Product number	Trivial name	MEAN ±SD HPLC $logP_{ow}^{pH\ 7.4}$[26]	ClogP [26]	MEAN ±SD K_{IAM} IAM-HPLC	MEAN ±SD Pm IAM-HPLC	MEAN ±SD %PPB HSA-HPLC	MEAN ±SD LogK HSA-HPLC
(6S,10bR)-6-(4-((fluoromethyl)thio)phenyl)-1,2,3,5,6,10b-hexahydropyrrolo[2,1-a]isoquinoline	4381 ABX	**(+)-Fluoromethyl-McN 5652**	4.35 ±0.18	4.34	101 ±5	0.32 ±0.01	89 ±2	0.88 ±0.08
1-fluoro-3-(2-nitro-1H-imidazol-1-yl)propan-2-ol	1410 ABX	**Fluoromisonidazole (FMISO)**	-1.54 ±0.66	-0.54	5 ±1	0.02 ±0.01	0	2.00
1-(1-(4-(4-fluorophenyl)-4-oxobutyl)piperidin-4-yl)-3-methyl-1H-benzo[d]imidazol-2(3H)-one	2760 ABX	**FNMB**	3.55 ±0.07	3.5	124 ±2	0.31 ±0.01	78 ±0.4	0.54 ±0.01
3-fluoro-5-(pyridin-2-ylethynyl)benzonitrile	3572 ABX	**FPEB Standard**	3.15 ±0.04	2.86	50 ±1	0.22 ±0	73 ±1	0.42 ±0.01
(R)-methyl 4-(2-(3,4-dichlorophenyl)acetyl)-3-(pyrrolidin-1-ylmethyl)piperazine-1-carboxylate	2070 ABX	**GR89696 fumarate**	3.02 ±0.04	4.17	116 ±3	0.22 ±0.01	72 ±0.5	0.40 ±0.01
7-methoxy-1-methyl-9H-pyrido[3,4-b]indole	1755 ABX	**Harmine**	2.98 ±0.02	3.13	82 ±0	0.39 ±0	79 ±0.3	0.57 ±0.01
(6S,10bR)-6-(4-(methylthio)phenyl)-1,2,3,5,6,10b-hexahydropyrrolo[2,1-a]isoquinoline	4370 ABX	**(+)-McN 5652**	4.33 ±0.17	4.16	121 ±6	0.41 ±0.02	85 ±0.2	0.72 ±0.01
2,3-dimethoxyphenyl)(1-(4-fluorophenethyl)piperidin-4-yl)methanol	1860 ABX	**MDL100151**	3.13 ±0.05	3.29	103 ±19	0.28 ±0.05	72 ±1	0.39 ±0.01
(R)-(2,3-dimethoxyphenyl)(1-(4-fluorophenethyl)piperidin-4-yl)methanol	1850 ABX	**MDL100907**	3.11 ±0.04	3.29	113 ±3	0.30 ±0.01	67 ±1	0.30 ±0.01
(R)-methyl 1-(1-phenylethyl)-1H-imidazole-5-carboxylate	1760 ABX	**(R)-Metomidate hydrochloride**	2.07 ±0.15	2.14	19 ±0.3	0.07 ±0	61 ±1	0.19 ±0.02
4-fluoro-N-(2-(4-(2-methoxyphenyl)piperazin-1-yl)ethyl)-N-(pyridin-2-yl)benzamide	3250 ABX	**MPPF**	2.83 ±0.06	3.49	43 ±0.4	0.10 ±0	71 ±1	0.37 ±0.01
(8aS,14bR)-7-(cyclopropylmethyl)-14-methyl-5,6,7,8,8a,9,14,14b-octahydro-4,8-methanobenzofuro[2,3-a]pyrido[4,3-b]carbazole-1,8a-diol	2810 ABX	**N-Methylnaltrindole**	4.28 ±0.17	2.42	229 ±8	0.54 ±0.02	83 ±0.5	0.67 ±0.01

IUPAC	Product number	Trivial name	MEAN ±SD HPLC $logP_{ow}^{pH 7.4}$ [26]	ClogP [26]	MEAN ±SD K_{IAM} IAM-HPLC	MEAN ±SD Pm IAM-HPLC	MEAN ±SD %PPB HSA-HPLC	MEAN ±SD LogK HSA-HPLC
2-(4-(methylamino)phenyl)benzo[d]thiazol-6-ol	5140 ABX	**6-OH-BTA-1 (free base) (PiB)**	3.94 ±0.19	3.70	200 ±4	0.78 ±0.02	84 ±0.1	0.70 ±0.01
(1R,2S,3S,5S)-methyl 8-((E)-3-iodoallyl)-3-(p-tolyl)-8-azabicyclo[3.2.1]octane-2-carboxylate	4170 ABX	**PE2I**	4.55 ±0.22	4.87	228 ±7	0.54 ±0.02	73 ±1	0.43 ±0.02
(4R,4aR,10bR)-9-hydroxy-4-propyl-3,4,4a,5,6,10b-hexahydro-2H-naphtho[1,2-b][1,4]oxazin-4-ium	1645 ABX	**(+)-PHNO hydrochloride**	2.00 ±0.16	2.79	39 ±0.2	0.16 ±0	62 ±1	0.20 ±0.02
N-(sec-butyl)-1-(2-chlorophenyl)-N-methylisoquinoline-3-carboxamide	1611 ABX	**(R,S)-PK11195**	3.25 ±0.03	4.62	123 ±2	0.35 ±0.05	80 ±0.2	0.57 ±0.01
(S)-3,5-dichloro-N-((1-ethylpyrrolidin-2-yl)methyl)-2-hydroxy-6-methoxybenzamide	1520 ABX	**Raclopride**	1.47 ±0.23	4.06	44 ±1	0.13 ±0	66 ±1	0.27 ±0.02
4-(3-(cyclopentyloxy)-4-methoxyphenyl)pyrrolidin-2-one	6000 ABX	**Rolipram**	1.69 ±0.20	1.71	19 ±0.4	0.07 ±0	64 ±1	0.24 ±0.02
(1-methylpiperidin-4-yl)methyl 8-amino-7-chloro-2,3-dihydrobenzo[b][1,4]dioxine-5-carboxylate	1882 ABX	**SB207145**	1.62 ±0.22	2.79	54 ±3	0.16 ±0.01	76 ±0.5	0.47 ±0.01
(R)-8-chloro-3-methyl-5-phenyl-2,3,4,5-tetrahydro-1H-benzo[d]azepin-7-ol	1464 ABX	**SCH-23390 hydrochloride**	3.11 ±0.03	3.24	180 ±4	0.55 ±0.01	81 ±0.3	0.60 ±0.01
6-(2-(4-(4-fluorobenzoyl)piperidin-1-yl)ethyl)-7-methyl-2H-thiazolo[3,2-a]pyrimidin-5(3H)-one	1830 ABX	**Setoperone**	2.36 ±0.15	1.95	39 ±1	0.10 ±0	66 ±1	0.27 ±0.02
N-(2-(4-(2-methoxyphenyl)piperazin-1-yl)ethyl)-N-(pyridin-2-yl)cyclohexanecarboxamide	W108-5MG, Sigma-Aldrich	**WAY-100635**	2.88 ±0.03	4.09	57 ±0.4	0.14 ±0	69 ±1	0.34 ±0.02
Total Mean			2.90 ±1.19	3.15 ±1.06	98 ±68	0.28 ±0.19	69 ±16	0.43 ±0.35

In the first column of **table 1** the IUPAC name of the tested compounds is given, whereas in column 3 the trivial names in alphabetical order are listed. Column 2 is showing the product number of the compounds. From column four to nine the mean results of HPLC $logP_{ow}^{pH7.4}$, ClogP, K_{IAM}, Pm, %PPB and LogK of BBB penetrating compounds with standard deviation are shown. All measurements were performed at least in a triplicate (n≥3). Total group means of the parameters are given in the last row. HPLC$ClogP_{ow}^{pH7.4}$ and the ClogP results were taken from a previously published manuscript [26].

Table 2

Results of the HPLC $logP_{ow}^{pH7.4}$, ClogP, the membrane coefficient (K_{IAM}), the permeability (Pm), plasma protein binding (%PPB) and LogK value of BBB non-penetrating compounds using high performance chromatography.

IUPAC	Product number	Trivial name	MEAN ±SD HPLC $logP_{ow}^{pH\ 7.4}$	ClogP	MEAN ±SD K_{IAM} IAM-HPLC	MEAN ±SD Pm IAM-HPLC	MEAN ±SD %PPB HSA-HPLC	MEAN ±SD LogK HSA-HPLC
1-{[(Cyclohexyloxy)carbonyl]oxy}ethyl 2-ethoxy-1-{[2'-(1H-tetrazol-5-yl)-4-biphenylyl]methyl}-1H-benzimidazole-7-carboxylate	SML0245-10MG	**Candesartan cilexetil**	3.38 ±0.08	7.34	95 ±17	0.16 ±0.03	91 ±0.1	0.95 ±0.01
(2S)-3-(3,4-Dihydroxyphenyl)-2-hydrazino-2-methylpropanoic acid	C1335-25MG	**Carbidopa**	-0.69 ±0.54	-0.45	n.q	n.q.	26 ±4	-0.47 ±0.10
4-[5-(4-Methylphenyl)-3-(trifluoromethyl)-1H-pyrazol-1-yl]benzenesulfonamide **[**	PZ0008-5MG	**Celecoxib**	3.66 ±0.08	4.37	191 ±8	0.5 ±0.02	89 ±0.04	0.88 ±0.00
(2-{4-[(4-Chlorophenyl)(phenyl)methyl]-1-piperazinyl}ethoxy)acetic acid	C3618-50MG	**Cetirizin**	2.08 ±0.14	2.08	12 ±7	0.03 ±0.05	74 ±0.5	0.44 ±0.01
5-Chloro-1-{1-[3-(2-hydroxy-1H-benzimidazol-1-yl)propyl]-4-piperidinyl}-1H-benzimidazol-2-ol	D122-25MG	**Domperidon**	3.20 ±0.03	4.80	148 ±8	0.34 ±0.02	85 ±0.3	0.71 ±0.01
(2E)-2-Cyano-3-(3,4-dihydroxy-5-nitrophenyl)-N,N-diethylacrylamide	SML0654-10MG	**Entacapone**	0.73 ±0.34	1.76	n.q	n.q.	92 ±0.4	1.03 ±0.02
(7α,17β)-7-{9-[(4,4,5,5,5-Pentafluoropentyl)sulfinyl]nonyl}estra-1(10),2,4-triene-3,17-diol	I4409-25MG	**Fulvestrant**	4.37 ±0.18	5.79	0.7 ±0.3	0.001 ±0	92 ±0.1	0.99 ±0.00
(3α,4α,5α,8α,9β,11α,13α,14β,16β,17Z)-16-Acetoxy-3,11-dihydroxy-4,8,14-trimethyl-18-norcholesta-17,24-dien-21-oic acid	F0756-1G	**Fusidic acid**	3.09 ±0.05	7.28	42 ±3	0.08 ±0.05	85 ±1	0.72 ±0.03
5-Chloro-N-[2-(4-{[(E)-(cyclohexylimino)(hydroxy)methyl]sulfamoyl}phenyl)ethyl]-2-methoxybenzenecarboximidic acid	G0639-5G	**Glibenclamide**	2.17 ±0.14	4.58	25 ±1	0.05 ±0.003	89 ±0.4	0.87 ±0.02

IUPAC	Product number	Trivial name	MEAN ±SD HPLC $logP_{ow}^{pH\ 7.4}$	ClogP	MEAN ±SD K_{IAM} IAM-HPLC	MEAN ±SD Pm IAM-HPLC	MEAN ±SD %PPB HSA-HPLC	MEAN ±SD LogK HSA-HPLC
3-Ethyl-4-methyl-N-[2-(4-{[(trans-4-methylcyclohexyl)carbamoyl]sulfamoyl}phenyl)ethyl]-2-oxo-2,5-dihydro-1H-pyrrole-1-carboxamide	G2295-50MG	**Glimepiride**	2.16 ±0.13	3.96	17 ±2.5	0.04 ±0.005	88 ±0.3	0.83 ±0.01
6-Chloro-3,4-dihydro-2H-1,2,4-benzothiadiazine-7-sulfonamide 1,1-dioxide	CS-O-30942	**Hydrochlorothiazide**	0.61 ±0.37	-0.36	9 ±3	0.029 ±0.088	48 ±1	-0.05 ±0.01
2-sec-Butyl-4-{4-[4-(4-{[(2R,4S)-2-(2,4-dichlorophenyl)-2-(1H-1,2,4-triazol-1-ylmethyl)-1,3-dioxolan-4-yl]methoxy}phenyl)-1-piperazinyl]phenyl}-2,4-dihydro-3H-1,2,4-triazol-3-one	I6657-100MG	**Itraconazole**	4.51 ±0.20	5.99	293 ±52	0.4 ±0.02	89 ±1	0.89 ±0.04
1-[4-(4-{[(2R,4S)-2-(2,4-Dichlorophenyl)-2-(1H-imidazol-1-ylmethyl)-1,3-dioxolan-4-yl]methoxy}phenyl)-1-piperazinyl]ethanone	K1003-100MG	**Ketoconazole**	3.48 ±0.09	3.64	90 ±12	0.17 ±0.02	84 ±0.1	0.71 ±0.00
8-(3-Amino-1-piperidinyl)-7-(2-butyn-1-yl)-3-methyl-1-[(4-methyl-2-quinazolinyl)methyl]-3,7-dihydro-1H-purine-2,6-dione	CS-O-30970	**Linagliptin**	1.54 ±0.22	1.91	42 ±1.2	0.09 ±0.03	71 ±1	0.37 ±0.02
Ethyl 4-(8-chloro-5,6-dihydro-11H-benzo[5,6]cyclohepta[1,2-b]pyridin-11-ylidene)-1-piperidinecarboxylate	L9664-10MG	**Loratadine**	3.62 ±0.09	5.05	192 ±11	0.5 ±0.03	88 ±0.1	0.82 ±0.00
3-[1-hydroxy-2-(methylamino)propyl]phenol	3400 ABX	**mHED / 3-[1-Hydroxy-2-(methylamino)propyl]phenol**	-2.10 ±0.73	0.22	10 ±2	0.05 ±0.02	37 ±6	-0.25 ±0.11
(5α,17R)-17-(Cyclopropylmethyl)-3,14-dihydroxy-17-methyl-6-oxo-4,5-epoxymorphinan-17-ium bromide	SML0277-5MG	**Methylnaltrexone bromide**	-1.79 ±0.69	-2.64	12 ±2	0.03 ±0	54 ±3	0.07 ±0.05
1-{2-[(2,4-Dichlorobenzyl)oxy]-2-(2,4-dichlorophenyl)ethyl}-1H-imidazole	PHR1618-1G	**Miconazol**	4.61 ±0.21	5.81	901 ±110	2.2 ±0.3	93 ±1	1.07 ±0.06
(2R,3S)-5-{2-Hydroxy-3-[(2-methyl-2-propanyl)amino]propoxy}-1,2,3,4-tetrahydro-2,3-naphthalenediol	N1892-1G	**Nadolol**	-1.07 ±0.58	0.38	14 ±2	0.05 ±0.01	29 ±1	-0.38 ±0.02

IUPAC	Product number	Trivial name	MEAN ±SD HPLC $logP_{ow}^{pH\ 7.4}$	ClogP	MEAN ±SD K_{IAM} IAM-HPLC	MEAN ±SD Pm IAM-HPLC	MEAN ±SD %PPB HSA-HPLC	MEAN ±SD LogK HSA-HPLC
(1R,2R,4S,5S,7s,9R)-9-Butyl-7-{[(2S)-3-hydroxy-2-phenylpropanoyl]oxy}-9-methyl-3-oxa-9-azoniatricyclo[3.3.1.$0^{2,4}$]nonane	S7882-1G	**N-Butylscopolamine**	-0.30 ±0.48	-0.89	24 ±3	0.07 ±0.01	41 ±2	-0.16 ±0.04
3-[(Dimethylcarbamoyl)oxy]-N,N,N-trimethylanilinium	N2001-1G	**Neostigmine**	-2.03 ±0.75	-2.81	4 ±0	0.02 ±0	29 ±2	-0.41 ±0.05
N-{[4-(5-Methyl-3-phenyl-1,2-oxazol-4-yl)phenyl]sulfonyl}propanamide	32152-25MG	**Parecoxib**	1.04 ±0.29	2.05	5 ±1	0.01 ±0	84 ±1	0.68 ±0.03
4-Butyl-1,2-diphenyl-3,5-pyrazolidinedione	79184-50MG	**Phenylbutazone**	0.82 ±0.32	3.39	7 ±1	0.02 ±0	84 ±3	0.70 ±0.09
2-Ethoxy-4-[2-({(1S)-3-methyl-1-[2-(1-piperidinyl)phenyl]butyl}amino)-2-oxoethyl]benzoic acid	R9028-50MG	**Repaglinid**	2.89 ±0.03	5.30	48 ±7	0.11 ±0.02	88 ±1	0.82 ±0.03
4-[4-(Methylsulfonyl)phenyl]-3-phenyl-2(5H)-furanone	SML0613-10MG	**Rofecoxib**	2.74 ±0.06	1.80	19 ±2	0.06 ±0.01	69 ±1	0.34 ±0.02
(3R,4S,5S,6R,7R,9R,10E,11S,12R,13S,14R)-6-{[(2S,3R,4S,6R)-4-(Dimethylamino)-3-hydroxy-6-methyltetrahydro-2H-pyran-2-yl]oxy}-14-ethyl-7,12,13-trihydroxy-4-{[(2R,4R,5S,6S)-5-hydroxy-4-methoxy-4,6-dimeth yltetrahydro-2H-pyran-2-yl]oxy}-10-{[(2-methoxyethoxy)methoxy]imino}-3,5,7,9,11,13-hexamethyloxacyclotetradecan-2-one	R4393-1G	**Roxithromycin**	0.88 ±0.32	n.c.	126 ±8	0.15 ±0.01	43 ±4	-0.13 ±0.06
(3R)-3-Amino-1-[3-(trifluoromethyl)-5,6-dihydro[1,2,4]triazolo[4,3-a]pyrazin-7(8H)-yl]-4-(2,4,5-trifluorophenyl)-1-butanone	Y0001812	**Sitagliptin**	1.06 ±0.30	0.69	31 ±1	0.08 ±0	31 ±2	-0.35 ±0.03
N-{4-[1-Hydroxy-2-(isopropylamino)ethyl]phenyl}methanesulfonamide	S0278-25MG	**Sotalol**	-1.93 ±0.71	0.23	11 ±1	0.04 ±0	30 ±3	-0.39 ±0.07
Ristomycin A 34-O-[2-(acetylamino)-2-deoxy-.beta.-D-glucopyranosyl]-22,31-dichloro-7-demethyl-64-O-demethyl-19-deoxy-56-O-[2-deoxy-2-[(8-methyl-1-oxononyl)amino]-.beta.-D-glucopyranosyl]-42-O-.alpha.-D-mannopyranosyl-	T0578-100MG	**Teicoplanin**	1.92 ±0.17	n.c.	11 ±4	0.01 ±0	90 ±0.1	0.92 ±0.00
4-{4-[Hydroxy(diphenyl)methyl]-1-piperidinyl}-1-[4-(2-methyl-2-propanyl)phenyl]-1-butanol	T9652-5G	**Terfenadine**	4.55 ±0.24	6.07	943 ±219	2 ±0.5	91 ±1	0.95 ±0.03

IUPAC	Product number	Trivial name	MEAN ±SD HPLC $logP_{ow}^{pH\ 7.4}$	ClogP	MEAN ±SD K_{IAM} IAM-HPLC	MEAN ±SD Pm IAM-HPLC	MEAN ±SD %PPB HSA-HPLC	MEAN ±SD LogK HSA-HPLC
Total Mean			1.6 ±2.1	2.76 ±2.89	119 ±238	0.26 ±0.54	69 ±25	0.47 ±0.58

In the first column of **table 2** the IUPAC names of the tested compounds are given, whereas in column 3 the trivial name in alphabetical order is given. Column 2 is showing the product number of the compounds. From column four to nine the mean results of HPLC logPowpH7.4, ClogP, KIAM, Pm, %PPB and LogK of BBB non-penetrating compounds with standard deviation are shown. Not calculable value (n.c.) and not quantifiable measurement (n.q.). All measurements were performed at least in a triplicate ($n \geq 3$). Total group means of the parameters are illustrated in the last row.

Table 3

Results of the HPLC $logP_{ow}^{pH7.4}$, ClogP, the membrane coefficient (K_{IAM}), the permeability (Pm), plasma protein binding (%PPB) and LogK value of compounds showing interactions to various efflux transporters.

IUPAC	Product number	Trivial name	MEAN ±SD HPLC $logP_{ow}^{pH\ 7.4}$	ClogP	MEAN ±SD K_{IAM} IAM-HPLC	MEAN ±SD Pm IAM-HPLC	MEAN ±SD %PPB HSA-HPLC	MEAN ±SD LogK HSA-HPLC
2-Amino-N,N'-bis[(6S,9R,10S,13R,18aS)-6,13-diisopropyl-2,5,9-trimethyl-1,4,7,11,14-pentaoxohexadecahydro-1H-pyrrolo[2,1-i][1,4,7,10,13]oxatetraazacyclohexadecin-10-yl]-4,6-dimethyl-3-oxo-3H-phenoxazin e-1,9-dicarboxamide	A1410-2MG	**Actinomycin D**	3.68 ±0.08	n.c.	121 ±4	0.1 ±0	65 ±1	0.25 ±0.02
(3S)-Tetrahydro-3-furanyl [(2S,3R)-4-{[(4-aminophenyl)sulfonyl](isobutyl)amino}-3-hydroxy-1-phenyl-2-butanyl]carbamate	SML0685-5MG	**Amprenavir**	2.69 ±0.06	3.29	40 ±0.1	0.08 ±0	70 ±0.1	0.36 ±0.00
N-{(1S)-2-[(3S)-3-Hydroxy-1-pyrrolidinyl]-1-phenylethyl}-N-methyl-2,2-diphenylacetamide	SML1261-5MG	**Asimadoline**	3.12 ±0.07	3.87	164 ±1	0.39 ±0	82 ±0.4	0.64 ±0.01
(3R,5R)-7-[2-(4-Fluorophenyl)-5-isopropyl-3-phenyl-4-(phenylcarbamoyl)-1H-pyrrol-1-yl]-3,5-dihydroxyheptanoic acid	PZ0001-5MG	**Atorvastatin**	2.38 ±0.10	4.46	20 ±1	0.04 ±0	82 ±0.3	0.65 ±0.01
2,2'-{9,10-Anthracenediylbis[(Z)methylylidene(2Z)-1-hydrazinyl-2-ylidene]}bis(4,5-dihydro-1H-imidazole)	B4563-10MG	**Bisantrene**	3.10 ±0.04	3.40	1017 ±32	2.5 ±0.08	100 ±0	2.00 ±0.00
1-Cyano-2-methyl-3-(2-{[(4-methyl-1H-imidazol-5-yl)methyl]sulfanyl}ethyl)guanidine	PHR1075	**Cimetidine**	-0.63 ±0.53	0.19	9 ±0.6	0.03 ±0.04	24 ±3	-0.38 ±0.06
(11β)-11,21-Dihydroxypregn-4-ene-3,20-dione	27840-100MG	**Corticosterone**	2.11 ±0.14	0.39	29 ±1	0.08 ±0.001	69 ±1	0.33 ±0.01
(3S,6S,9S,12R,15S,18S,21S,24S,30S,33S)-30-Ethyl-33-[(1R,2R,4E)-1-hydroxy-2-methyl-4-hexen-1-yl]-6,9,18,24-tetraisobutyl-3,21-diisopropyl-1,4,7,10,12,15,19,25,28-nonamethyl-1,4,7,10,13,16,19,22,25,28,3 1-undecaazacyclotritriacontane-2,5,8,11,14,17,20,23,26,29,32-undecone	30024-25MG	**Cyclosporin A**	4.31 ±0.20	n.c.	355 ±8	0.34 ±0.01	78.03 ±0.5	0.53 ±0.01

IUPAC	Product number	Trivial name	MEAN ±SD HPLC $logP_{ow}^{pH\ 7.4}$	ClogP	MEAN ±SD K_{IAM} IAM-HPLC	MEAN ±SD Pm IAM-HPLC	MEAN ±SD %PPB HSA-HPLC	MEAN ±SD LogK HSA-HPLC
(1S,3S)-3-Acetyl-3,5,12-trihydroxy-10-methoxy-6,11-dioxo-1,2,3,4,6,11-hexahydro-1-tetracenyl 3-amino-2,3,6-trideoxy-α-L-lyxo-hexopyranoside	D8809-1MG	**Daunorubicin**	3.34 ±0.10	0.84	177 ±4.4	0.34 ±0.01	88 ±1	0.82 ±0.04
(11β,16α)-9-Fluoro-11,17,21-trihydroxy-16-methylpregna-1,4-diene-3,20-dione	D1756-25MG	**Dexamethasone**	2.10 ±0.14	0.135	27 ±0.1	0.07 ±0	60 ±0.5	0.16 ±0.01
(3β,5β,12β)-3-{[2,6-Dideoxy-β-D-ribo-hexopyranosyl-(1->;4)-2,6-dideoxy-β-D-ribo-hexopyranosyl-(1->4)-2,6-dideoxy-β-D-ribo-hexopyranosyl]oxy}-12,14-dihydroxycard-20(22)-enolide	D6003-100MG	**Digoxin**	2.20 ±0.13	n.c.	11 ±0.3	0.01 ±0.01	0	0
(2S,3S)-5-[2-(Dimethylamino)ethyl]-2-(4-methoxyphenyl)-4-oxo-2,3,4,5-tetrahydro-1,5-benzothiazepin-3-yl acetate	D2521-1G	**Diltiazem**	2.89 ±0.04	3.65	86 ±1	0.2 ±0	69 ±1	0.34 ±0.02
(1S,3S)-3-Glycoloyl-3,5,12-trihydroxy-10-methoxy-6,11-dioxo-1,2,3,4,6,11-hexahydro-1-tetracenyl 3-amino-2,3,6-trideoxy-α-L-lyxo-hexopyranoside	44583-1MG	**Doxorubicin**	3.12 ±1.36	0.32	114 ±3	0.21 ±0.01	87 ±1	0.80 ±0.05
N-{4-[2-(6,7-Dimethoxy-3,4-dihydro-2(1H)-isoquinolinyl)ethyl]phenyl}-5-methoxy-9-oxo-9,10-dihydro-4-acridinecarboxamide	SML0486-10MG	**Elacridar/ GF120918**	4.86 ±0.25	4.21	1254 ±27	2.22 ±0.05	92 ±0.1	1.01 ±0.00
(1S,3S)-3-Glycoloyl-3,5,12-trihydroxy-10-methoxy-6,11-dioxo-1,2,3,4,6,11-hexahydro-1-tetracenyl 3-amino-2,3,6-trideoxy-α-L-arabino-hexopyranoside	E9406-5MG	**Epirubicin**	3.61 ±0.08	0.32	144 ±6	0.26 ±0.01	88 ±1	0.84 ±0.03
N-(3-Ethynylphenyl)-6,7-bis(2-methoxyethoxy)-4-quinazolinamine	CDS022564-10MG	**Erlotinib**	3.22 ±0.03	3.20	64 ±1.5	0.2 ±0	79 ±0.1	0.56 ±0.00
(5S,5aR,8aR,9R)-9-(4-Hydroxy-3,5-dimethoxyphenyl)-8-oxo-5,5a,6,8,8a,9-hexahydrofuro[3',4':6,7]naphtho[2,3-d][1,3]dioxol-5-yl 4,6-O-[(1R)-ethylidene]-β-D-glucopyranoside	E1383-25MG	**Etoposide**	1.57 ±0.22	0.0298	n.q.	n.q.	64.30 ±0.63	0.24 ±0.01

IUPAC	Product number	Trivial name	MEAN ±SD HPLC $logP_{ow}^{pH\ 7.4}$	ClogP	MEAN ±SD K_{IAM} IAM-HPLC	MEAN ±SD Pm IAM-HPLC	MEAN ±SD %PPB HSA-HPLC	MEAN ±SD LogK HSA-HPLC
2-[4-(1-Hydroxy-4-{4-[hydroxy(diphenyl)methyl]-1-piperidinyl}butyl)phenyl]-2-methylpropanoic acid	F9427-10MG	**Fexofenadine**	1.99 ±0.16	1.96	22 ±0.1	0.04 ±0	57 ±1	0.12 ±0.02
2'-(4-Ethoxyphenyl)-5-(4-methyl-1-piperazinyl)-1H,1'H-2,5'-bibenzimidazole	B2261-25MG	**Hoechst 33342**	3.29 ±0.07	6.04	512 ±56	1.13 ±0.1	95 ±0.2	1.16 ±0.02
(11β)-11,17,21-Trihydroxypregn-4-ene-3,20-dione	H4001-1G	**Hydrocortisone**	1.60 ±0.21	-0.86	17 ±0.16	0.05 ±0	49 ±1	-0.03 ±0.01
(2S)-1-[(2S,4R)-4-Benzyl-2-hydroxy-5-{[(1S,2R)-2-hydroxy-2,3-dihydro-1H-inden-1-yl]amino}-5-oxopentyl]-N-(2-methyl-2-propanyl)-4-(3-pyridinylmethyl)-2-piperazinecarboxamide	Y0000788	**Indinavir**	2.67 ±0.06	3.68	31 ±0.3	0.05 ±0	55 ±1	0.08 ±0.02
4-[4-(4-Chlorophenyl)-4-hydroxy-1-piperidinyl]-N,N-dimethyl-2,2-diphenylbutanamide	L4762-5G	**Loperamide**	3.59 ±0.08	4.66	499 ±18	1.1 ±0.04	85 ±0.1	0.71 ±0.00
(2S)-N-[(2S,4S,5S)-5-{[(2,6-Dimethylphenoxy)acetyl]amino}-4-hydroxy-1,6-diphenyl-2-hexanyl]-3-methyl-2-(2-oxotetrahydro-1(2H)-pyrimidinyl)butanamide	CDS022154-10MG	**Lopinavir**	3.66 ±0.08	6.10	164 ±3	0.26 ±0.01	86 ±0.1	0.75 ±0.00
(2-Butyl-4-chloro-1-{[2'-(1H-tetrazol-5-yl)-4-biphenylyl]methyl}-1H-imidazol-5-yl)methanol	61188-100MG	**Losartan**	1.50 ±0.23	4.10	5 ±0.1	0.01 ±0	82 ±0.3	0.62 ±0.01
(3S,4aS,8aS)-2-[(2R,3R)-2-Hydroxy-3-[(3-hydroxy-2-methylbenzoyl)amino]-4-(phenylsulfanyl)butyl]-N-(2-methyl-2-propanyl)decahydro-3-isoquinolinecarboxamide	CDS021783-50MG	**Nelfinavir**	3.85 ±0.11	3.77	665 ±7	1.17 ±0.01	91 ±0.1	0.96 ±0.00
2-[Benzyl(methyl)amino]ethyl methyl 2,6-dimethyl-4-(3-nitrophenyl)-1,4-dihydro-3,5-pyridinedicarboxylate	N7510-1G	**Nicardipine**	4.17 ±0.15	5.23	276 ±18	0.6 ±0.04	84 ±1	0.70 ±0.04

IUPAC	Product number	Trivial name	MEAN ±SD HPLC $logP_{ow}^{pH\ 7.4}$	ClogP	MEAN ±SD K_{IAM} IAM-HPLC	MEAN ±SD Pm IAM-HPLC	MEAN ±SD %PPB HSA-HPLC	MEAN ±SD LogK HSA-HPLC
9-Methyl-3-[(2-methyl-1H-imidazol-1-yl)methyl]-1,2,3,9-tetrahydro-4H-carbazol-4-one	O3639-10MG	**Ondansetron**	2.09 ±0.15	2.72	36 ±0.4	0.12 ±0	78 ±1	0.52 ±0.03
(4S,7S,13S)-7-Benzyl-3,3,14,14-tetramethyl-6,9,12-trioxo-13-(L-tyrosylamino)-1,2-dithia-5,8,11-triazacyclotetradecane-4-carboxylic acid	E3888-1MG	**[D-Penicillamine2,5]-enkephaline (DPDPE)**	0.39 ±0.39	0.97	n.q.	n.q.	32 ±1	-0.33 ±0.02
N^4-(6-Chloro-2-methoxy-9-acridinyl)-N^1,N^1-diethyl-1,4-pentanediamine	Q3251-25G	**Quinacrine**	3.89 ±0.12	6.72	156 ±5	0.39 ±0.01	94 ±0.4	1.13 ±0.03
(9S)-6'-Methoxycinchonan-9-ol	Q0750-5G	**Quinidine**	2.74 ±0.06	2.78	120 ±4	0.37 ±0.01	76 ±2	0.49 ±0.03
(E)-N-{2-[({5-[(Dimethylamino)methyl]-2-furyl}methyl)sulfanyl]ethyl}-N'-methyl-2-nitro-1,1-ethenediamine	R101-1G	**Ranitidine**	-1.09 ±0.59	0.67	9 ±0.4	0.03 ±0	53.00 ±1	0.04 ±0.01
6-Amino-9-[2-(methoxycarbonyl)phenyl]-3H-xanthen-3-iminium	83702-10MG	**Rhodamine123**	2.11 ±0.15	1.51	220 ±8	0.6 ±0.02	85 ±0.3	0.74 ±0.01
(1E,2S)-N-[(2S,4S,5S)-4-Hydroxy-5-{(E)-[hydroxy(1,3-thiazol-5-ylmethoxy)methylene]amino}-1,6-diphenyl-2-hexanyl]-2-[(E)-(hydroxy{[(2-isopropyl-1,3-thiazol-4-yl)methyl](methyl)amino}methylene)amino]-3-methylbutanimidic acid	SML0491-10MG	**Ritonavir**	3.32 ±0.20	6.10	108 ±3	0.15 ±0	82 ±0.1	0.64 ±0.00
N-[2-(3,4-Dimethoxyphenyl)ethyl]-N-methyl-3-[2-(2-naphthyl)-1,3-dithian-2-yl]-1-propanamine	112933-5G	**Ro 11-2933/ Acetanilide**	0.07 ±0.43	6.11	9 ±0.1	0.02 ±0	12 ±3	-0.86 ±0.12
N-[2-({4-[2-(6,7-Dimethoxy-3,4-dihydro-2(1H)-isoquinolinyl)ethyl]phenyl}carbamoyl)-4,5-dimethoxyphenyl]-3-quinolinecarboxamide	HY-10550A	**Tariquidar**	4.81 ±0.24	5.55	809 ±47	1.25 ±0.07	90 ±0.2	0.92 ±0.01
(5S,5aR,8aR,9R)-9-(4-Hydroxy-3,5-dimethoxyphenyl)-8-oxo-5,5a,6,8,8a,9-hexahydrofuro[3',4':6,7]naphtho[2,3-d][1,3]dioxol-5-yl 4,6-O-(2-thienylmethylene)-β-D-glucopyranoside	SML0609-10MG	**Teniposide**	2.65 ±0.06	-0.58	34 ±0.5	0.05 ±0	80 ±0.2	0.59 ±0.00

IUPAC	Product number	Trivial name	MEAN ±SD HPLC $logP_{ow}^{pH\ 7.4}$	ClogP	MEAN ±SD K_{IAM} IAM-HPLC	MEAN ±SD Pm IAM-HPLC	MEAN ±SD %PPB HSA-HPLC	MEAN ±SD LogK HSA-HPLC
(11β,16*α*)-9-Fluoro-11,16,17,21-tetrahydroxypregna-1,4-diene-3,20-dione	T6376-50MG	**Triamcinolone**	1.03 ±0.29	-0.35	10 ±0.3	0.03 ±0	39 ±0.5	-0.20 ±0.01
2-(3,4-Dimethoxyphenyl)-5-{[2-(3,4-dimethoxyphenyl)ethyl](methyl)amino}-2-isopropylpentanenitrile hydrochloride (1:1)	V4629-1G	**(±)-Verapamil hydrochloride**	3.34 ±0.04	4.47	132 ±2	0.29 ±0.01	78 ±1	0.54 ±0.01
dimethyl (2β,3β,4β,5*α*,12β,19*α*)-15-[(5*S*,9*S*)-5-ethyl-5-hydroxy-9-(methoxycarbonyl)-1,4,5,6,7,8,9,10-octahydro-2*H*-3,7-methanoazacycloundecino[5,4-b]indol- 9-yl]-3-hydroxy-16-methoxy-1-methyl-6,7-didehydroaspidospermidine-3,4-dicarboxylate	V1377-1MG	**Vinblastine**	3.10 ±0.05	n.c.	164 ±4	0.2 ±0	75 ±1	0.47 ±0.01
(3a*R*,3a1*R*,4*R*,5*S*,5a*R*,10b*R*)-Methyl 4-acetoxy-3a-ethyl-9-((5*S*,7*S*,9*S*)-5-ethyl-5-hydroxy-9-(methoxycarbonyl)-2,4,5,6,7,8,9,10-octahydro-1*H*-3,7-methano[1]azacycloundecino[5,4-*b*]indol-9-yl)-6-formyl-5-hydroxy-8-methoxy-3a,3a1,4,5,5a,6,11,12-octahydro-1*H*-indolizino[8,1-cd]carbazole-5-carboxylate	V8388-1MG	**Vincristine**	2.73 ±0.06	n.c.	99 ±0.9	0.12 ±0	67 ±1	0.29 ±0.02
Total Mean			2.7 ±1.3	2.9 ±2.3	203 ±292	0.40 ±0.58	71 ±23	0.48 ±0.5

In the first column of **table 3** the IUPAC names of the tested compounds are given, whereas in column 3 the trivial name in alphabetical order is given. Column 2 is showing the product number of the compounds. From column four to nine the mean results of HPLC $logP_{ow}^{pH7.4}$, ClogP, K_{IAM}, Pm, %PPB, LogK of compounds which interact with efflux transporters with standard deviation are shown. Not calculable value (n.c.) and not quantifiable measurement (n.q.). All measurements were performed at least in a triplicate (n≥3). Total group means of the parameters are illustrated in the last row.

Table S1

Relative standard deviation (RSD%) of all injections of IAM chromatography for each method (different acetonitrile and buffer content) for CNS positive compounds.

Trivial name	RSD % Injection shift 50/50	RSD % Injection shift 55/45	RSD % Injection shift 60/40	RSD % Injection shift 65/35
ABP688	0.6	0.4	1.0	1.2
Altanserin	1.5	1.0	1.1	0.8
Azidomazenil	0	0.4	0	2.6
beta-CIT	2.1	1.6	1.6	2.2
(R,S)-Carazolol	0.1	1.8	1.9	2.5
Carfentanil oxalate	0.6	6.4	6.7	0.5
CITFE	0.4	0.4	0.7	1.0
CITFP	0.4	0.9	1.3	2.4
CPFPX	0.4	0.4	0.6	0.7
DASB	0.7	0.8	0.3	1.9
DMFEAN	0.5	1.0	1.5	1.1
Epidepride	2.1	1.9	1.9	2.5
(R)-Etomidate	0.9	3.3	0.5	0.5
Fallypride	0.3	0.5	0.5	0.7
2-FE-beta-CIT	1.6	1.5	1.5	2.3
FLB 457	1.9	1.7	1.8	2.4

Trivial name	RSD % Injection shift 50/50	RSD % Injection shift 55/45	RSD % Injection shift 60/40	RSD % Injection shift 65/35
Flumazenil or Ro 15-1788	0.4	1.6	0.5	1.6
Fluoroethyl-Carfentanil hydrochloride	0.9	0.9	0.5	0.4
(R)-Fluoroethyl-Etomidate (FETO)	1.5	5.3	0.4	0.7
Fluoroethylflumazenil (FFMZ)	1.2	0.5	0.2	0.8
Fluoroethyl-spiperone (FESP)	0.6	0.7	0.4	1.4
(+)-Fluoromethyl-McN 5652	2.0	1.8	2.1	3.1
Fluoromisonidazole (FMISO)	4.8	8.2	5.0	6.2
FNMB	0.7	0.7	0.2	0.8
FPEB Standard	0.4	0.8	0.5	0.6
GR89696 fumarate	0.9	0.5	1.4	1.6
Harmine	0.7	0.7	0.3	0.2
(+)-McN 5652	2.2	2.3	2.2	3.5
MDL100151	0.7	1.0	1.4	2.0
MDL100907	0.9	0.7	1.3	1.9

Trivial name	RSD % Injection shift 50/50	RSD % Injection shift 55/45	RSD % Injection shift 60/40	RSD % Injection shift 65/35
(R)-Metomidate hydrochloride	0.8	6.2	0.7	1.3
MPPF	0.5	0.4	0.5	0.4
N-Methylnaltrindole	0.9	1.2	1.5	2.4
6-OH-BTA-1 (free base) (PiB)	1.1	2.2	1.4	1.7
PE2I	0.2	0.6	0.6	2.0
(+)-PHNO hydrochloride	0.4	0.4	0.3	0.3
(R,S)-PK11195	0.3	1.0	0.9	0.9
Raclopride	0.8	0.5	0.9	0.9
Rolipram	0.6	0.4	0.2	0.5
SB207145	1.9	2.0	2.1	2.8
SCH-23390 hydrochloride	1.2	1.0	0.8	1.9
Setoperone	0.7	0.2	0.4	1.1
WAY-100635	0.4	0.5	0.5	0.4

Table S2

Relative standard deviation (RSD%) of all injections of IAM chromatography for each method (different acetonitrile and buffer content) for CNS negative compounds.

Trivial name	RSD % Injection shift 50/50	RSD % Injection shift 55/45	RSD % Injection shift 60/40	RSD % Injection shift 65/35
Candesartan cilexetil	2.3	2.1	3.7	4.9
Celecoxib	12.7	12.6	9.9	5.4
Cetirizin	6.1	3.0	4.1	2.6
Domperidon	13.3	12.6	9.4	7.10
Fulvestrant	1.1	1.2	1.1	1.2
Fusidic acid	3.9	4.7	2.5	3.8
Glibenclamide	5.1	6.3	4.4	5.3
Glimepiride	4.8	4.5	6.3	2.3
Hydrochlorothiazide	2.2	11.3	10.7	3.0
Itraconazole	2.8	5.2	6.2	4.7
Ketoconazole	9.4	12.2	9.9	11.7
Linagliptin	6.7	6.1	4.5	3.9
Loratadine	13.3	13.8	10.4	6.9
mHED / 3-[1-Hydroxy-2-(methylamino)propyl]phenol	1.6	2.4	2.5	3.7
Methylnaltrexone bromide	3.9	4.3	4.5	5.1
Miconazol	2.6	3.1	6.3	3.6
Nadolol	3.0	2.9	3.5	3.7
N-Butylscopolamine	3.3	3.1	1.9	3.0
Neostigmine	0.9	0.2	0.2	0.5
Parecoxib	1.4	1.6	2.7	1.4
Phenylbutazone	1.5	2.4	1.8	2.2
Repaglinid	4.7	7.2	5.9	6.5
Rofecoxib	3.1	9.4	3.5	3.8
Roxithromycin	10.7	10.0	7.9	6.8
Sitagliptin	6.9	7.0	5.7	4.8
Sotalol	1.2	1.3	1.4	1.7
Teicoplanin	1.4	1.5	2.3	1.2
Terfenadine	1.2	1.3	2.0	15.1

Table S3

Relative standard deviation (RSD%) of all injections of IAM chromatography for each method (different acetonitrile and buffer content) for Drugs interacting with efflux transporters.

Trivial name	RSD% Injection shift 50/50	RSD% Injection shift 55/45	RSD% Injection shift 60/40	RSD% Injection shift 65/35
Actinomycin D	0.4	0.2	0.5	2.7
Amprenavir	0.3	0.2	0.3	0
Asimadoline	0.6	0.8	1.1	1.0
Atorvastatin	0.6	0.2	1.1	1.4
Bisantrene	2.4	4.2	2.3	3.8
Cimetidine	0.4	0	2.7	0.2
Corticosterone	0	0.4	0.0	0.7
Cyclosporin A	0.6	0.8	1.4	1.9
Daunorubicin	0.3	0.6	0.8	1.6
Dexamethasone	0.24	0	0.3	0.2
Digoxin	0.3	0.3	2.5	0.2
Diltiazem	0.7	0.8	0.9	1.0
Doxorubicin	2.3	2.1	3.0	1.8
Elacridar/ GF120918	2.8	2.4	0.3	2.5
Epirubicin	2.6	1.4	1.9	2.4
Erlotinib	0.2	0.8	0.7	1.5
Fexofenadine	0	0.1	0.1	0.2
Hoechst 33342	2.6	5.0	5.4	6.9
Hydrocortisone	0.2	0.0	0.2	0.3
Indinavir	0.2	0.1	0.5	0.4
Loperamide	0.2	1.1	4.2	2.4
Lopinavir	0.2	0.8	1.2	1.6
Losartan	0.6	0.4	0.8	0.5
Nelfinavir	1.5	2.3	1.3	0.8
Nicardipine	1.0	1.1	1.6	5.8
Ondansetron	0.5	0.7	0.8	0.6
Quinacrine	0.8	1.6	1.2	2.2
Quinidine	2.5	1.8	2.9	2.5
Ranitidine	0.5	1.0	1.0	0.9
Rhodamine123	2.4	3.4	3.3	3.1
Ritonavir	0.5	0.9	1.2	1.9
Ro 11-2933/ Acetanilide	0	0.2	0.1	0.2
Tariquidar	1.4	1.8	1.7	6.0
Teniposide	0.2	0.5	0.7	0.6
Triamcinolone	0.5	0.2	0.2	0.2
(±)-Verapamil hydrochloride	1.4	2.1	2.4	1.5
Vinblastine	1.1	3.4	2.2	1.9
Vincristine	0.5	0.8	1.0	0.6

Table S4

Comparison of K_{IAM} values using extrapolation or using the retention time of 100% aqueous phase.

Compound	K_{IAM} extrapolated	K_{IAM} of 100% buffer
mHED	10	51
Hydrochlorothiazide	9	101
Methylnaltrexone bromide	12	149

Table S5

Comparison of K_{IAM} values using different amounts data points (runs) for extrapolation

	DASB
K_{IAM} extrapolated (4 data points)	136
K_{IAM} extrapolated (first, second & third data point)	105
K_{IAM} extrapolated (second, third & fourth data point)	158
K_{IAM} extrapolated (third & fourth data point)	229

3.1.4 Manuscript IV

Vraka C, Dumanic M, Racz T, Pichler F, Philippe C, Balber T, Klebermass EM, Wagner KH, Hacker M, Wadsak W, Mitterhauser M. A New Model for the Prediction of the Interaction of Radiotracers with the P-glycoprotein (P-gp) transporter. Submitted, 2017 November 13th, Journal of Nuclear Medicine and Biology(NUCMEDBIO_2017_285).

A New Model for the Prediction of the Interaction of Radiotracers with the P-glycoprotein (P-gp) Transporter

Authors: Chrysoula Vraka[1,2], Monika Dumanic[1], Teresa Racz[1], Florian Pichler[1,3], Cecile Philippe[1], Theresa Balber[1,6], Eva-Maria Klebermass[1], Karl-Heinz Wagner[2], Marcus Hacker[1], Wolfgang Wadsak[1,4,5] and Markus Mitterhauser[1,6,7]

Affiliation

[1]*Department of Biomedical Imaging and Image-guided Therapy, Division of Nuclear Medicine, Medical University of Vienna, Vienna, Austria*
[2]*Department for Nutritional Science, University of Vienna, Vienna, Austria*
[3]*Department of Engineering, University of Applied Sciences Wiener Neustadt, Austria*
[4]*Department of Inorganic Chemistry, University of Vienna, Vienna, Austria*
[5]*CBmed, Graz, Austria*
[6]*Department of Pharmaceutical Technology and Biopharmaceuticals (PTB), University of Vienna, Vienna, Austria*
[7]*Ludwig Boltzmann Institute Applied Diagnostics, Vienna, Austria*

This work was supported by the Austrian Science Fund (FWF P26502-B24, M. Mitterhauser).

*Corresponding author:
Prof. Dr. Markus Mitterhauser
Ludwig Boltzmann Institute Applied Diagnostics, Vienna, Austria
General Hospital of Vienna
Waehringer Guertel 18-20
A-1090 Vienna / AUSTRIA
Email: markus.mitterhauser@meduniwien.ac.at
Telephone: +43 1 40400 55340
Fax: +43 1 40400 15590

Abstract

In drug development, biomarkers for cerebral applications have a lower success rate compared to cardiovascular drugs or tumor therapeutics. One reason is the missing blood brain barrier penetration, caused by the tracer's interaction with efflux transporters such as the P-gp (MDR1 or ABCB1). Aim of this study was the development of a reliable model to predict the interaction of radiotracers with the human efflux transporter P-gp at an early stage of development. LigandTracer Technology® was used with the wildtype cell line MDCKII and the equivalent cell line overexpressing human P-gp (MDCKII-hMDR1). The method was evaluated based on established PET tracers with known interaction with the human P-gp transporter and in nanomolar concentration (15nM). [^{11}C]SNAP-7941 and [^{18}F]FE@SNAP were classified as P-gp substrates by comparing the real-time model with an uptake assay and µPET images. [^{11}C]DASB [^{11}C]Harmine, [^{18}F]FMeNER and [^{18}F]FE@SUPPY were classified as tracers without interactions with P-gp. For [^{11}C]Me@HAPTHI, we hypothesize an *in vivo* interaction with the efflux transporter BCRP. The developed real-time kinetic model uses directly PET tracers in a compound concentration, which is reflecting the *in vivo* situation. This method may be used at an early stage of radiopharmaceutical development to predict interactions to P-gp before conducting animal experiments.

Keywords: ABCB1, efflux transporter, MDR1, PET tracer, P-gp-substrate.

Introduction

According to the World Health Organization, there is an incident rate of ~1:4 to suffer from mental disorders once in a lifetime. Currently, more than 450 million people worldwide are affected [1]. Still, none of these disorders are fully understood and the underlying neurobiology changes and the pathway of medication are discussed controversially. Positron emission tomography (PET) is currently the most sensitive and specific imaging technique for the quantification of these biochemical changes of the involved neurotransmitter systems, since it contributes to the elucidation with minimal invasive effort. Therefore, the demand of PET tracers targeting the brain is expanding rapidly. In comparison to drugs targeting cancer or cardiovascular diseases, medications for the central nervous system (CNS) have a lower success rate (< 15% in phase III compared to > 30%)[2]. Pardridge et al. stated that about ~98% of all small molecules are not transported through the blood brain barrier (BBB)[3]. In addition, central uptake of exogenous compounds is limited by efflux transporters[4,5].

Efflux transporters belong to the ATP binding cassette (ABC) super family and can be found in organs of mammalian species ubiquitously. Furthermore, ABC efflux transporters were found in a plethora of tumor membranes thereby limiting effective therapies with cytotoxic agents and targeted anticancer drugs (multiple drug resistance)[6–9]. Therefore, efflux transporters are significantly involved in drug pharmacokinetics. The most relevant efflux transporter is the permeability glycoprotein (P-gp), also known as MDR1 (genetic name) or ABCB1 (family name). Interestingly, a wide range of P-gp substrates with different chemical structures and pharmacological functions are known (e.g. anticancer drugs, protease inhibitors, peptides, steroids, calcium channel blockers and antihistamines)[9,10]. Solely based on structure or chemical properties, an upfront identification of P-gp substrates is impossible. For that reason, there is a need for *in vitro* technologies that reliably predict interactions between newly developed drugs and the efflux transporter P-gp already at early

stages of PET tracer development.

Objective of the study was to set up a real-time kinetic model to distinguish between P-gp-substrates and biomarkers without any interaction with the human P-gp (hMDR1) transporter.

Materials & Methods

Animal preparation

All procedures and protocols using animals were conducted in compliance and approval by the Institutional Animal Care and Use Committee of the Medical University of Vienna, Austria, as well as by the Austrian Ministry of Science, Research and Economy (BMWFW-66.009/0029-WF/V/3b/2015; BMWFW-66.009/0209-WF/V/3b/2015). The manuscript adheres to the Directive European law (2010/63/EU) and to the ARRIVE guidelines for reporting animal experiments.

Real-time kinetic model

The Madin-Darby Canine Kidney cell line, overexpressing human P-gp, (MDCKII-hMDR1) and the MDCKII-wildtype (MDCKII-WT) cell lines were purchased from the Netherlands Cancer Institute (NKI, Amsterdam, Netherlands). MDCKII-hMDR1 and MDCKII-WT cell lines were cultivated in DMEM GlutaMAX™ (Gibco® 61965-026), 10% FCS (Gibco® 10270-106) and 0.5% Pen/Strep (Gibco® 15140). 2.5 x 10^5 cells were seeded two days before experiments in the oblique plane of a cell culture dish (100/20mm, Greiner Bio-one, cellstar 664160) to allow attachment to only one side of the dish. After 24 hours, the cell culture dishes were positioned horizontally. Prior to experiments, cells were treated with serum free medium to avoid unspecific binding of the tracer to fetal calf serum. For the blocking experiments on theMDCKII-hMDR1 cells (±)-Verapamil hydrochloride purchased from Sigma Aldrich (St. Louis, Missouri, USA) diluted in DMSO was used. To avoid effects of Verapamil, the MDCKII-WT cells were also treated with (±)-Verapamil hydrochloride in DMSO. Blocking concentration was 10µM and concentration of organic solvent was less than 0.5%. For the assessment of P-gp binding or P-gp mediated transport, real-time kinetics with the PET tracers [^{18}F]FE@SNAP, [^{18}F]FE@SUPPY, [^{11}C]SNAP-7941, [^{18}F]FMeNER-D2, [^{11}C]DASB, [^{11}C]Harmine and [^{11}C]Me@HAPTHI were performed using

LigandTracer®Yellow and LigandTracer®White technology (Ridgeview Instruments AB, Uppsala, Sweden). During one revolution of the petri dish, two positions were measured for 3 seconds with a delay of 2 seconds. One of these positions (within the cell pole) serves as signal- and the other (cell free area) as background measurement. Appropriate tracer concentrations (0.1-625 nM) were added within the linearity range of the instrument's detector. The results with 15 nM compound concentration were used for comparison of the different tracer kinetics. Calculations and drafting of the kinetics were performed by using GraphPadPrism Version 6.01 © 1992-2012 GraphPad Software, Inc. (CA, USA). Single results are represented as CPS over time, whereas overall mean results are normalized to % signal of the maximum CPS.

Conventional internalization experiments

MDCKII-WT and MDCKII-hMDR1 cells were cultivated in 6-well plates ($1x10^5$ cells per well) two days prior to the experiments. One hour before the experiments, cells were washed with DPBS (Gibco® 14190-094) and serum free medium was added. The cells were incubated with the tracers [^{11}C]SNAP-7491 or [^{18}F]FE@SNAP. In an additional setup, both cell lines were treated with 10 µM (±)-Verapamil hydrochloride (DMSO < 0.5%) for 0.5 h before the respective tracer was added. After tracer incubation for 0.5 h, the medium was removed, the cells were washed with 1 mL DPBS, scratched off and removed from the well with an additional washing step. The cell fraction and the supernatant were counted in the calibrated Gamma-Counter (Perkin Elmer, Waltham, Massachusetts, USA), calibrated for [^{18}F]fluoride and [^{11}C]carbon. Furthermore, the internalization protocol for [^{11}C]SNAP-7941 was performed with additional washing steps with glycine buffer to account for unspecific binding of the tracer at the membrane surface[11]. The data were processed with Microsoft Excel Version 14.00 © Microsoft Cooperation (WA, USA) or GraphPadPrism Version 6.01 © 1992-2012 GraphPad Software, Inc. (CA, USA).

µPET imaging

In vivo imaging experiments were conducted with a small animal computed tomography (CT) and positron emission tomography (PET) scanner (Siemens Inveon Multimodal µSPECT/CT, dedicated µPET; Siemens Medical Solutions, Knoxville, USA). Twelve to fourteen weeks old male Sprague Dawley rats (HIM:OFA, Himberg, Austria) weighing 420 ± 42 g were kept under controlled laboratory conditions (22 ± 1°C; 12 hours light/dark cycle) with food and water access *ad libitum*. Anesthetized rats (1.5–2% isoflurane vaporized in oxygen 1 – 1.5 L/min) were prepared for the imaging experiments and positioned in the center of the field of view. Physiological parameters and the depth of anesthesia were constantly monitored and adapted throughout the experiment. All animals received the P-gp/BCRP inhibitor tariquidar methanesulfonate, hydrate (TQD, HY-10550A, MedChemExpress Europe, Sollentuna, Sweden) (15 mg/kg body weight; 500 µL intravenously) or 2.5 % glucose solution as vehicle 60 min before the administration (i.v.) of the respective radiotracer ([^{11}C]SNAP-7941 [12]; [^{18}F]FE@SNAP, 46.62 ± 5.63 MBq, molar activity: 210.9 ± 240.6 GBq/µmol (range: 28.2-627.3 GBq/µmol); [^{11}C]ME@HAPHTI, 54.852 ± 4.89 MBq, mol. activity.: 43.9 ± 33.8 GBq/µmol (range: 20-87.6 GBq/µmol)). Once the radioligands were administered through the lateral tail vein, the PET data acquisition took 45 to 60 min to allow tracer kinetics to attain full equilibration. For statistical relevance, experiments were performed in triplicate.

The CT data was corrected for beam-hardening. PET list mode data was sorted into three-dimensional sinograms and reconstructed using an OSEM3D/OP-MAP with scatter and attenuation correction. All relevant corrections (e.g. normalization, dead time, random) for quantitative PET data were performed. Image data analysis was carried out using the Inveon Research Workplace (IRW; Siemens Medical Solutions, Knoxville, USA). Volumes of interest (VOIs), comprising the brain of rats was outlined on the CT and transferred to the PET images. Time–activity curves (TACs) were calculated and expressed as standardized uptake values normalized to the body weight of the animal (SUV_{BW}).

Radiosynthesis

[^{18}F]FE@SNAP, [^{18}F]FMeNER-D2, [^{18}F]FE@SUPPY, [^{11}C]SNAP-7941, [^{11}C]Me@HAPTHI, [^{11}C]DASB and [^{11}C]Harmine were synthesized following previously published procedures [13–19].

Results

Real-time kinetic model

At all used concentrations (0.1 to 625 nM), qualitative and reproducible results were obtained (uptake or no uptake) for all tested PET tracers. For quantification of the kinetics, only experiments using 15 nM concentration of the respective tracer were taken into account.

P-gp substrates

The direct comparison of the curves shows different uptake behavior for **[**^{18}F]FE@SNAP and [^{11}C]SNAP-7941 in the three described experimental setups: A clear uptake of the respective tracers was visible in the MDCKII-WT cells. A significant uptake on the cell side was also obtained when MDCKII-hMDR1 cells were treated with (±)-Verapamil (pre-blocking). On the other hand, no cell uptake was measured on untreated MDCKII-hMDR1 cells.

Fig. 1 illustrates the kinetics of [^{11}C]SNAP-7941 (signal in [CPS]). (A) shows the kinetics on MDCKII-WT cells. (B) shows the signal on the MDCKII-hMDR1 cells, where the transporter was blocked with (±)-Verapamil. (C) exemplifies that the signal of the tracer on the P-gp transporter expressing cell line is due to unspecific accumulation. The red signal represents the background measurement (plastic surface of the petri dish) and the blue signal the kinetics of the tracers on the target area (cells), whereas the black signal shows the corrected signal (target minus background).

When all results with 15 nM of tracer concentration were superimposed, both compounds exhibited a comparable kinetic on the MDCKII-WT cell line as well as on the MDCKII-hMDR1 cells, where P-gp was inhibited with (±)-Verapamil (figure 2A). In contrast, for the MDCKII-hMDR1 cells both PET tracers showed no uptake (diffuse widespread signal, cf. figure 2B).

Fig. 2 shows the uptake of [^{18}F]FE@SNAP (n=7) and [^{11}C]SNAP-7941 (n=6) on the MDCKII-wildtype and MDCKII-hMDR1 cells pre-blocked with (±)-Verapamil (means of the experiments, normalized to 100% uptake, standard deviations are illustrated with red bars (A)) and the non-treated hMDR1 cell line (B).

Compounds with no interaction with the P-gp transporter

No difference was observed regarding the kinetics of [^{11}C]Harmine, [^{11}C]DASB, [^{11}C]Me@HAPTHI, [^{18}F]FE@SUPPY and [^{18}F]FMeNER-D2 (figure 3 and 4). In figure 3, exemplary curves are presented for [^{11}C]Harmine. An uptake can be observed after background subtraction on both cell lines.

Fig. 3 exemplifies the kinetics of the PET tracer [^{11}C]Harmine, which is known to have no interactions with the P-gp transporter. The red signal represents the background measurement (plastic surface of the petri dish) and the blue signal the kinetics of the tracers on the target area (cells), whereas the black signal shows the corrected signal (target minus background). There are no differences displayed in the kinetics at all examined setups (A-C).

In direct comparison, overall overlaid and normalized results (figure 4) show no differences in the uptake behavior or the kinetics of [^{11}C]Harmine, [^{11}C]DASB, [^{18}F]FE@SUPPY and [^{18}F]FMeNER-D2 (figure 4A).

Fig. 4 shows the signal means (colored lines) of all performed experiments with the PET tracers [^{11}C]Harmine, [^{11}C]DASB, [^{18}F]FE@SUPPY, [^{18}F]FMeNER-D2 and [^{11}C]Me@HAPTHI in all setups (4A). Fig. 4B and C illustrate the curves with standard deviations (red bars), splitted by the different kinetic properties of the respective PET tracer (B: [^{11}C]Harmine, [^{11}C]DASB, [^{18}F]FE@SUPPY and [^{18}F]FMeNER-D2 and C: [^{11}C]Me@HAPTHI).

The kinetics of [^{11}C]Me@HAPTHI showed a slower uptake behavior in contrast to the results of [^{11}C]Harmine, [^{11}C]DASB, [^{18}F]FE@SUPPY and [^{18}F]FMeNER-D2, but a clear uptake on both cell lines.

Conventional internalization experiments

The cell internalization assay with [^{11}C]SNAP-7941 and [^{18}F]FE@SNAP showed an increased uptake in the MDCKII-WT cells in contrast to MDCKII-hMDR1 cells. Same results were observed when P-gp was blocked in MDCKII-hMDR1 cells (figure 5). Internalization ratios were calculated for MDCKII-WT/MDCKII-hMDR1 and pre-blocked MDCKII-hMDR1/MDCKII-hMDR1. No significant differences were found using a multiple

comparison test and Sidak correction (figure 5B). Unspecific binding measured with two additional washing steps was < 5% for each setup and cell line.

Fig. 5 shows the ratio of tracer internalization of wildtype versus MDR1 cells and blocked MDR1 versus untreated MDR1 cells of [^{11}C]SNAP-7941 and [^{18}F]FE@SNAP. Standard deviations are illustrated as black bars. There was no significant difference between the ratios (Multiple comparison test, Sidak correction).

PET-Imaging

[^{18}F]FE@SNAP in rats

VOIs comprising the brain were outlined on the images resulting in 0.31 ± 0.07 SUV_{BW} for the vehicle group (A) and 0.75 ± 0.17 SUV_{BW} for the TQD treated group (B) (cf. figure 6A and B).

Fig. 6 shows representative µPET/CT images of a rat brain in axial, coronal and sagittal planes of [^{18}F]FE@SNAP (A, B) and [^{11}C]ME@HAPHTI (C, D). The animals received the P-gp/BCRP inhibitor TQD (15 mg/kg body weight; intravenously) (B, D) or the respective vehicle (A, C) 60min before µPET acquisition.

[^{11}C]SNAP-7941 in rats

As previously reported, mean brain TACs of [^{11}C]SNAP-7941 in rats were 0.22 ± 0.0 SUV_{BW} 55 min after tracer injection. In rats, pre-treated with TQD the SUV increased to 1.04 ± 0.1 SUV_{BW} at 55 min after tracer injection (4.72 fold increase) [12].

[^{11}C]Me@HAPTHI in rats

VOIs comprising the brain were outlined in the images resulting in 0.19 ± 0.04 SUV_{BW} for the vehicle group (figure 6C) and 0.56 ± 0.21 SUV_{BW} for the TQD treated group (cf. figure 6D).

[^{18}F]FE@SUPPY

In a previously published study it was shown that efflux inhibition with TQD did not change

the brain uptake of [^{18}F]FE@SUPPY. Peak brain activity was similar in the baseline scans (1.56±0.01 SUV) and the group which was pre-treated with TQD (1.53±0.01 SUV) [20].

Discussion

General

It is undisputed that P-gp and associated efflux transporters of the ABC family play an important role for the pharmacokinetics and therapeutic efficiency of drugs. Drug-drug interactions resulting from inhibition or induction of P-gp are a recognized clinical concern and highlighted in the "Food and Drug Administration Concept" of the FDA [21–25]. Consequently, the development of selective efflux transporter inhibitors should be emphasized as an additional medication for tumor therapeutics to avoid multiple drug resistance [9,26]. Hence, it is pivotal to assess any interaction of newly developed drugs with these transporters in the preclinical or even *pre vivo* phase. So far, there are several methods for this purpose, however, none of them directly addressing the pure interaction of the PET tracer with the P-gp. Molecular imaging of the efflux transporters at the BBB, based on PET, has become increasingly interesting in recent years. However, the binding characteristics of the respective tracers to these transporters are different and not yet fully understood. These differences can be concentration dependent processes as described for Verapamil: in a nanomolar range, Verapamil is supposed to be a substrate, whereas at micromolar ranges, it becomes an inhibitor [27]. For other tracers, shared (dual) interactions with the transporter variants are known: e.g. Tariquidar binds to P-gp and is transported by BCRP [28,29]. The authors conclude that currently available labeled inhibitors may not be suitable for imaging the efflux transporter density. Therefore, there is a need for optimized PET imaging protocols and for PET tracers with high affinity (Ki < 5 nM) [30,31]. The present study aimed at the establishment of a general experimental real-time model for the direct quantification of the interactions of PET tracers with the human P-gp transporter in nanomolar concentration.

Real-time kinetic model

The developed real-time kinetic assay is highly robust, rapid and needs less preparation and experimental time in comparison to the cell internalization assay. Theoretically, the identification of a P-gp substrate can be assessed in a single experiment on P-gp expressing cells, showing high background to target ratio of the labelled molecules. This experiment can be performed on pre-blocked cells (with the disadvantage of a required second setup) or in real-time, where the inhibitor is added after equilibrium of the tracer. In that case, the signal on the cell side increases immediately, if the tracer is a P-gp substrate. For comparison, three setups were chosen: experiments with the MDCKII-WT, the MDCKII-hMDR1 cells as well as pre-blocking of the P-gp transporter with (±)-Verapamil. In prior experiments and by treatment of the WT, we excluded vehicle effects as well as effects of Verapamil itself on the MDCKII cells.

Currently available methods are not efficient, as they are time consuming and require the use of long-lived radionuclides. Other assays, derived from toxicology studies (e.g. calcein-AM assay, rhodamine 123 assay or digoxin assays), indirectly measure the dependence of the toxic effect on the P-gp blockade [32–36].

The established new application for the LigandTracer® technology directly uses the PET tracer in very small activities. Main advantage of this method is the insight into the kinetic behavior of the uptake process in real- time enabling a direct interpretation of the underlying mechanism such as the affinity towards the P-gp transporter [26] and the distinction between substrates and compounds without any protein interaction. Therefore, it may be used for quantification of the equilibrium inhibitory constant (K_i) of newly developed P-gp inhibitors. Furthermore, this method is not limited to the use of high energy gamma detection as for PET and SPECT nuclides, but also applicable for beta emitters.

P-gp transporter substrates

The two SNAP derivatives [^{18}F]FE@SNAP and [^{11}C]SNAP-7941 were confirmed to be highly potent P-gp-substrates. The kinetic changes were obvious: no signal could be observed on the P-gp expressing cell line, whereas WT cells and cell lines pre-blocked with (±)-Verapamil exhibited a significantly increased signal with a similar curve shape (cf. figure 1 and 2). Further experiments were conducted with the MDCKII-hMDR1 cells treated with non-labeled Verapamil after incubation with the P-gp substrates during the real-time assay. The signal on the cell side increased instantly indicating that P-gp inhibition was also successful while performing the real-time assay.

Compounds with no interaction with the P-gp transporter

The PET tracers [^{11}C]Harmine, [^{11}C]DASB and [^{18}F]FMeNER-D2, which are described to have no interaction with the human P-gp transporter (established brain tracer) showed the same kinetic behavior in all tested setups and all used concentrations (prior-experiments, data not shown). Hence, they were classified as non-P-gp-substrates. [^{18}F]FE@SUPPY shows comparable uptake behavior in the real-time assay. In previously published PET data, [^{18}F]FE@SUPPY shows no increasing brain uptake after inhibition with Tariquidar, which is in accordance to the findings of the *in vitro* assay. However, AUC levels were increased after inhibition [20]. In baseline scans with [^{11}C]Me@HAPTHI, we observed a slight brain uptake. At that stage, we hypothesized that the PET tracer could be a P-gp-substrate. This assumption was not proven by *in vitro* experiments (real-time model), since [^{11}C]Me@HAPTHI shows uptake in both cell lines independent of blocking. However, the time to equilibrium was slower for [^{11}C]Me@HAPTHI than of the other non-interacting PET tracers (cf. figure 4A and C). We hypothesize that this observed change is due to differences in permeability efficiency, especially bearing in mind, that MDCKII cell lines are a widely used model for the assessment of permeability features of compounds [37,38] and that [^{11}C]Me@HAPTHI may

interact with other efflux transporter like BCRP (breast cancer resistance protein), which are also natively expressed in the MDCKII cell lines. The latter becomes conclusive by overlapping the kinetics of SNAP PET tracer and [^{11}C]Me@HAPTHI (figure 7C and D) and interpreting the imaging data.

Fig. 7 shows the signal means (colored lines, see legend) of all performed experiments with the PET tracers [^{11}C]SNAP-7941, [^{18}F]FE@SNAP and [^{11}C]Me@HAPTHI using all setups.

Conventional internalization experiments

The interactions of [^{11}C]SNAP-7941 and [^{18}F]FE@SNAP with the P-gp transporter were also evaluated using a conventional cell internalization assay. Comparing the real-time assay with the conventional internalization assay, the established real-time model is easy, needs fewer activities and achieves the same results in less time with lower standard deviation. Calculation of the uptake ratio between (1) WT versus non-treated hMDR1 cell lines and (2) pre-blocked hMDR1 versus untreated hMDR1 cell line of the PET tracers [^{18}F]FE@SNAP and [^{11}C]SNAP-7941 show that the uptake in the WT and the pre-blocked MDCKII-hMDR1 cell line increased by the same factor. Therefore, the results were in the same ratio and did not differ significantly. Hence, the two SNAP derivatives can also be classified as P-gp substrates in this internalization assay.

PET Imaging

Animal experiments were conducted under baseline (vehicle) and TQD blocking conditions (15 mg/kg bodyweight) in rats. Currently, TQD is the gold standard for *in vivo* inhibition of P-gp in preclinical and clinical settings, but also known as an inhibitor for BCRP (dual inhibitor) [39]. Therefore, *in vivo* PET studies using this inhibitor cannot distinguish between interactions of the PET tracer with BCRP and P-gp. However, conducting animal experiments with (±)-Verapamil is impossible since it is a highly potent calcium channel blocker with a variety of severe cardiovascular and central side-effects. Based on our µPET results with

[^{18}F]FE@SNAP and [^{11}C]SNAP-7941, a clear assignment of the efflux effect to human BCRP, P-gp or both, respectively, is not possible. Yet, our *in vitro* assay shows that there is a strong interaction with the human P-gp. In contrast, the imaging results of [^{11}C]Me@HAPTHI show a significant brain uptake after inhibition with TQD, whereas no effect can be seen *in vitro*. This leads to the hypothesis that this PET tracer might be a substrate of human BCRP (*in vivo*), but not a substrate of P-gp.

Conclusion

A rapid *in vitro* real-time kinetic model was developed for a qualitative prediction of P-gp interactions for early stage PET tracer development. These data correlate with *in vivo* PET quantifications. Hence, PET tracers can be clearly categorized into P-gp substrates or substances without P-gp interaction (neither inhibitory effect nor efflux) based on their kinetic behavior.

Acknowledgements

We gratefully acknowledge the support of Markus Zeilinger, MSc for his proper expertise in LigandTracer Technologies, Prof Dr Oliver Langer for fruitful discussions, Dr Verena Pichler, and Neydher Berroteran, MSc for synthesis of the diverse PET tracers and their support. This work was supported by the Austrian Science Fund (FWF P26502-B24, M. Mitterhauser).

Authors Contribution

CV, TB, E-MK, TR, CP, FP, MD performed the experiments. MM, CV, WW, MH and K-HW planned the experiments. CV, MM, MD and CP composed the draft. WW, MH, K-HW, and FP reviewed the manuscript. CV, TB, E-MK, TR, FP, MD and MM performed the calculations and analyses.

Disclosure/Conflict of interest

We have nothing to disclose.

Sentence regarding supplementary information

No supplementary information provided.

Abbreviations

AUC area under the curve

BCRP breast cancer resistance protein

K_i equilibrium inhibitory constant

hMDR1 human multiple drug resistance 1

MDCKII Madin-Darby Canine Kidney cell line

MRP-1 Multiple drug resistance protein 1

PET Positron emission tomography

VERA Verapamil

WT Wildtype

TQD Tariquidar

References

[1] World Health Organization. World Health Report. Geneva: n.d.

[2] Alavijeh MS, Chishty M, Qaiser MZ, Palmer AM. Drug metabolism and pharmacokinetics, the blood-brain barrier, and central nervous system drug discovery. NeuroRX 2005;2:554–71.

[3] Pardridge WM. Drug transport across the blood–brain barrier. J Cereb Blood Flow Metab 2012;32:1959–72. doi:10.1038/jcbfm.2012.126.

[4] Abbott NJ, Patabendige AAK, Dolman DEM, Yusof SR, Begley DJ. Structure and function of the blood–brain barrier. Neurobiol Dis 2010;37:13–25.

[5] Pike VW. PET radiotracers: crossing the blood–brain barrier and surviving metabolism. Trends Pharmacol Sci 2009;30:431–40.

[6] Sharom FJ. ABC multidrug transporters: structure, function and role in chemoresistance. Pharmacogenomics 2008;9:105–27. doi:10.2217/14622416.9.1.105.

[7] Endres CJ, Hsiao P, Chung FS, Unadkat JD. The role of transporters in drug interactions. Eur J Pharm Sci Off J Eur Fed Pharm Sci 2006;27:501–17.

[8] Agnani D, Acharya P, Martinez E, Tran TT, Abraham F, Tobin F, et al. Fitting the elementary rate constants of the P-gp transporter network in the hMDR1-MDCK confluent cell monolayer using a particle swarm algorithm. PloS One 2011;6:e25086.

[9] Chen Z, Shi T, Zhang L, Zhu P, Deng M, Huang C, et al. Mammalian drug efflux transporters of the ATP binding cassette (ABC) family in multidrug resistance: A review of the past decade. Cancer Lett 2016;370:153–64.
[10] Wanek T, Mairinger S, Langer O. Radioligands targeting P-glycoprotein and other drug efflux proteins at the blood–brain barrier. J Label Compd Radiopharm 2013;56:68–77.
[11] Fischer C, Vomstein S, Mindt T. A Bombesin-Shepherdin Radioconjugate Designed for Combined Extra- and Intracellular Targeting. Pharmaceuticals 2014;7:662–75.
[12] Philippe C, Nics L, Zeilinger M, Kuntner C, Wanek T, Mairinger S, et al. Preclinical in vitro &in vivo evaluation of [(11)C]SNAP-7941 - the first PET tracer for the melanin concentrating hormone receptor 1. Nucl Med Biol 2013;40:919–25.
[13] Rami-Mark C, Zhang M-R, Mitterhauser M, Lanzenberger R, Hacker M, Wadsak W. [18F]FMeNER-D2: Reliable fully-automated synthesis for visualization of the norepinephrine transporter. Nucl Med Biol 2013;40:1049–54.
[14] Philippe C, Zeilinger M, Mitterhauser M, Dumanic M, Lanzenberger R, Hacker M, et al. Parameter evaluation and fully-automated radiosynthesis of [11C]harmine for imaging of MAO-A for clinical trials. Appl Radiat Isot 2015;97:182–7.
[15] Philippe C, Nics L, Zeilinger M, Schirmer E, Spreitzer H, Karanikas G, et al. Preparation and First Preclinical Evaluation of [18F]FE@SNAP: A Potential PET Tracer for the Melanin-Concentrating Hormone Receptor-1 (MCHR1). Sci Pharm 2013;81:625–39.
[16] Philippe C, Schirmer E, Mitterhauser M, Shanab K, Lanzenberger R, Karanikas G, et al. Radiosynthesis of [11C]SNAP-7941—the first PET-tracer for the melanin concentrating hormone receptor 1 (MCHR1). Appl Radiat Isot 2012;70:2287–94.
[17] Haeusler D, Mien L-K, Nics L, Ungersboeck J, Philippe C, Lanzenberger RR, et al. Simple and rapid preparation of [11C]DASB with high quality and reliability for routine applications. Appl Radiat Isot 2009;67:1654–60.
[18] Rami-Mark C, Berroterán-Infante N, Philippe C, Foltin S, Vraka C, Hoepping A, et al. Radiosynthesis and first preclinical evaluation of the novel norepinephrine transporter pet-ligand [11C]ME@HAPTHI. EJNMMI Res 2015;5.
[19] Wadsak W, Mien L-K, Shanab K, Ettlinger DE, Haeusler D, Sindelar K, et al. Preparation and first evaluation of [18F]FE@SUPPY: a new PET tracer for the adenosine A3 receptor. Nucl Med Biol 2008;35:61–6.
[20] Haeusler D, Kuntner C, Nics L, Savli M, Zeilinger M, Wanek T, et al. [18F]FE@SUPPY: a suitable PET tracer for the adenosine A3 receptor? An in vivo study in rodents. Eur J Nucl Med Mol Imaging 2015;42:741–9.
[21] Prueksaritanont T, Chu X, Gibson C, Cui D, Yee KL, Ballard J, et al. Drug–Drug Interaction Studies: Regulatory Guidance and An Industry Perspective. AAPS J 2013;15:629–45.
[22] Zhang L, Strong JM, Qiu W, Lesko LJ, Huang S-M. Scientific Perspectives on Drug Transporters and Their Role in Drug Interactions †. Mol Pharm 2006;3:62–9.
[23] Brinkmann U, Roots I, Eichelbaum M. Pharmacogenetics of the human drug-transporter gene MDR1: impact of polymorphisms on pharmacotherapy. Drug Discov Today 2001;6:835–9.
[24] Englund G, Hallberg P, Artursson P, Michaëlsson K, Melhus H. Association between the number of coadministered P-glycoprotein inhibitors and serum digoxin levels in patients on therapeutic drug monitoring. BMC Med 2004;2.
[25] Balayssac D, Authier N, Cayre A, Coudore F. Does inhibition of P-glycoprotein lead to drug-drug interactions? Toxicol Lett 2005;156:319–29.
[26] Zeilinger M, Pichler F, Nics L, Wadsak W, Spreitzer H, Hacker M, et al. New approaches for the reliable in vitro assessment of binding affinity based on high-resolution real-time data acquisition of radioligand-receptor binding kinetics. EJNMMI Res 2017;7.

[27] Römermann K, Wanek T, Bankstahl M, Bankstahl JP, Fedrowitz M, Müller M, et al. (R)-[11C]verapamil is selectively transported by murine and human P-glycoprotein at the blood–brain barrier, and not by MRP1 and BCRP. Nucl Med Biol 2013;40:873–8.
[28] Kannan P, Telu S, Shukla S, Ambudkar SV, Pike VW, Halldin C, et al. The "Specific" P-Glycoprotein Inhibitor Tariquidar Is Also a Substrate and an Inhibitor for Breast Cancer Resistance Protein (BCRP/ABCG2). ACS Chem Neurosci 2011;2:82–9.
[29] Weidner LD, Fung KL, Kannan P, Moen JK, Kumar JS, Mulder J, et al. Tariquidar Is an Inhibitor and Not a Substrate of Human and Mouse P-glycoprotein. Drug Metab Dispos 2016;44:275–82.
[30] Kannan P, John C, Zoghbi SS, Halldin C, Gottesman MM, Innis RB, et al. Imaging the Function of P-Glycoprotein With Radiotracers: Pharmacokinetics and In Vivo Applications. Clin Pharmacol 38 Ther 2009;86:368–77.
[31] Kannan P, Pike VW, Halldin C, Langer O, Gottesman MM, Innis RB, et al. Factors that limit positron emission tomography imaging of p-glycoprotein density at the blood-brain barrier. Mol Pharm 2013;10:2222–9. doi:10.1021/mp400011g.
[32] Keogh JP, Kunta JR. Development, validation and utility of an in vitro technique for assessment of potential clinical drug-drug interactions involving P-glycoprotein. Eur J Pharm Sci Off J Eur Fed Pharm Sci 2006;27:543–54.
[33] Rautio J, Humphreys JE, Webster LO, Balakrishnan A, Keogh JP, Kunta JR, et al. In vitro p-glycoprotein inhibition assays for assessment of clinical drug interaction potential of new drug candidates: a recommendation for probe substrates. Drug Metab Dispos Biol Fate Chem 2006;34:786–92.
[34] Doan KMM, Humphreys JE, Webster LO, Wring SA, Shampine LJ, Serabjit-Singh CJ, et al. Passive Permeability and P-Glycoprotein-Mediated Efflux Differentiate Central Nervous System (CNS) and Non-CNS Marketed Drugs. J Pharmacol Exp Ther 2002;303:1029–37.
[35] Polli JW, Wring SA, Humphreys JE, Huang L, Morgan JB, Webster LO, et al. Rational Use of in Vitro P-glycoprotein Assays in Drug Discovery. J Pharmacol Exp Ther 2001;299:620–8.
[36] Dörner B, Kuntner C, Bankstahl JP, Wanek T, Bankstahl M, Stanek J, et al. Radiosynthesis and in vivo evaluation of 1-[18F]fluoroelacridar as a positron emission tomography tracer for P-glycoprotein and breast cancer resistance protein. Bioorg Med Chem 2011;19:2190–8.
[37] Di L, Whitney?Pickett C, Umland JP, Zhang H, Zhang X, Gebhard DF, et al. Development of a new permeability assay using low?efflux MDCKII cells. J Pharm Sci 2011;100:4974–85.
[38] Irvine JD, Takahashi L, Lockhart K, Cheong J, Tolan JW, Selick HE, et al. MDCK (Madin-Darby Canine Kidney) Cells: A Tool for Membrane Permeability Screening. J Pharm Sci 1999;88:28–33.
[39] Bauer M, Karch R, Zeitlinger M, Stanek J, Philippe C, Wadsak W, et al. Interaction of 11C-Tariquidar and 11C-Elacridar with P-glycoprotein and Breast Cancer Resistance Protein at the Human Blood-Brain Barrier. J Nucl Med Off Publ Soc Nucl Med 2013;54.

Captions

Fig. 1 illustrates the kinetics of [^{11}C]SNAP-7941 (signal in [CPS]). (A) shows the kinetics on MDCKII-WT cells. (B) shows the signal on the MDCKII-hMDR1 cells, where the transporter was blocked with (±)-Verapamil. (C) exemplifies that the signal of the tracer on the P-gp transporter expressing cell line is due to unspecific accumulation. The red signal represents the background measurement (plastic surface of the petri dish) and the blue signal the kinetics of the tracers on the target area (cells), whereas the black signal shows the corrected signal (target minus background).

Fig. 2 shows the uptake of [^{18}F]FE@SNAP (n=7) and [^{11}C]SNAP-7941 (n=6) on the MDCKII-wildtype and MDCKII-hMDR1 cells pre-blocked with (±)-Verapamil (means of the experiments, normalized to 100% uptake, standard deviations are illustrated with red bars (A)) and the non-treated hMDR1 cell line (B).

Fig. 3 exemplifies the kinetics of the PET tracer [11C]Harmine, which is known to have no interactions with the P-gp transporter. The red signal represents the background measurement (plastic surface of the petri dish) and the blue signal the kinetics of the tracers on the target area (cells), whereas the black signal shows the corrected signal (target minus background). There are no differences displayed in the kinetics at all examined setups (A-C).

Fig. 4 shows the signal means (colored lines) of all performed experiments with the PET tracers [^{11}C]Harmine, [^{11}C]DASB, [^{18}F]FE@SUPPY, [^{18}F]FMeNER-D2 and [^{11}C]Me@HAPTHI in all setups (4A). Fig. 4B and C illustrate the curves with standard

deviations (red bars), splitted by the different kinetic properties of the respective PET tracer (B: [^{11}C]Harmine, [^{11}C]DASB, [^{18}F]FE@SUPPY and [^{18}F]FMeNER-D2 and C: [^{11}C]Me@HAPTHI).

Fig. 5 shows the ratio of tracer internalization of wildtype versus MDR1 cells and blocked MDR1 versus untreated MDR1 cells of [^{11}C]SNAP-7941 and [^{18}F]FE@SNAP. Standard deviations are illustrated as black bars. There was no significant difference between the ratios (Multiple comparison test, Sidak correction).

Fig. 6 shows representative µPET/CT images of a rat brain in axial, coronal and sagittal planes of [^{18}F]FE@SNAP (A, B) and [^{11}C]ME@HAPHTI (C, D). The animals received the P-gp/BCRP inhibitor TQD (15 mg/kg body weight; intravenously) (B, D) or the respective vehicle (A, C) 60min before µPET acquisition.

Fig. 7 shows the signal means (colored lines, see legend) of all performed experiments with the PET tracers [^{11}C]SNAP-7941, [^{18}F]FE@SNAP and [^{11}C]Me@HAPTHI using all setups.

Fig.1

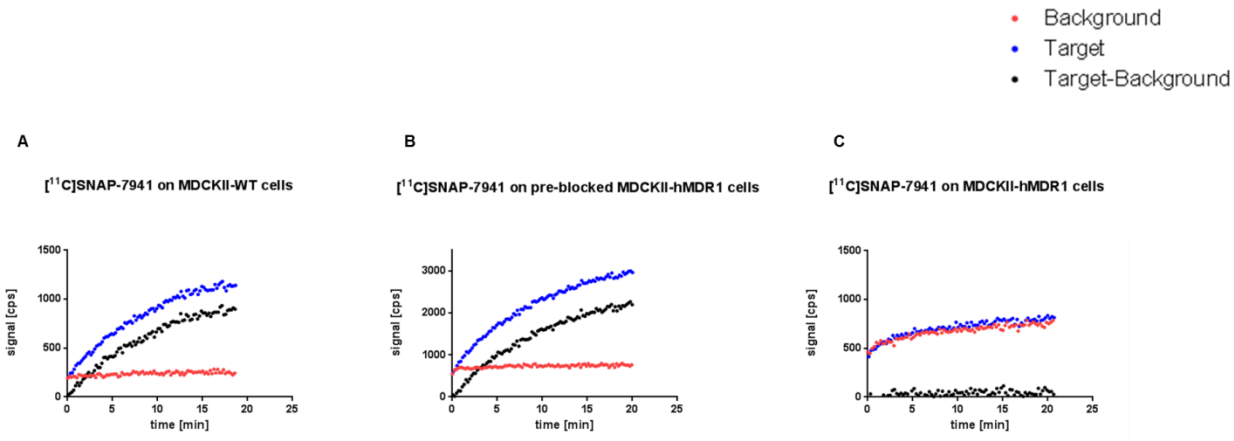

Figr.2

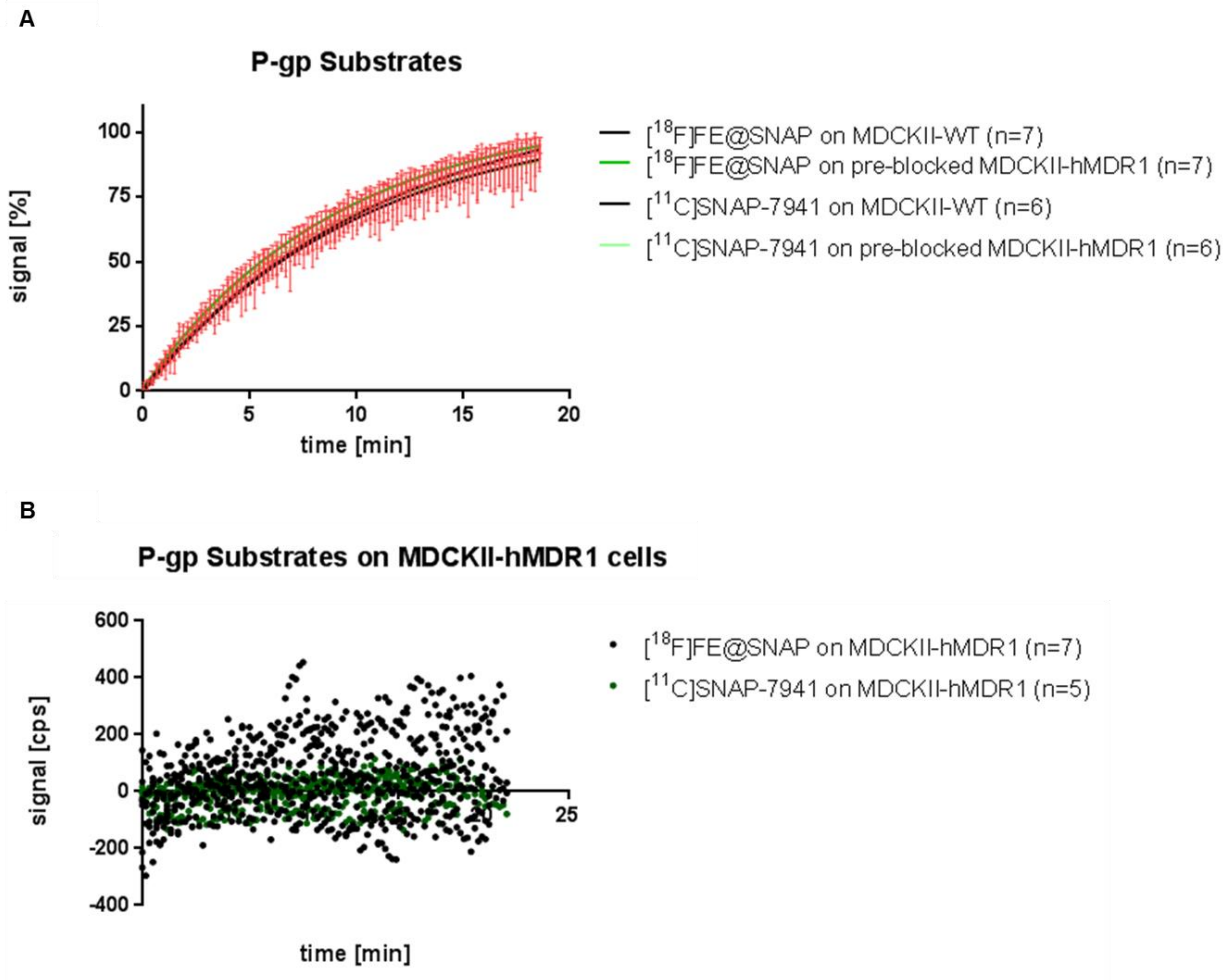
A
P-gp Substrates
signal [%]
time [min]
[18F]FE@SNAP on MDCKII-WT (n=7)
[18F]FE@SNAP on pre-blocked MDCKII-hMDR1 (n=7)
[11C]SNAP-7941 on MDCKII-WT (n=6)
[11C]SNAP-7941 on pre-blocked MDCKII-hMDR1 (n=6)
B
P-gp Substrates on MDCKII-hMDR1 cells
signal [cps]
time [min]
[18F]FE@SNAP on MDCKII-hMDR1 (n=7)
[11C]SNAP-7941 on MDCKII-hMDR1 (n=5)

Fig.3

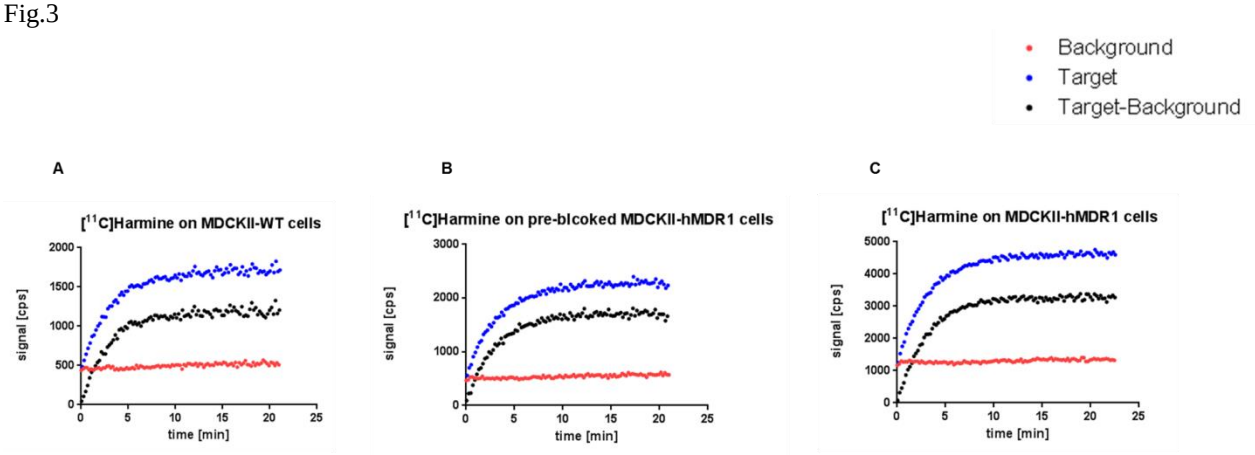
Background
Target
Target-Background
A
[11C]Harmine on MDCKII-WT cells
signal [cps]
time [min]
B
[11C]Harmine on pre-blcoked MDCKII-hMDR1 cells
signal [cps]
time [min]
C
[11C]Harmine on MDCKII-hMDR1 cells
signal [cps]
time [min]

Fig. 4

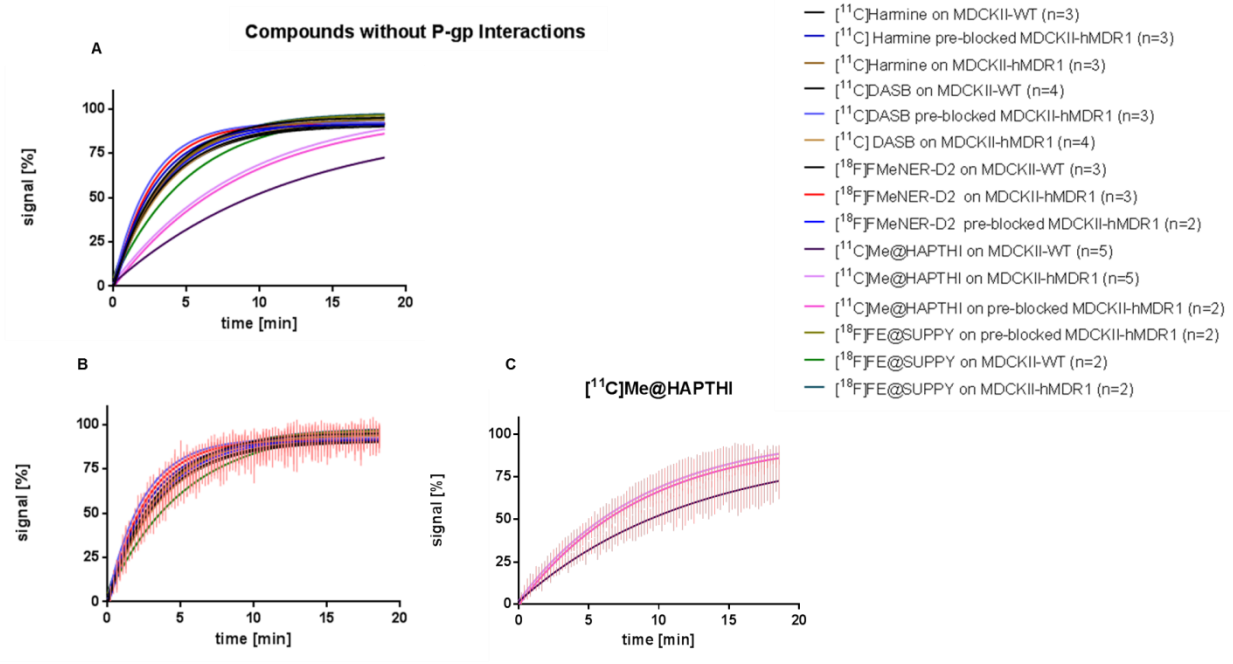
Compounds without P-gp Interactions
A
signal [%]
time [min]
B
C
[11C]Me@HAPTHI
[11C]Harmine on MDCKII-WT (n=3)
[11C] Harmine pre-blocked MDCKII-hMDR1 (n=3)
[11C]Harmine on MDCKII-hMDR1 (n=3)
[11C]DASB on MDCKII-WT (n=4)
[11C]DASB pre-blocked MDCKII-hMDR1 (n=3)
[11C] DASB on MDCKII-hMDR1 (n=4)
[18F]FMeNER-D2 on MDCKII-WT (n=3)
[18F]FMeNER-D2 on MDCKII-hMDR1 (n=3)
[18F]FMeNER-D2 pre-blocked MDCKII-hMDR1 (n=2)
[11C]Me@HAPTHI on MDCKII-WT (n=5)
[11C]Me@HAPTHI on MDCKII-hMDR1 (n=5)
[11C]Me@HAPTHI on pre-blocked MDCKII-hMDR1 (n=2)
[18F]FE@SUPPY on pre-blocked MDCKII-hMDR1 (n=2)
[18F]FE@SUPPY on MDCKII-WT (n=2)
[18F]FE@SUPPY on MDCKII-hMDR1 (n=2)

Fig.5

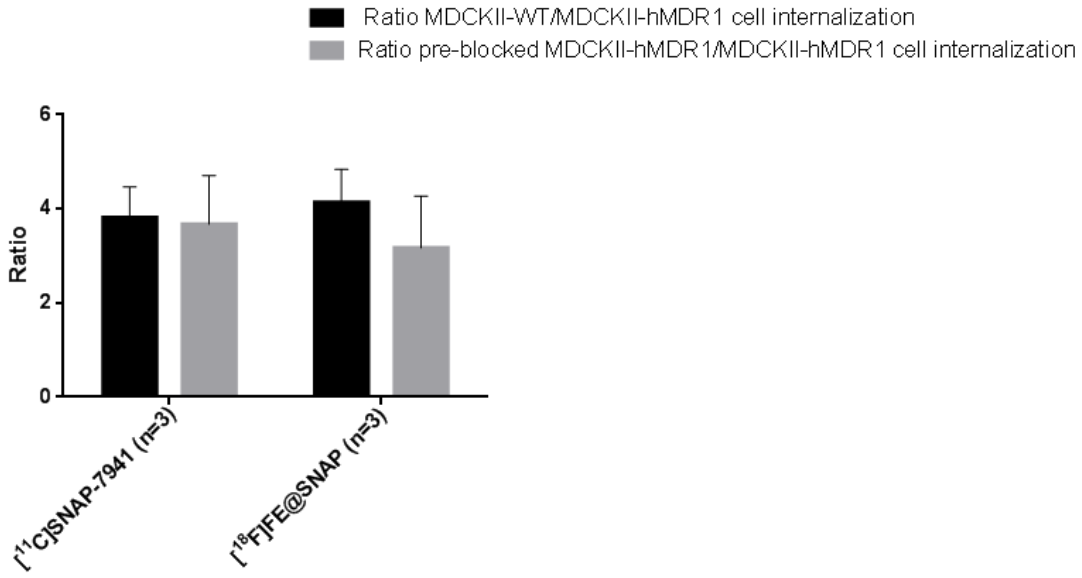
Ratio MDCKII-WT/MDCKII-hMDR1 cell internalization
Ratio pre-blocked MDCKII-hMDR1/MDCKII-hMDR1 cell internalization
Ratio
6
4
2
0
[11C]SNAP-7941 (n=3)
[18F]FE@SNAP (n=3)

Fig.6

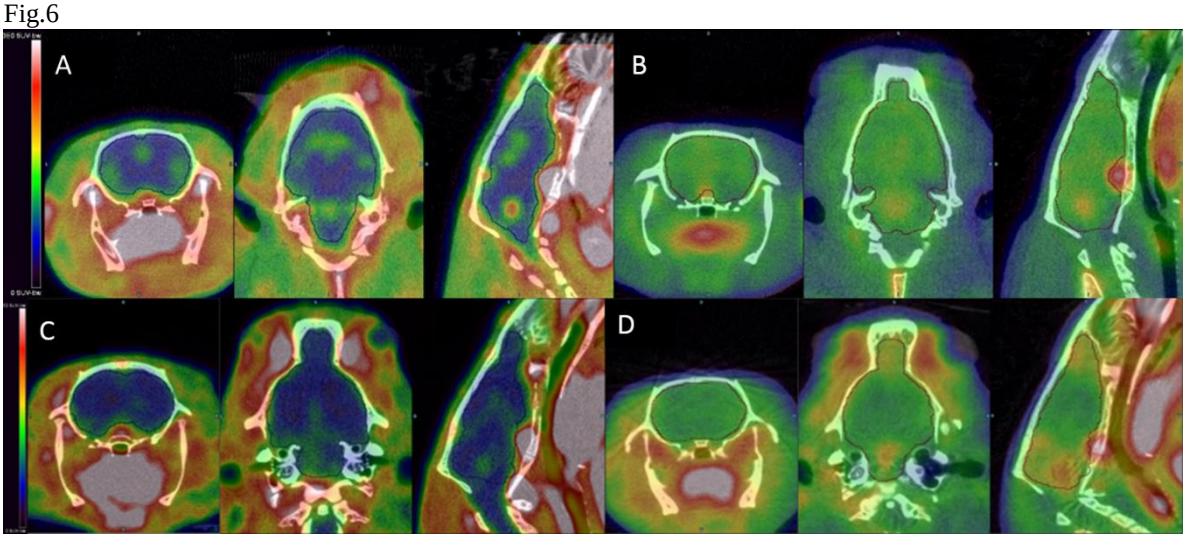

Fig. 7

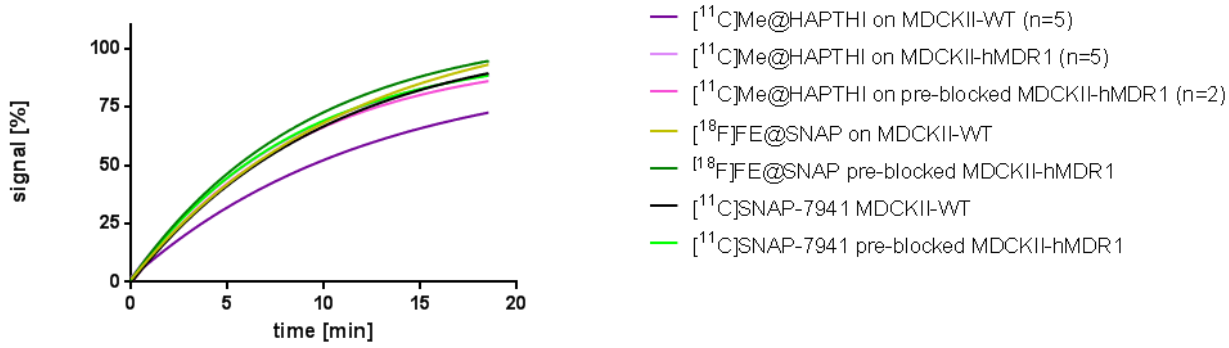
signal [%]
100
75
50
25
0
0
5
10
15
20
time [min]
[11C]Me@HAPTHI on MDCKII-WT (n=5)
[11C]Me@HAPTHI on MDCKII-hMDR1 (n=5)
[11C]Me@HAPTHI on pre-blocked MDCKII-hMDR1 (n=2)
[18F]FE@SNAP on MDCKII-WT
[18F]FE@SNAP pre-blocked MDCKII-hMDR1
[11C]SNAP-7941 MDCKII-WT
[11C]SNAP-7941 pre-blocked MDCKII-hMDR1

3.1.5 Manuscript V

Rami-Mark C, Bornatowicz B, Fink C, Otter P, Ungersboeck J, **Vraka C**, Haeusler D, Nics L, Spreitzer H, Hacker M, Mitterhauser M, Wadsak W. Synthesis, radiosynthesis and first in vitro evaluation of novel PET-tracers for the dopamine transporter: [(11)C]IPCIT and [(18)F]FE@IPCIT. Bioorg Med Chem. 2013 Dec 15;21(24):7562-9.

Bioorganic & Medicinal Chemistry 21 (2013) 7562–7569

Contents lists available at ScienceDirect

Bioorganic & Medicinal Chemistry

journal homepage: www.elsevier.com/locate/bmc

Synthesis, radiosynthesis and first in vitro evaluation of novel PET-tracers for the dopamine transporter: [^{11}C]IPCIT and [^{18}F]FE@IPCIT

Christina Rami-Mark [a,b], Birgit Bornatowicz [c], Cornel Fink [a], Paul Otter [a], Johanna Ungersboeck [a], Chrysoula Vraka [a,d], Daniela Haeusler [a], Lukas Nics [a,d], Helmut Spreitzer [c], Marcus Hacker [a], Markus Mitterhauser [a], Wolfgang Wadsak [a,*]

[a] Division of Nuclear Medicine, Radiochemistry and Biomarker Development Unit, Department of Biomedical Imaging and Image-guided Therapy, Medical University of Vienna, Waehringer Guertel 18-20, A-1090 Vienna, Austria
[b] Department of Inorganic Chemistry, University of Vienna, Waehringer Strasse 42, A-1090 Vienna, Austria
[c] Department of Drug and Natural Product Synthesis, University of Vienna, Althanstrasse 14, A-1090 Vienna, Austria
[d] Department of Nutritional Sciences, University of Vienna, Althanstrasse 14, A-1090 Vienna, Austria

ARTICLE INFO

Article history:
Received 27 August 2013
Revised 17 October 2013
Accepted 29 October 2013
Available online 7 November 2013

Keywords:
Transporter
Dopamine
PET
IPCIT
Carbon-11
Radiosynthesis
Fluorine-18

ABSTRACT

Introduction: Present data indicate that merging beneficial structural elements from previously published DAT-ligands highest DAT affinity, selectivity and a suitable metabolic profile should be achieved. This combination led to the development of IPCIT and FE@IPCIT.
Methods: Precursor synthesis was done starting from cocaine in a six step reaction. *O*-[^{11}C]-methylation was established using [^{11}C]methyl iodide, optimized and subsequently automated. Small scale ^{18}F-fluoroethylation as well as optimization of reaction parameters and automation were performed. Affinity and selectivity of the candidate substances were tested in standard binding experiments on human membranes. Metabolic stability and blood–brain-barrier (BBB) penetration were determined.
Results: Precursor compound, IPCITacid, and reference compounds, IPCIT and FE@IPCIT, were obtained in 4.9%, 12.7% and 4.1% yield, respectively. Automated radiosynthesis of [^{11}C]IPCIT yielded 1.9 ± 0.7 GBq (12.5 ± 4%, corrected for decay). Optimum parameters for ^{18}F-fluoroethylation were 110 °C for 15 min under TBAH catalysis, yielding 67 ± 16% radiochemical incorporation. Affinity was determined as 1.7 ± 0.6 nM for IPCIT, 1.3 ± 0.2 nM for FE@IPCIT and 37 ± 13 nM for the precursor molecule, IPCIT-acid. Results from in vitro and in silico evaluations revealed high stability but also high lipophilicity.
Conclusion: Present data indicate high affinity and stability of both IPCIT and FE@IPCIT. Radiolabelling, optimization of reaction parameters and automation succeeded. On the other hand, data concerning BBB-penetration are not promising.

1. Introduction

The dopamine transporter (DAT) has attracted the attention of neuro-researchers due to its involvement in many neurodegenerative and psychiatric diseases; amongst these Parkinson's disease, attention deficit hyperactivity disorder and schizophrenia.[1–4] As membrane bound monoamine transporter, it facilitates the re-uptake of dopamine into the cytosol and controls the concentration of dopamine in the synaptic cleft. For in vitro and in vivo visualization of DAT, and therefore also for diagnostic investigations of neurodegenerative brain disorders, many SPECT and PET tracers have been developed. These established ligands are mostly based on the nortropane structure of cocaine, such as [^{123}I]β-CIT, [^{11}C]β-CIT, [^{11}C]CFT, [^{18}F]FE@CIT, [^{18}F]FECNT and iodinated nortropane derivatives like [^{123}I]-IPT or [^{125}I]altropane.[5–14] Considering the high concentration of DAT in human brain (B_{max} ~ 200 pmol/g, human putamen), this transporter can be targeted straight-forwardly.[8] Although a variety of radioligands has been described and used in clinical applications, there is still controversy regarding the optimum features for precise quantification of DAT. Low selectivity, slow kinetics, metabolic degradation or problems with blood-brain-barrier (BBB)-penetration put some constraints on their applicability in clinical trials, thus better suitable DAT-PET ligands are still of interest.[15–17]

Halldin and co-workers presented [^{11}C]PE2I and [^{18}F]FE-PE2I as new cocaine congeners and evaluated these in vitro and in vivo.[18–21] These ligands are exhibiting good selectivity and affinity,

* Corresponding author. Tel.: +43 1 40400 5255; fax: +43 1 40400 1559.
E-mail address: wolfgang.wadsak@meduniwien.ac.at (W. Wadsak).

0968-0896/$ - see front matter © 2013 Elsevier Ltd. All rights reserved.
http://dx.doi.org/10.1016/j.bmc.2013.10.046

but display certain limitations due to their metabolic fate: two radiometabolites were observed in all brain regions and amongst these one is showing also specific binding to striatum.[22,23] Furthermore, these metabolic transformations show a high inter-individual variability.[22]

Therefore, it was our aim to synthesize novel derivatives combining the para-iodosubstituted phenyl ring, as in the widespread used β-CIT molecule (with good metabolic stability[24]), with an iodopropenyl moiety on the tropane-*N* (derived from the altropane and PE2I structure), as well as with a methyl- or fluoroethyl-ester at the 2β-carbomethoxy function (high affinity and selectivity). This combination led to the development of IPCIT (methyl 8-[(2*E*)-3-iodoprop-2-en-1-yl]-3-(4-iodophenyl)-8-azabicyclo[3.2.1]octane-2-carboxylate and FE@IPCIT (2-fluoroethyl 8-[(2*E*)-3-iodoprop-2-en-1-yl]-3-(4-iodophenyl)-8-azabicyclo[3.2.1]octane-2-carboxylate) (Fig. 1), two DAT tracers with expected high metabolic stability.

In the present work, the objective was to evaluate the affinity and selectivity of the candidate substances and of β-CIT (for comparison) in membrane binding experiments expressing the human monoamine transporters. Moreover, metabolic stability was examined and radiolabelling was optimized with ^{11}C and ^{18}F in small scale experiments and automation was intended.

2. Materials and methods

2.1. Materials

Acetonitrile (ACN) for synthesis of DNA, ⩾99.9% (GC) and ACN (HPLC grade), tetrabutylammonium hydroxide 30-hydrate (TBAH), methanol (MeOH, CHROMASOLV®, for HPLC, ⩾99.9%), ammonium formate, ammonium acetate, acetic acid (⩾99%) and ethanol (absolute) were obtained from Sigma Aldrich (Vienna, Austria). Iodine (sublimated grade for analysis; ACS, Pharm.Eur.) was purchased from Merck (Darmstadt, Germany).

For formulation of the product, 0.9% saline solution from B. Braun (Melsungen, Germany), 3% saline solution (Landesapotheke Salzburg, Austria), sodium dihydrogenphosphate monohydrate and disodiumhydrogenphosphate dihydrate (both from Merck, Darmstadt, Germany) and TWEEN® 80 (polyoxyethylenesorbitan monooleate, Sigma Aldrich, Vienna, Austria) were used. Anion-exchange cartridges (PS-HCO_3) for [^{18}F]fluoride trapping were purchased from Macherey-Nagel (Dueren, Germany). 2-bromoethyl triflate (BET) was synthesized in cooperation with the Department of Drug and Natural Product Synthesis of the University of Vienna (Austria) according to a literature method.[25] Sterile water was purchased from Meditrade Medicare Medizinprodukte (Kufstein, Austria). Phosphate buffer (125 mM) was prepared by dissolving 0.224 g sodium dihydrogenphosphate–monohydrate and 1.935 g disodiumhydrogenphosphate–dihydrate in 100 mL sterile water. For solid phase extraction C18 plus SepPak® cartridges were purchased from Waters (Waters® Associates Milford, USA). Low-protein binding Millex® GS 0.22 μm sterile filters were obtained from Millipore (Bedford, USA). All other chemicals and solvents for the syntheses and radiosyntheses were obtained from Merck (Darmstadt, Germany) and Sigma-Aldrich (Vienna, Austria) with at least analytical grade and used without further purification.

2.2. Instrumentation

[^{11}C]CO_2 was produced within a GE PETtrace cyclotron (General Electric Medical System, Uppsala, Sweden) by a $^{14}N(p,\alpha)^{11}C$ nuclear reaction under irradiation of a gas target (Aluminium) filled with N_2 (+1% O_2) (Messer Gases, Vienna, Austria). The production of [^{11}C]CH_3I and [^{11}C]CH_3OTf was performed within a Tracerlab™ FX C Pro synthesizer (GE Healthcare, Uppsala, Sweden). [^{18}F]Fluoride was produced within a GE PETtrace cyclotron via $^{18}O(p,n)^{18}F$ reaction (16.5 MeV protons; GE Medical Systems, Uppsala, Sweden). $H_2{}^{18}O$ (HYOX18; >98%) was obtained from Rotem Europe (Leipzig, Germany).

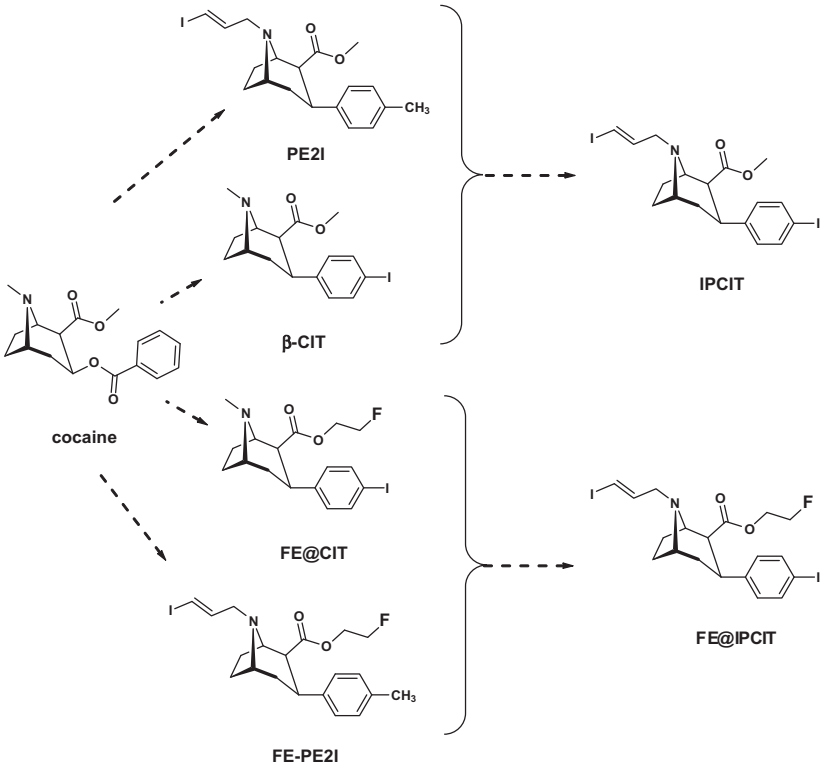

Figure 1. Structures of cocaine and derived DAT ligands.

Evaluation of reaction conditions was performed manually in a lead-shielded hood with small quantities of radioactivity (<1 GBq). After optimization, [^{11}C]IPCIT-synthesis was automated in the Tracerlab™ FX C Pro synthesizer, whereas [^{18}F]FE@IPCIT-synthesis was automated within a Nuclear Interface synthesizer (both GE Medical Systems, Sweden), remotely controlled by a standard laptop with suitable processing software.

Purification of [^{11}C]IPCIT was performed by semi-preparative reversed phase HPLC using the built-in semi-preparative HPLC system equipped with a radioactivity (Bertholdt Technologies, Bad Wildbach, Germany), a UV-detector (Linear Instruments Model 200 Detector UV/vis) and a LaPrep HPLC pump (VWR International, Radnor, USA). A Phenomenex® Gemini, C-18 with TMS endcapping, 10 μm, 250 × 10 mm column (Phenomenex®, Aschaffenburg, Germany) with a mobile phase of MeOH/0.1 M ammonium formate 71/29 v/v containing 1% NEt_3 at a flow rate of 8 mL/min was used for purification.

Analytical HPLC for both tracers was performed on Merck-Hitachi LaChrom HPLC system (L-7100 pump; LaChrom L-7400 UV detector at 254 nm) and a NaI radio-detector (Bertholdt Technologies, Bad Wildbach, Germany) using Raytest software (Raytest, Straubenhardt, Germany). A Chromolith® Performance RP-18e, 5 μm, 100 × 4.6 mm (Merck, Germany) column with a mobile phase consisting of (water/acetic acid 97.5/2.5 v/v; 2.5 g/L ammonium acetate; pH 3.5)/ACN 75/25 v/v at a flow rate of 2 mL/min was used. Osmolality was measured with a Wescor osmometer Vapro® 5600 (Sanova Medical Systems, Vienna, Austria) and pH was measured using a WTW inoLab 740 pH meter (WTW, Weilheim, Germany).

All intermediates and products were analysed spectroscopically via NMR, MS, and HRMS. For NMR analysis, the solvent signal was used as an internal standard which was related to TMS with δ = 7.26 ppm (^{1}H in $CDCl_3$) and δ = 77.0 ppm (^{13}C in $CDCl_3$). NMR: Bruker Avance DPX-200 Spectrometer at 27 °C (200.13 MHz for ^{1}H, 50.32 MHz for ^{13}C); MS: GC/MS-Q95050 GC-17A SHIMADZU; HRMS: Finnigan MAT 8230 (EI, 70 eV) and Finnigan MAT 900 S (ESI, 4 kV, 3 μA CH_3CN/MeOH). NMR analysis (^{1}H and ^{13}C) of intermediates were in full accordance with the literature.

2.3. Methods

2.3.1. Precursor chemistry

Syntheses of precursor and reference compounds were done with some modifications according to previously reported methods (Scheme 1).[26–29] Detailed reaction conditions are given in the Supplementary data.

2.3.2. Radiochemistry

2.3.2.1. Preparation of [^{11}C]IPCIT. *2.3.2.1.1. Production of [^{11}C]CH_3I.* [^{11}C]CO_2 production was stopped as soon as the desired activity (45.7 ± 8 GBq) at currents between 45 and 54 μA was achieved (10–15 min). [^{11}C]CH_3I was produced using a gas phase conversion described by Larsen et al.[30] within the GE Tracerlab™ FX C Pro synthesizer adopting modifications described by Kniess et al.[31] Briefly, [^{11}C]CO_2 was trapped on a molecular sieve (4 Å) within the module and subsequently converted into [^{11}C]CH_4 by a Ni-catalysed reduction with H_2 at 400 °C. The resulting [^{11}C]CH_4 was reacted in a re-circulating process for 4 min with sublimated iodine at 720 °C to give [^{11}C]CH_3I. The produced [^{11}C]CH_3I was trapped on-line on a Porapak® N column and finally released by heating the trap to 190 °C.

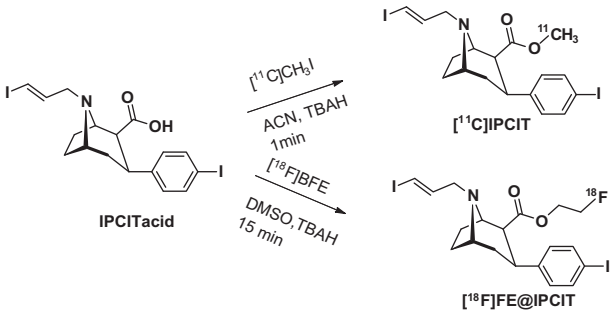

Scheme 2. Radiosyntheses of [^{11}C]IPCIT and [^{18}F]FE@IPCIT.

2.3.2.1.2. [^{11}C]IPCIT: small scale experiments and optimization. [^{11}C]methyl iodide was trapped in 500 μL ACN and split for further experiments. All evaluation reactions were, if not stated otherwise, performed in triplicates and executed manually (lead shielded hood, <1 GBq). The impact of reaction time (0.5, 1 and 2 min) and temperature (RT, 50 °C, 75 °C) as well as precursor concentration (0.25, 0.5, 1, 1.5 and 2 mg/mL) were investigated. Final reaction volumes of small-scale reactions were 50–200 μL. In Scheme 2 the radiosyntheses are outlined.

2.3.2.1.3. [^{11}C]IPCIT: automation of synthesis. [^{11}C]-*O*-methylation was automated within a Tracerlab™ FX C Pro syntheziser.[32] Freshly produced [^{11}C]CH_3I was trapped at RT within a glass reactor (2 mL) containing IPCITacid (0.25 mg, 0.48 μmol) and 1 μL of an aqueous TBAH-solution (1 mg/μL) in 250 μL ACN. After stirring for 0.5 min at ambient temperature, the reaction was quenched and diluted by addition of 1 mL water. The crude mixture was transferred to the injection loop and automatically (fluid detector controlled) injected onto the semi-preparative HPLC column. The [^{11}C]IPCIT peak was cut into a bulb, and subsequently diluted with 80 mL water. The aqueous product solution was subjected to solid phase extraction by transfer over a preconditioned (10 mL EtOH, air, 20 mL water, air) C18plus SPE cartridge. After rinsing the C18plus SepPak® with water, the pure product was eluted with 1.5 mL EtOH into a vial containing 100 μL TWEEN®-80 and the

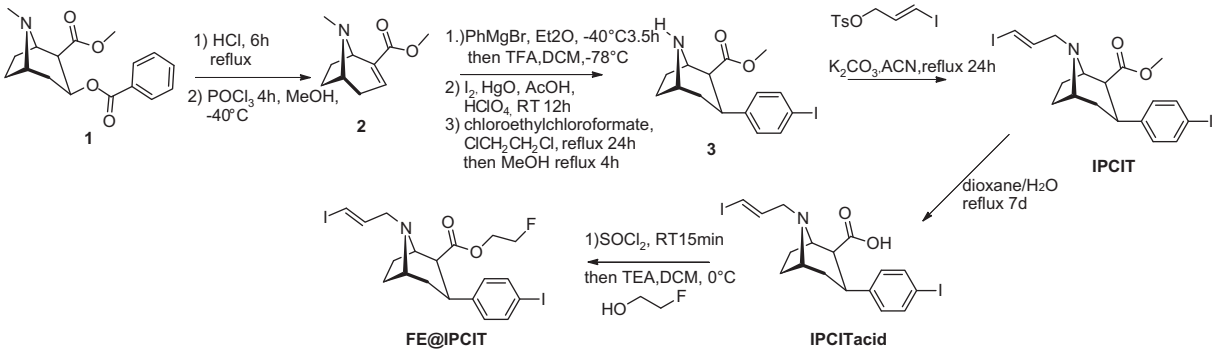

Scheme 1. Syntheses of precursor IPCITacid and reference standards IPCIT and FE@IPCIT.

cartridge and transfer lines were washed with 5 mL 0.9% saline. After sterile filtration (0.22 μm), formulation with further 9 mL 0.9% saline, 1 mL 3% saline and 1 mL 125 mM phosphate buffer was performed under aseptic conditions (laminar air flow hot cell, class A) to avoid microbial contamination.

2.3.2.2. Preparation of [^{18}F]FE@IPCIT. *2.3.2.2.1. Synthesis of 1-bromo-2-[^{18}F]fluoroethane (BFE).* Cyclotron produced [^{18}F]fluoride in $H_2{}^{18}O$ was trapped on a PS-HCO_3 cartridge, and eluted with 0.8 mL of solution A, containing K_2CO_3 (4.5 mg/mL, 33.2 μmol/mL), Kryptofix 2.2.2 (4,7,13,16,21,24-hexaoxa-1,10-diaza-bi-cyclo [8.8.8]hexacosane; 20 mg/mL, 53.2 μmol/mL) in ACN/H2O (70/30 %v/v). Azeotropic drying was performed iteratively by threefold addition of 0.5 mL of ACN. [^{18}F]BFE was synthesized according to Zuhayra et al.[33] A mixture of 30 μL BrEtOTf in 500 μL 1,2-dichlorobenzene (*o*-DCB) was added to the azeotropically dried [^{18}F]fluoride and heated to 100 °C for 10 min. The resulting [^{18}F]BFE was purified by distillation at 100 °C and trapped in 0.5 mL of DMSO at 0 °C.[34] Radiochemical and chemical purity was assessed by analytical HPLC (for conditions see Section 2.1).

2.3.2.2.2. [^{18}F]FE@IPCIT: small scale experiments and optimization. To the resulting [^{18}F]BFE solution in DMSO a solution of precursor IPCITacid and base in DMSO was added. All evaluation reactions were performed manually (shielded hood; starting activity <1 GBq). The influence of reaction time (1, 5, 10 and 15 and 60 min), reaction temperature (RT, 75 °C, 110 °C, 130 °C), base (TBAH, K_2CO_3, Cs_2CO_3, succinic anhydride, NaI, KI, NaH triethylamine and LiOH) and precursor concentration (0.25, 0.5, 1 and 2 mg/mL) was investigated. Finale reaction volumes of small-scale reactions were 50–400 μL. The reaction scheme is presented in Scheme 2.

2.3.2.2.3. [^{18}F]FE@IPCIT: automation of synthesis. Automation of fluoroalkylation was performed within a Nuclear Interface synthesiser. Cyclotron produced [^{18}F]F^- was trapped automatically on an anion exchange cartridge, eluted with 0.8 mL of solution A into the first reactor and iteratively azeotropically dried. Then a solution of 30 μL BET in 500 μL *o*-DCB was added, the vessel sealed and the mixture heated to 100 °C for 10 min. The resulting [^{18}F]BFE was distilled under a smooth He-stream (40 mL/min) into the precooled (0 °C) second reaction vessel containing 0.4 mL DMSO. To this, the precursor (2 mg/mL final concentration), 1 μL of an aqueous TBAH solution (2.4 mg/μL) in 0.2 mL DMSO was added and the sealed reaction vessel heated to 110 °C for 15 min. The crude reaction mixture was cooled to RT and radiochemical conversion checked by analytical HPLC.

2.3.3. Quality control

According to the European Pharmacopoeia, chemical and radiochemical impurities were identified by UV- and radio-HPLC, osmolality and pH were tested with designated equipment. Sterility, absences of endotoxins and residual solvents were determined by routine procedures at the PET Centre of the Vienna General Hospital, Medical University of Vienna. Specific radioactivity was assessed by quantification of the non-radioactive product (HPLC UV channel at 254 nm) and determination of overall radiochemical yield (GBq at end of synthesis).

2.3.4. Statistical analysis

All quantitative data (both in text and figures) are given as arithmetic mean ± standard deviation. A Student *t*-test (two-tailed) was performed for determination of significance; that is, *P* values of <0.05 were considered significant. If not stated otherwise, error bars in figures are representing the standard deviation; if not visible they are within the margin of the symbol.

2.3.5. Membrane binding studies

Affinity of candidate substances was tested in standard DAT-membrane binding experiments.[35,36] A 100 mM NaCl and 50 mM Tris–HCl pH 7.4 was used for the assay. The competitive binding experiments were performed in glass test tubes, filled with 350 μL of the new 'cold' (=non-radioactive) reference compounds, 100 μL of the membrane suspension (in assay buffer; 12.7 μg protein/unit, RBHDATM400UA, Perkin Elmer, Waltham, USA) and 50 μL of a 3 nM ^{3}H-WIN 35,428 (=β-CFT) solution (in assay buffer, 60–87 Ci/mmol, NET1033001MC; Perkin Elmer). For non-specific binding 10 μM GBR 12909 (Sigma–Aldrich, Vienna, Austria) was used; and for total binding (control) only ^{3}H-WIN35,428, buffer and membrane suspension were incubated. After 2 h incubation time at 4 °C, binding was quenched with ice cold buffer, and membrane bound radioactivity was recovered by centrifugation at about 40,000*g* for 15 min. The supernatant was wasted and the pellets were washed two times with 4 mL ice cold assay buffer. After addition of a β-scintillation cocktail (2 mL Ultima GoldTM, biodegradable, Perkin Elmer), the tubes were shaken for 20 min and then counted. Data from the competition plots were analyzed; IC_{50} and K_i values were calculated using GraphPad Prism® 5 software (San Diego, USA). (Arithmetic means of values derived from three different assays, in triplicate for each compound.)

Selectivity of the candidate compounds was tested in NET and SERT membrane studies, similarly to those described for DAT above. NET and SERT expressing membranes were used instead of DAT-membranes (hSERT: 9 μg protein/unit, RBHSTM400UA, Perkin Elmer and hNET: 3 μg protein/unit, RBHNETM400AU, Perkin Elmer). ^{3}H-Nisoxetine*HCl solution (in assay buffer, 70–87 Ci/mmol, NET1084; Perkin Elmer) was as radioligand for the NET assay, ^{3}H-Imipramin*HCl (in assay buffer, NET576; 40–70 Ci/mmol, Perkin Elmer) was used for SERT testing, respectively. IC_{50} and K_i values were obtained in analogy to NET experiments and ratios NET/DAT and SERT/DAT were determined.

2.3.6. Lipophilicity and blood brain barrier penetration

Lipophilicity was tested with HPLC according to Donovan and Pescatore.[37] The candidate substances were injected in a mix of Toluene and Triphenylene (known log*D* and *k*′) in a short polymeric ODP-50 column (20 × 4.0 mm, 5 μm, Shodex®, Showa Denko Europe GmbH, Munich, Germany) using a linear gradient from 10% MeOH/90% 25 mM Phosphate buffer to 100% methanol within 9.4 min at a flow-rate of 1.5 mL/min. As log*D* values are poor predictors for blood brain barrier (BBB) penetration, additional calculation of tPSA (total polar surface area) and IAM chromatography experiments were performed according to Yoon et al. and Tavares et al.;[38,39] tPSA was calculated using ChemBioDraw Ultra 12.0 (CamebridgeSoft, PerkinElmer). For IAM-chromatography, a Reditech IAM.PC.DD2 (Regis Technologies Inc., Morton Grove, USA) column (150 m × 4.6 mm) was used isocratically with 0.01 M phosphate buffer and ACN in different ratios (1 mL/min). Resulting P_m (permeability) and K_m (membrane partition coefficient) were obtained after data analysis and the data were compared with those derived from PE2I and β-CIT as external standards, compounds known to penetrate BBB.

2.3.7. Metabolic stability testing

Metabolic stability was assessed using three different methods. First, plasma stability was determined over a period of 60 min.[40] Therefore, 10 μL of [^{11}C]IPCIT or [^{18}F]FE@IPCIT were incubated in 500 μL pooled human plasma (Innovative Research, Peary Court Novi, Li Heparin, X1693B) at 37 °C using a thermocycler (NB: 2% ethanol in the final incubation solution should not be exceeded, in order to avoid enzymatic side reactions). At the respective time points, an aliquot of the tracer-plasma mixture was quenched with

one volume of an ice-cold methanol/ACN mixture (10/1 v/v). The mixtures were vortexed and centrifuged (4 min, 5 °C, 23,000*g*), and the obtained supernatants were analyzed by radio-HPLC. As result, percentage of metabolized compound per time was obtained.

To investigate the further metabolic fate of [^{11}C]IPCIT and [^{18}F]FE@IPCIT, stability against pooled human liver microsomes (BD Biosciences, Woburn, 20 mg/mL in sucrose) was determined. These microsomes are subcellular fractions containing many drug-metabolizing enzymes (cytochrome P450, flavinmonooxygenases, epoxid hydrolases, etc.). Microsomal incubation was performed similarly to the plasma stability assay described above. Microsome solution in sucrose were pre-incubated for 5 min under physiological conditions (pH 7.4, Phosphate buffer, 37 °C) with a NADPH-generating system (NADP+, glucose-6-phosphate, magnesium-chloride in H_2O and Glucose-6-phosphate dehydrogenase in sodium citrate). Subsequently, 6 μL of the formulated radiotracer were incubated in a final volume of 300 μL microsome solution (NB: 2% ethanol in the final incubation solution should not be exceeded, in order to avoid inhibition of various enzymes like CYPs and UDP-GA).[40] Enzymatic reactions were stopped at the respective time points by quenching with one volume MeOH/ACN (10/1). After vortexing and centrifugation, the supernatants were analyzed by radio-HPLC and the percentage of intact tracer was determined.

Furthermore, stability against carboxylic ester hydrolase (CES) was tested as well. Therefore, 20 μL of a 1/1/1 (v/v/v) mixture of human CES1b, human CES1c and CES2 (each BD Biosciences, Bedford, 5 mg/mL, Cat. No. 453320, 453321, 453322) was prepared and diluted with 270 μL phosphate buffer (pH 7.4). To this 6 μL of the respective radiotracer were added and incubated, stopped and analyzed as described above.

3. Results

3.1. Chemistry

Precursor and reference compounds were synthesized successfully; overall-yields of 4.9% for IPCITacid, 12.7% for IPCIT and 4.1% for FE@IPCIT were achieved.

Briefly, after hydrolysis of cocaine with 6 M HCl, and elimination of the resulting alcohol moiety with $POCl_3$ and MeOH, the anhydroecgonine methyl ester **2** was obtained and purification by distillation yielded 94.3%. After Michael addition of the unsaturated methyl ester with PhMgBr, followed by introduction of the para-iodo substituent at the phenyl ring and N-demethylation with chloroethyl chloroformate in 1,2-dichloroethane, nortropane **3** was obtained in 21.2% yield. N-Alkylation with the (*E*)-3-iodoallyl 4-methylbenzenesulfonate gave the reference compound IPCIT in 63.3% yield. Precursor IPCIT acid was obtained via hydrolysis in dioxane/water in 38.7% yield. Fluoroethylation of IPCITacid resulted in 85.0% of the reference compound FE@IPCIT. Spectroscopic data were in full accordance with the proposed structures (see Supplementary data).

3.2. Radiochemistry

3.2.1. ^{11}C-Radiolabelling

^{11}C-O-methylation evinced no difference whether [^{11}C]methyl iodide or [^{11}C]methyl triflate was used. Using precursor amounts below 0.5 mg/mL, radiochemical incorporation yields (RCIY) were below 30.5%. At 0.5 mg/mL 60% radiochemical incorporation was observed, above 0.5 mg/mL a plateau of 66% RCIY was found (Fig. 2). Base catalysis was in all experiments performed with 1 μL of an aqueous TBAH solution per 500 μL of precursor dissolved in ACN. Increasing temperature from RT to 50 °C or 75 °C appears to play a subordinate role, thus it did not result in a significant increase in radiochemical incorporation. RCIYs for 1 mg/mL precursor concentration at RT ranged from 65.0% for short reaction times (0.5 min at RT) up to 66.4% for longer reaction times (2 min). Hence, small scale experiments revealed optimum conditions of 1 mg/mL precursor concentration, RT, 1 min and TBAH catalysis.

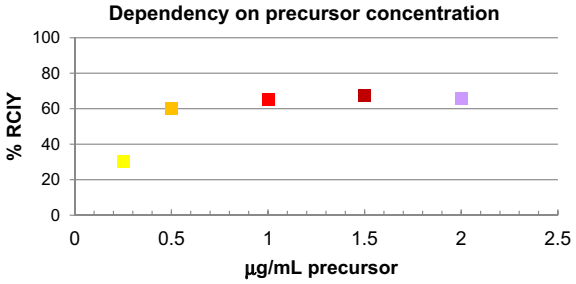

Figure 2. Dependency of RCIY on precursor concentration.

In Table 1, synthesis steps, conversion and yields for large scale preparations are outlined. After preparative HPLC (ret. time [^{11}C]CH_3I = 2.0 min; [^{11}C]ICPIT = 11.5 min) and SPE, the pure product was eluted from the C18plus SepPak® with ethanol and the tubings rinsed with 5 mL saline 0.9%. Sterile filtration was attempted over a 0.22 μm PVDF (polyvinyliden fluoride) or a 0.22 μm MCE (mixed cellulose esters) sterile filter with product solutions with different EtOH concentration. In Figure 3, product passing the sterile filter is depicted. Best conditions were achieved when adding 100 μL TWEEN®-80 to the product solution before sterile filtration.

So far, 5 fully automated radiosyntheses have been performed, yielding 1.9 ± 0.7 GBq [^{11}C]IPCIT (6.4 ± 4%, corr. EOB) within 36 min (for details see Table 1). Specific radioactivities were sufficient with 24 ± 5 GBq/μmol (calculated using an HPLC-based method). Radiochemical and chemical purity were always ⩾98%, osmolality and pH were found to be in a physiological range. GC analysis evinced ACN <5 ppm and methanol <20 ppm. Retention times in the analytical HPLC were 1.05–1.4 min (k' = 0–0.33) for [^{11}C]CH_3I, 2.1–3.0 min (k' = 1.0–1.86) for precursor IPCITacid, and 5.0–5.9 min (k' = 3.76–4.6) for [^{11}C]IPCIT. In Figure 4 a spiked analytical chromatogram of [^{11}C]IPCIT is shown (IPCIT reference standard in 50 μg/mL)

3.2.2. ^{18}F-Radiolabelling

[^{18}F]BFE was obtained in sufficient yields (26.4 ± 6%) and high purity (⩾95%) after distillation. ^{18}F-Fluoroethylation was performed in small scale experiments investigating the influence of base, reaction temperature and precursor concentration. Regarding the reaction temperature, very low RCIYs (2.9%) were obtained for reactions at RT, whereas high RCIYs were achieved at 110 °C (55.1–78.1%) after 15 min. Elevation of temperature to 130 °C did not result in further increase in radiochemical incorporation. Elongation of reaction time did not affect RCIY. Using precursor amounts of more than 1 mg/mL did not show a beneficial effect either. No conversion of [^{18}F]BFE to [^{18}F]FE@IPCIT was observed for reactions below 0.5 mg/mL. In Table 2 the effects of base catalysis are summarized. Advantages of addition of NaI or KI could not be confirmed for this reaction. Hence, optimum conditions were obtained using 1 mg/mL IPCITacid at 100 °C with TBAH catalysis (1 μL, aqueous solution).

Although the optimum conditions were used for automation in larger scale, unexpectedly poor radiochemical incorporation yields (below 6%) were achieved.

Table 1
Fully automated preparation of [^{11}C]IPCIT with $n \geqslant 5$ (∗at end of synthesis)

$n \geqslant 5$	GBq	% of initial activity (corr. for decay)	Δt to EOB (min)
[^{11}C]CO_2 targetactivity	45.7 ± 8.7	100	0
[^{11}C]CH_3I activity trapped in reactor	19.8 ± 2.2	71.7 ± 9.1	14 ± 1
Residual in reactor after transfer to HPLC	1.0 ± 0.6	3.8 ± 2.2	16 ± 1
Residual in HPLC injection loop waste	1.1 ± 1.0	4.2 ± 4.5	16 ± 1
Collected [^{11}C]IPCIT before sterile filtration	2.1 ± 0.4	13.8 ± 1.9	33 ± 1
[^{11}C]IPCIT final product yield	1.9 ± 0.7	12.5 ± 4.4	36 ± 2
Specific activity	24 ± 5		

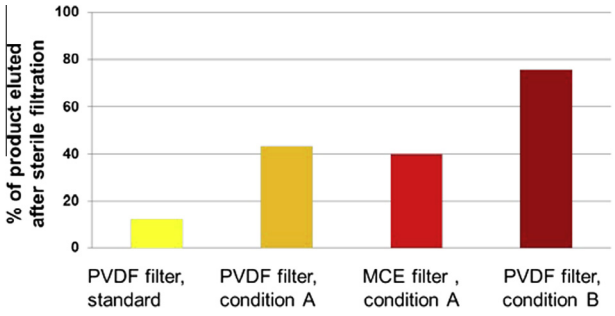

Figure 3. Percentage of product passing the 0.22 μm sterile filter using different conditions for product transfer over sterile filter: *standard:* 9 mL 0.9% saline, 1 mL 3% saline, 1 mL 125 mM phosphate buffer; 1.5 mL EtOH; *condition A*: 5 mL 0.9% saline, 1.5 mL EtOH; *condition B*: 5 mL 0.9% saline, 1.5 mL EtOH, 100 μL Tween® 80).

The radiochemical and chemical purity was assessed via analytical HPLC (see Section 2.1), the retention times were: [^{18}F]F$^-$: 1.6-1.8 min (k' = 0–0.1), IPCITacid: 2.05–2.2 min (k' = 0.28–0.38), [^{18}F]BFE: 3.8–4.2 min (k' = 1.37-1.63) and [^{18}F]FE@IPCIT: 5.0-6.5 min (k' = 2.1-3.06). In Figure 4 an exemplary analytical HPLC chromatogram is shown (co-injection with FE@IPCIT reference standard 50 μg/mL)

3.3. Affinity and selectivity testing, lipophilicity and blood brain barrier penetration

Optimum conditions for DAT-affinity testing were found to be incubation at 25 °C in a buffer containing 100 mM NaCl and 50 mM TRIS*HCl at pH 7.4. K_i values of reference compounds were determined as 37 ± 13 nM for precursor IPCITacid, 1.7 ± 0.6 nM for IPCIT and 1.3 ± 0.2 nM for FE@IPCIT ($n \geqslant 5$ triplicates). For testing of selectivity of our candidate compounds, affinity towards NET and SERT was determined similarly, revealing an 11-fold selectivity for IPCIT and a 115-fold selectivity for FE@ICPIT towards DAT as compared to NET. Selectivity towards SERT was found to be poor for IPCIT, but tolerable for FE@IPCIT (SERT/DAT: 1.8-fold).

Log$D$ was determined as 0.87 for precursor IPCITacid, 5.29 for IPCIT and 5.39 for FE@IPCIT. Regarding BBB-penetration a tPSA value of 29.54 was calculated both for IPCIT and FE@IPCIT. IAM-chromatography experiments revealed permeability (P_m) values of 0.04 for IPCITacid, 7.74 for IPCIT and 8.94 for FE@IPCIT. For comparison P_m was also determined for PE2I (3.15) and β-CIT (0.31), two compounds known to penetrate the BBB. In Table 3, all tested preclinical parameters including K_i, P_m, PSA and log$D$ are outlined.

3.4. Metabolic stability testing

The aim of this molecular design was to obtain a DAT PET tracer with both high affinity and metabolic stability. Therefore, three different metabolizing systems were used to determine the metabolic fate of our novel candidate tracers over a period of 1 h, representative for the PET measurement duration. In Figure 5, an overview of the degradation is given. Hereby, no metabolism was observed in human plasma, thus 100% of the tracers were intact after 1 h of incubation. Using human liver microsomes, a significant metabolic degradation was observed. After 1 h of incubation 46.4 ± 0.6% of [^{11}C]IPCIT and 71.6 ± 2.7% [^{18}F]FE@IPCIT were found to be intact. After incubation with CES, 92% of the candidate tracers were found to be intact after 60 min.

4. Discussion

The rationale of this work was to combine the structural advantages of β-CIT and PE2I, aiming at DAT-ligands with high affinity, stability and selectivity. Synthesis of precursor and reference compounds was achieved successfully. In preliminary preclinical examinations, affinity was found to be high; also selectivity was sufficient due to the high abundance of DAT in human brain as compared to other monoamine transporters.

Optimized O-^{11}C-methylation was leading to good radiochemical incorporation yields with low amounts of precursor at ambient temperature. Furthermore, also purification of crude mixture via preparative HPLC and SPE succeeded. Sterile filtration was optimized using 100 μL TWEEN®-80. Automation of ^{11}C-radiosynthesis yielded 1.9 ± 0.7 GBq [^{11}C]IPCIT within 36 min, enabling large scale preparations (starting activities: 40–50 GBq [^{11}C]CO_2) under maximum radiation safety compliance.

Specific activities were moderate with 24 ± 5 GBq/μmol, due to difficulties with [^{12}C]CO_2 impurities in the target gas (nota bene: this was observed for all ^{11}C-labelled tracers at that time, but was resolved in the meantime). Quality control of [^{11}C]IPCIT showed high purity (<99%) of all batches of the formulated product observing the European Pharmacopoeia and therefore allowing for further preclinical testing.

Preparation of [^{18}F]BFE was done successfully starting from [^{18}F]F$^-$ and 2-bromoethyltriflate in o-DCB and purified by distillation. Trace amounts of o-DCB turned out to hamper the reaction also in very small amounts, when present in the reaction mixture; therefore a rather smooth He-stream during distillation (⩽40 mL/min) was crucial. Fluoroalkylation of IPCITacid with [^{18}F]BFE was accomplished in small scale experiments in high radiochemical yields (up to 66.6 ± 16%) using 1 μL of an aqueous TBAH solution. Other alkaline compounds were evaluated as catalyst, amongst these only Cs_2CO_3 showed similar catalytic activity as TBAH. The addition of small amounts of KI or NaI to the reaction mixture was reported to be beneficial, however this was not observed for this specific ^{18}F-fluoroalkylation reaction. On the contrary, lower RCIYs were observed when adding KI or NaI.[24] Increasing the reaction temperature also did not result in further increase in radiochemical incorporation, thus maximum conversion was observed at 110 °C for 15 min. Automation using optimum parameters did not lead to RCIYs higher than 6%.

In a first preclinical evaluation, we found high affinity towards DAT for both candidate compounds. The DAT-affinity of IPCIT is 10-fold higher than the affinity displayed by PE2I towards DAT. A more than 13-fold affinity was determined for FE@IPCIT at DAT as compared to PE2I. Unfortunately, selectivity DAT/SERT is poor for both ligands. Thus, the hypothesis of this molecular design, did not lead to ligands with higher selectivity. Nevertheless, the selectivity is tolerable, as also known from other DAT radioligands in clinical use (e.g., [^{123}I]FP-CIT, DATScan®).

Metabolic stability was expected to be high due to the favorable combination of structural elements from PE2I and β-CIT (no benzylic oxidation possible), but displayed to be high only against human plasma and human carboxyl esterase, and moderate against human liver microsomes. Here, only polar metabolites were

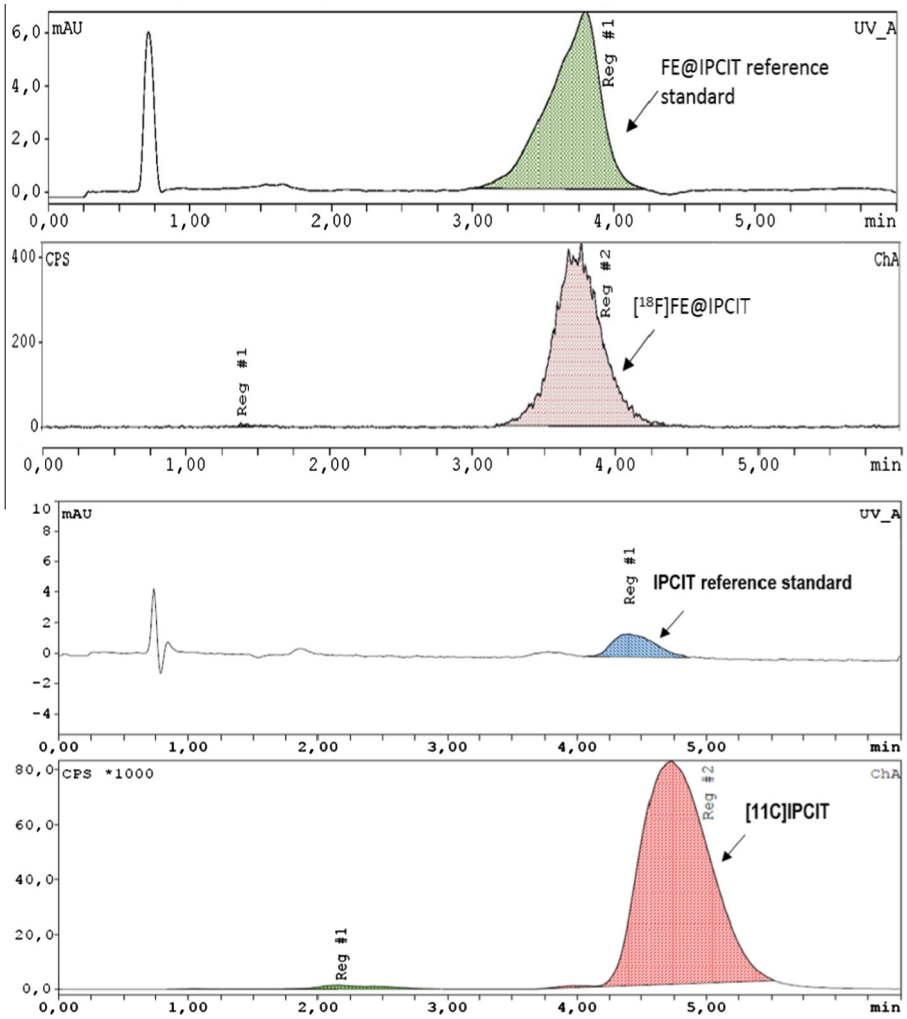

Figure 4. Co-injected analytical HPLC chromatograms of [^{11}C]IPCIT and IPCIT reference standard and [^{18}F]FE@IPCIT and FE@IPCIT reference standard.

Table 2
Effects of different bases on RCI of ^{18}F-fluoroethylation of IPCITacid (110 °C, 15 min, 1 mg/mL IPCITacid)

FE@IPCIT base catalysis	TBAH	Cs_2CO_3	LiOH	Na_2 succinate	KI + Cs_2CO_3	NEt_3	KOH, NaOH, KI, NaH, TRIS, NaI or KI + NaH
% RCI	78	75	70	31	21	2	0

Table 3
Overview on tested preclinical parameters of DAT ligands

					K_i (nM)		
	log*D*	tPSA[a]	K_M	P_m	DAT	NET	SERT
IPCITacid	0.87	40.54	21.26	0.04	36.99 ± 13	785 ± 179	71.4 ± 25.5
IPCIT	5.29	29.54	4157.34	7.74	1.72 ± 0.6	20 ± 10	1.5 ± 0.4
FE@IPCIT	5.39	29.54	5086.15	8.94	1.33 ± 0.2	153 ± 53	2.4 ± 1
PE2I	4.71[a]	29.54	1340.99	3.15	17 ± 7[42]	>1000[42]	500 ± 30[42]
b-CIT	3.69[a]	29.54	120.43	0.31	6.34 ± 1.7[22]	32.77 ± 13.41[22]	29.17 ± 6.4[22]

[a] Calculated with ChemBioDraw Ultra 12).

formed. Thus, no critical interaction on the target sites in vivo can be expected. Overall, metabolic stability tests indicate higher stability than for previously published DAT ligands.[7,13,16,20]

Considering a potential in vivo application of [^{11}C]IPCIT or [^{18}F]FE@IPCIT as DAT-PET tracer, also BBB-penetration was examined. Therefore, log*D* was measured and tPSA calculated. According to Yoon et al. a tPSA value below 60 seems to predict possible BBB-penetration.[38] We found a tPSA value of 29.54 for both IPCIT and FE@IPCIT. Nevertheless, being aware of the high log*D* value of >5 for both candidate ligands, and a measured high P_m value (>8) in IAM experiments, crossing of BBB and high specific brain uptake might be doubted.

Since previously published DAT ligands also showed high lipophilicity (e.g., [^{123}I]IPT[41]) and lack a testing of IAM chromatography and tPSA values, a possible BBB penetration cannot be totally excluded for our candidate DAT tracers although the found values

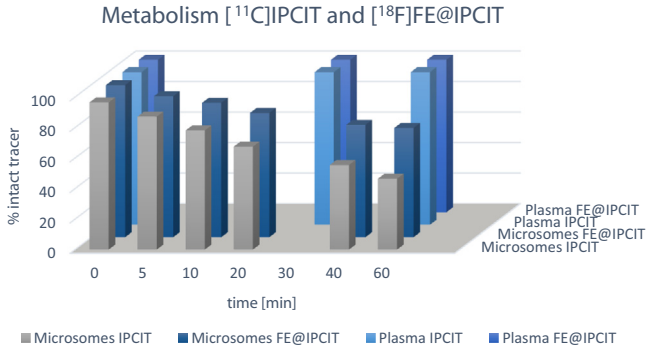

Figure 5. Metabolic stability of [^{11}C]IPCIT and [^{18}F]FE@IPCIT against human CES, plasma and microsomes.

suggest otherwise. Further examinations of the candidate ligands in biodistribution studies could be performed to clarify whether a significant brain uptake is possible or not. However, in respect to the 'three Rs-principle' (reduction, refinement, replacement)[42] we think that such additional animal (in vivo and ex vivo) experiments are not justified enough. Therefore, we think that data concerning BBB-penetration from in vitro and in silico experiments are representative and allow to judge the suitability of our molecules to be used in further studies.

Consequently, we acknowledge that merging two structurally beneficial elements did, in this case, not result in an improved DAT-PET ligand for in vivo application.

5. Conclusion

Synthesis and radiosyntheses of the candidate compounds were performed successfully. Membrane binding experiments revealed high affinity for both methylated and fluoroethylated compounds; selectivity and metabolic stability turned out tolerable. Both candidate compounds displayed high log$D$ and P_m values, making BBB-penetration questionable.

Acknowledgement

The authors thank Dr. Michael Berger, Matthias Hendl, Ing. Thomas Zenz and Ing. Andreas Krcal for their support.

Supplementary data

Supplementary data associated with this article can be found, in the online version, at http://dx.doi.org/10.1016/j.bmc.2013.10.046.

References and notes

1. Tissingh, G.; Bergmans, P.; Booij, J.; Winogrodzka, A.; van Royen, E. A.; Stoof, J. C.; Wolters, E. C. *J. Neurol.* **1998**, *245*, 10.
2. Dougherty, D. D.; Bonab, A. A.; Spencer, T. J.; Rauch, S. L.; Madras, B. K.; Fischman, A. J. *Lancet* **1999**, *354*, 2132.
3. Laasonen-Balk, T.; Kuikka, J.; Viinamäki, H.; Husso-Saastamoinen, M.; Lehtonen, J.; Tiihonen, J. *Psychopharmacology* **1999**, *144*, 282.
4. Halldin, C.; Gulyás, B.; Langer, O.; Farde, L. Q. *J. Nucl. Med.* **2001**, *2001*, 139.
5. Malison, R. T.; Kung, H. F.; Vessotskie, J. M.; Kung, M.-P.; McElgin, W.; Romaniello, G.; Kim, H.-J.; Goodman, M. M. *J. Nucl. Med.* **1995**, *36*, 2290.
6. Mitterhauser, M.; Wadsak, W.; Mien, L.-K.; Hoepping, A.; Viernstein, H.; Dudczak, R.; Kletter, K. *Synapse* **2005**, *55*, 73.
7. Muller, L.; Halldin, C.; Farde, L.; Karlsson, P.; Hall, H.; Swahn, C. G.; Neumeyer, J.; Gao, Y.; Milius, R. *Nucl. Med. Biol.* **1993**, *20*, 249.
8. Madras, B. K.; Gracz, L. M.; Fahey, M. A.; Elmaleh, D.; Meltzer, P. C.; Liang, A. Y.; Stopa, E. G.; Babich, J.; Fischman, A. J. *Synapse (N.Y.)* **1998**, *29*, 116.
9. Stehouwer, J. S.; Jarkas, N.; Zeng, F.; Voll, R. J.; Williams, L.; Camp, V. M.; Malveaux, E. J.; Votaw, J. R.; Howell, L.; Owens, M. J.; Goodman, M. M. *J. Med. Chem.* **2008**, *51*, 7788.
10. Koivula, T.; Marjamaki, P.; Haaparanta, M.; Fagerholm, V.; Gronroos, T.; Lipponen, T.; Perhola, O.; Vepsalainen, J.; Solin, O. *Nucl. Med. Biol.* **2008**, *35*, 177.
11. Mozley, P. D.; Kim, H.-J.; Gur, R. C.; Tatsch, K.; Muenz, L. R.; McElgin, W. T.; Kung, M.-P.; Mu, M.; Myers, A. M.; Kung, H. F. *J. Nucl. Med.* **1996**, *37*, 1965.
12. Goodman, M. M.; Kung, M.-P.; Kabalka, G. W.; Kung, H. F.; Switzer, R. *J. Med. Chem.* **1994**, *37*, 1535.
13. Goodman, M. M.; Kilts, C. D.; Keil, R.; Shi, B.; Martarello, L.; Xing, D.; Votaw, J.; Ely, T. D.; Lambert, P.; Owens, M. J.; Camp, V. M.; Malveaux, E.; Hoffman, J. M. *Nucl. Med. Biol.* **2000**, *27*, 1.
14. Riss, P. J.; Stockhofe, K.; Roesch, F. *J. Labelled Compd. Radiopharm.* **2013**, *56*, 149.
15. Farde, L.; Halldin, C.; Müller, L.; Suhara, T.; Karlsson, P.; Hall, H. *Synapse* **1994**, *16*, 93.
16. Shetty, H. U.; Zoghbi, S.; Liow, J.-S.; Ichise, M.; Hong, J.; Musachio, J.; Halldin, C.; Seidel, J.; Innis, R.; Pike, V. *Eur. J. Nucl. Med. Mol. Imaging* **2007**, *34*, 667.
17. Zoghbi, S. S.; Shetty, H. U.; Ichise, M.; Fujita, M.; Imaizumi, M.; Liow, J.-S.; Shah, J.; Musachio, J. L.; Pike, V. W.; Innis, R. B. *J. Nucl. Med.* **2006**, *47*, 520.
18. Varrone, A.; Steiger, C.; Schou, M.; Takano, A.; Finnema, S. J.; Guilloteau, D.; Gulyas, B.; Halldin, C. *Synapse (Hoboken, NJ, U. S.)* **2009**, *63*, 871.
19. Stepanov, V.; Krasikova, R.; Raus, L.; Loog, O.; Hiltunen, J.; Halldin, C. *J. Labelled Compd. Radiopharm.* **2012**, *55*, 206.
20. Schou, M.; Steiger, C.; Varrone, A.; Guilloteau, D.; Halldin, C. *Bioorg. Med. Chem. Lett.* **2009**, *19*, 4843.
21. Halldin, C.; Erixon-Lindroth, N.; Pauli, S.; Chou, Y.-H.; Okubo, Y.; Karlsson, P.; Lundkvist, C.; Olsson, H.; Guilloteau, D.; Emond, P.; Farde, L. *Eur. J. Nucl. Med. Mol. Imaging* **2003**, *30*, 1220.
22. Emond, P.; Guilloteau, D.; Chalon, S. *CNS Neurosci. Ther.* **2008**, *14*, 47.
23. Shetty, H. U.; Zoghbi, S. S.; Liow, J.-S.; Ichise, M.; Hong, J.; Musachio, J. L.; Halldin, C.; Seidel, J.; Innis, R. B.; Pike, V. W. *Eur. J. Nucl. Med. Mol. Imaging* **2007**, *34*, 667.
24. Nics, L.; Haeusler, D.; Wadsak, W.; Wagner, K.-H.; Dudczak, R.; Kletter, K.; Mitterhauser, M. *Nucl. Med. Biol.* **2011**, *38*, 13.
25. Zhang, M.-R.; Furutsuka, K.; Yoshida, Y.; Suzuki, K. *J. Labelled Compd. Radiopharm.* **2003**, *46*, 587.
26. Meltzer, P. C.; Liang, A. Y.; Brownell, A. L.; Elmaleh, D. R.; Madras, B. K. *J. Med. Chem.* **1993**, *36*, 855.
27. Xu, L.; Trudell, M. L. *J. Heterocycl. Chem.* **1996**, *33*, 2037.
28. Boja, J. W.; Kuhar, M. J.; Kopajtic, T.; Yang, E.; Abraham, P.; Lewin, A. H.; Carroll, F. I. *J. Med. Chem.* **1994**, *37*, 1220.
29. Peng, X.; Zhang, A.; Kula, N. S.; Baldessarini, R. J.; Neumeyer, J. L. *Bioorg. Med. Chem. Lett.* **2004**, *14*, 5635.
30. Larsen, P.; Ulin, J.; Dahlstrøm, K.; Jensen, M. *Appl. Radiat. Isot.* **1997**, *48*, 153.
31. Kniess, T.; Rode, K.; Wuest, F. *Appl. Radiat. Isot.* **2008**, *66*, 482.
32. GE Healthcare, U., Sweden.
33. Zuhayra, M.; Alfteimi, A.; Papp, L.; Luetzen, U.; Luetzen, A.; Von, F. C.; Meller, B.; Henze, E. *Bioorg. Med. Chem.* **2008**, *16*, 9121.
34. Wadsak, W.; Mien, L.-K.; Ettlinger, D. E.; Eidherr, H.; Haeusler, D.; Sindelar, K.-M.; Keppler, B. K.; Dudczak, R.; Kletter, K.; Mitterhauser, M. *Nucl. Med. Biol.* **2007**, *34*, 1019.
35. Allard, P.; Marcusson, J. O.; Ross, S. B. *Brain Res.* **1996**, *706*, 347.
36. Mark, C.; Bornatowicz, B.; Mitterhauser, M.; Hendl, M.; Nics, L.; Haeusler, D.; Lanzenberger, R.; Berger, M. L.; Spreitzer, H.; Wadsak, W. *Nucl. Med. Biol.* **2013**, *40*, 295.
37. Donovan, S. F.; Pescatore, M. C. *J. Chromatogr. A* **2002**, *952*, 47.
38. Yoon, C. H.; Kim, S. J.; Shin, B. S.; Lee, K. C.; Yoo, S. D. *J. Biomol. Screen.* **2006**, *11*, 13.
39. Tavares, A. A.; Lewsey, J.; Dewar, D.; Pimlott, S. L. *Nucl. Med. Biol.* **2012**, *39*, 127.
40. Nics, L.; Vraka, C.; Hendl, M.; Haeusler, D.; Wagner, K.-H.; Shanab, K.; Spreitzer, H.; Dudczak, R.; Wadsak, W.; Mitterhauser, M. *Nuklearmed-Nucl. Med.* **2011**, *50*, A176.
41. Kung, M.-P.; Essman, W. D.; Frederick, D.; Meegalla, S.; Goodman, M.; Mu, M.; Lucki, I.; Kung, H. F. *Synapse* **1995**, *20*, 316.
42. Russell, W. M. S.; Burch, R. L. *The Principles of Humane Experimental Technique*; Methuen: London, 1959.

3.1.6 Manuscript VI

Rami-Mark C, Berroterán-Infante N, Philippe C, Foltin S, **Vraka C**, Hoepping A, Lanzenberger R, Hacker M, Mitterhauser M, Wadsak W. Radiosynthesis and first preclinical evaluation of the novel norepinephrine transporter pet-ligand [(11)C]ME@HAPTHI. EJNMMI Res. 2015 Dec;5(1):113.

Rami-Mark et al. EJNMMI Research (2015) 5:34
DOI 10.1186/s13550-015-0113-3

EJNMMI Research
a SpringerOpen Journal

ORIGINAL RESEARCH Open Access

Radiosynthesis and first preclinical evaluation of the novel norepinephrine transporter pet-ligand [^{11}C]ME@HAPTHI

Christina Rami-Mark[1,2], Neydher Berroterán-Infante[1,2], Cecile Philippe[1,3], Stefanie Foltin[1], Chrysoula Vraka[1], Alexander Hoepping[4], Rupert Lanzenberger[5], Marcus Hacker[1], Markus Mitterhauser[1,3*†] and Wolfgang Wadsak[1,2†]

Abstract

Background: The norepinephrine transporter (NET) has been demonstrated to be relevant to a multitude of neurological, psychiatric and cardiovascular pathologies. Due to the wide range of possible applications for PET imaging of the NET together with the limitations of currently available radioligands, novel PET tracers for imaging of the cerebral NET with improved pharmacological and pharmacodynamic properties are needed.

Methods: The present study addresses the radiosynthesis and first preclinical evaluation of the novel NET PET tracer [^{11}C]Me@HAPTHI by describing its affinity, selectivity, metabolic stability, plasma free fraction, blood–brain barrier (BBB) penetration and binding behaviour in in vitro autoradiography.

Results: [^{11}C]Me@HAPTHI was prepared and displayed outstanding affinity and selectivity as well as excellent in vitro metabolic stability, and it is likely to penetrate the BBB. Moreover, selective NET binding in in vitro autoradiography was observed in human brain and rat heart tissue samples.

Conclusions: All preclinical results and radiosynthetic key-parameters indicate that the novel benzothiadiazole dioxide-based PET tracer [^{11}C]Me@HAPTHI is a feasible and improved NET radioligand and might prospectively facilitate clinical NET imaging.

Keywords: NET; PET; Autoradiography; Radiosynthesis; HAPTHI

Background

The noradrenergic system—and specifically the presynaptic norepinephrine transporter (NET)—is proposed to be altered in a variety of neurological, neuropsychiatric and cardiovascular diseases. For example, alterations have been shown in Alzheimer's disease, Morbus Parkinson, major depressive disorder and attention deficit hyperactivity disorder [1–9]. Therefore, a reliable non-invasive molecular imaging technique—such as positron emission tomography (PET)—would be of great benefit for early stage in vivo diagnostics, visualization of treatment response and further elucidation of underlying pathophysiological mechanisms.

Great efforts have been made to develop PET tracers for the NET over the last two decades. Focus was primarily placed on reboxetine-derived ligands [10–14]. However, previous studies have shown that the in vivo and in vitro behaviour of these reboxetine analogues, more specifically [^{11}C]MeNER ([^{11}C]MRB, ((S,S)-2-(α-(2-[^{11}C]methoxyphenoxy)benzyl)morpholine), [^{11}C]MeNET and [^{18}F]FMeNER-D_2 ((S,S)-2-(α-(2-[^{18}F]fluoro[$^{2}H_2$] methoxyphenoxy)benzyl) morpholine), is not favourable for viable imaging of the NET by PET. Limitations include their metabolic stability, late reaching of equilibrium, unexplainable striatal uptake and complexity of radiosynthesis [10, 15–18]. Recently, we aimed at the preparation of a benzo[d]imidazolone derivative—[^{11}C]Me@APPI as new NET PET tracer [19]. Despite its favourable properties and straightforward production, its affinity was not sufficient

* Correspondence: markus.mitterhauser@meduniwien.ac.at
†Equal contributors
[1]Department of Biomedical Imaging and Image-guided Therapy, Division of Nuclear Medicine, Medical University of Vienna, Vienna, Austria
[3]Faculty of Life Sciences, Department of Technology and Biopharmaceutics, University of Vienna, Vienna, Austria
Full list of author information is available at the end of the article

and its lipophilicity high. Hence, there is ample demand for a novel, improved radioligand for in vivo NET imaging.

Therefore, this study highlights a novel, non-reboxetine-based NET PET tracer based on a benzothiadiazole scaffold: [^{11}C]Me@HAPTHI ((S)-1-(3-hydroxy-4-([^{11}C]methylamino)butyl)-3-phenyl-1,3-dihydrobenzo[c][1, 2, 5]thiadiazole 2,2-dioxide) (Fig. 1). In general, the designed benzothidiazole dioxides exhibits excellent affinity and selectivity as well as slightly reduced flexibility compared to other previously published benzoimidazolones [20, 21]. Hence, these substances offer an ideal basis for the further development of novel NET ligands for PET imaging.

The objectives of this investigation were as follows:

- The set-up of a small-scale radiosynthetic procedure for the preparation of the carbon-11 labelled [^{11}C]Me@HAPTHI and its optimization;
- The up-scaling and set-up of a fully automated preparation of [^{11}C]Me@HAPTHI, including purification and formulation;
- The in vitro evaluation of Me@HAPTHI and its precursor HAPTHI. Evaluation includes binding studies for the determination of affinity and selectivity of both Me@HAPTHI and its precursor HAPTHI towards NET using NET, serotonin transporter (SERT) and dopamine transporter (DAT) expressing membranes, metabolic stability testing in vitro against Cytochrom P 450 enzymes, logP analysis and immobilized artificial membrane (IAM) chromatography for indirect measurement of the blood–brain barrier (BBB) penetration and determination of plasma free fraction.
- Comparative in vitro autoradiography on human and rodent tissue slices.

Methods

Materials

Precursor, HAPTHI ((S)-1-(4-amino-3-hydroxybutyl)-3-phenyl-1,3-dihydrobenzo[c][1, 2, 5]thiadiazole 2,2-dioxide, and cold reference compound Me@HAPTHI ((S)-1-(3-hydroxy-4-(methylamino)butyl)-3-phenyl-1,3-dihydrobenzo[c][1, 2, 5]thiadiazole 2,2-dioxide) were custom-synthesized by ABX Advanced Biochemical Compounds (Radeberg, Germany). Briefly, synthesis of (2S)-4-(2,2-dioxido-3-phenyl-2,1,3-benzothiadiazol-1(3H)-yl)-1-(methylamino)butan-2-ol followed the route described by Neill et al. [20, 21]. For more details, see Additional file 1.

2-Butanone (MEK, <99.0 % ACS reagent), acetonitrile (ACN, HPLC grade), dimethylsulfoxide (DMSO), tetrabutylammonium hydroxide 30-hydrate (TBAH), ammonium formate, ammonium acetate, sodium hydroxide, triethylamine and ethanol (absolute) were purchased from Sigma-Aldrich (Vienna, Austria) in the highest available grades. In addition, iodine (sublimated grade for analysis; ACS, Pharm. Eur.) was obtained from Merck (Darmstadt, Germany). Silver triflate impregnated carbon was prepared by reaction of 1 g of silver trifluoromethanesulfonate (Sigma Aldrich, Vienna, Austria) in 20 mL ACN with 3 g of Graphpac-GC (80/100 mesh, Alltech, Deerfield, USA). The suspension was stirred under protection from light and in an argon atmosphere for 30 min. After removal of the solvent, the resulting powder was dried under protection from light for further 2 h under reduced pressure.

For formulation of the product, 0.9 % saline solution from B. Braun (Melsungen, Germany), 3 % saline solution (Landesapotheke Salzburg, Austria) and sodium dihydrogenphosphate-monohydrate and disodiumhydrogenphosphate-dihydrate (both from Merck, Darmstadt, Germany)

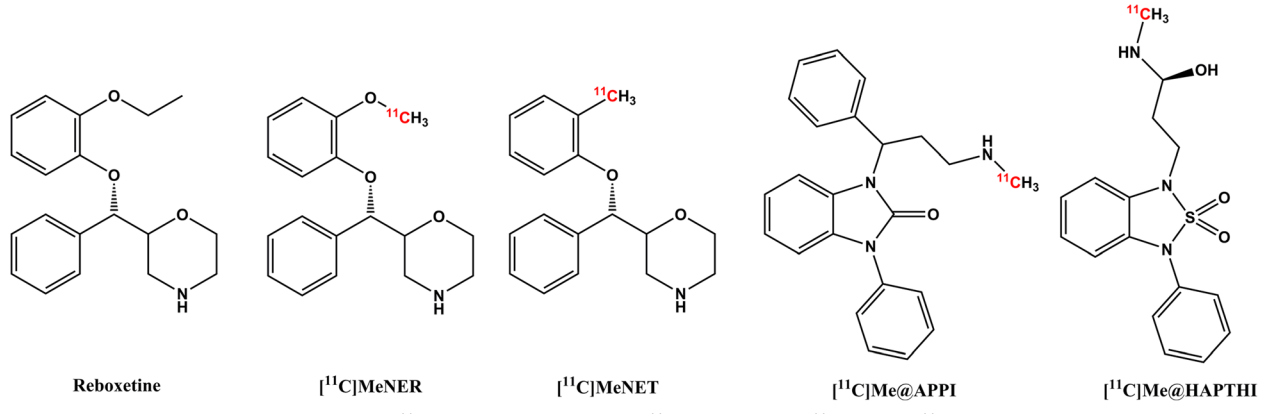

Fig. 1 Chemical structures of reboxetine and ^{11}C-labelled NET PET tracers [^{11}C]Me@APPI and [^{11}C]MeNER, [^{11}C]MeNET and our novel NET PET ligand [^{11}C]ME@HAPTHI. The *red coloured atom* indicates the position of the radioisotope introduced by radiolabeling

were used. Sterile water was purchased from Meditrade Medicare Medizinprodukte (Kufstein, Austria). Phosphate buffer (125 mM) was prepared by dissolving 0.224 g sodium dihydrogenphosphate-monohydrate and 1.935 g disodiumhydrogenphosphate-dihydrate in 100 mL sterile water. For solid phase extraction, C18 plus SepPak® cartridges were purchased from Waters (Waters® Associates, Milford, USA). Low-protein binding Millex® GS 0.22 μm sterile filters were obtained from Millipore (Bedford, USA).

All other chemicals and solvents for the radiosyntheses were obtained from Merck (Darmstadt, Germany) and Sigma-Aldrich (Vienna, Austria) with at least analytical grade and used without further purification.

NET, DAT and SERT expressing membrane preparations were obtained from Perkin Elmer (MA, USA). An ODP-50 column (20 × 4.0 mm, 5 μm) was purchased from Shodex® (Showa Denko Europe GmbH, Munich, Germany). For prediction of BBB penetration, a Redistech IAM.PC.DD2 column (Regis Technologies Inc., Morton Grove, USA) was used.

Microsomal preparations (human/rat liver microsomes) for stability testing were obtained from BD Bioscience (NJ, USA). Pooled human and rat plasma was obtained from Innovative Research (MI, USA).

The human *postmortem* tissue (7–9 h *postmortem* time, no history of neurological diseases) was obtained from the Neurobiobank of the Medical University of Vienna and approved by the local ethics committee ("Molecular neuropathologic investigation of neurodegenerative diseases" Nr.396/2011) following the principles of the Helsinki Declaration. Wild-type male rats were deeply anesthesized by isoflurane and sacrificed by decapitation. The organs of interest (i.e. brain, heart and testis) were removed and quick-frozen in *i*-pentan. Research using animal tissue was carried out under institutional approval in accordance with the Austrian Animal Care Law. Tissues were cut at −20 °C in a micro-cryotome (Microm HM 560, Thermo Scientific, Austria). Frozen slices were thaw-mounted onto superfrost slides (Menzel-Gläser SUPERFROST plus microscopy slides, Thermo Scientific, Germany). A barrier pen (Mini PAP Pen, Invitrogen, USA) was used for immunohistochemistry only. For detection of autoradiography, a Cyclone Phospho-Imager (Cyclone Plus Storage Phosphor System, Perkin Elmer, Germany) and Phosphor Imager plates (Multisensitive Phosphor Screens Long Type MS, PPN 7001724, Perkin Elmer, Germany) were used. The lead shielded and light-protected cassettes (Fisher Biotech Autoradiography Cassette FBCS 1417) were purchased from Fisher Scientific (PA, USA).

The NET-antibody (SLC6A2 Antibody H-67, sc-67216) was purchased from Santa Cruz Biotechnology (TX, USA). An endogenous Avidin-Biotin blocking kit (ab64212) as well as the DAB (=3,3′-diaminobenzidine) substrate kit (94665) was obtained from abcam (Cambridge, UK). A rabbit primary antibody isotype control was purchased from Invitrogen (CA, USA). A peroxidase-based Vectastain ABC kit (Rabbit IgG, PK-4001) was obtained from Vector Laboratories (CA, USA). Phosphate buffered saline (PBS pH 7.4, tenfold concentrate, 11237) was obtained from Morphisto Evolutionsforschung und Anwendung GmbH (Germany). Mayer's Hemalaun solution was purchased from Merck Millipore (Germany). Histofluid (Marienfeld Superior, Germany) was used as a mounting medium. Coverslips from Menzel Gläser (24 × 60 mm, Thermo Fisher Scientific, Germany) were used for conservation of mounted slides. All other chemicals were obtained from Sigma-Aldrich.

Instrumentation

$[^{11}C]CO_2$ was produced within a GE PETtrace cyclotron (General Electric Medical System, Uppsala, Sweden) by a $^{14}N(p,\alpha)^{11}C$ nuclear reaction under irradiation of a gas target filled with N_2 (+1 % O_2) (Air Liquide Austria GmbH, Schwechat, Austria).

The evaluation of the reaction conditions was performed manually with starting activities <2 GBq. After optimization of the reaction parameters, [^{11}C]Me@HAPTHI-synthesis was transferred to the TRACERlab™ FX C Pro synthesizer and a fully automated synthesis was established.

Crude [^{11}C]Me@HAPTHI was purified by semi-preparative reversed phase HPLC using the built-in semi-preparative HPLC system equipped with a radioactivity and a UV detector (Linear Instruments Model 200 Detector UV/VIS) and a LaPrep HPLC pump (VWR International, Radnor, USA). A Supelcosil™ LC-ABZb, 5 μm, 250 × 10 mm (Supelco®, Bellefonte, PA, USA) column was used with a mobile phase of ACN/0.1 M ammonium acetate 40/60 *v*/*v*% at a flow rate of 6 mL/min.

The analytical HPLC was performed on a Merck-Hitachi LaChrom HPLC system (L-7100 pump; LaChrom L-7400 UV detector) using a NaI radio-detector (Bertholdt Technologies, Bad Wildbach, Germany) and a GinaStar® processing software (Raytest, Straubenhardt, Germany). A Phenomenex® Prodigy, Phenyl-3(PH-3), 5 μm, 250 × 4.6 mm (Phenomenex®, Aschaffenburg, Germany) column with a mobile phase consisting of ACN/0.1 M ammonium formate 50/50 *v*/*v*% at a flow rate of 2 mL/min was used while detection of the cold compounds was performed at 280 nm.

The osmolality of the final sterile product was measured with a Wescor osmometer Vapro® 5600 (Sanova Medical Systems, Vienna, Austria).

Methods

Radiochemistry

Production of [^{11}C]CH_3I and [^{11}C]CH_3OTf

The cyclotron production of [^{11}C]CO_2 was terminated at desired target activities between 40 and 50 GBq at currents between 48 and 53 μA (20–25 min) and trapped upon delivery on a molecular sieve (4 Å) within the Tracerlab FxC Pro synthesizer. Subsequently, [^{11}C]CO_2 was converted into [^{11}C]CH_4 by a Ni-catalysed reduction with H_2 at 400 °C. [^{11}C]CH_3I was produced within the same synthesizer using the dry method (gas phase conversion) described by Larsen et al. [22] with adopted modifications described by Kniess et al. [23]. Briefly, the resulting [^{11}C]CH_4 was reacted with sublimated iodine at 738 °C in a recirculating process for 4 min to give [^{11}C]CH_3I. The produced [^{11}C]CH_3I was trapped on-line on a Porapak® N column and finally released by heating the trap to 190 °C. [^{11}C]CH_3OTf was prepared on-line at the passage of [^{11}C]CH_3I through a pre-heated (200 °C) column containing 300 mg silver triflate impregnated graphitized carbon at a flow rate of 40 mL/min [24].

Small-scale reactions

For optimization of reaction conditions, small-scale reactions using [^{11}C]CH_3I or [^{11}C]CH_3OTf were performed. Either [^{11}C]CH_3I or [^{11}C]CH_3OTf was trapped in 500 μL of the solvent of choice at room temperature (RT) and aportioned for further experiments in 1 mL Wheaton v-vials. All evaluation reactions were performed manually (shielded hood; starting activity <2 GBq). The influence of various reaction conditions was investigated:

- Reaction temperature: 25 °C, 75 °C
- Base as catalyst: NaOH, triethylamine (TEA) and TBAH
- Precursor concentration: 1 or 2 mg/mL
- Solvent: MEK or DMSO

Finale reaction volumes of small-scale reactions were 10–200 μL. The reactions were quenched with an equivolume solution of ammonium acetate (aq., pH 3.5), and the radiochemical yield (RCY) was determined using analytical radio-HPLC. In Fig. 2, the reaction scheme is presented.

Full automation of radiosyntheses

The automation of the *N*-^{11}C-methylation reaction was done on the TRACERlab™ FX C Pro (GE Healthcare). A schematic flowchart of the synthesis is depicted in Fig. 3.

After conversion of cyclotron-produced [^{11}C]CO_2 to [^{11}C]methane, [^{11}C]methyl iodide and [^{11}C]CH_3OTf, it was trapped at RT in a glass reactor containing precursor HAPTHI (1 mg, 3 μmol) and 0.5 μL of an aqueous NaOH-solution (5 M) in 500 μL MEK. After heating of the sealed reaction vessel to 75 °C for 2 min, the crude reaction mixture was cooled to 25° and quenched by addition of 1 mL HPLC eluent. The entire volume was then transferred to the 5 mL injection loop. The crude mixture was (fluid detector controlled) injected into the semi-preparative HPLC column (Fig. 4). The pure [^{11}C]Me@HAPTHI peak was cut into a round bulb, containing 80 mL of distilled water. The now predominantly

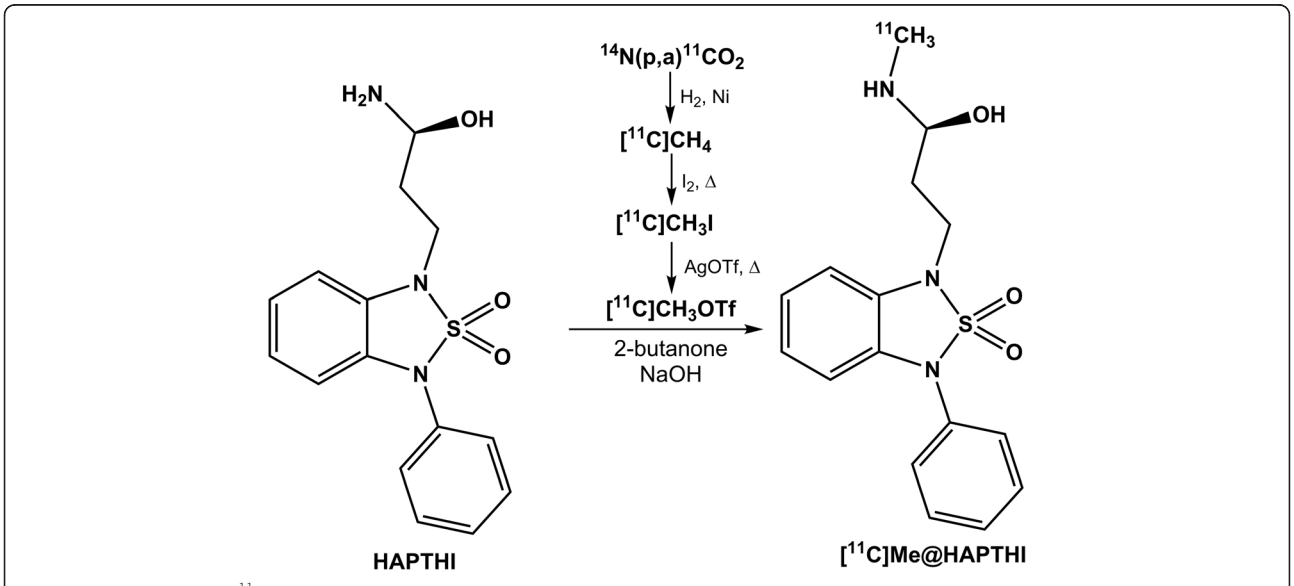

Fig. 2 Radiosynthesis of [^{11}C]Me@HAPTHI starting from the precursor molecule HAPTHI

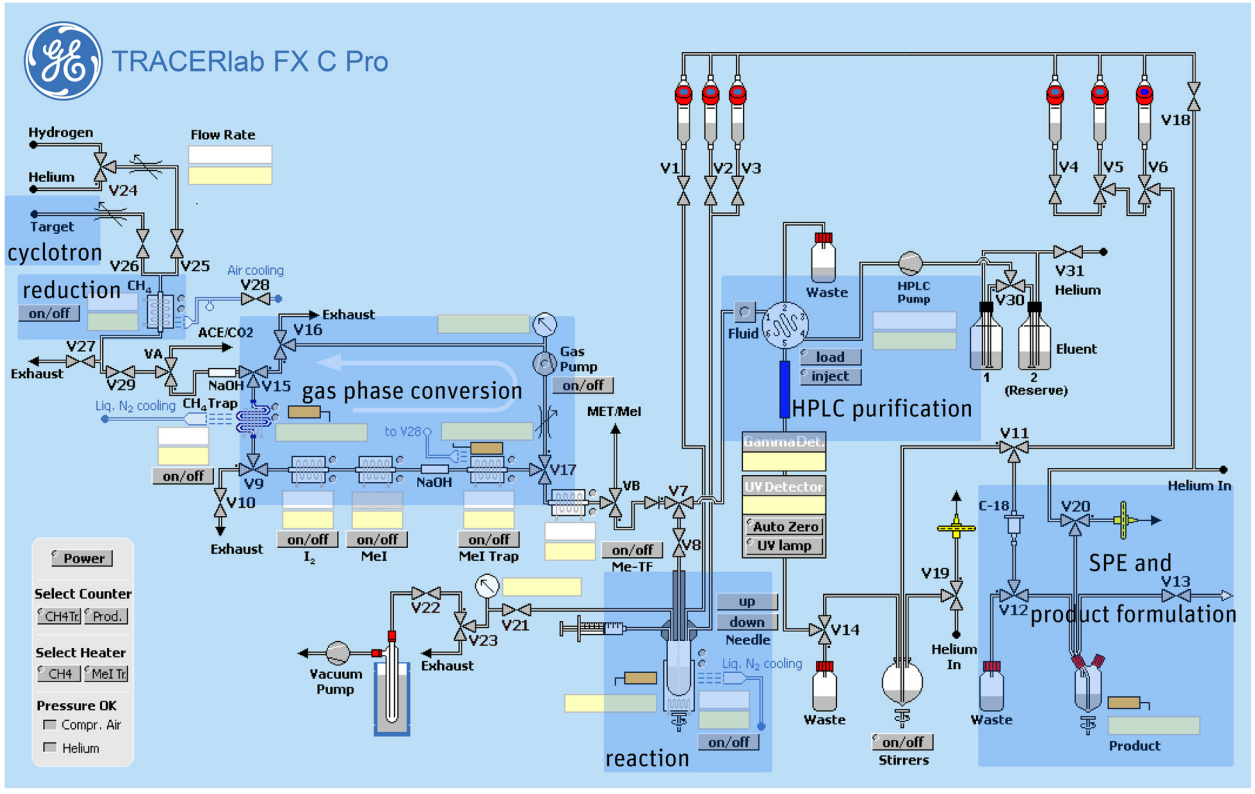

Fig. 3 Flow scheme of the fully automated radiosynthesis of [^{11}C]Me@HAPTHI

aqueous product solution was subjected to solid phase extraction by transferring over a preconditioned (10 mL EtOH, air, 20 mL water) C18 SPE cartridge. After rinsing of the C18 SepPak® with water (V6) for complete removal of residual HPLC solvents, the pure product was eluted with 1.5 mL EtOH (V5) into a two-neck vial and the cartridge and transfer lines rinsed with further 5 mL 0.9 % saline into the same vial. After formulation with 9 mL 0.9 % saline, 1 mL 3 % saline and 1 mL 125 mM phosphate buffer, sterile filtration (0.22 μm) was performed

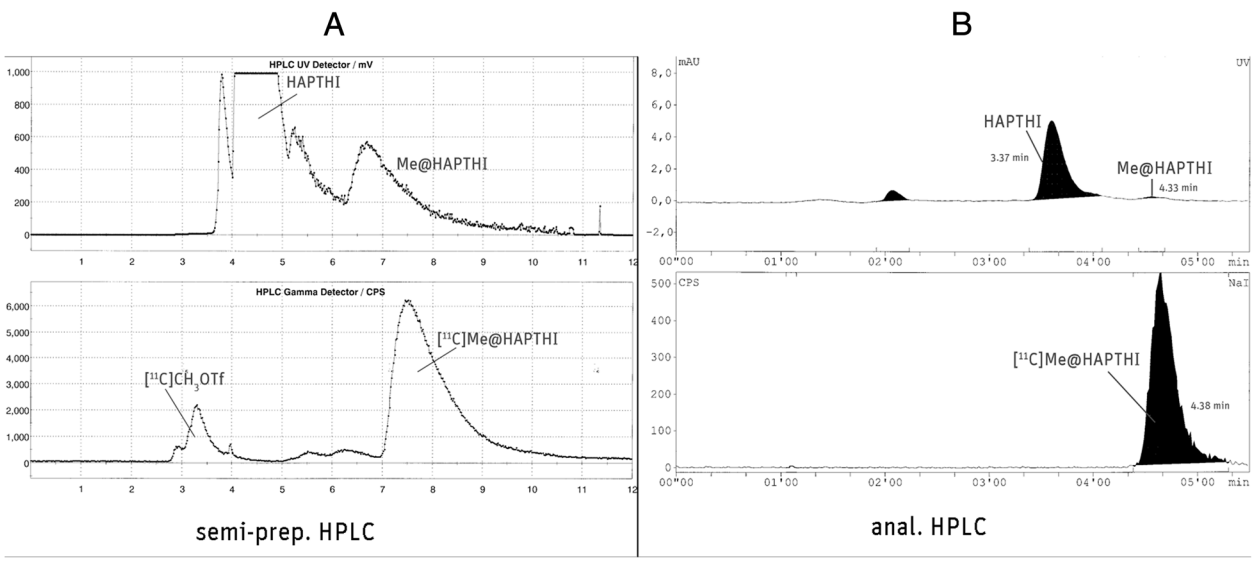

Fig. 4 a Semi-preparative and **b** analytical HPLC chromatogram

under aseptic conditions (laminar air flow hot cell, class A) to avoid microbial contamination.

Quality control

Chemical and radiochemical impurities were assessed using analytical radio- and UV-HPLC according to the monograph in the European Pharmacopoeia [25]. Radiochemical identity and purity were measured via analytical radio-HPLC by comparison of retention times with authentic samples. Specific radioactivity was determined by quantification of the non-radioactive product (HPLC UV channel at 280 nm) and inclusion of the overall radiochemical yield (GBq at end of synthesis). Sterility, absence of endotoxins, pH, osmolality and residual solvents were determined by standard procedures routinely performed at the PET Centre of the Vienna General Hospital/Medical University of Vienna and follow the respective monograph in the European Pharmacopoeia [25].

Statistical analysis

All quantitative data described in the text and figures are specified as arithmetic mean ± standard deviation. For the determination of significance, a Student's two-tailed t test (α = 0.95) was performed using Microsoft® Excel. P values of <0.05 were considered to be significant. Unless otherwise stated, error bars in figures represent the standard deviation; if not visual, they are within the icon margin.

NET-expressing membrane binding studies

The affinity of new radiolabelled ligand was determined in a NET-expressing membrane binding protocol [26, 27]. For details, see Additional file 1.

Data from the competition plots (as arithmetic means of values derived from three different assays, each in triplicate for each compound) were analyzed and subsequently IC_{50} and K_i values were calculated using GraphPad Prism® software (San Diego, USA).

Assays similar to those described for NET were performed in order to determine the selectivity of the tested compounds towards NET in comparison to DAT and SERT. IC_{50} and K_i values were obtained in analogy to NET experiments. Ratios DAT/NET and SERT/NET were determined.

LogD analysis, IAM chromatography and blood–brain barrier penetration

LogD values were assessed using a HPLC-based protocol according to Donovan and Pescatore [28]. All compounds (as cold reference standards) were injected together with two known compounds—with known logD and k' values—according to a standard protocol. A polymeric ODP-50 column was used; a linear gradient from 10 % MeOH 90 % 25 mM phosphate buffer (pH 7.4) to 100 % methanol within 9.4 min at a flow-rate of 1.5 mL/min was applied. Internal standards were triphenylene and toluene; detection was performed at 260 and 285 nm.

As lipophilicity alone was shown to be a tenuous predictor for blood–brain barrier penetration, other in vitro methods have been described, such as immobilized artificial membrane (IAM) chromatography and further calculation of total polar surface area (tPSA) values [29–31]. Therefore, IAM chromatography was performed using a Redistech IAM.PC.DD2 column (15 cm × 4.6 mm) according to previously published methods [19, 32–35]. For analysis, 0.01 M phosphate buffer (pH 7.4) and ACN (in different ratios) were used isocratically as mobile phase at a flow rate of 1 mL/min. Resulting K_m (membrane partition coefficient) and P_m (permeability) values were obtained after data analysis using Microsoft Excel. The resulting data were compared with those derived from compounds known to penetrate BBB as external standard. Additionally, tPSA values were determined in silico using Chem Bio Draw Ultra (Cambridge Software, Perkin Elmer, USA).

Metabolic stability testing

Pooled human and rat liver microsomes are subcellular fractions that are rich in endoplasmatic reticuli, which contain many drug-metabolizing enzymes, e.g. cytochrome P450s, flavin monooxygenases and epoxide hydrolase. Microsomal incubations were performed in order to investigate the metabolization of [^{11}C]Me@HAPTHI. As the results, both the percentage of test compound metabolized after a certain time and the biological half-life were determined.

Plasma protein binding

For the determination of free fraction in human pooled plasma, an ultrafiltration protocol according to previously published methods was used [35–38]. Briefly, aliquots of pooled human plasma were spiked with [^{11}C]Me@HAPTHI and centrifuged using ultrafiltration vials (Amicon Centrifree; Millipore, Bedford, USA). The plasma free fraction was calculated, and the percentage of unspecific binding of [^{11}C]Me@HAPTHI to the filter matrix evaluated. For a detailed method, see Additional file 1.

Autoradiography, Nissl staining and immunohistochemistry

Human brain tissue (cortex, thalamus, hippocampus, cerebellum and hypothalamus) was obtained deeply frozen from the Neurobiobank of the Medical University Vienna and was stored at −80 °C. Before cutting, tissue blocks were thawed slowly within 12 h to −20 °C. The organs were cut at −20 °C in a micro-cryotome into 10-

μm-thick slices and thaw mounted onto object slides. Slices were again stored at −80 °C until the beginning of the experiment.

In vitro autoradiography was performed with slight modifications according to previously published protocols [13, 39, 40]. Non-specific binding was determined by co-incubation with excess Nisoxetine (10 μM). For competition experiments, non-radioactive FMeNER-D2, an established NET PET tracer, and Me@HAPTHI were added to the incubation solution in different concentrations. After 1 h at room temperature, incubation was stopped and slices were processed on phosphor imaging films.

All data was exported to Microsoft Excel for statistical analysis, and the percentage of total specific binding was calculated.

Post-autoradiographic processing of the slices was done by Nissl staining in order to facilitate morphological mapping of hot areas in the autoradiography. The same tissue slices were stained after autoradiography with cresyl violet [28, 41, 42] to demonstrate the Nissl substance in the neurons and cell nuclei. For a detailed procedure, see Additional file 1.

Immunohistochemical staining experiments were performed on rat and human tissue cryo-slices, vicinal to the slices used for autoradiographic experiments. The staining procedure was a modification of a general protocol as published previously in detail [28, 43].

Results

Radiochemistry

The optimum parameters were examined in small-scale reactions. Thus, the influence of different ^{11}C-methylation agents, solvent, precursor concentration, reaction temperature and base were investigated (Fig. 5a–d). Radiochemical yields (RCY) of [^{11}C]Me@HATPHI were below 6 % for all examined conditions using [^{11}C]CH_3I as methylation agent. Hereby, DMSO proved to be the best solvent for the SN_2 reaction using [^{11}C]methyl iodide. In contrast, very promising results were obtained using [^{11}C]CH_3OTf as radio-methylation agent (Fig. 5c–d). Interestingly, the use of DMSO as solvent did not result in high yields, less than 1 % RCY was observed using [^{11}C]CH_3OTf. Applying 2-butanone resulted in high radiochemical yields. Furthermore, the influence of basic catalysis was examined: TBAH catalysis could not shift the reaction kinetics to favourable outcomes, as it did not result in any methylation of HAPTHI. Up to 12.8 ± 4.7 % RCY was observed when using 0.5 μL triethylamine instead. Conducting the experiments with 0.5 μL of 1 M NaOH (aq.), however, yielded 42.9 ± 5.2 % radiochemical yield with 1 mg/mL precursor concentration and even above 50 % RCY were obtained with 2 mg/mL precursor concentration. A further increase in basicity—facilitated by 0.5 μL 5 M NaOH (aq.) instead of 1 M NaOH (aq.)—did not lead to improved results (in a total reaction volume of 100 μL); only <0.5 % RCY were obtained.

Hence, the best results were obtained with NaOH-catalysis in 2-butanone for 2 min at 75 °C using 2 mg/mL precursor HAPTHI. Thereby, 54.0 ± 8.3 % radiochemical yield was achieved.

Therefore, these optimum reaction parameters were transferred to the fully automated radiosynthesis within the Tracerlab FxC Pro synthesizer. In Table 1, an overview on the automated syntheses, their conversion and yield is given. The crude reaction mixture was purified via semi-preparative radio-HPLC using isocratic conditions (0.1 M ammonium acetate and acetonitrile (60/40; *v*/*v*)) at a flow rate of 5 mL/min. An exemplary semi-preparative HPLC chromatogram is outlined in Fig. 4a. The precursor HAPTHI was found to be eluted at a retention time of 4.5 min (k' = 0.55) and the product [^{11}C]Me@HAPTHI at 7.6 min (k' = 1.62), respectively.

Overall, seven large-scale radiosyntheses were performed, yielding 2.2 ± 2.0 GBq (18.9 ± 13.3 %, corrected

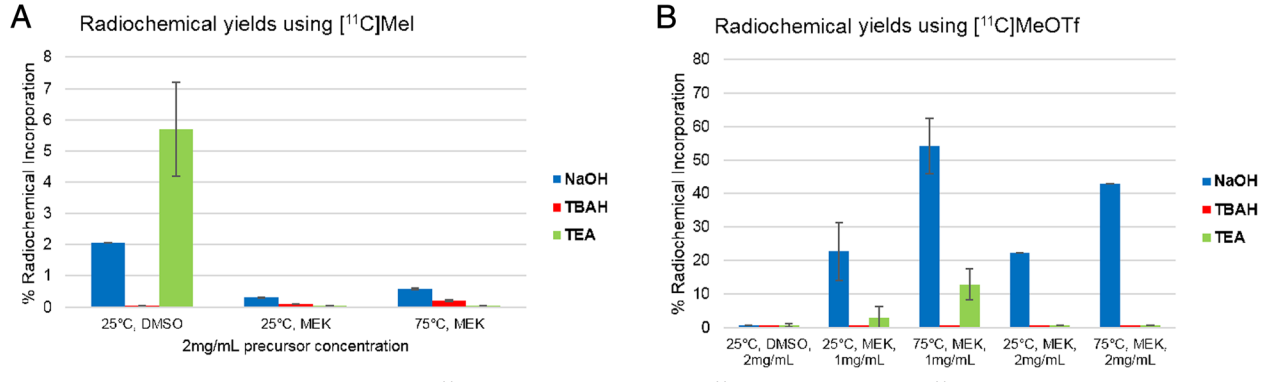

Fig. 5 Dependence of the radiochemical yield of [^{11}C]Me@HAPTHI ($n \geq 3$) on the ^{11}C-methylation agent **a** [^{11}C]methyliodide or **b** [^{11}C]methyltriflate) in DMSO and 2-butanone using different bases (NaOH, triethylamine or TBAH) at 2-min reaction time

Table 1 Overview on the fully automated, large-scale radiosyntheses of [^{11}C]Me@HAPTHI

[^{11}C]Me@HAPTHI (n = 7)	Mean	SD	Median
Starting activity [^{11}C]CO2	53.4	2.4	53.9
Trapped [^{11}C]CH4	34.6	4.6	32
Trapped [^{11}C]CH3I	29.6	2.4	29
Trapped [^{11}C]CH3OTf in reactor	16.6	5.5	17.2
After quenching	8.8	3.6	8.9
Loss during injection in loop waste	1.0	0.5	0.8
Product [^{11}C]Me@HAPTHI (EOS)	2.2	2.0	1.9
Yield (decay corr. to EOB)	13.7	13.5	15.9
Specific activity [GBq/μmol] (EOS)	43.4	29.7	59.2

Reaction conditions: [^{11}C]MeOTf, NaOH, MEK, 2 mg/mL precursor concentration
EOS end of synthesis, *EOB* end of bombardment

for decay to EOB) of sterile, formulated [^{11}C]Me@HAPTHI within 41 min including 5 min of radiopharmaceutical quality control. A mean specific activity of 46.8 ± 28.5 GBq/μmol was found in the large-scale syntheses (calculated using an HPLC-based method). A representative analytical HPLC chromatogram of the purified, sterile [^{11}C]Me@HAPTHI is shown in Fig. 4b. The retention times in the analytical HPLC assay were 3.37 min (k' = 2.17) for precursor HAPTHI, 1.8 min (k' = 0.7) for [^{11}C]MeOH, 2.7 min (k' = 1.55) for [^{11}C]CH_3OTf and 3.1 min (k' = 1.9) for [^{11}C]CH_3I, respectively. The product [^{11}C]Me@HAPTHI was eluted at a retention time of 4.38 min (k' = 3.08). Radiochemical purity always exceeded 98 %. Osmolality and pH values were at all times found to be in a physiological range. Residual solvent analysis using GC revealed MEK <5 ppm and ACN <20 ppm, besides 8.5 % ethanol present in the product formulation (total product volume 17.5 mL). Moreover, sterility and absence of endotoxins was approved for all produced batches of [^{11}C]Me@HAPTHI upon complete decay of radioactivity as *in-process* control.

Affinity and selectivity testings

Affinity of reference compounds (Me@HAPTHI and its radiolabeling progenitor HAPTHI) was determined using human NET membranes as K_d = 0.21 ± 0.07 nM for Me@HAPTHI and 24.2 ± 10.9 nM for HAPTHI, respectively ($n \geq 9$ triplicates). For determination of selectivity, the affinity of both reference substances was assessed on human DAT and SERT membranes and revealed >10 μM for both compounds for DAT and 409 ± 43 nM (Me@HAPTHI) and 10,274 ± 1207 nM (HAPTHI) towards SERT, respectively, ($n \geq 5$ triplicates). Hence, selectivity of Me@HAPTHI towards NET was determined as DAT/NET >1947.6 and SERT/NET = 9757. Both values clearly elucidate the ideal binding properties of our novel NET PET ligand [^{11}C]Me@HAPTHI.

LogD analysis, IAM chromatography and blood–brain barrier penetration

The lipophilicity of the novel NET PET radioligand Me@HAPTHI was found to be in a decent range (logD = 2.27 ± 0.01) for a potential penetration of the BBB. The precursor HAPTHI showed a logD value of 2.30 ± 0.01. Additionally, BBB penetration experiments using IAM chromatography revealed a permeability of P_m = 1.15 ± 0.25 for Me@HAPTHI and P_m = 1.14 ± 0.27 for the precursor HAPTHI, respectively. Both values were within the identical, ideal range (P_m = 0.01–4.21) from other PET tracers, known to easily penetrate the BBB [34].

Metabolic stability testing

Stability testing using human liver microsomes (n = 4) revealed no significant metabolism of [^{11}C]Me@HAPTHI within the tested timeframe. After 60 min, 99.6 ± 0.3 % of the tracer was found to be still intact. Incubation of [^{11}C]Me@HAPTHI with pooled male rat liver microsomes revealed a higher metabolic degradation. The percentage of intact tracer over time is presented in Fig. 6. Overall, 29.3 ± 1.9 % tracer was still intact after 1-h incubation time. Thus, the stability of the novel NET PET tracer [^{11}C]Me@HAPTHI is encouraging in a human and rodent setting and superior to the established reboxetine-derived PET tracer [^{18}F]FMeNER-D2.

Plasma protein binding

The mean percentage of plasma free fraction (ff) and percentage of unspecific binding to the filter matrix of the Centrifuge vials was determined. A plasma free fraction of ff = 8.2 ± 0.3 % (n = 7 triplicates) as well as an unspecific filter retention of 51.26 ± 0.78 % was found. Overall, the ff of our novel NET PET tracer [^{11}C]Me@HAPTHI was in the same range as that of [^{11}C]ADAM [35].

In vitro autoradiography, immunohistochemistry and Nissl staining

In the autoradiographic experiments, the highest uptake of [^{11}C]Me@HAPTHI was observed in NET-rich regions identified with immunohistochemistry (Fig. 7). Blocking was performed with non-radioactive NET ligands FMeNER-D2 and Me@HAPTHI in two different concentrations each (100 nM, 1 μM). A concentration-dependent binding displacement was observed using human tissue samples for both cold competitors. In Table 2, an overview on the percentage of specific displaceable binding of [^{11}C]Me@HAPTHI and fmol/mm^2 values of relative transporter protein density on the different tissue sections is given. All values are given in % as mean $n \geq 3$ triplicates. Autoradiography of human

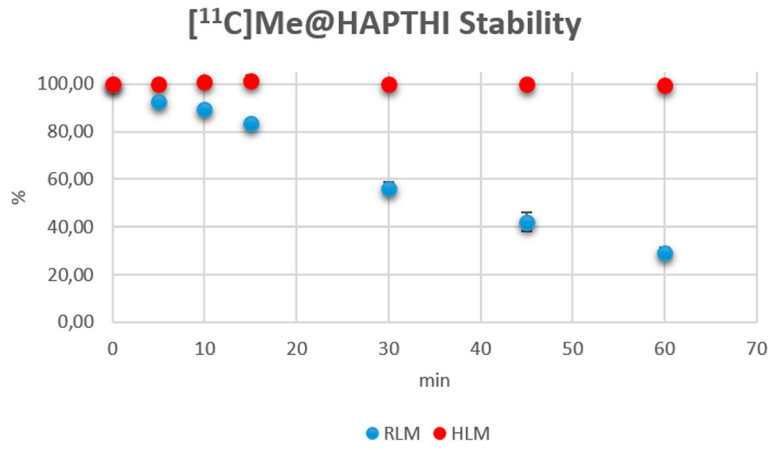

Fig. 6 Metabolic stability of [^{11}C]Me@HAPTHI against human and rat liver microsomes

cerebellum revealed NET specific uptake in NET-rich regions identified with IHC, though blocking experiments were not possible due to the vast inhomogeneity of the tissue samples. In human nucleus caudatus, a region known to be low in NET density, only unspecific binding was observed.

Immunohistochemical staining was used to allocate areas with high uptake in autoradiography with regions known high NET abundance. Hence, the NET antibody-dye complexes were found highly abundant in the heart fibres, hippocampus, thalamus and hypothalamus and to a minor extent in all other brain regions (Fig. 7). NET specificity of staining was validated using a rabbit antibody isotype control.

Moreover, harvesting experiments with [^{11}C]Me@HAPTHI using hNET expressing membranes were performed according to the affinity testing protocol. Thereby, a concentration-dependent displacement of [^{11}C]Me@HAPTHI was observed for all tested competitor substances (cold FMeNER-D2 or Me@HAPTHI), and the counts were corrected for decay (Fig. 8). Using Graph Pad Prism, data correlation revealed akin-binding displacement behaviour for both cold Me@HAPTHI as well as the established NET ligand FMeNER-D2 ($n \geq 3$ triplicates).

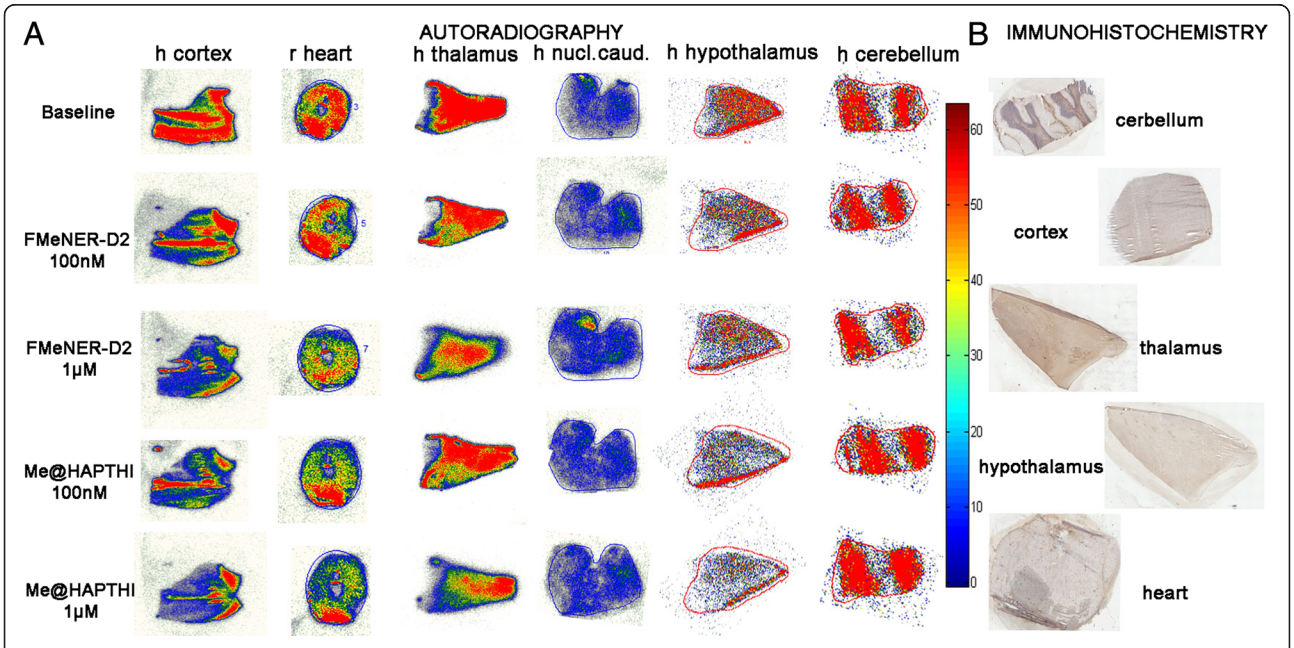

Fig. 7 a NET-autoradiography and **b** immunohistochemistry of [^{11}C]Me@HAPTHI on 10 µm slices of human cortex, thalamus, hypothalamus, cerebellum and nucleus caudatus as well as rat heart tissue and blocking with 100 nM FMeNER-D2, 1 µM FMeNER-D2, 100 nM Me@HAPTHI and 1 µM Me@HAPTHI. The scale shows the radioactivity from high (*red*) to low levels of radiotracer present on the Phosphor imager film

Table 2 Overview of specific NET binding of the radioligand [^{11}C]Me@HAPTHI vs. Me@HAPTHI and FMeNER-D2 on rat and human tissue origin

$n \geq 3$	[^{11}C]Me@HAPTHI	
	% BL-competitor	fmol
Rat heart		
FMeNER 1 μM	88.8 ± 11.2	<0.01
FMeNER 100nM	99.00 ± 0.07	<0.01
Me@HAPTHI 1 μM	92.5 ± 7.5*	<0.01
Me@HAPTHI 100nM	104.5 ± 4.5	<0.01
Human cortex		
FMeNER 1 μM	71.9 ± 7.9*	0.86
FMeNER 100nM	86.3 ± 11.2*	<0.01
Me@HAPTHI 1 μM	66.3 ± 5.9*	1.32
Me@HAPTHI 100nM	82.1 ± 13.9*	0.02
Human thalamus		
FMeNER 1 μM	68.36 ± 2.11	0.71
FMeNER 100nM	77.6 ± 9.8	0.47
Me@HAPTHI 1 μM	85.9 ± 18.5	0.09
Me@HAPTHI 100nM	92.5 ± 17.3	0.26
Human hypothalamus		
FMeNER 1 μM	77.4 ± 14.5	0.02
FMeNER 100 nM	97.8 ± 14.6	0.11
Me@HAPTHI 1 μM	62.0 ± 3.6*	0.04
Me@HAPTHI 100 nM	83.7 ± 1.7*	0.05
Human hippocampus		
FMeNER 1 μM	67.3 ± 8.2	<0.01
FMeNER 100 nM	97.1 ± 10.3	<0.01
Me@HAPTHI 1 μM	68.3 ± 5.3	<0.01
Me@HAPTHI 100 nM	84.1 ± 9.3	<0.01
Human nucleus caudatus		
FMeNER 1 μM	107.6 ± 17.7	n.d.
FMeNER 100nM	102.6 ± 14.5	n.d.
Me@HAPTHI 1 μM	110.0 ± 21.0	n.d.
Me@HAPTHI 100nM	93.5 ± 12.5	nd
Human cerebellum		
FMeNER 1 μM	108.2 ± 17.3	n.d.
FMeNER 100nM	103.9 ± 12.2	n.d.
Me@HAPTHI 1 μM	107.2 ± 20.8	n.d.
Me@HAPTHI 100nM	124.7 ± 10.8	n.d.

fmol values reflect calculated relative concentration (fmol/mm^2) of transporter protein). Limit of detection = 0.01 fmol; BL=baseline
n.d. not determined
*$p < 0.05$

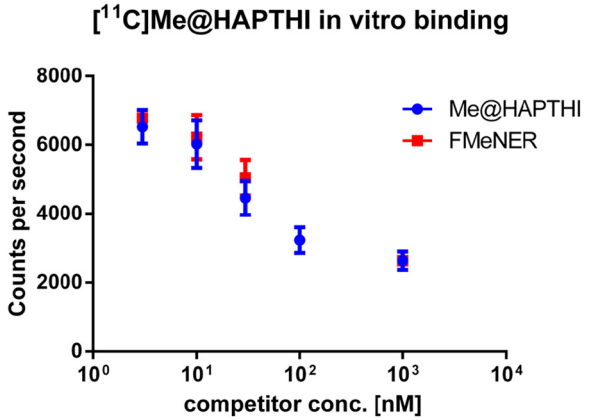

Fig. 8 NET-binding of [^{11}C]Me@HAPTHI on human NET expressing cell membranes using a harvesting protocol. Competition was done using different concentrations of Me@HAPTHI and FMeNER-D2 (1, 3, 10, 30, 100 and 1000 nM)

Discussion

[^{11}C]Me@HAPTHI presents a large stride towards an improved, novel, conveniently producible PET tracer for NET imaging. This study comprises the first radiochemical preparation, quality control and in vitro evaluation of this novel candidate PET-tracer. We describe its affinity, selectivity, lipophilicity and its potential to penetrate the BBB as well as metabolic stability. Moreover, the in vitro binding behaviour of [^{11}C]Me@HAPTHI to human NET cell membranes as well as human and rodent tissue slices was examined.

The excellent affinity of Me@HAPTHI (K_d hNET = 0.21 ± 0.07 nM) and exceptional selectivity of our candidate NET PET ligand present the ideal ground for a further evaluation of this tracer. Moreover, a lower non-specific binding can be expected, as the described radioligand is less lipophilic than previous NET PET tracers based on reboxetine (logD Me@HAPTHI = 2.21, logD FMeNER-D2 = 2.73). Based on the in vitro data acquired, successful BBB penetration by [^{11}C]Me@HAPTHI may be expected. This assumption is supported by immobilized artificial membrane chromatography results showing Me@HAPTHI to be within the discussed range of permeability P_m values.

Additionally, the high radiochemical yields and feasible radiosynthetic availability favour our newly developed NET radioligand. The employed ^{11}C-methylation reaction can be implemented at any PET facility with a cyclotron. Hence, this study presents a large stride towards a highly affine, selective and routinely available radiotracer. Moreover, in vitro stability of [^{11}C]Me@HAPTHI against human liver microsomes, containing all human liver cytochrome P450 enzymes, is excellent (99.6 ± 0.3 % intact tracer after 60 min). In contrast, other existing PET tracers show significant metabolic degradation within this timeframe (e.g. [^{11}C]MeNER, [^{11}C]DASB or [^{11}C]WAY-100635 [15, 44, 45]). Also in the rodent setting, where highly increased turnover rates of the enzymes are present, a

sufficient metabolic stability of [^{11}C]Me@HAPTHI was observed (29.26 ± 1.95 % intact, 60 min).

Furthermore, a plasma free fraction of 8.4 % was determined in ultrafiltration experiments, which was in a similar range with other clinically successful PET-tracers (e.g. [^{11}C]ADAM).

In vitro binding studies revealed specific displaceable binding in human brain regions and rat heart, indicating towards a promising further use of this tracer in in vivo studies. Binding displacement was observed in competition experiments with different NET ligands FMeNER-D2 and Me@HAPTHI in a concentration-dependent manner. The high radiotracer uptake areas matched with the high NET-density regions identified by immunohistochemistry. Therefore, specific NET uptake of [^{11}C]Me@HAPTHI can be affirmed. While this specific NET binding may be valid on ex vivo tissue, the question of binding behaviour on a cellular level was raised. Therefore, in vitro binding studies on human NET membranes were performed in a cell harvesting protocol. In these cell-based experiments, which used the same parameters as autoradiography studies (i.e. incubation time and buffer), a comparable concentration-dependent binding displacement was found for both competitors FMeNER-D2 and Me@HAPTHI. Therefore, selective NET-uptake for our novel PET ligand [^{11}C]Me@HAPTHI could be confirmed on a cellular and on a human and rat tissue level.

Thus, [^{11}C]Me@HAPTHI was showing highly promising results in vitro so far and might therefore become an improved, routine NET PET tracer. As a next step, small animal experiments will be performed to further elucidate the in vivo behaviour of [^{11}C]Me@HAPTHI.

Conclusions

A number of key properties have been discussed in the presented study, indicating that the benzothiadiazole dioxide [^{11}C]Me@HAPTHI presents a viable and improved NET PET tracer.

We demonstrated its outstanding affinity and selectivity, its great stability in human liver microsomes, as well as promising results from in vitro autoradiography. Therefore, these data encourage us for an in vivo application of this compound in small animal PET experiments in the future. On these grounds, [^{11}C]Me@HAPTHI might improve clinical NET imaging.

Additional file

Additional file 1: Supplementary data on affinity testing, metabolic stability assessments and autoradiography. Detailed methods for synthesis of precursor and reference compounds, the affinity testing of the new radiolabelled ligand via NET-expressing membrane binding protocol, as well as detailed procedures to autoradiography, immunohistochemistry and metabolic stability testings.

Competing interests
Dr. Alexander Hoepping is a full employee at the ABX Advanced Biochemical Compounds. All other authors declare that they have no competing interests.

Authors' contributions
CRM performed all radiosyntheses and preclinical in vitro experiments, autoradiography, immunohistochemistry and writing of the paper. NB contributed to all radiosyntheses and metabolite studies. CP contributed to in vitro autoradiography and immunohistochemistry. SF contributed to the affinity and selectivity testing procedures. CV contributed to IAM chromatography experiments and plasma free fraction. AH performed the synthesis of the cold reference standard Me@HAPTHI and the precursor HAPTHI. RL participated in the design of the study and proofread the manuscript. MH designed parts of the research and proofread the manuscript. MM conceived and supervised the preclinical experiments and proofread the manuscript. WW conceived and supervised the radiosyntheses and proofread the manuscript. All authors read and approved the manuscript.

Acknowledgements
The authors would like to thank Vanessa Fröhlich and Thomas Zenz for their practical and technical support. The authors are grateful to Marie Spies, MD, for native English editing.

Author details
[1]Department of Biomedical Imaging and Image-guided Therapy, Division of Nuclear Medicine, Medical University of Vienna, Vienna, Austria. [2]Department of Inorganic Chemistry, University of Vienna, Vienna, Austria. [3]Faculty of Life Sciences, Department of Technology and Biopharmaceutics, University of Vienna, Vienna, Austria. [4]ABX Advanced Biochemical Compounds, Radeberg, Germany. [5]Department of Psychiatry and Psychotherapy, Division of Biological Psychiatry, Medical University of Vienna, Vienna, Austria.

Received: 10 April 2015 Accepted: 22 May 2015
Published online: 10 June 2015

References

1. Zhou J. Norepinephrine transporter inhibitors and their therapeutic potential. Drugs Future. 2004;29:1235–44.
2. Zhou J, Zhang A, Klaess T, Johnson KM, Wang CZ, Ye YP, et al. Biaryl analogues of conformationally constrained tricyclic tropanes as potent and selective norepinephrine reuptake inhibitors: synthesis and evaluation of their uptake inhibition at monoamine transporter sites. J Med Chem. 2003;46:1997–2007.
3. Curatolo P, D'Agati E, Moavero R. The neurobiological basis of ADHD. Ital J Pediatr. 2010;36:79.
4. Mash DC, Ouyang Q, Qin Y, Pablo J. Norepinephrine transporter immunoblotting and radioligand binding in cocaine abusers. J Neurosci Methods. 2005;143:79–85.
5. Schlessinger A, Geier E, Fan H, Irwin JJ, Shoichet BK, Giacomini KM, et al. Structure-based discovery of prescription drugs that interact with the norepinephrine transporter, NET. Proc Natl Acad Sci U S A. 2011;108:15810–5.
6. Vazey EM, Aston-Jones G. The emerging role of norepinephrine in cognitive dysfunctions of Parkinson's disease. Front Behav Neurosci. 2012;6:48.
7. Moldovanova I, Schroeder C, Jacob G, Hiemke C, Diedrich A, Luft FC, et al. Hormonal influences on cardiovascular norepinephrine transporter responses in healthy women. Hypertension. 2008;51:1203–9.
8. Harik S, Duckrow R, LaManna J, Rosenthal M, Sharma V, Banerjee S. Cerebral compensation for chronic noradrenergic denervation induced by locus ceruleus lesion: recovery of receptor binding, isoproterenol- induced adenylate cyclase activity, and oxidative metabolism. J Neurosci. 1981;1:641–9.
9. Rommelfanger KS, Edwards GL, Freeman KG, Liles LC, Miller GW, Weinshenker D. Norepinephrine loss produces more profound motor deficits than MPTP treatment in mice. Proc Natl Acad Sci U S A. 2007;104:13804–9.
10. Wilson AA, Patrick Johnson D, Mozley D, Hussey D, Ginovart N, Nobrega J, et al. Synthesis and in vivo evaluation of novel radiotracers for the in vivo imaging of the norepinephrine transporter. Nucl Med Biol. 2003;30:85–92.
11. Takano A, Gulyás B, Varrone A, Halldin C. Comparative evaluations of norepinephrine transporter radioligands with reference tissue models in

rhesus monkeys: (S, S)-[18F]FMeNER-D2 and (S, S)-[11C]MeNER. Eur J Nucl Med Mol Imaging. 2009;36:1885–91.
12. Schou M, Halldin C, Sóvágó J, Pike VW, Hall H, Gulyás B, et al. PET evaluation of novel radiofluorinated reboxetine analogs as norepinephrine transporter probes in the monkey brain. Synapse. 2004;53:57–67.
13. Gulyás B, Brockschnieder D, Nag S, Pavlova E, Kása P, Beliczai Z, et al. The norepinephrine transporter (NET) radioligand (S, S)-[18F]FMeNER-D2 shows significant decreases in NET density in the human brain in Alzheimer's disease: a post-mortem autoradiographic study. Neurochem Int. 2010;56:789–98.
14. Rami-Mark C, Zhang MR, Mitterhauser M, Lanzenberger R, Hacker M, Wadsak W. [^{18}F]FMeNER-D2: reliable fully-automated synthesis for visualization of the norepinephrine transporter. Nucl Med Biol. 2013;40:1049–54.
15. Schou M, Zoghbi S, Shetty H, Shchukin E, Liow J-S, Hong J, et al. Investigation of the metabolites of (S, S)-[11C]MeNER in humans, monkeys and rats. Mol Imaging Biol. 2009;11:23–30.
16. Zeng F, Jarkas N, Stehouwer JS, Voll RJ, Owens MJ, Kilts CD, et al. Synthesis, in vitro characterization, and radiolabeling of reboxetine analogs as potential PET radioligands for imaging the norepinephrine transporter. Bioorg Med Chem. 2008;16:783–93.
17. Zeng F, Mun J, Jarkas N, Stehouwer JS, Voll RJ, Tamagnan GD, et al. Synthesis, radiosynthesis, and biological evaluation of carbon-11 and fluorine-18 labeled reboxetine analogues: potential positron emission tomography radioligands for in vivo imaging of the norepinephrine transporter. J Med Chem. 2008;52:62–73.
18. Zeng F, Stehouwer JS, Jarkas N, Voll RJ, Williams L, Camp VM, et al. Synthesis and biological evaluation of 2β,3α-(substituted phenyl)nortropanes as potential norepinephrine transporter imaging agents. Bioorg Med Chem Lett. 2007;17:3044–7.
19. Mark C, Bornatowicz B, Mitterhauser M, Hendl M, Nics L, Haeusler D, et al. Development and automation of a novel NET-PET tracer: [^{11}C]Me@APPI. Nucl Med Biol. 2013;40:295–303. doi:10.1016/j.nucmedbio.2012.11.009.
20. O'Neill DJ, Adedoyin A, Bray JA, Deecher DC, Fensome A, Goldberg JA, et al. Discovery of novel selective norepinephrine inhibitors: 1-(2-morpholin-2-ylethyl)-3-aryl-1,3-dihydro-2,1,3-benzothiadiazole 2,2-dioxides (WYE-114152). J Med Chem. 2011;54:6824–31. doi:10.1021/jm200733r.
21. O'Neill DJ, Adedoyin A, Alfinito PD, Bray JA, Cosmi S, Deecher DC, et al. Discovery of novel selective norepinephrine reuptake inhibitors: 4-[3-aryl-2,2-dioxido-2,1,3-benzothiadiazol-1(3H)-yl]-1-(methylamino)butan-2-ols (WYE-103231). J Med Chem. 2010;53:4511–21.
22. Larsen P, Ulin J, Dahlstrøm K, Jensen M. Synthesis of [^{11}C]iodomethane by iodination of [^{11}C]methane. Appl Radiat Isot. 1997;48:153–7.
23. Kniess T, Rode K, Wuest F. Practical experiences with the synthesis of [^{11}C]CH3I through gas phase iodination reaction using a TRACERlabFXC synthesis module. Appl Radiat Isot. 2008;66:482–8.
24. Jewett DM. A simple synthesis of [^{11}C]methyl triflate. Int J Radiat Appl Instrum Part A. 1992;43:1383–5.
25. Council of Europe. Radioactive pharmaceuticals (European Pharmacopoeia (Europäisches Arzneibuch). 6th ed. Vienna: Verlag Österreich GmbH; 2008.
26. Zeng F, Jarkas N, Owens MJ, Kilts CD, Nemeroff CB, Goodman MM. Synthesis and monoamine transporter affinity of front bridged tricyclic 3β-(4′-halo or 4′-methyl)phenyltropanes bearing methylene or carbomethoxymethylene on the bridge to the 2β-position. Bioorg Med Chem Lett. 2006;16:4661–3.
27. Tejani-Butt SM. [3H]nisoxetine: a radioligand for quantitation of norepinephrine uptake sites by autoradiography or by homogenate binding. J Pharmacol Exp Ther. 1992;260:427–36.
28. Donovan SF, Pescatore MC. Method for measuring the logarithm of the octanol-water partition coefficient by using short octadecyl-poly(vinyl alcohol) high-performance liquid chromatography columns. J Chromatogr A. 2002;952:47–61.
29. Naik P, Cucullo L. In vitro blood–brain barrier models: current and perspective technologies. J Pharm Sci. 2012;101:1337–54.
30. Neuhaus W, Freidl M, Szkokan P, Berger M, Wirth M, Winkler J, et al. Effects of NMDA receptor modulators on a blood–brain barrier in vitro model. Brain Res. 2011;1394:49–61.
31. Yoon CH, Kim SJ, Shin BS, Lee KC, Yoo SD. Rapid screening of blood–brain barrier penetration of drugs using the immobilized artificial membrane phosphatidylcholine column chromatography. J Biomol Screen. 2006;11:13–20.
32. Tavares AA, Lewsey J, Dewar D, Pimlott SL. Radiotracer properties determined by high performance liquid chromatography: a potential tool for brain radiotracer discovery. Nucl Med Biol. 2012;39:127–35.
33. Rami-Mark C, Bornatowicz B, Fink C, Otter P, Ungersboeck J, Vraka C, et al. Synthesis, radiosynthesis and first in vitro evaluation of novel PET-tracers for the dopamine transporter: [(11)C]IPCIT and [(18)F]FE@IPCIT. Bioorg Med Chem Lett. 2013;21:7562–9.
34. Vraka C, Nics L, Weiss V, Wagner K-H, Hacker M, Wadsak W, et al. Combination of high throughput HPLC methods for rapid prediction of blood brain barrier penetration of newly developed radiotracers—EANM 14. Eur J Nucl Med Mol Imaging. 2014;41:442.
35. Huang Y, Hwang D-R, Narendran R, Sudo Y, Chatterjee R, Bae S-A, et al. Comparative evaluation in nonhuman primates of five PET radiotracers for imaging the serotonin transporters[^{11}C]McN 5652, [^{11}C]ADAM, [^{11}C]DASB, [^{11}C]DAPA, and [^{11}C]AFM. J Cereb Blood Flow Metab. 2002;22:1377–98.
36. Gandelman MS, Baldwin RM, Zoghbi SS, Zea-Ponce Y, Innis RB. Evaluation of ultrafiltration for the free-fraction determination of single photon emission computed tomography (SPECT) radiotracers: beta-CIT, IBF, and iomazenil. Thai J Pharm Sci. 1994;83:1014–9.
37. Price JC, Mayberg HS, Dannals RF, Wilson AA, Ravert HT, Sadzot B. Measurement of benzodiazepine receptor number and affinity in humans using tracer kinetic modeling, positron emission tomography, and [^{11}C]flumazenil. Journal of cerebral blood flow and Metabolism. 1993;13:656–67.
38. Sadzot B, Price JC, Mayberg HS, Douglass KH, Dannals RF, Lever JR, et al. Quantification of human opiate receptor concentration and affinity using high and Low specific activity [^{11}C]diprenorphine and positron emission tomography. J Cereb Blood Flow Metab. 1991;11:204–19.
39. Schou M, Halldin C, Pike VW, Mozley PD, Dobson D, Innis RB, et al. Post-mortem human brain autoradiography of the norepinephrine transporter using (S, S)-[18F]FMeNER-D2. Eur Neuropsychopharmacol. 2005;15:517–20.
40. Philippe C, Haeusler D, Fuchshuber F, Spreitzer H, Viernstein H, Hacker M, et al. Comparative autoradiographic in vitro investigation of melanin concentrating hormone receptor 1 ligands in the central nervous system. Eur J Pharmacol. 2014;735:177–83.
41. Kádár A, Wittmann G, Liposits Z, Fekete C. Improved method for combination of immunocytochemistry and Nissl staining. J Neurosci Methods. 2009;184:115–8.
42. Fukuda T, Koelle GB. The cytological localization of intracellular neuronal acetylcholinesterase. J Biophys Biochem Cytol. 1959;5:433–40.
43. Immunohistochemistry HF. Current protocols in immunology. 2001.
44. Någren K, Halldin C, Pike VW, Allonen T, Hietala J, Swahn CG, et al. Radioactive metabolites of the 5-HT1A receptor pet radioligand, [carbonyl-11C]way-100635, measured in human plasma samples. J Label Compd Radiopharm. 2001;44:S472–4.
45. Parsey RV, Ojha A, Ogden RT, Erlandsson K, Kumar D, Landgrebe M, et al. Metabolite considerations in the in vivo quantification of serotonin transporters using 11C-DASB and PET in humans. J Nucl Med. 2006;47:1796–802.

3.1.7 Manuscript VII

Wenzel B, Mollitor J, Deuther-Conrad W, Dukic-Stefanovic S, Kranz M, **Vraka C**, Teodoro R, Günther R, Donat C, Ludwig F-A, Fischer S, Smits R, Wadsak W, Mitterhauser M, Steinbach J, Hoepping A, Brust P. On the development of a novel non-peptidic 18F-labeled radiotracer for in vivo imaging of oxytocin receptors with positron emission tomography. J Med Chem. 2016 Mar 10;59(5):1800-17.

Journal of Medicinal Chemistry

Article

pubs.acs.org/jmc

Development of a Novel Nonpeptidic ^{18}F-Labeled Radiotracer for in Vivo Imaging of Oxytocin Receptors with Positron Emission Tomography

Barbara Wenzel,[*,†,#] Jan Mollitor,[‡,#] Winnie Deuther-Conrad,[†] Sladjana Dukic-Stefanovic,[†] Mathias Kranz,[†] Chrysoula Vraka,[§] Rodrigo Teodoro,[†] Robert Günther,[†] Cornelius K. Donat,[†] Friedrich-Alexander Ludwig,[†] Steffen Fischer,[†] Rene Smits,[‡] Wolfgang Wadsak,[§] Markus Mitterhauser,[§] Jörg Steinbach,[†] Alexander Hoepping,[‡] and Peter Brust[†]

[†]Helmholtz-Zentrum Dresden-Rossendorf, Institute of Radiopharmaceutical Cancer Research, Research Site Leipzig, Department of Neuroradiopharmaceuticals,, Permoserstr. 15, 04318 Leipzig, Germany

[‡]ABX Advanced Biochemical Compounds GmbH, 01454 Radeberg, Germany

[§]Radiopharmacy and Experimental Nuclear Medicine, Division of Nuclear Medicine, Medical University of Vienna, A-1090 Vienna, Austria

ABSTRACT: With the aim of imaging and quantification of oxytocin receptors (OTRs) in living brain using positron emission tomography (PET), we developed a ^{18}F-labeled small molecule radiotracer and investigated its in vivo pharmacokinetics in mice and pig. [^{18}F]**6b** (K_D = 12.3 nM) was radiolabeled by a two-step procedure using a microwave system with radiochemical yields of 26.9 ± 4.7%. Both organ distribution and small animal PET studies revealed limited brain uptake of [^{18}F]**6b** in mouse (mean SUV of 0.04 at 30 min pi). Besides, significant radioactivity uptake in the pituitary gland was observed (SUV of 0.7 at 30 min pi). In a dynamic PET study in one piglet, we detected a higher uptake of [^{18}F]**6b** in the olfactory bulb (SUV of 0.34 at 30 min pi) accompanied by a low uptake in the whole brain. In vitro autoradiographic studies on porcine brain sections indicated interaction of [^{18}F]**6b** with several off-target receptors.

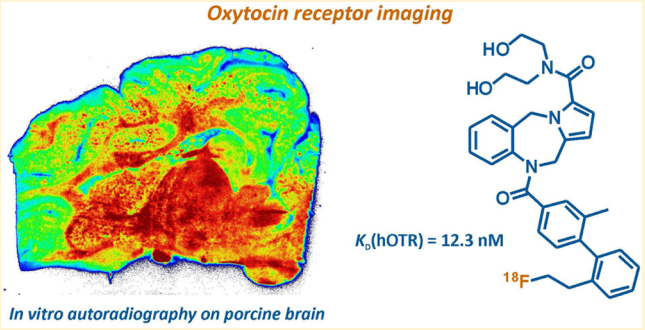

1. INTRODUCTION

The small peptide oxytocin consists of nine amino acids arranged in a disulfide-bonded cyclic structure with a short "tail". It is mainly synthesized in the paraventricular nuclei of the hypothalamus as a large prohormone, cleaved into the biologically active oxytocin and neurophysin I during passage in the neurohypophysis, and secreted upon activation of the neurosecretory cells by multiple physiological stimuli.[1] It binds to the oxytocin receptor (OTR), a 389 amino acid polypeptide (human OTR) belonging to the G-protein coupled receptor (GPCR) family. OTRs are peripherally expressed mainly in the uterus, the mammary gland, the ovary, the testis, the prostate, the kidney, the heart, and bone.[2] In the uterus, they mediate the contracting effect of oxytocin, the first discovered action of this hormone. Beside peripheral physiological functions,[2,3] oxytocin also plays an important role in the central nervous system, where it acts as putative neurotransmitter and neurohormone in different brain regions. The OTR expression in brain is strongly species-dependent,[2] which hampers the comparability between data obtained in animals and human. Main OTR expressing brain regions in human are basal ganglia, hypothalamic nuclei, brain stem, basal nucleus of Meynert, and the lateral septal nucleus.[2] Although investigated by autoradiography,[4] no quantitative data on OTR expression in human brain are available yet. A semiquantitative study on monkey brain revealed comparatively high expression in hippocampus and moderate expression in nucleus basalis of Meynert and some cortical and hindbrain regions.[5] In rats, however, beside the basal ganglia and the hypothalamus, OTRs are also abundantly expressed (~200−400 fmol [^{3}H]OT/mg protein) in the olfactory system (anterior olf nucl), the bed nucleus of stria terminalis, and the peduncular cortex.[2,6,7] In addition, Freund-Mercier et al.[8] have shown that neurophysins rather than OTR are involved in binding of [^{3}H]oxytocin in the neural lobe of the pituitary.

Central behavioral effects of the OT system are extensively investigated in animals[9−11] and in humans.[12−15] The involvement in social and maternal behavior, trust and empathy, partnership bonding, sexual behavior, stress-related behavior, and learning and memory has been demonstrated.[12,16] Moreover, the impact of oxytocin on psychiatric disorders such as schizophrenia,[17] depression,[18] and autism[19,20] is the object of recent studies. Research in this field is mainly

Received: August 18, 2015
Published: January 21, 2016

DOI: 10.1021/acs.jmedchem.5b01080
J. Med. Chem. 2016, 59, 1800−1817

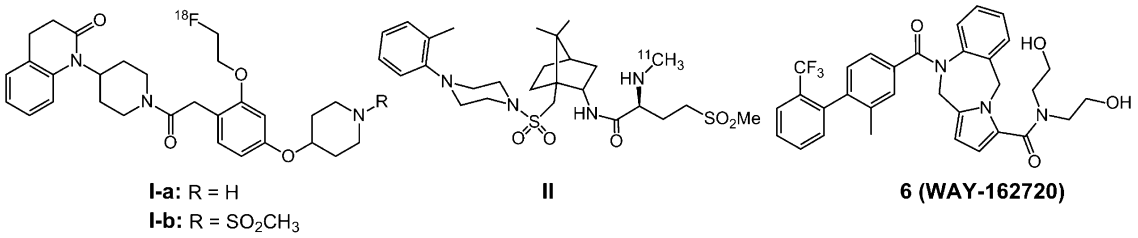

Figure 1. Reported PET radiotracers for OTR (**I-a**, **I-b**, and **II**); **6** as lead structure.

Scheme 1. Synthetic Route of Series A Derivatives 6a−6f and Precursor 7[a]

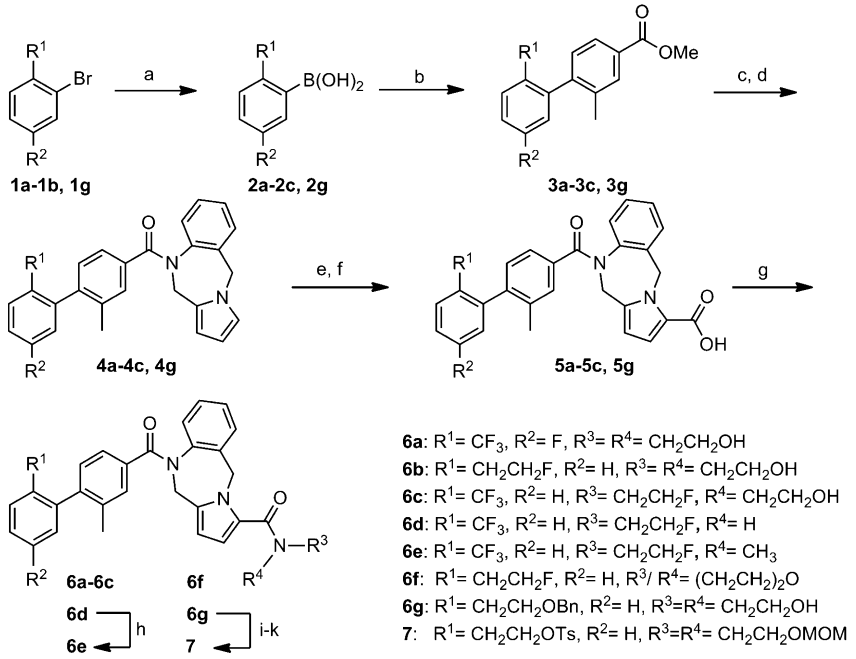

[a]Reagents and conditions: (a) $B(OMe)_3$, *n*-BuLi, THF, −78 °C to rt; (b) methyl 4-bromo-3-methylbenzoate, $Pd(PPh_3)_4$, Na_2CO_3, H_2O, EtOH, toluene, 14 h, 90 °C; (c) 1 M NaOH, THF, 12 h, reflux; (d) (i) $SOCl_2$, 2 h, reflux, (ii) 10,11-dihydro-5*H*-pyrrolo[2,1-*c*][1,4]benzodiazepine (**8**), Hünig's base, CH_2Cl_2, 0 °C to rt, overnight; (e) trichloroacetyl chloride, Hünig's base, CH_2Cl_2, 2 h, 0 °C to rt achieving intermediates **15**, **18**, and **19**; (f) 2.5 M NaOH, acetone, 12 h, rt; (g) amidation with the corresponding amine (for **6a**,**b**,**g**, diethanolamine; for **6c**, diethanolamine and DAST, CH_2Cl_2, 12 h, rt; for **6d**,**6e**, 2-fluoroethylamine; for **6f**, morpholine) HOBt/EDCI, COMU, or TBTU, 12−20 h, rt; (h) NaH, CH_3I, DMF, 1 h, rt; (i) MOMBr, TBAC, Hünig's base, CH_2Cl_2, 24 h, 0 °C to rt achieving intermediate **16**; (j) H_2, $Pd(OH)_2$/C, MeOH, 20 h, rt achieving intermediate **17**; (k) TsCl, triethylamine, 4-DMAP, CH_2Cl_2, 12 h, 0 °C to rt.

conducted by behavioral monitoring after drug administration or functional magnetic resonance imaging (fMRI), the latter based on changes in the blood flow in certain brain regions.[14] An investigation of disease-specific changes in the expression of OTR in the brain has been limited so far.

Positron emission tomography (PET) is a noninvasive imaging method that can provide selective information on a single biological target or biochemical process, when a target specific radiotracer is used. Therefore, a radiotracer, binding specifically to the OTR, would allow direct quantification of these receptors in the living brain and open new options for diagnosis and therapy monitoring of the diseases mentioned above.

In 2012 and 2013, Smith et al. reported for the first time structurally different PET tracers intended for OTR imaging (see **I-a**, **I-b**, and **II** in Figure 1), labeled with fluorine-18 and carbon-11, the most commonly used short-lived positron emitting radionuclides.[21−23] These compounds are based on two nonpeptidic antagonists of the OTR developed by Merck Research Laboratories in the early 1990s as drug candidates for premature labor.[24,25] Although these small molecule radiotracers showed appropriate physicochemical properties regarding blood−brain barrier (BBB) permeability, the authors observed a very poor brain uptake in rats and cynomolgus monkeys insufficient for OTR imaging.

In parallel to this work, we started to develop a ^{18}F-labeled PET radiotracer for imaging of OTR in brain. As lead structure, *N*,*N*-bis(2-hydroxyethyl)-10-(2-methyl-2′-(trifluoromethyl)-[1,1′-biphenyl]-4-carbonyl)-10,11-dihydro-5*H*-benzo[*e*]-pyrrolo[1,2-*a*][1,4]diazepine-3-carboxamide, **6** (**WAY-162720**;[26] Figure 1), was selected, an OTR antagonist described to be able to penetrate the BBB in mice.[27] We synthesized two series of derivatives and determined the binding affinity toward human OTR (hOTR) in vitro as well as their lipophilicity (log *D*) and permeability values (P_m) by different HPLC methods. The most promising candidate was labeled with [^{18}F]fluoride and investigated by in vitro autoradiography on pig brain slices. Furthermore, the pharmacokinetics of the novel ^{18}F-labeled PET radiotracer

DOI: 10.1021/acs.jmedchem.5b01080
J. Med. Chem. 2016, 59, 1800−1817

Scheme 2. Synthetic Route of Series B Derivatives 12a−12d, 13a, 13b, and 14[a]

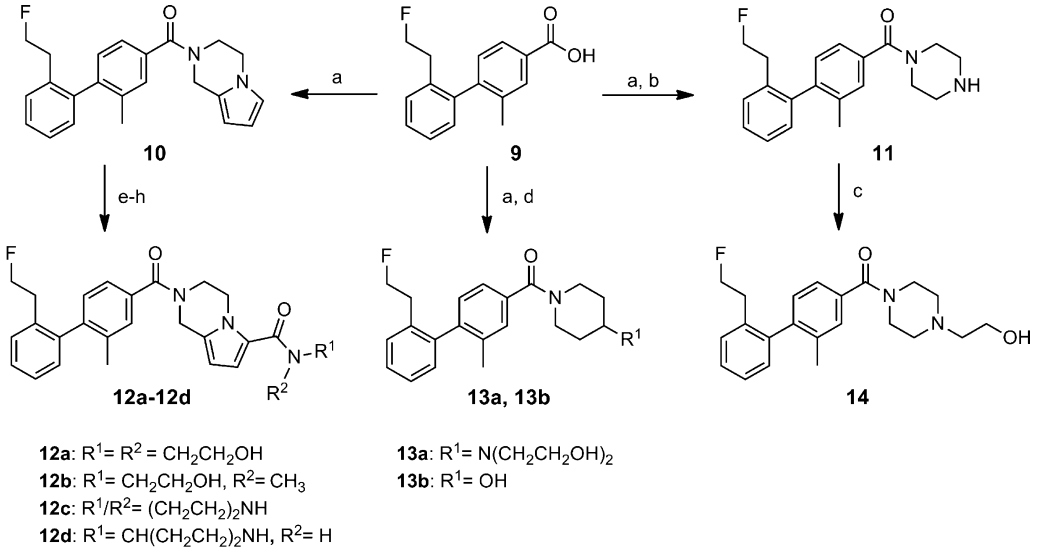

[a]Reagents and conditions: (a) (i) $SOCl_2$, 1 h, reflux; (ii) Hünig's base, CH_2Cl_2, and 1,2,3,4-tetrahydro-pyrrolo[1,2-*a*]pyrazine for **12a−d**, 4-piperidone for **13a,b**, and intermediate **24**, *N*-Boc-piperazine for **14** and intermediate **25**, 4 h, 0 °C to rt; (b) trifluoroacetic acid, CH_2Cl_2, 2.5 h, rt; (c) 2-bromoethanol, K_2CO_3, CH_3CN, 12 h, reflux; (d) diethanolamine, $Na(OAc)_3BH$, AcOH, 1,2-dichloroethane, 12 h, rt; (e) trichloroacetyl chloride, Hünig's base, CH_2Cl_2, 2 h, 0 °C to rt achieving intermediate **20**; (f) 2.5 M NaOH, acetone, 12 h, rt achieving intermediate **21**; (g) amidation with the corresponding amine (**12a**, diethanolamine; **12b**, *N*-methylethanolamine; **12c** and intermediate **22**, *N*-Boc-piperazine; **12d** and intermediate **23**, 4-amino-1-Boc-piperidine) HOBt/EDCI, COMU, or TBTU, 12−20 h, rt; (h) **12c,d**, trifluoroacetic acid, CH_2Cl_2, 2,5 h, rt.

was investigated in mice and pig by ex vivo analyses and dynamic PET studies.

2. RESULTS AND DISCUSSION

2.1. Organic Chemistry. The synthesis of the new derivatives is based on the synthesis of **6** described previously.[26] Key steps of the synthetic routes are a Suzuki coupling between appropriately substituted phenylboronic acids and methyl 4-bromo-3-methylbenzoate to form the desired biaryl framework, followed by an amidation using a tricyclic benzodiazepine (series A, Scheme 1) or other *N*-heterocycles like piperazine, piperidine, and pyrrolopyrazine (series B, Scheme 2).

All derivatives of series A (**6a−6f**) contain a primary, secondary, or cyclic alkyl side chain at the *N*-heterocyclic unit with varying substituents and side chain length. To additionally investigate the influence of the substituents at the biphenyl ring system, different fluorine and alkyl fluorine substituted systems were synthesized with respect to the intended ^{18}F-fluorination.

In general, the synthesis of the compounds **6a−6f** of series A (Scheme 1) started with differently substituted 2-bromophenyl substrates (**1a−1b**), which were converted to the corresponding boronic acids (**2a−2b**; **2c** was commercially available) using *n*-BuLi and trimethyl borate. Following Suzuki cross coupling with commercially available methyl 4-bromo-3-methylbenzoate afforded the corresponding biaryl units (**3a−3c**). To couple the biaryl units with the benzopyrrolodiazepine moiety, the methyl ester functionality was hydrolyzed and converted to its acid chloride. Subsequent reaction with 10,11-dihydro-5*H*-pyrrolo-[2,1-*c*][1,4]benzodiazepine, **8**, synthesized according to reported procedures,[28−30] provided the desired biaryl functionalized benzopyrrolodiazepines (**4a−4c**). To introduce a carboxyl group solely at the 3-position of the tricycle, aromatic acylation with trichloroacetyl chloride in the presence of Hünig's base was performed followed by a haloform type reaction with aqueous NaOH to give the corresponding carboxylic acids (**5a−5c**). The final amidation could be effectively achieved by treating **5a−5c** with 1-ethyl-3-(3-dimethylamino-propyl) carbodiimide hydrochloride (EDCI) and 1-hydroxybenzotriazole (HOBt) as coupling agents followed by the addition of the corresponding amine. For some substrates, the use of (1-cyano-2-ethoxy-2-oxoethylidenaminooxy)dimethylamino-morpholino-carbenium hexafluorophosphate (COMU) or (benzotriazol-1-yl)-*N*,*N*,*N*′,*N*′-tetramethyluronium tetrafluoroborate (TBTU) proved to be superior to the combination of EDCI/HOBt.

For some of the derivatives, the synthetic route was slightly changed. Thus, the synthesis of **6c** was accomplished by fluorination of **6** using one equivalent of diethylaminosulfur trifluoride (DAST). Compound **6e** was synthesized by *N*-methylation of **6d**. Derivative **7** with the 4-tosyloxyethyl side chain was synthesized as a precursor compound for the intended radiosynthesis of [^{18}F]**6b**. The synthetic route started from the benzyl protected 2-(2-bromophenyl)-ethanol **1g**, which was converted to the corresponding boronic acid **2g** for subsequent Suzuki coupling. After haloform type reaction and amidation with diethanolamine, the two primary hydroxyl groups of the resulting derivative **6g** were protected as methyloxymethyl ether to avoid side reactions during radiosynthesis. To introduce an appropriate leaving group for nucleophilic radiofluorination, the benzyl protecting group of the ethoxy side chain was removed by hydrogenolysis and replaced by a tosylate function (**7**).

The synthetic route for the series B derivatives **12a−12d**, **13a**, **13b**, and **14** is shown in Scheme 2. The biaryl carboxylic acid **9**, obtained after fluorination of 2-(2-bromo-phenyl)-ethanol followed by Suzuki coupling with the corresponding boronic acids **2b** and subsequent methyl ester hydrolyses, served as starting material. For the synthesis of **12a−12d**, the reaction sequence of carboxylation and amide formation was applied. The required 1,2,3,4-tetrahydro-pyrrolo[1,2-*a*]pyrazine

DOI: 10.1021/acs.jmedchem.5b01080
J. Med. Chem. 2016, 59, 1800−1817

was synthesized as reported[31] via in situ formation of formaldehyde imine of 2-(1*H*-pyrrol-1-yl)ethanamine, followed by an intramolecular aza-Friedel–Crafts reaction. The synthesis of **12a** and **12b** was accomplished by amidation of the carboxylic acid with the appropriate secondary amine. To gain access to **12d**, the 4-amino-1-Boc-piperidine was used for amidation followed by Boc deprotection. In the same way, mono-Boc-protected piperazine was introduced to obtain **12c**. Boc-protected piperazine was also utilized for the synthesis of **14**. After amidation and deprotection, the secondary amine **11** was finally alkylated with 2-bromoethanol to obtain the product **14**. Compound **13a** was synthesized by amide formation with 4-piperidone followed by reductive amination using diethanolamine. A side product of this reaction obtained by reduction of the ketone functionality to the corresponding secondary alcohol was derivative **13b**.

2.2. Binding Affinity and Estimation of BBB Permeability in Vitro. For determination of the binding affinities of the new derivatives toward hOTR, competitive binding studies were performed using a cell line stably transfected with hOTR gene and [^{3}H]oxytocin as radioligand. The calculated K_i values are summarized in Table 1.

Table 1. In Vitro Binding Affinity, Lipophilicity, and Permeability Data of New Derivatives

compd	K_i [nM][a]	lipophilicity (log D)[b]	permeability (P_m)[c]
		Series A	
6	8.7 ± 1.1	3.21 ± 0.02	3.21 ± 1.23
6a	21.5 ± 8.8	3.31 ± 0.04	4.49 ± 0.80
6b	13.3 ± 7.1	3.14 ± 0.01	6.28 ± 5.64
6c	17.7 ± 5.1	4.89 ± 0.30	24.70 ± 8.81
6d	96.6 ± 7.5	4.18 ± 0.18	34.20 ± 9.32
6e	27.3 ± 6.4	5.20 ± 0.36	25.71 ± 3.49
6f	66.3 ± 14.9	4.08 ± 0.16	7.09 ± 3.06
		Series B	
12a	>1000	nd[d]	nd
12b	>1000	nd	nd
12c	>1000	nd	nd
12d	>1000	nd	nd
13a	>1000	nd	nd
13b	>1000	nd	nd
14	>1000	nd	nd

[a] K_i values in nM (mean ± SD, $n \geq 2$) were derived from IC_{50} values according to the Cheng–Prusoff equation;[32] K_D ([^{3}H]oxytocin) = 2.56 ± 0.95 nM. [b] Log D values (mean ± SD, $n \geq 3$, pH 7.4) were determined by HPLC.[33] [c] P_m values (mean ± S.D., $n \geq 3$) were determined by IAM-chromatography.[34] [d] nd: not determined.

Compounds **6a**, **6b**, and **6c** bind with only slightly lower affinity to hOTR compared to the lead structure **6**. This indicates that minor structural modifications at the biphenyl moiety and at the carbamide functionality are well accepted by the receptor binding site. In contrast, a more pronounced modification of the substituents at the nitrogen of the carbamide function results in a remarkable decrease in binding affinities (**6d** and **6f**). Considering the compounds of series B, we observed almost no relevant interaction with the hOTR (K_i values of >1 μM), which is probably caused by the exchange of the benzopyrrolodiazepine moiety.

To estimate the BBB permeability of the new derivatives, their lipophilicity and permeability was investigated using two different HPLC methods. An established criterion for a passive diffusion of molecules through the BBB is the lipophilicity with a log P or log D value in the range of 1 to 4.[35−37] The log D values of the derivatives of series A (Table 1) were determined according to the HPLC method of Donovan and Pescatore.[33] The log D values of **6**, **6a**, and **6b** are in the range of 3.1−3.3, which indicates at least a moderate passage across the BBB.[35,36] Compounds **6c**−**6f** are considerably more lipophilic with values of >4.1. On one hand, a higher lipophilicity is assumed to enhance the passive diffusion across biological membranes but also increases plasma protein binding which might decrease drug availability. In addition, P. Wils and co-workers[38] have shown that the transport of a drug across intestinal epithelial cells is decreased with increasing lipophilicity (log D values ranging from 3.5 to 5.2), a phenomenon which was explained by successive aqueous−lipid interphases that a higher lipophilic drug has to cross. Correspondingly, a parabolic relationship exists between lipophilicity and brain uptake,[39,40] making derivatives with higher log D values unsuitable as ligands for PET imaging in brain.

Lipophilicity is only one of several physicochemical parameters when discussing BBB permeability, and recent studies have shown that log D values are not generally appropriate predictors for BBB penetration.[41] Therefore, we performed in addition permeability (P_m) measurements according to Taillardat-Bertschinger et al. using immobilized artificial membrane (IAM) chromatography.[34,42] Those IAMs mimic the lipid environment of cell membranes and are formed by synthetic phospholipid analogues covalently bound on the silica support. This modified stationary phase is packed as a solid matrix in a liquid chromatography column. The calculated P_m value correlates with the retention time of the tested compound in the chromatogram. For the IAM measurements of the derivatives of series A, an IAM.PC.DD2 column was used in isocratic mode with phosphate buffer and acetonitrile in different ratios. Data analysis was performed as described in detail in the Experimental Section. As basis, a series of 20 reference compounds was investigated which comprise molecules known to penetrate the BBB by passive diffusion[43] (e.g., raclopride 0.1 ± 0.01, DASB 0.4 ± 0.15, fluoroethylcarfentanil 1.5 ± 0.58, altanserin 2.2 ± 0.8, and elacridar 4.0 ± 2.7). Accordingly, P_m values between 0 and 4 obtained with this test system allowed expectation of a good BBB penetration.[43]

Table 1 shows the P_m values of the derivatives of series A. Within this series, **6** is expected to be the compound with the highest BBB permeability (P_m value of 3.21). As mentioned earlier, this compound was described to be brain penetrable[27] and was therefore chosen as lead structure for the current study. By contrast, the P_m values of compounds **6c**, **6d**, and **6e** are considerably higher (P_m = 24 to 34) and indicate poor permeability. This could be caused by the high lipophilicity of these derivatives hampering the transport of the compounds across a membrane as mentioned.[38] For the derivatives **6a**, **6b**, and **6f**, a moderate BBB permeability may be expected according to P_m values between 4.5 and 7.

On the basis of the highest in vitro binding affinity in combination with the moderate lipophilicity and permeability data, **6b** was selected as candidate for further ^{18}F-labeling and in vivo investigation.

2.3. Radiochemistry. The new radioligand [^{18}F]**6b** was prepared in a two-step synthesis by nucleophilic substitution of a methoxymethyl (MOM) ether protected tosylate precursor (**7**) using anhydrous K[^{18}F]F-$K_{2.2.2}$-carbonate complex in

DOI: 10.1021/acs.jmedchem.5b01080
J. Med. Chem. 2016, 59, 1800−1817

Scheme 3. ^{18}F-Radiolabeling of [^{18}F]**6b**[a]

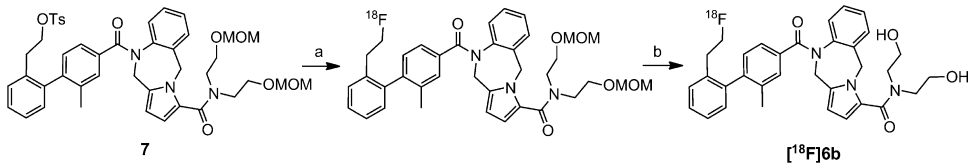

[a]Reagents and conditions: (a) [^{18}F]F$^-$/$K_{2.2.2}$/K_2CO_3, ACN, with thermal heating (90 °C) or microwave heating (85−95 °C; 75 W); (b) 1 mL 2.0 M HCl, with thermal heating (90 °C) or microwave heating (75−85 °C, 50 W).

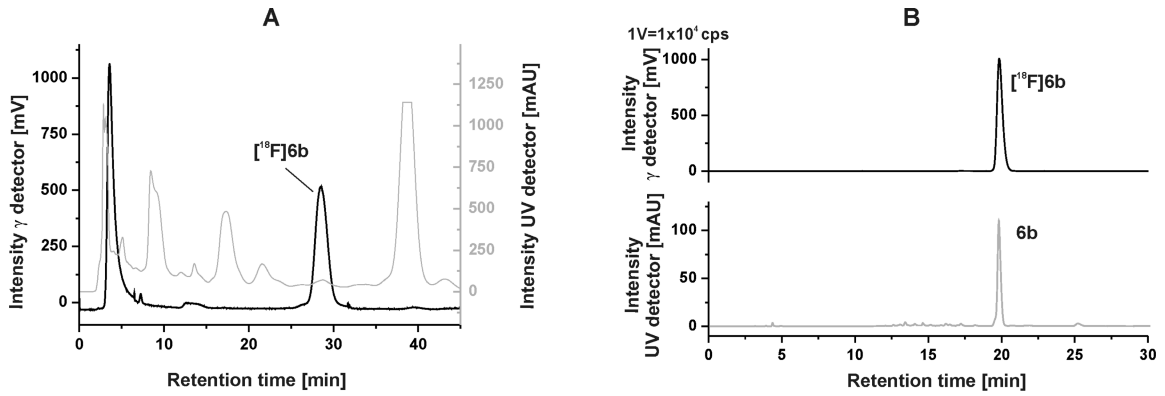

Figure 2. (A) Semipreparative UV- and radio-HPLC chromatograms of [^{18}F]**6b** (conditions: Reprosil-Pur C18-AQ, 250 mm × 10 mm, 44% ACN/20 mM NH_4OAc_{aq}, 4 mL/min). (B) Analytical UV- and radio-HPLC chromatograms of the final product of [^{18}F]**6b** spiked with the reference **6b** (conditions: Reprosil-Pur C18-AQ, 250 mm × 4.6 mm, gradient with eluent A 10% ACN/20 mM NH_4OAc aq and eluent B 90% ACN/20 mM NH_4OAc aq: 0−5′ 100% A, 5−10′ up to 55% B, 10−25′ 55% B, 25−30 up to 100% B, 30−40′ 100% B, 40−45′ up to 100% A, and 45−55′ 100% A).

acetonitrile followed by the deprotection of the two hydroxyl groups using aqueous HCl (Scheme 3).

The ^{18}F-labeling process was investigated under thermal and microwave heating. In general, higher labeling yields in shorter reaction times were achieved under microwave conditions. Using 75 W and a temperature interval of 85−95 °C, the formation of the product was completed within 6−9 min and labeling yields of 67.8 ± 9.4% (n = 11) were achieved. By contrast, under conventional heating at 90 °C, 15 min reaction time was needed until no further increase of labeled product was observed, resulting in labeling yields of 51.7 ± 14.0% (n = 10). Beside [^{18}F]fluoride, no radioactive byproduct was observed under both conditions tested. Moreover, the precursor remained quite stable as proven by HPLC. The deprotection step was also investigated with the two heating methods and different concentrations of hydrochloric acid (0.5, 1.0, and 2.0 M HCl each 1 mL). Using 1 mL of 2.0 M HCl and microwave settings of 50 W/75−85 °C, the deprotection was completed within 5 min. When lower concentrations of HCl were used, longer reaction times were needed. Also for thermal heating at 90 °C, 2.0 M HCl was most appropriate, however, 15 min reaction time was necessary to remove both protecting groups quantitatively. With increasing reaction time the formation of a byproduct (<5%) was observed, which appeared to be slightly more lipophilic than the product according to HPLC analysis.

For isolation of [^{18}F]**6b**, the reaction mixture was neutralized with appropriate amounts of 6.0 M NaOH and injected into the semipreparative HPLC system. The product was collected at a retention time of 27−30 min (A in Figure 2), purified using solid phase extraction on an RP cartridge, and formulated in sterile isotonic saline containing 10% of EtOH for better solubility. Analytical HPLC of the final product, spiked with the unlabeled reference compound, confirmed the identity of [^{18}F]**6b** (B in Figure 2). Finally, the radiotracer was obtained with a radiochemical purity of ≥97% in radiochemical yields of 20.9 ± 4.1% (n = 4, decay corrected) with thermal heating and 26.9 ± 4.7% (n = 6, decay corrected) with microwave heating and specific activities between 35−160 GBq/μmol. Because of the short reaction time and the slightly higher radiochemical yield, the microwave heating system was preferred for the radiosynthesis of [^{18}F]**6b**.

The in vitro stability of the radiotracer was investigated by incubation at 40 °C in the following solutions: (i) 0.9% aq NaCl, (ii) phosphate-buffered saline (PBS), and (iii) pig plasma samples. [^{18}F]**6b** proved to be stable in all media, and no defluorination or degradation was observed within 30 min of incubation time.

The n-octanol-buffer partition coefficient (log D at pH 7.4) of [^{18}F]**6b** was determined for the n-octanol/PBS system by the shake-flask method. The obtained value of 2.87 ± 0.15 (n = 3) is slightly lower than the log D value of 3.14 determined by the HPLC method for the nonradioactive reference compound **6b**.

2.4. In Vitro Affinity and Plasma Free Fraction of [^{18}F]6b. The equilibrium dissociation constant of [^{18}F]**6b** was determined in a homologous competitive binding experiment with K_D = 12.3 nM, which is consistent with the above-reported K_i value of 13.3 nM for the nonradioactive reference compound **6b**.

The plasma free fraction f_p of [^{18}F]**6b**, determined by ultrafiltration of a plasma sample prepared from pooled pig blood and incubated with the radiotracer, was 0.02. This value corresponds with the log D value and indicates sufficient availability of the radiotracer for penetration of the BBB.

2.5. In Vitro Autoradiographic Studies. The distribution of binding sites of [^{3}H]oxytocin and [^{18}F]**6b** in porcine brain is shown in parts A and B of Figure 3, respectively. For [^{18}F]**6b**, we detected the following ranking order: chiasma opticus (CO)

DOI: 10.1021/acs.jmedchem.5b01080
J. Med. Chem. 2016, 59, 1800−1817

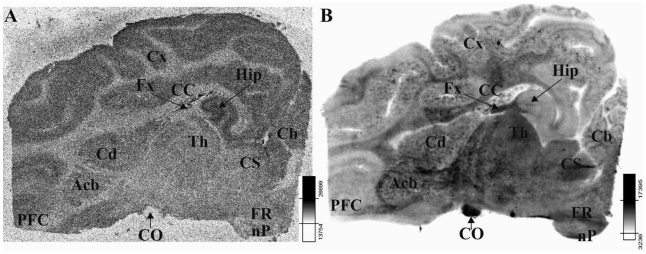

Figure 3. Distribution of the binding sites of (A) [^{3}H]oxytocin (6 nM) and (B) [^{18}F]**6b** (~10 nM) in porcine brain in vitro. Abbreviations: Acb = nucleus accumbens, Cb = cerebellum, CC = corpus callosum, Cd = nucleus caudatus, CO = chiasma opticus, Cx = cortex, CS = colliculus superior, Fx = fornix, FR = formatio reticularis, Hip = hippocampus, nP = nuclei pontis, Th = thalamus, PFC = prefrontal cortex.

> fornix (Fx) > basal ganglia (Acb, Cd) ~ brainstem (FR, nP) > corpus callosum (CC) > cerebellum (Cb) ~ hippocampus (Hip) ~ cortex (Cx) > prefrontal cortex (PFC). By contrast, for [^{3}H]oxytocin, a clearly different pattern was detected: Hip > Cx > Cb ~ PFC > Cd > Th ~ Acb > Fx ~ CC > CO. This quite sparse and very restricted distribution has also been observed in the human and the brain of the titi monkey by [^{125}I]OVTA and [^{3}H]oxytocin autoradiography.[4,44] Therefore, we supposed that these results suggest binding of [^{18}F]**6b** to both OTR as well as other targets. To test this assumption, we performed appropriate competitive binding studies. We noticed a considerable and overall reduction of binding sites of [^{18}F]**6b** by the $GABA_A$ receptor ligand THIP and a localized reduction by oxytocin and the glutamate receptor ligand L-quisqualic acid. In selected brain regions, the binding of [^{18}F]**6b** was both increased and decreased by the vasopressin receptor ligands tolvaptan and SR49059 as well as the σ1/2 receptor ligand siramesine (data not shown). We hypothesize that this substantial off-target binding can be related to the presence of the 1,4-benzodiazepine moiety in [^{18}F]**6b**. In particular, 1,4-benzodiazepine derivatives have been used among others as anxiolytic, hypnotic, anticonvulsant, or antiarrhythmic drugs as well as inhibitors or ligands of a variety of GPCRs such as cholecystokinin, fibrinogen, integrin, vasopressin, bradykinin, or κ-opioid receptors.[45] It might be expected that such features hamper the applicability of benzodiazepine-related OTR ligands such as [^{18}F]**6b** for the PET imaging of OTR in the central nervous system.

2.6. Metabolism of [^{18}F]6b. The metabolism of [^{18}F]**6b** was investigated in plasma samples of female CD1 mice obtained at 30 min pi of the radiotracer. Figure 4 shows a typical analytical HPLC chromatogram of the metabolite profile of the radiotracer. For preparation of RP-HPLC samples, the proteins were precipitated and extracted two times with ACN, with a reproducible recovery of ~82% of the starting radioactivity in the supernatant. We assume that the radioactivity remaining in the pellet mainly attributes to hydrophilic radiometabolites. To verify this assumption, a plasma sample was incubated in vitro with the parent radiotracer and processed under identical conditions as the in vivo experiments. As a result, in vitro more than 99% of the radiotracer could be transferred into the supernatant, leading to the conclusion that the radiotracer is recovered quantitatively also in the in vivo samples. On the basis of this finding, we were able to correct the percentage of intact radiotracer in dependence of the recovery. Therefore, the intensities (mV/min; correlating to the count rates) of each signal in the radio-HPLC chromatograms were summed and related to 82%. This ratio was used to calculate the percentage of intact radiotracer based on its peak intensity in the chromatogram. Accordingly, 20% of intact radiotracer is available in plasma at 30 min pi, which is slightly less than the uncorrected value of 25%.

During the dynamic PET study in pig, we also determined the fraction of nonmetabolized [^{18}F]**6b** in plasma samples taken at 2, 8, 30, and 60 min pi of the radiotracer and processed them as described for the plasma samples of mouse. The metabolite RP-HPLC profile is comparable to the profile observed for the mouse samples at 30 min pi. However, for samples collected at later time points, we detected a considerable decrease of recovery of radioactivity ranging from 97% at 2 min pi to 64% at 60 min pi. Therefore, the percentage of intact radiotracer at each time point was calculated as described and the corrected values are given in Table 2. Accordingly, intact tracer accounts for 31% of total activity in plasma at 30 min pi.

2.7. In Vivo Characterization of [^{18}F]6b. To assess brain uptake and pharmacokinetics of this type of tricyclic benzodiazepine in more detail, biodistribution of [^{18}F]**6b** was investigated in female CD-1 mice 5 and 30 min after intravenous injection of ~220 kBq of the radioligand. With 0.41% ID/g (SUV = 0.11) at 5 min pi, a rather low brain uptake was observed, followed by a fast washout (0.11% ID/g or SUV = 0.03 at 30 min pi). In addition, we detected high uptake of radioactivity in the pituitary gland (Figure 5; 8.36% ID/g, SUV

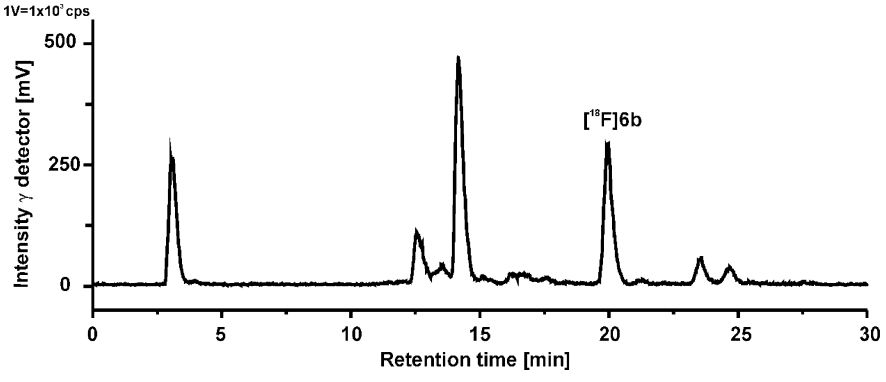

Figure 4. Analytical radio-HPLC chromatogram of a plasma sample of [^{18}F]**6b** 30 min pi. Conditions: Reprosil-Pur C18-AQ; 250 mm × 4.6 mm; flow 1.0 mL/min; gradient mode see Experimental Section.

DOI: 10.1021/acs.jmedchem.5b01080
J. Med. Chem. 2016, 59, 1800−1817

Table 2. Percentage of [^{18}F]6b in Plasma Samples of Pig

time of sampling [min pi]	radioactivity recovery [%]	peak area [^{18}F]6b[a] [mV/min]	peak area total[b] [mV/min]	[^{18}F]**6b** noncorr[c] [%]	[^{18}F]**6b** corr[d] [%]
2	97	461	467	99	96
8	77	55	77	71	55
30	69	76	172	44	31
60	64	11	70	16	10

[a]Values are taken from radio-HPLC chromatograms. [b]Sum of values of all signals taken from each radio-HPLC chromatogram. [c]Percentage values without correlation to the recovery of radioactivity. [d]Percentage values with correlation to the recovery of radioactivity.

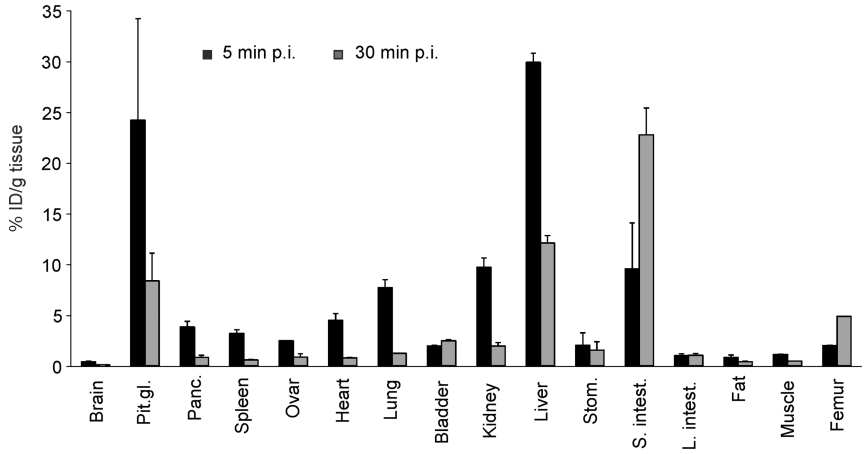

Figure 5. Organ distribution of [^{18}F]**6b** in mice (data are presented as mean values ± sd; n = 2 per time point).

= 2.1 at 30 min pi), a region outside of the BBB with known OTR expression.[46] This uptake might indicate a specific binding of [^{18}F]**6b** to OTRs but could also be caused by the binding to the oxytocin specific carrier protein neurophysin.[8] The excretory organs small intestine and liver showed the highest accumulation of radioactivity at 30 min pi (22.8% ID/g and 12.1% ID/g, respectively). The increasing accumulation in the femur may indicate some defluorination of the radiotracer, although OTR expression has also been found in bone marrow.[47]

To analyze the kinetics of the brain uptake of [^{18}F]**6b** and to assess an interaction of this particular tricyclic benzodiazepine with efflux transporters of the blood–brain barrier, pharmacokinetics was further studied by dynamic PET scans under baseline and blocking conditions in female CD-1 mice. The results obtained by these PET studies revealed a very low uptake of [^{18}F]**6b** in the mouse brain during the 60 min acquisition, with peak radioactivity in whole brain of SUV 0.07 at 5 and 0.04 at 60 min pi (Figure 6). A considerably higher accumulation of radioactivity (SUV 0.7 at 60 min pi) was detected in the pituitary gland. To investigate a possible interaction of [^{18}F]**6b** with the efflux transporter P-glycoprotein (P-gp) as cause for the low brain uptake, additional PET studies under pretreatment with the known P-gp inhibitor cyclosporin[48] were performed. However, neither in brain nor in the pituitary gland of mice was an increase in the uptake of [^{18}F]**6b** observed.

Finally, [^{18}F]**6b** failed to image brain OTR in vivo in mouse, most probably due to lack of brain penetration. However, the log D and P_m values at physiological pH are assumed to be compatible with at least a moderate brain permeation of [^{18}F]**6b**. In addition, the absence of an effect of cyclosporine on the brain uptake of the radiotracer indicates no substantial interaction of [^{18}F]**6b** with the P-gp. However, an important aspect of preclinical evaluation of brain targeting PET

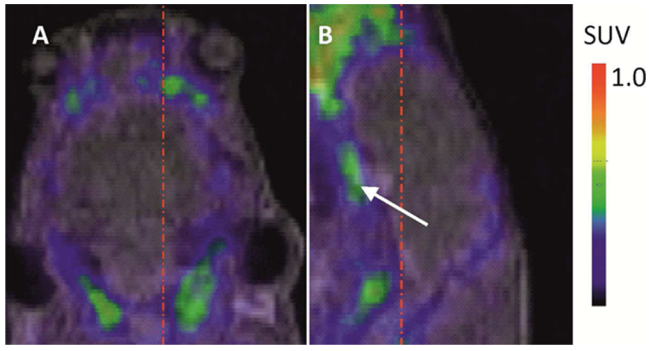

Figure 6. Representative image of a PET scan of [^{18}F]**6b** at 60 min pi of a brain of a female CD-1 mouse. The arrow is pointing to the pituitary gland and the crosshairs designating the slice location of the transverse and sagittal slice. (A) Transverse slice. (B) Sagittal slice.

radiotracers is species specificity as reflected by, e.g., higher brain uptake of [^{11}C]GR205171 and [^{18}F]altanserin in humans and monkey than in rats[49] and of the α7 nicotinic acetylcholine receptor ligand [^{18}F]NS14490 in pig than in mouse.[50,51] To test if such behavior is also relevant for the tricyclic benzodiazepines under investigation in the current study, we decided to proceed with the evaluation of [^{18}F]**6b** in one pig.

Although this single PET study in pig confirmed a low BBB permeability of [^{18}F]**6b** with a maximum SUV of 0.34 in brain at 30 min pi, this value reflects an about 10-fold higher brain uptake in pig than in mouse (SUV 0.03–0.04 at 30 min pi). Interestingly, the uptake in the olfactory bulb (SUV = 0.33 at 30 min pi) was considerably higher than in other brain regions, which is consistent with a comparably high OTR expression found in rats.[7]

Despite a slightly better penetration of [^{18}F]**6b** across the BBB in pig than in mouse, the total brain uptake is rather low and hampers reliable imaging and quantification of OTR in the

DOI: 10.1021/acs.jmedchem.5b01080
J. Med. Chem. 2016, 59, 1800–1817

living brain. To disclose the reason for the low brain penetration is ambitious. As often reported, the magnitude of brain uptake of a compound is mainly determined by its size, lipophilicity, H-bonding capacity, polar surface area (PSA), and molecular flexibility.[36,37] The lipophilicity of [^{18}F]**6b** with an experimentally determined log *D* value of 2.8 is in the range for BBB penetrating compounds[35,36] and gives therefore no valuable information. However, with a molecular weight of 555 g/mol, the size of the compound is considerably higher than the limit of 400 g/mol, reported by Waterbeemd et al. for a set of 125 CNS-active and inactive drugs.[37] In this study, additional to the size dependency, also the PSA was specified as significant criterion for BBB penetration and estimated to be <90 Å^2 for CNS-active drugs. Later on, Kelder et al. suggested an even more stringent cutoff of PSA < 60 Å^2 based on calculations with a data set of more than 700 CNS-active drugs.[52] Therefore, with a calculated TPSA (topological PSA) value[53] of 86 Å^2 for [^{18}F]**6b**, a passage across the BBB seems to be not favored (TPSA values are comparable to PSA values[54]). Because the PSA is defined as the surface area occupied by nitrogen and oxygen atoms and the polar hydrogens attached to them,[55] it also reflects the hydrogen bonding capacity and polarity of a compound. Thus, in particular, the two OH groups, acting as H-bond donors, contribute to the high TPSA value. Additionally, the free rotation and steric availability of these aliphatic OH groups may hamper the diffusion across a lipophilic membrane. We are aware that the requirements for BBB penetration are more complex and not only simply related to physicochemical properties. However, these considerations may serve as a first explanation for the observed poor brain uptake of [^{18}F]**6b**.

3. SUMMARY AND CONCLUSION

With the 10,11-dihydro-5*H*-benzo[*e*]pyrrolo[1,2-*a*][1,4]-diazepine derivative **6b**, a novel ligand with high affinity for the oxytocin receptor was synthesized and radiolabeled with fluorine-18 and the binding affinity in vitro and pharmacokinetics in vivo were evaluated.

Because of the very low brain uptake of [^{18}F]**6b** in mouse and pig, this radiotracer is not suitable for examining the oxytocin receptor in the living brain. The molecular size of [^{18}F]**6b** and the relatively high polar surface area with two easily accessible OH groups might account for the low brain penetration. This is also reflected by the in vitro permeability (P_m) determined by IAM chromatography, which is not in the ideal range of brain penetrating compounds.[43] The lipophilicity, characterized by the log *D* value, was not a good predictor for BBB penetration of [^{18}F]**6b**. Moreover, on the basis of blockade PET studies in mice, we could show that [^{18}F]**6b** does not significantly interact with the efflux transporter P-gp, a further parameter that can strongly influence the brain uptake of a compound.

Furthermore, in vitro autoradiographic blocking studies on porcine brain indicated interaction of the radioligand at binding sites of several off-target receptors, which hampers the applicability of [^{18}F]**6b** as specific OTR-PET tracer. This low selectivity is assumed to be caused by the 1,4-benzodiazepine moiety in [^{18}F]**6b**, which is part of numerous drugs and ligands for several GPCRs. However, as we have shown with the series B compounds, this 1,4-benzodiazepine moiety is essential for high affinity to the OTR binding site.

Finally, we conclude that the selected OTR antagonist **6** is not suitable as lead structure for the development of PET tracers for the oxytocin receptor because of the observed poor brain penetration and limited target selectivity of its analogue [^{18}F]**6b**.

4. EXPERIMENTAL SECTION

4.1. Organic Chemistry. *General.* All reactions were carried out under argon atmosphere, in dry glassware, with dried solvents and anhydrous conditions, unless otherwise stated. Reagents were purchased with a minimum commercial quality of 95% and used without further purification. Analytical thin layer chromatography (TLC) was performed on 0.25 mm silica gel plates Alugram SIL G/UV$_{254}$ (Machery-Nagel, Germany). The spots were visualized by using UV light or staining with ninhydrin, phosphomolybdic acid, or vanillin followed by heating. Column chromatography for purification of the crude products was carried out on silica gel (60, particle size 0.040−0.063 mm, Machery-Nagel). NMR spectra were recorded on Bruker AV 500 Ultra instruments and calibrated using residual nondeuterated solvents as an internal reference. Following abbreviations were used to describe the multiplicities: s = singlet, d = doublet, t = triplet, q = quartet, m = multiplet, dt = doublet of triplet, td = triplet of doublet, dd = doublet of doublet.

Analysis of all final compounds was performed by TLC, MS, and ^{1}H- and ^{13}C NMR spectroscopy. The purity of the final compounds was ≥95% and was confirmed by LC/MS analysis employing a Thermo SCIENTIFIC Ultimate 3000 system consisting of a quaternary pump, a diode array detector, and an autosampler. Electrospray ionization mass spectra were obtained using a MSQ mass detector (Thermo SCIENTIFIC). An Ascentic Express Peptide ES-C18 column 150 mm × 2.1 mm (SUPELCO) was used in gradient mode (eluent: acetonitrile/H$_2$O + 0.1% HCOOH (v); 5% to 100% ACN over 12 min with a flow rate of 0.4 mL/min), and the chromatograms were monitored at 220 nm.

Chemical names of compounds were generated by ChemDraw Ultra 10.0.

TPSA values were calculated using the free Molecular Property Calculation service of Molinspiration (molinspiration.com).

*Synthesis of the Precursor **7**. Benzyl 2-(2-Bromophenyl)ethyl Ether (**1g**).* A solution of 7.44 g (37 mmol) of 2-bromophenylethyl alcohol in 60 mL of THF was added under argon atmosphere to an ice-cooled suspension of 2.25 g (56 mmol, 60% in mineral oil) NaH in 60 mL of THF. After stirring for 30 min at rt, the suspension was heated to 50 °C for 30 min and cooled to 0 °C for the addition of 5.4 mL (7.77 g, 45 mmol) benzyl bromide. The reaction mixture was stirred at rt overnight. Then 50 mL of H$_2$O were slowly added and the organic solvent was removed under reduced pressure. The aqueous layer was extracted with diethyl ether, and the organic layer was dried over Na$_2$SO$_4$. Column chromatography (petroleum ether (PE): diethyl ether = 15:1) of the crude product afforded 10 g (93%) of **1g** as a colorless oil. ^{1}H NMR (500 MHz, CDCl$_3$) δ [ppm]: 3.09 (t, J = 7.0 Hz, 2H), 3.73 (t, 7.0 Hz, 2H), 4.55 (s, 2H), 7.08 (td, J = 7.5 Hz, J = 1.5 Hz, 1H), 7.24 (td, J = 7.5 Hz, J = 1.5 Hz, 1H), 7.27−7.36 (m, 6H), 7.54 (dd, J = 8.0 Hz, J = 1.0 Hz, 1H).

*Benzyl 2-(2-Boronophenyl)ethyl Ether (**2g**).* To a solution of 8.9 g (31 mmol) of **1g** in 150 mL of dry THF, *n*-BuLi (14.8 mL, 2.5 M in *n*-hexane) was added at −78 °C and the mixture was stirred for 1 h at this temperature. After addition of 4.1 mL (3.8 g, 37 mmol) of trimethyl borate, the cooling bath was removed and the reaction mixture was stirred at rt overnight, quenched with 100 mL of 1.0 M aqueous HCl, and stirred for 1 h. The organic layer was separated, and the aqueous layer was extracted with CH$_2$Cl$_2$ (2 × 100 mL). The combined organic layers were washed with brine and dried over Na$_2$SO$_4$ and the solvent was removed in vacuum. The obtained 7.9 g (99%) of the crude product **2g** was used in the next step without any further purification.

*2′-(2-Benzyloxyethyl)-2-methylbiphenyl-4-carboxylic Acid Methyl Ester (**3g**).* A stirred solution of 7.9 g (31 mmol) of **2g**, 7.0 g (31 mmol) of methyl 4-bromo-3-methylbenzoate, and 14.2 g (134 mmol) of Na$_2$CO$_3$ in 360 mL of H$_2$O/ethyl alcohol/toluene (1:1:2) was degassed for 30 min with argon. The catalyst Pd(PPh$_3$)$_4$ (1.78 g, 1.5

DOI: 10.1021/acs.jmedchem.5b01080
J. Med. Chem. 2016, 59, 1800−1817

mmol) was added, and the obtained yellow solution was refluxed at 90 °C for 14 h. After cooling to rt, 150 mL of ethyl acetate (EtOAc) was added and the aqueous layer was separated. The organic layer was washed with brine and dried over Na_2SO_4. After removal of the solvents, the crude product was purified by column chromatography (*n*-hexane:EtOAc = 10:1) to yield 9.5 g (85%) of **3g** as colorless oil. ^{1}H NMR (500 MHz, $CDCl_3$) δ [ppm]: 2.06 (s, 3H), 2.60 (dt, J = 14.0 Hz, J = 7.0 Hz, 1H), 2.75 (dt, J = 14.0 Hz, J = 7.0 Hz, 1H), 3.45 (t, J = 7.5 Hz, 2H), 3.95 (s, 3H), 4.37 (s, 2H), 7.06 (dd, J = 7.5 Hz, J = 1.5 Hz, 1H), 7.14 (d, J = 7.5 Hz, 1H), 7.16−7.18 (m, 2H), 7.24−7.36 (m, 6H), 7.85 (dd, J = 8.0 Hz, J = 1.5 Hz, 1H), 7.93 (s, 1H).

*10,11-Dihydro-5H-pyrrolo[2,1-c][1,4]benzodiazepine (**8**).* Compound **8** was synthesized according to the literature[28−30] by *N*-alkylation of pyrrole-2-carboxaldehyde with 2-nitrobenzyl bromide followed by reductive ring closure of 1-(2-nitrobenzyl)-2-pyrrolecarboxaldehyde. ^{1}H NMR (500 MHz, $CDCl_3$) δ [ppm]: 4.18 (br s, 1H), 4.46 (d, J = 4.0 Hz, 2H), 5.19 (s, 2H), 6.02−6.05 (m, 2H), 6.49 (dd, J = 8.0 Hz, J = 1.0 Hz, 1H), 6.63 (td, J = 7.5 Hz, 1.0 Hz, 1H), 6.68−6.69 (m, 1H), 6.98−7.05 (m, 2H).

*(5H,11H-Benzo[e]pyrrolo[1,2-a][1,4]diazepin-10-yl)-[2′-(2-benzyloxyethyl)-2-methylbiphenyl-4-yl]methanone (**4g**).* To a stirred solution of 9.5 g (26 mmol) of **3g** in 190 mL of THF, a solution of 96 mL of 1.0 M aqueous NaOH was added and the mixture was stirred under reflux overnight. The complete consumption of the starting material was confirmed by TLC (PE:*n*-hexane = 9:1). After removal of THF, 1.0 M aqueous HCl was added to adjust a pH value of 3 and the product was extracted with EtOAc. The combined organic layers were dried over Na_2SO_4. Removal of the solvent afforded 8.5 g (94%) of the corresponding carboxylic acid as white solid, which was used directly in the next step; mp 61−64 °C. ^{1}H NMR (500 MHz, DMSO-d_6) δ [ppm]: 2.00 (s, 3H), 2.50 (dt, J = 14.0 Hz, J = 7.0 Hz, 1H), 2.67 (dt, J = 14.0 Hz, J = 7.0 Hz, 1H), 3.40 (t, J = 7.0 Hz, 2H), 4.31 (s, 2H), 7.06 (dd, J = 7.5 Hz, J = 1.5 Hz, 1H), 7.12−7.18 (m, 3H), 7.22−7.30 (m, 4H), 7.33 (td, J = 7.5 Hz, J = 1.5 Hz, 1H), 7.40 (m, 1H), 7.78 (dd, J = 8.0 Hz, J = 1.5 Hz, 1H), 7.87 (d, J = 1.5 Hz, 1H), 12.93 (br s, 1H).

A solution of 4.5 g (13 mmol) of 2′-(2-benzyloxy-ethyl)-2-methylbiphenyl-4-carboxylic acid in 25 mL of thionyl chloride was refluxed under argon atmosphere for 2 h. The excess of thionyl chloride was removed under vacuum, and the residue was diluted three times with 10 mL of toluene followed by removal of the solvent. The resultant acid chloride was dissolved in 25 mL of CH_2Cl_2 and added dropwise to an ice-cold solution of 2.8 g (15 mmol) of **8** and 5.1 mL (30 mmol) of Hünig's base in 100 mL of CH_2Cl_2. The cooling bath was removed, and the mixture was stirred at rt overnight. After hydrolysis with 50 mL of H_2O, the aqueous layer was extracted three times with CH_2Cl_2. The combined organic layers were dried over Na_2SO_4, filtered, and concentrated in vacuum. The crude product was purified by column chromatography (PE:EtOAc = 4:1 to 1:1) to obtain 5.6 g (84%) of **4g** as colorless oil. ^{1}H NMR (500 MHz, DMSO-d_6) δ [ppm]: 1.83 (s, 3H), 2.38 (dt, J = 14.0 Hz, J = 7.0 Hz, 1H), 2.57 (dt, J = 14.0 Hz, J = 7.0 Hz, 1H), 3.30 (t, J = 7.0 Hz, 2H), 4.27 (s, 2H), 5.21 (br s, 2H), 5.31 (br s, 2H), 5.93 (dd, J = 3.0 Hz, J = 3.0 Hz, 1H), 5.97 (br s, 1H), 6.83−6.86 (m, 2H), 6.90−6.97 (m, 2H), 7.00−7.07 (m, 2H), 7.10−7.17 (m, 3H), 7.21−7.36 (m, 7H), 7.45 (d, J = 7.5 Hz, 1H).

*1-[10-[2′-(2-Benzyloxyethyl)-2-methylbiphenyl-4-carbonyl]-10,11-dihydro-5H-benzo[e]pyrrolo[1,2-a][1,4]diazepin-3-yl]-2,2,2-trichloroethanone (**15**; Intermediate of Reaction Step (e) in Scheme 1).* To an ice-cold solution of 5.5 g (11 mmol) of **4g** in 115 mL of CH_2Cl_2, Hünig's base was added (3.6 mL, 2.7 g, 22 mmol) under argon atmosphere. After the addition of 3.8 mL (6.2 g, 34 mmol) of trichloro acetyl chloride over 10 min, the cooling bath was removed and the mixture was stirred at rt overnight. The reaction mixture was diluted with 50 mL of H_2O, and the aqueous layer was extracted twice with CH_2Cl_2. The combined organic layers were washed with 100 mL of 1.0 M aqueous HCl and 50 mL of brine, dried over Na_2SO_4, filtered, and concentrated to remove the solvent. Column chromatography (PE:EtOAc = 2:1) afforded 6.4 g (92%) of the product **15** as a colorless solid; mp 80−85 °C. ^{1}H NMR (500 MHz, DMSO-d_6) δ [ppm]: 1.84 (s, 3H), 2.38 (dt, J = 14.0 Hz, J = 7.0 Hz, 1H), 2.57 (dt, J = 14.0 Hz, J = 7.0 Hz, 1H), 3.30 (t, J = 7.0 Hz, 2H), 4.28 (s, 2H), 5.30 (br s, 2H), 5.98 (br s, 2H), 6.38 (d, J = 4.5 Hz, 1H), 6.86 (d, J = 8.0 Hz, 1H), 6.90 (d, J = 8.0 Hz, 1H), 6.97 (dd, J = 7.5 Hz, J = 1.5 Hz, 1H), 7.01−7.07 (m, 2H), 7.12 (td, J = 7.5 Hz, J = 1.5 Hz, 1H), 7.15−7.17 (m, 2H), 7.21−7.35 (m, 7H), 7.42 (dd, J = 7.5, J = 1.5 Hz, 1H), 7.47 (d, J = 4.0 Hz, 1H).

*10-[2′-(2-Benzyloxyethyl)-2-methylbiphenyl-4-carbonyl]-10,11-dihydro-5H-benzo[e]pyrrolo[1,2-a][1,4]diazepine-3-carboxylic Acid (**5g**).* To a solution of 6.4 g (10 mmol) of **15** in 200 mL of acetone, 30 mL of 2.5 M aqueous NaOH was added and the mixture was stirred at rt overnight. After removal of the solvent, 25 mL of 2.0 M aqueous HCl was added and the mixture was extracted with EtOAc. The organic layer was dried over Na_2SO_4, filtered, and concentrated to remove the solvent. The crude product was purified by column chromatography (PE:EtOAc = 1:1) to provide 4.5 g (83%) of **5g** as a white solid; mp 64−68 °C. ^{1}H NMR (500 MHz, DMSO-d_6) δ [ppm]: 1.83 (s, 3H), 2.39 (dt, J = 14.0 Hz, J = 7.0 Hz, 1H), 2.58 (dt, J = 14.0 Hz, J = 7.0 Hz, 1H), 3.30 (t, J = 7.0 Hz, 2H), 4.28 (s, 2H), 5.20 (br s, 2H), 5.95 (br s, 2H), 6.12 (d, J = 4.0 Hz, 1H), 6.77 (d, J = 4.0 Hz, 1H), 6.83−6.87 (m, 2H), 6.95−7.02 (m, 3H), 7.09 (t, J = 7.0 Hz, 1H), 7.16 (t, J = 7.0 Hz, 2H), 7.21−7.35 (m, 8H), 12.34 (br s, 1H).

*10-[2′-(2-Benzyloxyethyl)-2-methylbiphenyl-4-carbonyl]-10,11-dihydro-5H-benzo[e]pyrrolo[1,2-a][1,4]diazepine-3-carboxylic Acid Bis(2-hydroxyethyl)amide (**6g**).* A mixture of 2.5 g (4.5 mmol) of **5g**, 0.66 g (6.3 mmol) of diethanolamine, 0.88 g (6.5 mmol) of HOBt, 1.12 g (5.9 mmol) of EDCI, and 1.3 mL (0.99 g, 7.7 mmol) of Hünig's base in 45 mL of DMF was stirred at rt overnight. The mixture was concentrated, diluted with 75 mL of H_2O, and extracted three times with 75 mL of EtOAc. The organic layer was washed twice with 50 mL of a saturated aqueous $NaHCO_3$ solution, dried over Na_2SO_4, filtered, and concentrated to remove the solvent. Purification by column chromatography (CH_2Cl_2:methanol = 95:5) afforded 2.46 g (85%) of **6g** as a white solid. ^{1}H NMR (500 MHz, $CDCl_3$) δ [ppm]: 1.89 (s, 3H), 2.50 (td, J = 7.5 Hz, J = 13.5 Hz, 1H), 2.64 (dt, J = 7.0 Hz, J = 14.0 Hz, 1H), 3.36 (t, J = 7.5 Hz, 2H) 3.44 (br s, 2H), 3.77 (t, J = 5.0 Hz, 4H), 3.88 (br s, 4H), 4.33 (dd, J = 12.0 Hz, J = 14.5 Hz, 2H), 5.30 (br s, 2H), 5.47 (br s, 2H), 6.01 (d, J = 4.0 Hz, 1H), 6.51 (d, J = 4.0, 1H), 6.79−6.85 (m, 2H), 6.96 (d, J = 8.0 Hz, 1H), 7.01 (t, J = 7.0 Hz, 1H), 7.10 (t, J = 7.0 Hz, 1H), 7.17−7.22 (m, 3H), 7.24−7.27 (m, 3H), 7.28−7.31 (m, 3H), 7.45 (dd, J = 1.5 Hz, J = 7.5 Hz, 1H).

*10-[2′-(2-Benzyloxyethyl)-2-methylbiphenyl-4-carbonyl]-10,11-dihydro-5H-benzo[e]pyrrolo[1,2-a][1,4]diazepine-3-carboxylic Acid Bis(2-methoxymethoxyethyl)amide (**16**; Intermediate of Reaction Step (i) in Scheme 1).* A solution of 1.39 g (2.2 mmol) of **6g** in 30 mL of CH_2Cl_2 was cooled on ice, and 1.6 mL (9.5 mmol) of Hünig's base, 65 mg (0.22 mmol) of tetrabutylammonium chloride, and 0.77 mL (9.5 mmol) of bromomethyl methyl ether were added. The resultant solution was allowed to warm to rt and stirred overnight. The mixture was diluted with H_2O, and the separated aqueous layer was extracted with CH_2Cl_2. The combined organic layers were dried over Na_2SO_4, filtered, and concentrated in vacuum. Flash chromatography (PE:EtOAc = 1:1) of the crude product afforded 1.4 g (87%) of **16** as an orange oil. ^{1}H NMR (500 MHz, $CDCl_3$) δ [ppm]: 1.83 (s, 3H), 2.38 (td, J = 7.5 Hz, J = 13.5 Hz, 1H), 2.57 (dt, J = 7.0 Hz, J = 14.0 Hz, 1H), 3.20−3.26 (m, 6H), 3.30 (t, J = 7.0 Hz, 2H), 3.58−3.73 (m, 8H), 4.27 (s, 2H), 4.57 (br s, 3H), 4.63 (br s, 1H), 5.20 (br s, 2H), 5.35 (br s, 2H), 6.05 (d, J = 3.5 Hz, 1H), 6.29 (d, J = 3.5 Hz, 1H), 6.83−6.88 (m, 2H), 6.96 (d, J = 7.0 Hz, 1H), 6.98−7.02 (m, 2H), 7.09 (t, J = 7.0 Hz, 1H), 7.16 (d, J = 7.0 Hz, 2H), 7.21−7.35 (m, 8H).

*10-[2′-(2-Hydroxyethyl)-2-methylbiphenyl-4-carbonyl]-10,11-dihydro-5H-benzo[e]pyrrolo[1,2-a][1,4]diazepine-3-carboxylic Acid Bis(2-methoxymethoxyethyl)amide (**17**; Intermediate of Reaction Step (j) in Scheme 1).* To a degassed solution of 860 mg (1.18 mmol) of compound **16** in 60 mL of methanol, $Pd(OH)_2/C$ (200 mg, 20 wt %, wet, 0.28 mmol) was added. The mixture was vigorously stirred at rt under a hydrogen atmosphere (balloon pressure) for 20 h. TLC analysis (100% EtOAc) indicated the complete consumption of the starting material. The reaction mixture was filtered through Celite and washed with methanol. The filtrate was concentrated and dried in vacuum to give 750 mg (99%) of the titled compound as yellowish viscous oil. The intermediate **17** was used in the next step without any further purification. ^{1}H NMR (500 MHz, DMSO-d_6) δ [ppm]: 1.86 (s,

DOI: 10.1021/acs.jmedchem.5b01080
J. Med. Chem. 2016, 59, 1800−1817

3H), 2.24−2.31 (m, 1H), 2.41−2.47 (m, 1H), 3.24−3.30 (m, 8H), 3.62−3.74 (m, 8H), 4.47 (t, J = 5.0 Hz, 1H), 4.55−4.78 (m, 4H), 5.15 (br s, 2H), 5.35 (br s, 2H), 6.05 (d, J = 3.5 Hz, 1H), 6.29 (d, J = 3.5 Hz, 1H), 6.88 (d, J = 8.0 Hz, 2H), 6.94 (d, J = 7.5 Hz, 1H), 7.02 (d, J = 7.5 Hz, 1H), 7.09 (t, J = 7.5 Hz, 1H), 7.16 (t, J = 7.5 Hz, 1H), 7.21 (td, J = 7.5 Hz, J = 1.5 Hz, 1H), 7.25 (s, 1H), 7.27 (td, J = 7.5 Hz, 1.5 Hz, 1H), 7.31 (dd, J = 7.5 Hz, 1.5 Hz, 1H), 7.36 (d, J = 7.5 Hz, 1H).

*Toluene-4-sulfonic Acid 2-(4′-[3-[Bis(2-methoxymethoxy-ethyl)-carbamoyl]-5H,11H-benzo[e]pyrrolo[1,2-a][1,4]diazepine-10-carbonyl]-2′-methylbiphenyl-2-yl)ethyl Ester (**7**).* A solution of 178 mg (0.93 mmol) of *p*-toluenesulfonyl chloride in 1 mL of CH_2Cl_2 was added under argon atmosphere to an ice-cooled solution of 104 mg (0.16 mmol) of compound **17**, 0.13 mL (0.93 mmol) of triethylamine, and 2 mg (0.02 mmol) of Steglich base (4-DMAP) in 3 mL of CH_2Cl_2. The mixture was stirred at rt overnight. The progress of the reaction was monitored by TLC (*n*-hexane:EtOAc = 1:1). After complete consumption of **17**, the reaction mixture was diluted with H_2O and extracted with CH_2Cl_2. The organic layer was dried over Na_2SO_4, filtered, and concentrated in vacuum. The resulting residue was purified by column chromatography (*n*-hexane:EtOAc = 2:3) to give 101 mg (78%) of **7** as a white solid; mp 75−80 °C. ^{1}H NMR (500 MHz, $CDCl_3$) δ [ppm]: 1.76 (s, 3H), 2.38 (td, J = 7.5 Hz, J = 13.5 Hz, 1H), 2.41 (s, 3H), 2.59 (dt, J = 7.0 Hz, J = 14.0 Hz, 1H), 3.25 (br s, 6H), 3.58−3.73 (m, 8H), 3.78−3.90 (m, 2H), 4.57 (br s, 3H), 4.64 (br s, 1H), 5.20 (br s, 2H), 5.36 (br s, 2H), 6.05 (d, J = 3.5 Hz, 1H), 6.30 (d, J = 3.5 Hz, 1H), 6.67 (d, J = 7.5 Hz, 1H), 6.82 (d, J = 6.0 Hz, 1H), 6.94−6.96 (m, 2H), 7.02 (t, J = 7.0 Hz, 1H), 7.12 (t, J = 7.5 Hz, 1H), 7.22 (s, 1H), 7.23−7.29 (m, 3H), 7.35 (d, J = 7.0 Hz, 1H), 7.41 (d, J = 8.0 Hz, 2H), 7.55 (d, J = 8.0 Hz, 2H). ^{13}C NMR (125 MHz, DMSO-d_6) δ [ppm]: 19.18, 20.95, 31.53, 45.97, 47.03, 54.59, 55.06, 64.65, 65.22, 69.70, 91.44, 92.66, 95.64, 107.61, 110.51, 125.07, 126.67, 126.80, 126.98, 127.28, 127.57, 128.39, 128.41, 128.63, 128.91, 129.12, 129.21, 129.61, 129.97, 132.03, 133.52, 134.67, 134.69, 134.82, 140.13, 141.30, 141.40, 144.73, 163.73, 169.17. LC/MS retention time: 10.80 min. MS (ESI) m/z = 796.2 $[M + H]^+$.

*Synthesis of **6a**. 5′-Fluoro-2-methyl-2′-trifluoromethylbiphenyl-4-carboxylic Acid Methyl Ester (**3a**).* The compound was synthesized using 1.0 g (4.8 mmol) of 5-fluoro-2-(trifluoromethyl)phenylboronic acid according to the procedure for the synthesis of **3g**. The obtained crude product was purified by column chromatography (*n*-hexane:EtOAc = 9:1) to yield 1.4 g (91%) of **3a** as a colorless oil. ^{1}H NMR (500 MHz, $CDCl_3$) δ [ppm]: 2.05 (s, 3H), 3.86 (s, 3H), 7.04 (d, J = 6.5 Hz, 1H), 7.10 (t, J = 6.5 Hz, 1H), 7.30 (s, 1H), 7.42−7.48 (m, 2H), 7.89 (dd, J = 7.5 Hz, J = 5.5 Hz, 1H).

*(5H,11H-Benzo[e]pyrrolo[1,2-a][1,4]diazepin-10-yl)-(5′-fluoro-2-methyl-2′-trifluoromethylbiphenyl-4-yl)methanone (**4a**).* According to the procedure described for the synthesis of **4g**, compound **3a** was hydrolyzed and 0.96 g (3.2 mmol) of the resulting carboxylic acid was used to react with 0.89 g (4.8 mmol) of **8**. The obtained crude product was purified by column chromatography (*n*-hexane:EtOAc = 4:1) to yield 1.4 g (94%) of **4a** as a colorless oil. ^{1}H NMR (500 MHz, DMSO-d_6) δ [ppm]: 1.89 (s, 3H), 5.10 (br s, 2H), 5.30 (br s, 2H), 5.93 (dd, J = 3.0 Hz, J = 3.0 Hz, 1H), 5.97 (br s, 1H), 6.83 (t, J = 2.5 Hz, 1H), 6.91−6.95 (m, 2H), 7.04 (d, J = 6.5 Hz, 1H), 7.10 (t, J = 6.5 Hz, 1H), 7.16−7.21 (m, 2H), 7.30 (s, 1H), 7.42−7.48 (m, 2H), 7.89 (dd, J = 7.5 Hz, J = 5.5 Hz, 1H).

*2,2,2-Trichloro-1-[10-(5′-fluoro-2-methyl-2′-trifluoromethylbiphenyl-4-carbonyl)-10,11-dihydro-5-benzo[e]pyrrolo[1,2-a][1,4]-diazepin-3-yl]ethanone (**18**; Intermediate of Reaction Step (e) in Scheme 1).* The compound was synthesized using 0.30 g (0.60 mmol) of **4a** according to the procedure for the synthesis of **15**. The obtained crude product was purified by column chromatography (*n*-hexane:EtOAc = 4:1) to yield 0.35 g (95%) of the titled product as a colorless oil. ^{1}H NMR (500 MHz, DMSO-d_6) δ [ppm]: 1.89 (s, 3H), 5.10 (br s, 2H), 5.30 (br s, 2H), 5.93 (dd, J = 3.0 Hz, J = 3.0 Hz, 1H), 5.97 (br s, 1H), 6.39 (d, J = 4.0 Hz, 1H), 6.79 (d, J = 7.0 Hz, 1H), 7.04 (d, J = 6.5 Hz, 1H), 7.10 (t, J = 6.5 Hz, 1H), 7.16−7.21 (m, 2H), 7.30 (s, 1H), 7.42−7.48 (m, 2H), 7.89 (dd, J = 7.5 Hz, J = 5.5 Hz, 1H).

*10-(5′-Fluoro-2-methyl-2′-trifluoromethylbiphenyl-4-carbonyl)-10,11-dihydro-5H-benzo[e]pyrrolo[1,2-a][1,4]diazepine-3-carboxylic Acid (**5a**).* According to the procedure for the synthesis of **5g** and using 0.35 g (0.57 mmol) of **18**, product **5a** was isolated as a white solid in 99% yield (0.29 g) and used in the next step without further purification. ^{1}H NMR (500 MHz, $CDCl_3$) δ [ppm]: 1.93 (s, 3H), 5.32 (br s, 2H), 5.98 (br s, 2H), 6.11 (d, J = 4.0 Hz, 1H), 6.79 (d, J = 7.0 Hz, 1H), 6.86 (dd, J = 8.5 Hz, J = 2.5 Hz, 1H), 6.91 (d, J = 8.0 Hz, 1H), 6.97−7.00 (m, 1H), 7.07 (t, J = 7.5 Hz, 1H), 7.09 (d, J = 4.0 Hz, 1H), 7.12−7.19 (m, 2H), 7.26 (s, 1H), 7.46 (d, J = 7.5 Hz, 1H), 7.72 (dd, J = 9.0 Hz, J = 5.5 Hz, 1H).

*10-(5′-Fluoro-2-methyl-2′-trifluoromethylbiphenyl-4-carbonyl)-10,11-dihydro-5H-benzo[e]pyrrolo[1,2-a][1,4]diazepine-3-carboxylic Acid Bis(2-hydroxyethyl) Amide (**6a**).* A mixture of 290 mg (0.57 mmol) of **5a**, 75 mg (0.72 mmol) of diethanol amine, 86 mg (0.63 mmol) of HOBt, 127 mg (0.66 mmol) of EDCI, and 0.15 mL (113 mg, 0.87 mmol) of Hünig's base in 4 mL of DMF was stirred at rt overnight. The mixture was concentrated, and the residue was diluted with 7 mL of H_2O and extracted three times with 7 mL of EtOAc. The organic layer was washed twice with 5 mL of a saturated aqueous $NaHCO_3$ solution, dried over Na_2SO_4, filtered, and concentrated to remove the solvent. Column chromatography (CH_2Cl_2:methanol = 95:5) followed by crystallization from EtOAc to remove traces of impurities afforded 190 mg (56%) of **5a** as a white solid; mp 100−107 °C. ^{1}H NMR (500 MHz, DMSO-d_6) δ [ppm]: 1.88 (s, 3H), 3.48−3.65 (m, 8H), 4.82 (t, J = 5.0 Hz, 2H), 5.25 (br s, 2H), 5.34 (br s, 2H), 6.03 (d, J = 3.0 Hz, 1H), 6.30 (d, J = 3.5 Hz, 1H), 6.87 (d, J = 6.0 Hz, 1H), 6.93 (d, J = 7.5 Hz, 1H), 7.01−7.07 (m, 2H), 7.13−7.18 (m, 2H), 7.28 (s, 1H), 7.38 (d, J = 7.0 Hz, 1H), 7.44 (td, J = 8.0 Hz, J = 2.5 Hz, 1H), 7.88 (dd, J = 9.0 Hz, J = 5.5 Hz, 1H). ^{13}C NMR (125 MHz, DMSO-d_6) δ [ppm] 19.29, 45.89, 47.03, 58. 45, 58. 56, 107.50, 110.23, 115.10 (d, J = 21.6 Hz), 118.30 (d, J = 22.1 Hz), 122.27, 123.50 (q, J = 29.9 Hz), 124.44, 124.51, 127.01, 127.36, 128.21, 128.44, 128.71, 128.75, 128.98 (m), 129.07, 129.29, 134.70, 135.07, 135.64, 138.42, 141.32, 142.03 (d, J = 7.6 Hz), 162.32, 163.76, 164.33, 169.04. LC/MS retention time: 8.94 min. MS (ESI) m/z = 596.4 $[M + H]^+$.

*Synthesis of **6b**. 2-(2-Fluoroethyl)phenyl Bromide (**1b**).* A mixture of 5 g (25 mmol) of 2-(2-hydroxyethyl)phenyl bromide and 3.5 mL (27 mmol) of DAST in 75 mL of dry CH_2Cl_2 was stirred at rt for 20 h. The reaction mixture was diluted with 150 mL of saturated aqueous $NaHCO_3$ solution and stirred for additional 30 min. The CH_2Cl_2 layer was separated, and the aqueous layer was extracted with CH_2Cl_2. The combined organic layers were dried over Na_2SO_4, filtered, and concentrated to remove the CH_2Cl_2. Purification by column chromatography (PE:EtOAc = 9:1) provided 3.2 g (63%) of **1b** as a colorless liquid. ^{1}H NMR (500 MHz, $CDCl_3$) δ [ppm]: 3.19 (dt, J = 22.5 Hz, J = 7.0 Hz, 2H), 4.66 (dt, J = 47.5 Hz, J = 6.5 Hz, 2H), 7.12 (td, J = 7.5 Hz, 2.0 Hz, 1H), 7.25−7.31 (m, 2H), 7.56 (dd, J = 7.5 Hz, J = 1.0 Hz, 1H).

*2-(2-Fluoroethyl)phenylboronic Acid (**2b**).* According to the procedure of **2g** described above, 3.0 g (15 mmol) of **1b**, 80 mL of dry THF, 7.2 mL of *n*-BuLi (2.5 M in *n*-hexane, 18 mmol), and 2.0 mL (18 mmol) of trimethyl borate reacted to give 2.0 g (79%) of the boronic acid **2b** as a clear, colorless oil. The crude product was used in the next step without any further purification.

*2′-(2-Fluoroethyl)-2-methylbiphenyl-4-carboxylic Acid Methyl Ester (**3b**).* The compound was synthesized using 136 mg (0.8 mmol) of **2b** according to the procedure for the synthesis of **3g**. The obtained crude product was purified by column chromatography (EtOAc:*n*-hexane = 1:19) to give 170 mg (78%) of compound **3b** as a colorless oil. ^{1}H NMR (500 MHz, $CDCl_3$) δ [ppm] 2.05 (s, 3H), 2.55−2.65 (m, 1H), 2.73−2.83 (m, 1H), 3.87 (s, 3H), 4.38 (t, J = 6.5 Hz, 1H), 4.47 (t, J = 6.5 Hz, 1H), 7.10 (d, J = 7.5 Hz, 1H), 7.25 (d, J = 8.0 Hz, 1H), 7.33 (td, J = 7.5 Hz, J = 1.5 Hz, 1H), 7.38 (td, J = 7.5 Hz, J = 1.5 Hz, 1H), 7.44 (d, J = 7.5 Hz, 1H), 7.83 (dd, J = 7.5 Hz, J = 1.5 Hz, 1H), 7.92 (s, 1H).

*(5H,11H-Benzo[e]pyrrolo[1,2-a][1,4]diazepin-10-yl)-[2′-(2-fluoroethyl)-2-methylbiphenyl-4-yl]methanone (**4b**).* According to the procedure described for the synthesis of **4g**, compound **3b** was hydrolyzed and 1.03 g (4.0 mmol) of the resulting carboxylic acid was used to react with **8**. The obtained crude product was purified by crystallization from EtOAc to give 1.60 g (99%) of **4b** as a colorless crystalline solid. ^{1}H NMR (500 MHz, $CDCl_3$) δ [ppm]: 1.86 (s, 3H),

DOI: 10.1021/acs.jmedchem.5b01080
J. Med. Chem. 2016, 59, 1800−1817

2.41−2.51 (m, 1H), 2.62−2.72 (m, 1H), 4.23 (t, J = 6.5 Hz, 1H), 4.32 (t, J = 6.5 Hz, 1H), 5.10 (br s, 2H), 5.31 (br s, 2H), 5.93 (dd, J = 3.5 Hz, J = 2.0 Hz, 1H), 5.97 (br s, 1H), 6.84 (t, J = 2.5 Hz, 1H), 6.89−6.95 (m, 2H), 7.01 (d, J = 6.5 Hz, 1H), 7.04 (d, J = 7.5 Hz, 1H), 7.09 (t, J = 7.5 Hz, 1H), 7.18 (t, J = 7.5 Hz, 1H), 7.25−7.34 (m, 3H), 7.37 (d, J = 7.5 Hz, 1H), 7.47 (d, J = 7.5 Hz, 1H).

*2,2,2-Trichloro-1-[10-[2′-(2-fluoroethyl)-2-methylbiphenyl-4-carbonyl]-10,11-dihydro-5H-benzo[e]pyrrolo[1,2-a][1,4]diazepin-3-yl]-ethanone (**19**; Intermediate of Reaction Step (e) in Scheme 1).* The compound was synthesized from 1.6 g (3.9 mmol) of **4b** according to the procedure for the synthesis of **15**. The obtained crude product was purified by column chromatography (EtOAc:*n*-hexane = 1:4) to give 2.1 g (95%) of the titled compound as a white solid. ^{1}H NMR (500 MHz, $CDCl_3$) δ [ppm]: 1.87 (s, 3H), 2.42−2.51 (m, 1H), 2.63−2.73 (m, 1H), 4.23 (t, J = 7.0 Hz, 1H), 4.33 (t, J = 7.0 Hz, 1H), 5.31 (br s, 2H), 5.99 (br s, 2H), 6.39 (d, J = 4.0 Hz, 1H), 6.89−6.93 (m, 2H), 7.02 (dd, J = 7.5 Hz, J = 1.5 Hz, 1H), 7.04−7.12 (m, 2H), 7.18 (td; J = 7.5 Hz, J = 1.5 Hz, 1H), 7.28 (td, J = 7.5 Hz, J = 1.5 Hz, 1H), 7.30−7.35 (m, 2H), 7.37 (d, 7.5 Hz, 1H), 7.44 (dd, 7.5 Hz, J = 1.5 Hz, 1H), 7.47 (d, J = 4.5 Hz, 1H).

*10-[2′-(2-Fluoroethyl)-2-methylbiphenyl-4-carbonyl]-10,11-dihydro-5H-benzo[e]pyrrolo[1,2-a][1,4]diazepine-3-carboxylic Acid (**5b**).* The compound was synthesized using 2.1 g (3.7 mmol) of **19** according to the procedure for the synthesis of **5g**. The obtained crude product was purified by column chromatography (EtOAc:*n*-hexane = 1:4) to give 1.6 g (92%) of **5b** as a white solid; mp 184−190 °C. ^{1}H NMR (500 MHz, $CDCl_3$) δ [ppm]: 1.86 (s, 3H), 2.42−2.51 (m, 1H), 2.62−2.73 (m, 1H), 4.23 (t, J = 7.0 Hz, 1H), 4.33 (t, J = 7.0 Hz, 1H), 5.19 (br s, 2H), 5.94 (br s, 2H), 6.12 (d, J = 4.0 Hz, 1H), 6.77 (d, J = 4.0 Hz, 1H), 6.86 (d, J = 7.5 Hz, 1H), 6.90 (d, J = 8.0 Hz, 1H), 7.00−7.06 (m, 3H), 7.14 (t, J = 7.0 Hz, 1H), 7.25−7.38 (m, 5H), 12.34 (br s, 1H).

*10-[2′-(2-Fluoroethyl)-2-methylbiphenyl-4-carbonyl]-10,11-dihydro-5H-benzo[e]pyrrolo[1,2-a][1,4]diazepine-3-carboxylic Acid Bis-(2-hydroxyethyl)amide (**6b**).* To an ice-cooled solution of 100 mg (0.21 mmol) of **5b** and 0.05 mL (0.42 mmol) of *N*-methylmorpholine in 2 mL of DMF, 91.4 mg of COMU (0.21 mmol) was added. After stirring for 10 min, a solution of 0.02 mL (0.21 mmol) of diethanolamine in 1 mL of DMF was added dropwise. The resultant bright-yellow solution was stirred for additional 30 min before the cooling bath was removed. The mixture was allowed to warm to rt overnight. The complete consumption of the starting material was confirmed by TLC (CH_2Cl_2:methanol = 95:5), and the reaction mixture was diluted with 5 mL of EtOAc. The organic layer was subsequently washed with aqueous $KHSO_4$ (5 wt %), aqueous $NaHCO_3$ (5 wt %), and brine and dried over Na_2SO_4. After filtration and removal of the solvent under reduced pressure the crude product was purified by column chromatography (CH_2Cl_2:methanol = 97:3) to give 73 mg (61%) of **6b** as a white solid; mp 90−94 °C. ^{1}H NMR (500 MHz, DMSO-d_6) δ [ppm]: 1.86 (s, 3H), 2.43−2.52 (m, 1H), 2.62−2.72 (m, 1H), 3.56 (br s, 8H), 4.23 (t, J = 6.5 Hz, 1H), 4.32 (t, J = 6.5 Hz, 1H), 4.83 (t, J = 5.0 Hz, 2H), 5.20 (br s, 2H), 5.34 (br s, 2H), 6.03 (d, J = 3.5 Hz, 1H), 6.30 (d, J = 3.5 Hz, 1H), 6.85−6.91 (m, 2H), 7.00−7.07 (m, 3H), 7.14 (t, J = 7.5 Hz, 1H), 7.25−7.29 (m, 2H), 7.32 (td, J = 1.5 Hz, J = 8.0 Hz, 1H), 7.37 (d, J = 7.5 Hz, 2H). ^{13}C NMR (125 MHz, DMSO-d_6) δ [ppm]: 19.32, 33.10 (d, J = 20 Hz), 45.83, 47.03, 58.55, 82.76 (d, J = 166 Hz), 107.50, 110.22, 125.11, 126.48, 126.97, 127.35, 127.55, 128.38, 128.51, 128.73, 128.91, 129.11, 129.60, 129.66, 134.05, 134.10, 134.77, 134.92, 140.26, 141.46, 141.62, 163.75, 169.23. LC/MS retention time: 8.61 min. MS (ESI) m/z = 556.2 $[M + H]^+$.

*Synthesis of **6c**. 10-(2-Methyl-2′-trifluoromethylbiphenyl-4-carbonyl)-10,11-dihydro-5H-benzo[e]pyrrolo[1,2-a][1,4]diazepine-3-carboxylic Acid (2-Fluoroethyl)-(2-hydroxyethyl)amide (**6c**).* To a solution of 50 mg (0.09 mmol) of **6** (synthesized according to literature[26]) in 0.4 mL of dry CH_2Cl_2, 0.01 mL (0.1 mmol) of DAST was added. The mixture was stirred at rt overnight. TLC analysis confirmed the complete consumption of the starting material. Purification via column chromatography (CH_2Cl_2:methanol = 95:5) provided 32 mg (64%) of **6c** as a white solid; mp 82−85 °C. ^{1}H NMR (500 MHz, DMSO-d_6) δ [ppm]: 1.85 (s, 3H), 2.83 (t, J = 5.0 Hz, 1H), 2.87−2.91 (m, 3H), 4.26 (t, J = 5.5 Hz, 2H), 4.46 (dt, J = 47.5 Hz, J = 5.0 Hz, 2H), 5.20 (br s, 2H), 5.93 (br s, 2H), 6.16 (d, J = 3.5 Hz, 1H), 6.85 (d, J = 3.5 Hz, 1H), 6.87 (d, J = 8.0 Hz, 1H), 6.91 (d, J = 8.0 Hz, 1H), 7.00−7.08 (m, 2H), 7.15 (td, J = 7.5 Hz, J = 1.0 Hz, 1H), 7.22 (d, J = 7.5 Hz, 1H), 7.27 (s, 1H), 7.37 (dd, J = 7.5 Hz, J = 1.0 Hz, 1H), 7.60 (t, J = 7.5 Hz, 1H), 7.69 (t, J = 7.5 Hz, 1H), 7.80 (d, J = 8.0 Hz, 1H). ^{13}C NMR (125 MHz, DMSO-d_6) δ [ppm]: 19.39, 45.99 (br s), 46.21, 47.39, 48.63 (d, J = 20 Hz), 63.12, 83.35 (d, J = 162 Hz), 109.25, 117.80, 121.46, 121.53, 123.73 (q, J = 272 Hz), 124.56, 125.90 (q, J = 5 Hz), 126.87 (q, J = 29 Hz), 127.15, 128.13, 128.35, 128.47, 128.59, 129.29, 130.37, 131.14, 132.19, 134.08, 134.87, 135.10, 138.86 (q, J = 1.5 Hz), 139.82, 141.15, 160.37, 169.17. LC/MS retention time: 9.39 min. MS (ESI) m/z = 580.1 $[M + H]^+$.

*Synthesis of **6d**−**6f**. 10-(2-Methyl-2′-trifluoromethylbiphenyl-4-carbonyl)-10,11-dihydro-5H-benzo[e]pyrrolo[1,2-a][1,4]diazepine-3-carboxylic Acid (**5c**).*[26] Compound **5c** was synthesized in five steps starting from 5.2 g (27 mmol) of commercially available **2c** and 6 g (26 mmol) of methyl 4-bromo-3-methylbenzoate according to the published procedure for the synthesis of **6**.[26] The obtained crude product was purified by crystallization from EtOAc to give 6.5 g (50%) of **5c** as a white solid; mp 230−234 °C. ^{1}H NMR (500 MHz, DMSO-d_6) δ [ppm]: 1.85 (3H, s), 5.19 (br s, 2H), 5.95 (br s, 2H), 6.12 (d, J = 4.0 Hz, 1H), 6.77 (d, J = 4.0 Hz, 1H), 6.87 (d, J = 7.5 Hz, 1H), 6.91 (d, J = 7.5 Hz, 1H), 7.01−7.07 (m, 2H), 7.15 (t, J = 7.5 Hz, 1H), 7.22 (d, J = 8.0 Hz, 1H), 7.27 (s, 1H), 7.34 (d, J = 7.0 Hz, 1H), 7.60 (t, J = 7.5 Hz, 1H), 7.69 (t, J = 8.0 Hz, 1H), 7.80 (d, J = 7.5 Hz, 1H), 12.33 (br s, 1H).

*10-(2-Methyl-2′-trifluoromethylbiphenyl-4-carbonyl)-10,11-dihydro-5H-benzo[e]pyrrolo[1,2-a][1,4]diazepine-3-carboxylic Acid (2-Fluoroethyl)amide (**6d**).* To a solution of 200 mg (0.41 mmol) of **5c** in 3.5 mL of THF, a mixture of 0.2 mL (0.98 mmol) Hünig's base, 66 mg (0.66 mmol) of 2-fluoroethylamine hydrochloride, and 170 mg (0.53 mmol) of TBTU was added. The mixture was stirred at rt overnight and diluted with 5 mL of a 0.5 M aqueous $NaHCO_3$ solution followed by extraction with EtOAc. The combined organic layers were dried over Na_2SO_4, filtered, and concentrated in vacuum. Purification by column chromatography (*n*-hexane:EtOAc = 2:1) afforded 176 mg (81%) of **6d** as a white solid; mp 197−200 °C. ^{1}H NMR (500 MHz, DMSO-d_6) δ [ppm]: 1.84 (s, 3H), 3.52 (dq, J = 30.0 Hz, J = 5.5 Hz, 2H), 4.52 (dt, J = 47.5 Hz, J = 5.0 Hz, 2H), 5.16 (br s, 2H), 5.94 (br s, 2H), 6.07 (d, J = 4.0 Hz, 1H), 6.72 (d, J = 4.0 Hz, 1H), 6.83 (d, J = 7.5 Hz, 1H), 6.90 (d, J = 7.5 Hz, 1H), 6.98−7.03 (m, 2H), 7.12 (td, J = 7.5 Hz, J = 1.0 Hz, 1H), 7.22 (d, J = 7.5 Hz, 1H), 7.26 (s, 1H), 7.32 (dd, J = 7.5 Hz, J = 1.0 Hz, 1H), 7.60 (t, J = 7.5 Hz, 1H), 7.69 (t, J = 7.5 Hz, 1H), 7.80 (d, J = 7.5 Hz, 1H). ^{13}C NMR (125 MHz, DMSO-d_6) δ [ppm]: 19.38, 45.89, 46.14 (br s), 64.79, 82.21 (d, J = 164.8 Hz), 108.45, 112.35, 123.74 (q, J = 272.4 Hz), 124.56, 125.75, 125.89 (q, J = 4.9 Hz), 126.89 (q, J = 29.3 Hz), 126.92, 128.11, 128.23, 128.35, 129.29, 131.09, 131.15, 132.17, 135.07, 135.31, 135.37, 138.90 (q, J = 1.6 Hz), 139.73, 141.00, 161.49, 169.16. LC/MS retention time: 10.16 min. MS (ESI) m/z = 536.1 $[M + H]^+$.

*10-(2-Methyl-2′-trifluoromethylbiphenyl-4-carbonyl)-10,11-dihydro-5H-benzo[e]pyrrolo[1,2-a][1,4]diazepine-3-carboxylic Acid (2-Fluoroethyl)methyl Amide (**6e**).* To a stirred solution of 164 mg (0.3 mmol) of **6d** in 0.3 mL of DMF, 44 mg (1.8 mmol, 60 wt % in mineral oil) of NaH was added followed by the addition of 0.11 mL (1.8 mmol) of methyl iodide. After stirring for 1 h at rt, the complete consumption of the reaction was confirmed by TLC analysis (*n*-hexane:EtOAc = 3:2). The mixture was quenched with 1 mL of H_2O followed by extraction with EtOAc. The combined organic layers were dried over Na_2SO_4, filtered, and concentrated in vacuum. The crude product was purified by column chromatography (*n*-hexane:EtOAc = 3:1) to obtain 80 mg (47%) of **6e** as a white solid; mp 165−168 °C. ^{1}H NMR (500 MHz, DMSO-d_6) δ [ppm]: 1.84 (s, 3H), 3.11 (br s, 3H), 3.80 (dt, J = 26.5 Hz, J = 5.0 Hz, 2H), 4.65 (dt, J = 47.5 Hz, J = 5.0 Hz, 2H), 5.17 (br s, 2H), 5.41 (br s, 2H), 6.07 (d, J = 3.5 Hz, 1H), 6.32 (d, J = 3.5 Hz, 1H), 6.86−6.92 (m, 2H), 7.00−7.08 (m, 2H), 7.15 (t, J = 7.5 Hz, 1H), 7.22 (d, J = 8.0 Hz, 1H), 7.26 (s, 1H), 7.37 (d, J = 7.0 Hz, 1H), 7.59 (t, J = 8.0 Hz, 1H), 7.68 (t, J = 7.5 Hz, 1H), 7.80 (d,

DOI: 10.1021/acs.jmedchem.5b01080
J. Med. Chem. 2016, 59, 1800−1817

J = 8.0 Hz, 1H). ^{13}C NMR (125 MHz, DMSO-d_6) δ [ppm]: 19.48, 45.88, 46.96, 80.87, 82.18, 107.72, 111.59, 120.46, 122.64, 124.51, 124.82, 125.87 (q, J = 5.0 Hz, 1C), 126.19, 126.54, 126.77, 126.99, 127.23, 128.11, 128.35, 128.45, 128.68, 129.10, 129.24, 129.66, 131.14, 132.17, 134.70, 135.08, 135.22, 138.87 (q), 139.78, 141.32, 163.28, 169.14. LC/MS retention time: 10.33 min. MS (ESI) m/z = 550.1 [M + H]$^+$.

*[2′-(2-Fluoroethyl)-2-methylbiphenyl-4-yl]-[3-(morpholino-4-carbonyl)-5H,11H-benzo[e]pyrrolo[1,2-a][1,4]diazepin-10-yl]-methanone (**6f**).* A mixture of 150 mg (0.32 mmol) of **5b**, 183 mg (0.48 mmol) of 1-bis(dimethylamino)methylene-1*H*-1,2,3-triazolo-[4,5-*b*]pyridinium-3-oxid hexafluorophosphate, (HATU) 0.32 mL (1.9 mmol) of Hünig's base, and 0.11 mL (1.28 mmol) of morpholine dissolved in 15 mL of DMF was stirred at rt overnight. The mixture was concentrated, and the residue was diluted with 7 mL of H_2O and extracted three times with 7 mL of EtOAc. The organic layer was washed twice with 5 mL of a saturated aqueous $NaHCO_3$ solution, dried over Na_2SO_4, filtered, and concentrated to remove the solvent. Column chromatography (*n*-hexane:EtOAc = 1:1) afforded 158 mg (92%) of **6f** as a white solid; mp 190−193 °C. ^{1}H NMR (500 MHz, DMSO-d_6) δ [ppm]: 1.86 (s, 3H), 2.42−2.52 (m, 1H), 2.62−2.71 (m, 1H), 3.63 (br s, 8H), 4.28 (dt, J = 47.0 Hz, J = 6.5 Hz, 2H), 5.17 (br s, 2H), 5.43 (br s, 2H), 6.08 (d, J = 4.0 Hz, 1H), 6.28 (d, J = 4.0 Hz, 1H), 6.86 (d, J = 7.5 Hz, 1H), 6.90 (d, J = 7.5 Hz, 1H), 7.00−7.07 (m, 3H), 7.15 (td, J = 7.5 Hz, J = 1.0 Hz, 1H), 7.25−7.29 (m, 2H), 7.32 (td, J = 7.5 Hz, J = 1.0 Hz, 1H), 7.37 (d, J = 7.5 Hz, 1H), 7.42 (dd, J = 7.5 Hz, J = 1.0 Hz, 1H). ^{13}C NMR (125 MHz, DMSO-d_6) δ [ppm]: 19.32, 33.1 (d, J = 20.4 Hz), 38.13, 45.84 (br s), 46.91, 66.14, 82.75 (d, J = 165.7 Hz), 107.86, 111.65, 125.12, 125.64, 126.47, 127.00, 127.55, 128.42, 128.50, 128.71, 128.90, 129.16, 129.62, 129.65, 129.95, 134.06 (d, J = 6.5 Hz), 134.74, 134.80, 134.93, 140.25, 141.39, 141.64, 161.73, 169.23. LC/MS retention time: 9.81 min. MS (ESI) m/z = 538.2 [M + H]$^+$.

*Synthesis of **12a** and **12b**. 2′-(2-Fluoroethyl)-2-methylbiphenyl-4-carboxylic Acid (**9**).* The compound was synthesized using 1.17 g (4.3 mmol) of **3b** according to the procedure for the synthesis of **4g**. After workup, 1.05 g (95%) of a white solid was obtained and used in the next step without any further purification; mp 128−130 °C. ^{1}H NMR (500 MHz, DMSO-d_6) δ [ppm]: 2.04 (s, 3H), 2.56−2.66 (m, 1H), 2.74−2.84 (m, 1H), 4.37 (t, J = 6.5 Hz, 1H), 4.47 (t, J = 6.5 Hz, 1H), 7.10 (d, J = 7.5 Hz, 1H), 7.22 (d, J = 8.0 Hz, 1H), 7.32 (td, J = 7.5 Hz, J = 1.5 Hz, 1H), 7.38 (td, J = 7.5 Hz, J = 1.5 Hz, 1H), 7.44 (d, J = 7.5 Hz, 1H), 7.82 (dd, J = 7.5 Hz, J = 1.5 Hz, 1H), 7.90 (s, 1H).

*(3,4-Dihydro-1H-pyrrolo[1,2-a]pyrazin-2-yl)-[2′-(2-fluoroethyl)-2-methylbiphenyl-4-yl]methanone (**10**).* A solution of 1.6 g (6.2 mmol) of **9** in 10 mL of thionyl chloride was refluxed under argon atmosphere for 1 h. The excess of thionyl chloride was removed under vacuum, and the residue was treated three times with 5 mL of toluene followed by removal of the solvent. The resultant acid chloride was dissolved in 10 mL of CH_2Cl_2 and added dropwise to an ice-cold solution of 0.85 g (7.0 mmol) of 1,2,3,4-tetrahydro-pyrrolo[1,2-*a*]pyrazine (synthesized according to procedures described[31]) and 2.5 mL (13.6 mmol) of Hünig's base in 30 mL of CH_2Cl_2. The cooling bath was removed and the mixture stirred for 4 h at rt. After hydrolysis of the reaction with 50 mL of H_2O, the aqueous layer was extracted three times with CH_2Cl_2. The combined organic layers were washed with an aqueous solution of $NaHCO_3$, dried over Na_2SO_4, filtered, and concentrated. The crude product was purified by column chromatography (EtOAc:*n*-hexane = 1:9) to obtain 1.5 g (67%) of **10** as a white foam; mp 50−54 °C. ^{1}H NMR (500 MHz, $CDCl_3$) δ [ppm]: 2.08 (s, 3H), 2.68−2.78 (m, 1H), 2.84−2.91 (m, 1H), 3.90 (br s, 2H), 4.10 (br s, 2H), 4.43 (dt, J = 47.5 Hz, J = 6.5 Hz, 2H), 4.80 (br s, 2H), 5.90 (br s, 1H), 6.19−6.25 (m, 1H), 6.63 (t, 1H), 7.11 (d, J = 7.5 Hz, 1H), 7.17 (d, J = 8 Hz, 1H), 7.29−7.32 (m, 2H), 7.36−7.39 (m, 3H).

*2,2,2-Trichloro-1-[2-[2′-(2-fluoroethyl)-2-methylbiphenyl-4-carbonyl]-1,2,3,4-tetrahydropyrrolo[1,2-a]pyrazin-6-yl]ethanone (**20**; Intermediate of Reaction Step (e) in Scheme 2).* The compound was synthesized using 1.4 g (3.9 mmol) of **10** according to the procedure for the synthesis of **15**. The obtained crude product was purified by column chromatography (*n*-hexane:EtOAc = 2:1) to yield 1.5 g (76%) of the titled product as a yellowish foam; mp 87−92 °C. ^{1}H NMR (500 MHz, DMSO-d_6) δ [ppm]: 2.04 (s, 3H), 2.61−2.72 (m, 1H), 2.77−2.88 (m, 1H), 4.88 (br s, 2H), 4.45 (dt, J = 47.5 Hz, J = 6.5 Hz, 2H), 4.46 (t, J = 5.5 Hz, 2H), 4.91 (br s, 2H), 6.34 (br s, 1H), 7.13 (dd, J = 7.5 Hz, J = 1.0 Hz, 1H), 7.21 (d, J = 7.5 Hz, 1H), 7.33 (td, J = 7.5 Hz, J = 1.0 Hz, 1H), 7.37−7.41 (m, 2H), 7.44−7.51 (m, 3H).

*2-[2′-(2-Fluoroethyl)-2-methylbiphenyl-4-carbonyl]-1,2,3,4-tetrahydropyrrolo[1,2-a]pyrazine-6-carboxylic Acid (**21**; Intermediate of Reaction Step (f) in Scheme 2).* According to the procedure for the synthesis of **5g** and using 1.2 g (2.4 mmol) of **20** in 50 mL of acetone and 10 mL (2.5 M) of an aqueous NaOH solution, 900 mg (91%) of the product was isolated as a white solid and used in the next step without further purification. ^{1}H NMR (500 MHz, DMSO-d_6)) δ [ppm]: 2.03 (s, 3H), 2.60−2.71 (m, 1H), 2.76−2.87 (m, 1H), 3.83 (br s, 2H), 4.41 (t, J = 7.0 Hz, 1H), 4.51 (t, J = 7.0 Hz, 1H), 4.53 (br s, 2H), 4.80 (br s, 2H), 6.05 (br s, 1H), 6.83 (br s, 1H), 7.13 (dd, J = 7.5 Hz, J = 1.5 Hz, 1H), 7.19 (d, J = 7.5 Hz, 1H), 7.33 (td, J = 7.5 Hz, 1.5 Hz, 1H), 7.35−7.40 (m, 2H), 7.44−7.46 (m, 2H), 12.07 (br s, 1H).

*2-[2′-(2-Fluoroethyl)-2-methylbiphenyl-4-carbonyl]-1,2,3,4-tetrahydropyrrolo[1,2-a]pyrazine-6-carboxylic Acid Bis(2-hydroxyethyl)amide (**12a**).* The compound was synthesized using 110 mg (0.28 mmol) of **21** and 52 mg (0.5 mmol) of diethanolamine according to the procedure for the synthesis of **6b**. The obtained crude product was purified by column chromatography (CH_2Cl_2:methanol = 97:3) to yield 25 mg (18%) of **12a** as a white foam; mp 72−75 °C. ^{1}H NMR (500 MHz, DMSO-d_6)) δ [ppm]: 2.03 (s, 3H), 2.60−2.71 (m, 1H), 2.76−2.87 (m, 1H), 3.55 (br s, 8H), 3.70−4.00 (br s, 2H), 4.12 (t, J = 5.0 Hz, 2H), 4.46 (dt, J = 47.0 Hz, 6.5 Hz, 2H), 4.78 (br s, 4H), 5.96 (br s, 1H), 6.47 (br s, 1H), 7.13 (dd, J = 7.5 Hz, J = 1.5 Hz, 1H), 7.19 (d, J = 7.5 Hz, 1H), 7.31−7.40 (m, 3H), 7.45 (br d, J = 7.5 Hz, 2H). ^{13}C NMR (125 MHz, DMSO-d_6) δ [ppm]: 19.44, 30.57, 33.14 (d, J = 20.1 Hz), 37.85, 46.87, 54.79, 65.78, 66.11, 83.05 (d, J = 165.5 Hz), 103.34 (br s), 123.07, 123.66, 124.26, 124.30, 126.49, 127.63, 128.52, 128.63, 129.04, 129.35, 129.48, 134.36 (d, J = 6.0 Hz), 135.75, 140.42, 161.52, 162.38. LC/MS retention time: 7.87 min. MS (ESI) m/z = 494.2 [M + H]$^+$.

*2-[2′-(2-Fluoroethyl)-2-methylbiphenyl-4-carbonyl]-1,2,3,4-tetrahydropyrrolo[1,2-a]pyrazine-6-carboxylic Acid (2-Hydroxyethyl)methyl Amide (**12b**).* The compound was synthesized using 110 mg (0.28 mmol) of **21** and 38 mg (0.5 mmol) of 2-methylaminoethanol according to the procedure for the synthesis of **6b**. The obtained crude product was purified by column chromatography (CH_2Cl_2:methanol = 97:3) to yield 50 mg (39%) of **12b** as a white solid; mp 125−129 °C. ^{1}H NMR (500 MHz, DMSO-d_6) δ [ppm]: 2.03 (s, 3H), 2.60−2.71 (m, 1H), 2.76−2.87 (m, 1H), 3.06 (br s, 3H), 3.53−3.58 (m, 4H), 3.78 (br s, 2H), 4.17 (t, J = 5.5 Hz, 2H), 4.46 (dt, J = 47.0 Hz, 6.5 Hz, 2H), 4.77 (br s, 3H), 5.97 (br s, 1H), 6.47 (br s, 1H), 7.13 (dd, J = 7.5 Hz, J = 1.5 Hz, 1H), 7.19 (d, J = 7.5 Hz, 1H), 7.31−7.40 (m, 3H), 7.44 (d, J = 7.5 Hz, 2H). ^{13}C NMR (125 MHz, DMSO-d_6) δ [ppm]: 19.45, 33.14 (d, J = 20.4 Hz), 44.05 (br s), 44.89 (br s), 54.79, 58.32, 83.05 (d, J = 165.5 Hz), 103.11, 112.23, 124.12, 124.25, 126.48, 127.62, 127.99, 128.50, 129.14, 129.34, 129.47, 134.36 (d, J = 6.0 Hz), 135.74, 140.42, 141.94, 162.90 (br s), 169.33 (br s). LC/MS retention time: 8.37 min. MS (ESI) m/z = 464.2 [M + H]$^+$.

*Synthesis of **12c**. 4-[2-[2′-(2-Fluoroethyl)-2-methylbiphenyl-4-carbonyl]-1,2,3,4-tetrahydropyrrolo[1,2-a]pyrazine-6-carbonyl]-piperazine-1-carboxylic Acid tert-Butyl Ester (**22**; Intermediate of Reaction Step (g) in Scheme 2).* The compound was synthesized using 200 mg (0.5 mmol) of **21** and 170 mg (0.9 mmol) of 1-Boc-piperazine according to the procedure for the synthesis of **6b**. The obtained crude product was purified by column chromatography (*n*-hexane:EtOAc = 2:3) to yield 170 mg (59%) of the titled product as a white solid; mp 95−98 °C. ^{1}H NMR (500 MHz, DMSO-d_6) δ [ppm]: 1.42 (s, 9H), 2.02 (s, 3H), 2.60−2.68 (m, 1H), 2.76−2.87 (m, 1H), 3.37 (br s, 4H), 3.61 (br s, 4H), 3.78 (br s, 2H), 4.17 (dd, J = 5.0 Hz, J = 5.0 Hz, 2H) 4.41 (t, J = 6.5 Hz, 1H), 4.50 (t, J = 6.5 Hz, 1H), 4.78 (br s, 2H), 6.02 (br s, 1H), 6.42 (br s, 1H), 7.12 (dd, J = 7.5 Hz, J = 1.5 Hz, 1H), 7.20 (d, J = 7.5 Hz, 1H), 7.30−7.38 (m, 3H), 7.45 (d, J = 7.5 Hz, 2H).

DOI: 10.1021/acs.jmedchem.5b01080
J. Med. Chem. 2016, 59, 1800−1817

*[2′-(2-Fluoroethyl)-2-methylbiphenyl-4-yl]-[6-(piperazine-1-carbonyl)-3,4-dihydro-1H-pyrrolo[1,2-a]pyrazin-2-yl]methanone (**12c**).* To an ice-cooled solution of 170 mg (0.3 mmol) of **22** in 5 mL of CH_2Cl_2, trifluoroacetic acid was added (0.6 mL, 0.8 mmol) under argon atmosphere. After stirring at rt for 2 h, the mixture was diluted with a saturated aqueous $NaHCO_3$ solution. The aqueous layer was extracted several times with CH_2Cl_2, the resultant organic layer washed with brine and dried over Na_2SO_4. After filtration, the solvent was removed under reduced pressure and the residue was dried in vacuum to give 120 mg (84%) of **12c** as a white solid; mp 125−130 °C. ^{1}H NMR (500 MHz, DMSO-d_6) δ [ppm]: 2.03 (s, 3H), 2.60−2.67 (m, 1H), 2.69 (dd, J = 5.0 Hz, J = 5.0 Hz, 4H), 2.76−2.87 (m, 1H), 3.55 (dd, J = 5.0 Hz, J = 5.0 Hz, 4H), 3.78 (br s, 2H), 4.17 (dd, J = 5.0 Hz, J = 5.0 Hz, 2H) 4.41 (t, J = 6.5 Hz, 1H), 4.50 (t, J = 6.5 Hz, 1H), 4.78 (br s, 2H), 5.99 (br s, 1H), 6.35 (br s, 1H), 7.13 (dd, J = 7.5 Hz, J = 1.5 Hz, 1H), 7.19 (d, J = 7.5 Hz, 1H), 7.31−7.39 (m, 3H), 7.44 (d, J = 7.5 Hz, 2H). ^{13}C NMR (125 MHz, DMSO-d_6) δ [ppm]: 19.44, 33.42 (d, J = 20.4 Hz), 43.94 (brs), 44.89 (brs), 45.31 (brs), 45.46, 83.05 (d, J = 165.1 Hz), 103.25 (brs), 112.11, 123.49, 124.27, 126.48, 127.62, 128.29 (brs), 128.53, 129.13, 129.35, 129.48, 134.36 (d, J = 6 Hz), 135.75, 140.41, 141.96, 161,41, 169.34 (brs). LC/MS retention time: 7.44 min. MS (ESI) m/z = 389.3 $[M - C_4H_9N_2]^+$, 475.2 $[M + H]^+$.

*Synthesis of **12d**. 4-([2-[2′-(2-Fluoroethyl)-2-methylbiphenyl-4-carbonyl]-1,2,3,4-tetrahydropyrrolo[1,2-a]pyrazine-6-carbonyl]-amino)piperidine-1-carboxylic Acid tert-Butyl Ester (**23**; Intermediate of Reaction Step (g) in Scheme 2).* The compound was synthesized using 200 mg (0.5 mmol) of **21** and 213 mg (0.9 mmol) of 4-amino-1-Boc-piperidine according to the procedure for the synthesis of **6b**. The obtained crude product was purified by column chromatography (n-hexane:EtOAc = 1:2) to yield 112 mg (38%) of the titled product as a yellow solid. ^{1}H NMR (500 MHz, DMSO-d_6) δ [ppm] 1.44 (s, 9H), 1.55−1.65 (m, 2H), 1.85−1.89 (m, 2H), 1.96 (s, 3H), 2.44−2.54 (m, 1H), 2.61−2.70 (m, 1H), 3.56 (br s, 4H), 3.71−3.85 (br s, 2H), 3.81−3.90 (m, 1H), 4.38−4.41 (m, 3H), 4.50 (t, J = 6.5 Hz, 1H), 4.75 (br s, 2H), 6.03 (d, J = 3.5 Hz, 1H), 6.30 (d, J = 3.5 Hz, 1H), 7.14 (dd, J = 7.5 Hz, J = 1.5 Hz, 1H), 7.18 (d, J = 7.5 Hz, 1H), 7.30−7.40 (m, 3H), 7.40−7.45 (m, 2H), 7.84 (d, J = 7.5 Hz, 1H). ^{13}C NMR (125 MHz, DMSO-d_6) δ [ppm] 19.32, 33.10 (d, J = 20 Hz), 45.83, 47.03, 58.55, 82.76 (d, J = 166 Hz), 107.50, 110.22, 125.11, 126.48, 126.97, 127.35, 127.55, 128.38, 128.51, 128.73, 128.91, 129.11, 129.60, 129.66, 134.05, 134.10, 134.77, 134.92, 140.26, 141.46, 141.62, 163.75, 169.23.

*2-[2′-(2-Fluoroethyl)-2-methylbiphenyl-4-carbonyl]-1,2,3,4-tetrahydropyrrolo[1,2-a]pyrazine-6-carboxylic Acid Piperidin-4-yl Amide (**12d**).* To a stirred solution of 112 mg (0.2 mmol) of **23** in 5 mL of CH_2Cl_2, 0.5 mL (0.7 mmol) of trifluoroacetic acid was added under argon atmosphere. After stirring for 2.5 h at rt, the complete consumption of the reaction was confirmed by TLC analysis (CH_2Cl_2:methanol = 9:1) and the mixture was diluted with a saturated aqueous $NaHCO_3$ solution. The aqueous layer was extracted several times with EtOAc, and the resultant organic layer washed with brine and dried over Na_2SO_4. After filtration, the solvent was removed under reduced pressure and the residue treated with diethyl ether. The precipitate was filtered and dried in vacuum to give 70 mg (71%) of **12d** as a yellow solid; mp 119−123 °C. ^{1}H NMR (500 MHz, DMSO-d_6) δ [ppm]: 1.53−1.61 (m, 2H), 1.82−1.86 (m, 2H), 2.03 (s, 3H), 2.60−2.71 (m, 1H), 2.76−2.87 (m, 3H), 3.18 (d, J = 13.0 Hz, 2H), 3.70−3.93 (m, 3H), 4.39−4.43 (m, 3H), 4.51 (t, J = 6.5 Hz, 1H), 4.77 (br s, 2H), 5.98 (br s, 1H), 6.88 (br s, 1H), 7.13 (dd, J = 7.5 Hz, J = 1.5 Hz, 1H), 7.19 (d, J = 7.5 Hz, 1H), 7.31−7.40 (m, 3H), 7.42−7.46 (m, 2H), 7.85 (d, J = 7.5 Hz, 1H). ^{13}C NMR (125 MHz, DMSO-d_6) δ [ppm]: 19.47, 28.46, 33.17 (d, J = 20.3 Hz), 42.25, 43.61, 44.69 (br s), 45.47, 83.08 (d, 165.1 Hz), 103.65 (br s), 112.53, 124.18, 124.28, 126.51, 127.66, 128.53, 129.16, 129.38, 129.50. 134.38 (d, J = 5.8 Hz), 135.77, 140.44, 142.00, 160.49, 169.33. LC/MS retention time: 7.57 min. MS (ESI) m/z = 489.2 $[M + H]^+$.

*Synthesis of **13a** and **13b**. 1-[2′-(2-Fluoroethyl)-2-methylbiphenyl-4-carbonyl]-piperidin-4-one (**24**; Intermediate of Reaction Step (a) in Scheme 2).* The compound was synthesized using 500 mg (2.0 mmol) of **9** and 338 mg (2.2 mmol) of 4-piperidone monohydrate hydrogen chloride according to the procedure for the synthesis of **6b** to give 600 mg (88%) of the titled compound. The obtained crude product was used for the next step without further purification. ^{1}H NMR (500 MHz, $CDCl_3$) δ [ppm]: 2.08 (s, 3H), 2.54 (br s, 4H), 2.67−2.78 (m, 1H), 2.80−2.90 (m, 1H), 3.94 (br s, 4H), 4.42 (dt, J = 47.0 Hz, J = 6.5 Hz, 2H), 7.09 (dd, J = 7.5 Hz, J = 1.0 Hz, 1H), 7.18 (d, J = 7.5 Hz, 1H), 7.27−7.40 (m, 5H). ^{13}C NMR (125 MHz, $CDCl_3$) δ [ppm] 19.96, 33.82 (d, J = 20.6 Hz), 41.23 (br s), 46.51 (br s), 83.31 (d, J = 168.5 Hz), 124.07, 126.69, 127.86, 128.71, 129.50, 129.70, 129.75, 134.19, 134.41 (d, J = 6.6 Hz), 136.79, 140.67, 142.99, 170.88, 206.62.

*{4-[Bis(2-hydroxyethyl)amino]-piperidin-1-yl]-[2′-(2-fluoroethyl)-2-methylbiphenyl-4-yl]methanone (**13a**) and (2′-(2-Fluoroethyl)-2-methyl-[1,1′-biphenyl]-4-yl)(4-hydroxypiperidin-1-yl)methanone (**13b**).* To a stirred solution of 370 mg (1.1 mmol) of **24** and 130 mg (1.2 mmol) of diethanolamine in 4 mL dichloroethane, $Na(OAc)_3BH$ (340 mg, 1.6 mmol) and acetic acid (72 mg, 1.2 mmol) were added. The mixture was stirred at rt overnight and diluted with 10 mL of a saturated aqueous $NaHCO_3$ solution. The aqueous layer was extracted with CH_2Cl_2 and the organic layer dried over Na_2SO_4. After filtration and removal of the solvent in vacuum, the crude product was purified by column chromatography (CH_2Cl_2:methanol:triethyl amine = 90:10:1) to give both compounds as white solids in a ratio of 1:3; 30 mg (6%) of **13a** (R_f = 0.3; CH_2Cl_2:methanol = 95:5) and 90 mg (24%) of **13b** (R_f = 0.7; CH_2Cl_2:methanol = 95:5).

13a: mp 55−60 °C. ^{1}H NMR (500 MHz, DMSO-d_6) δ [ppm] 1.35−1.45 (m, 2H), 1.65−1.85 (m, 2H), 2.01 (s, 3H), 2.57−2.69 (m, 5H), 2.75−2.86 (m, 3H), 3.05 (br s, 2H), 3.40 (br s, 4H), 3.72 (br s, 1H), 4.36 (br s, 1H), 4.45 (dt, 47.5 Hz, J = 6.5 Hz, 2H), 4.55 (br s, 1H), 7.12 (dd, J = 7.5 Hz, J = 1.5 Hz, 1H), 7.15 (d, J = 7.5 Hz, 1H), 7.25 (d, J = 7.5 Hz, 1H), 7.31 (dd, J = 7.5 Hz, J = 1.5 Hz, 1H), 7.33 (s, 1H), 7.37 (td, J = 7.5, J = 1.5 Hz, 1H), 7.44 (d, J = 7.5 Hz, 1H). ^{13}C NMR (125 MHz, DMSO-d_6) δ [ppm]: 19.46, 33.13 (d, J = 20 Hz), 40.97 (br s), 46.55 (br s), 52.98, 54.79, 59.10, 59.50 (br s), 83.04 (d, J = 165 Hz), 123.84, 126.47, 127.57, 128.13, 129.17 (d, J = 4.9 Hz), 129.44, 134.31, 134.36, 135.27, 135.55, 140.50, 141.34, 168.66. LC/MS retention time: 6.94 min. MS (ESI) m/z = 429.2 $[M + H]^+$.

13b: mp 132−134 °C. ^{1}H NMR (500 MHz, DMSO-d_6) δ [ppm] 1.35−1.45 (m, 2H), 1.65−1.85 (m, 2H), 2.01 (s, 3H), 2.57−2.69 (m, 1H), 2.75−2.85 (m, 1H), 3.21 (br s, 2H), 3.57 (br s, 1H), 3.72−3.78 (m, 1H), 4.03 (br s, 1H), 4.45 (dt, J = 47.0 Hz, J = 6.5 Hz, 2H), 4.79 (d, J = 4.0 Hz, 1H), 7.11 (dd, J = 7.5 Hz, J = 1.0 Hz, 1H), 7.14 (d, J = 7.5 Hz, 1H), 7.23 (dd, J = 7.5 Hz, J = 1.0 Hz, 1H), 7.29−7.33 (m, 2H), 7.36 (td, J = 7.5 Hz, J = 1.5 Hz, 1H), 7.43 (d, J = 7.5 Hz, 1H). ^{13}C NMR (125 MHz, DMSO-d_6) δ [ppm] 19.44, 33.13 (d, J = 20.3 Hz), 33.75 (br s), 34.41 (br s), 44.56 (br s), 65.41, 83.03 (d, J = 165.1 Hz), 123.77, 126.46, 127.56, 128.06, 129.19, 129.42, 134.34 (d, J = 6.4 Hz), 135.38, 135.54, 140.50, 141.29, 168.67. LC/MS retention time: 7.96 min. MS (ESI) m/z = 342.2 $[M + H]^+$.

*Synthesis of **14**. 4-[2′-(2-Fluoroethyl)-2-methylbiphenyl-4-carbonyl]-piperazine-1-carboxylic Acid tert-Butyl Ester (**25**; Intermediate of Reaction Step (a) in Scheme 2).* The compound was synthesized using 258 mg (1.0 mmol) of **9** and 230 mg (1.2 mmol) of N-Boc-piperazine according to the procedure for the synthesis of **6b**. The obtained crude product was purified by column chromatography (n-hexane:EtOAc = 3:2) to yield 414 mg (97%) of the titled product as a white solid; mp 55−58 °C. ^{1}H NMR (500 MHz, DMSO-d_6) δ [ppm]: 1.42 (s, 9H), 2.01 (s, 3H), 2.59−2.69 (m, 1H), 2.75−2.86 (m, 1H), 3.40 (br s, 6H), 3.57 (br s, 2H), 4.45 (dt, J = 47.0 Hz, J = 6.5 Hz, 2H), 7.10 (dd, J = 7.5 Hz, J = 1.5 Hz, 1H), 7.16 (d, J = 7.5 Hz, 1H), 7.28 (dd, J = 7.5 Hz, J = 1.5 Hz, 1H), 7.32 (td, J = 7.5 Hz, J = 1.5 Hz, 1H), 7.35−7.38 (m, 2H), 7.44 (d, J = 7.5 Hz, 1H).

*[2′-(2-Fluoroethyl)-2-methylbiphenyl-4-yl]-piperazin-1-yl-methanone (**11**).* To a stirred solution of 900 mg (2.1 mmol) of **25** in 50 mL of CH_2Cl_2 under argon atmosphere, 5 mL (65 mmol) of trifluoroacetic acid was added After stirring for 2.5 h at rt, the complete consumption of **25** was confirmed by TLC analysis (n-hexane:EtOAc = 1:1) and the mixture was diluted with a saturated aqueous $NaHCO_3$ solution. The aqueous layer was extracted several times with EtOAc, and the resultant organic layer washed with brine and dried over Na_2SO_4. After filtration, the solvent was removed under reduced pressure and the

DOI: 10.1021/acs.jmedchem.5b01080
J. Med. Chem. 2016, 59, 1800−1817

residue was treated with diethyl ether. The precipitate was filtered and dried in vacuum to give 700 mg (99%) of **11** as a white solid. ^{1}H NMR (500 MHz, DMSO-d_6) δ [ppm]: 2.01 (s, 3H), 2.58−2.69 (m, 1H), 2.75−2.85 (m, 4H), 3.20−3.70 (m, 6H), 4.45 (dt, J = 47.0 Hz, J = 6.5 Hz, 2H), 7.10 (dd, J = 7.5 Hz, J = 1.5 Hz, 1H), 7.15 (d, J = 7.5 Hz, 1H), 7.23−7.27 (m, 1H), 7.30−7.38 (m, 3H), 7.44 (d, J = 7.5 Hz, 1H).

*[2′-(2-Fluoroethyl)-2-methylbiphenyl-4-yl]-[4-(2-hydroxyethyl)-piperazin-1-yl]methanone (**14**).* To a stirred solution of 300 mg (0.9 mmol) of **11** in 7.5 mL of acetonitrile, 1.2 g (8.7 mmol) potassium carbonate and 0.1 mL (1.5 mmol) of 2-bromoethanol were added. After heating under reflux overnight, the consumption of the reactants was observed by TLC analysis (CH_2Cl_2:methanol = 9:1) and additional 0.05 mL (0.75 mmol) of 2-bromoethanol were added. After further refluxing for 4 h, the solvent was removed in vacuum and the residue was diluted with EtOAc. The resultant organic layer was washed with H_2O, dried over Na_2SO_4, filtered, and concentrated in vacuum. The crude product was purified by column chromatography (CH_2Cl_2:methanol = 95:5) to yield 200 mg (59%) of **14** as a white foam; mp 55−60 °C. ^{1}H NMR (500 MHz, DMSO-d_6) δ [ppm]: 2.01 (s, 3H), 2.43 (t, J = 6.0 Hz, 1H), 2.44 (br s, 5H), 2.58−2.69 (m, 1H), 2.75−2.85 (m, 1H), 3.40 (br s, 2H), 3.53 (q, J = 6.0 Hz, 2H), 3.62 (br s, 2H), 4.38−4.43 (m, 2H), 4.50 (t, J = 6.5 Hz, 1H), 7.11 (dd, J = 7.5 Hz, J = 1.0 Hz, 1H), 7.15 (d, J = 7.5 Hz, 1H), 7.24 (dd, 7.5 Hz, J = 1.5 Hz, 1H), 7.30−7.34 (m, 2H), 7.36 (td, J = 7.5 Hz, J = 1.5 Hz, 1H), 7.44 (d, J = 7.5 Hz, 1H). ^{13}C NMR (125 MHz, DMSO-d_6) δ [ppm]: 19.59, 33.17 (d, J = 20.3 Hz), 47.04, 52.99, 58.21, 59.81, 82.72 (d, J = 164.0 Hz), 123.42, 125.83, 126.94, 127.66, 128.55, 128.55, 128.78, 133.65 (d, J = 6.3 Hz), 134.26, 134.89, 139.73, 140.70, 167.71. LC/MS retention time: 6.72 min. MS (ESI) m/z = 371.2 $[M + H]^+$.

4.2. In Vitro Binding Studies. The studies were performed using membrane homogenates prepared from CHO cells stably transfected with human oxytocin receptor gene (hOTR-CHO; obtained from Bice Chini, Instituto di Neuroscienze, Consiglio Nazionale delle Ricerche, Milano, Italy). For the competitive binding studies, membrane preparation was incubated with [^{3}H]oxytocin (K_D = 2.56 nM ± 0.95 nM; [tyrosyl-2,6-^{3}H],1676 GBq/mmol; PerkinElmer LAS GmbH, Rodgau, Germany) at 1 nM and seven concentrations of test compounds (10 pM to 10 μM) in buffer consisting of 50 mM TRIS-HCl, pH 7.4, 5 mM $MgCl_2$, and 0.1% BSA for 60 min at 22 °C. The binding was terminated by rapid filtration (48-well semiautomated cell harvester; Brandel, Gaithersburg, USA) using GF/B glass fiber filter presoaked in 0.3% PEI for 60 min at rt. Radioactivity trapped on the filters was counted by liquid scintillation counting (Beckman LSC 6500; Beckman Coulter GmbH, Krefeld, Germany). Nonspecific binding was defined as binding remaining in the presence of 10 μM oxytocin. The assays were performed two times, each in duplicate. Experimental data were analyzed by nonlinear regression, and IC_{50} curves generated by a one-site competition model. The K_i values of the test compounds were calculated using the Cheng−Prusoff equation.

The equilibrium dissociation constant K_D of **6b** was determined performing a homologous binding experiment. [^{18}F]**6b** (specific activity: 160 GBq/μmol) at a radioactivity concentration of 57 kBq/mL (identical to a chemical concentration of 0.35 nM) was coincubated with various dilutions of **6b** (final concentration 0.1 nM−100 μM) with membranes obtained from hOTR-CHO cells in buffer consisting of 50 mM TRIS-HCl, pH 7.4, 5 mM $MgCl_2$, and 0.1% BSA for 60 min at 22 °C. The binding was terminated by rapid filtration (48-well semiautomated cell harvester; Brandel, Gaithersburg, USA) using GF/B glass fiber filter presoaked in 0.3% PEI for 60 min at rt. Radioactivity trapped on the filters was counted by gamma-counting (Wallac 1470 Wizard 3″; PerkinElmer LAS GmbH, Rodgau, Germany). CPM data were analyzed by nonlinear regression, and an IC_{50} curve generated by a one-site competition model. The K_D value of **6b** was calculated according to $K_D = IC_{50} - [\text{radioligand}]$, valid for the one-site homologous competition binding model.

4.3. Determination of log *D* and P_m Values. The log *D* values were determined by HPLC (Agilent 1100/1200 series) according to Donovan and Pescatore.[33] The compounds were injected (2 μL, 150 μg/mL) together with a mixture of toluene (0.5 mL) and triphenylene (5 mg) as internal standards in methanol (50 mL) to a short polymeric ODP-50 column (20 mm × 4 mm, 5 μm, Shodex, Showa Denko Europe GmbH, Munich, Germany) using a linear gradient from 10% methanol and 90% 10 mM sodium phosphate buffer to 100% methanol within 9.4 min at a flow rate of 1.5 mL/min and a pH of 7.4.

Permeability (P_m) measurements were performed according to Taillardat-Bertschinger et al. using immobilized artificial membrane (IAM) chromatography.[34,42] For IAM measurements, the same HPLC system and an IAM.PC.DD2 (150 mm × 4.6 mm, Regis Technologies Inc., Morton Grove, USA) column were used isocratically with 10 mM phosphate buffer and acetonitrile in different ratios (50/50, 55/45, 60/40, and 65/35) adjusted to pH 7.0 and 1 mL/min flow rate. P_m values are obtained by dividing membrane partition coefficient K_m by the molecular weight of the tracer candidates. K_m was calculated on the basis of the capacity factors k_{IAM} and correction of the column conditions (total volume of solvent within column (V_m) and volume of interphase (V_s)), at which the k_{IAM} factors are calculated and extrapolated to 100% aqueous phase.

4.4. Determination of Plasma-Free Fraction. Binding of [^{18}F]**6b** to plasma proteins was estimated by ultrafiltration. First, 1 mL of plasma obtained from pig was spiked with 60 μL of saline containing 10 MBq [^{18}F]**6b** and incubated for 30 min at 37 °C. The separation of protein-bound and free [^{18}F]**6b** was achieved by filtration through anisotropic hydrophilic Ultracel YM membrane (Amicon Centrifree, 30000 MW cutoff; MerckMilliporeAmicon Inc., USA) as specified by the manufacturer (2000*g*, 15 min, 21 °C). The radioactivity concentrations in the plasma obtained before centrifugation (C) and of the ultrafiltrate (C_u) were estimated by gamma counting of respective sample aliquots (Wallac 1470 Wizard 3″; PerkinElmer LAS GmbH, Rodgau, Germany). The value of plasma free fraction f_P was calculated according to the relation f_P (%) = C_u /C × 100.

4.5. Radiochemistry. No-carrier-added [^{18}F]fluoride was produced via the [^{18}O(p,n)^{18}F] nuclear reaction by irradiation of an [^{18}O]H_2O target (Hyox 18 enriched water, Rotem Industries Ltd., Israel) on a Cyclone 18/9 (iba RadioPharma Solutions, Belgium) with fixed energy proton beam using a Nirta [^{18}F]fluoride XL target. Microwave assisted radiofluorination was performed in a standard 4 mL V vial using a Discover PETWave Microwave (CEM, NC, USA).

Radio thin-layer chromatography (radio-TLC) was performed on silica gel (Polygram SIL G/UV_{254}) and aluminum oxide (Polygram Alox N/UV_{254}) precoated plates with EtOAc (EE)/PE (PE) 5/1 (for labeling product) and EE/EtOH 10/1 (for [^{18}F]**2**), respectively. The plates were exposed to storage phosphor screens (BAS-TR2025, FUJIFILM Co., Tokyo, Japan) and recorded using a bioimaging analyzer system (BAS-1800 II, FUJIFILM). Images were evaluated with the BASReader and AIDA 2.31 software (raytest Isotopenmessgeräte GmbH, Straubenhardt, Germany).

Analytical chromatographic separations were performed on a JASCO LC-2000 system, incorporating a PU-2080Plus pump, AS-2055Plus auto injector (100 μL sample loop), and a UV-2070Plus detector coupled with a gamma radioactivity HPLC detector (Gabi Star, raytest Isotopenmessgeräte GmbH). Data analysis was performed with the Galaxie chromatography software (Agilent Technologies) using the chromatograms obtained at 254 and 272 nm, respectively.

Semipreparative HPLC separations were performed on a JASCO LC-2000 system, incorporating a PU-2080-20 pump, a UV/vis-2075 detector coupled with a gamma radioactivity HPLC detector whose measurement geometry was slightly modified (Gabi Star, raytest Isotopenmessgeräte GmbH), and a fraction collector (Advantec CHF-122SC). Data analysis was performed with the Galaxie chromatography software (Agilent Technologies) using the chromatograms obtained at 254 nm.

The ammonium acetate (NH_4OAc) concentration stated as 20 mM NH_4OAc aq corresponds to the concentration in the aqueous component of an eluent mixture.

Radiosyntheses. No-carrier-added [^{18}F]fluoride in 2 mL of H_2O was trapped on a Chromafix 30 PS-HCO_3^- cartridge (Macherey-Nagel GmbH & Co. KG, Düren, Germany). The activity was eluted with 300 μL of an aqueous solution of potassium carbonate (K_2CO_3, 1.8 mg, 13

DOI: 10.1021/acs.jmedchem.5b01080
J. Med. Chem. 2016, 59, 1800−1817

μmol) into a 4 mL V vial and Kryptofix 2.2.2 ($K_{2.2.2}$, 11 mg, 29 μmol) in 1 mL of ACN was added. The aqueous [^{18}F]fluoride was azeotropically dried under vacuum and nitrogen flow within 7−10 min using a single mode microwave (75 W, at 50−60 °C, power cycling mode). Two aliquots of ACN (2 × 1.0 mL) were added during the drying procedure, and the final complex was dissolved in 1000 μL of ACN ready for labeling. The reactivity of the anhydrous K[^{18}F]F-$K_{2.2.2}$-carbonate complex as well as the reproducibility of the drying procedure were checked via the standard reaction with 2 mg (5.4 μmol) of ethylene glycol ditosylate (Sigma-Aldrich, Germany) at 80 °C for 10 min in ACN. Thereafter, a solution of 2.0−2.5 mg of precursor in 500 μL of ACN was added and the ^{18}F-labeling was performed under thermal heating (90 °C, 15 min) or microwave-assisted irradiation (75W, 85−95 °C, 9 min, power cycling mode). To analyze the reaction mixture and to determine labeling yields, samples were taken for radio-HPLC and radio-TLC. Moreover, the stability of the tosylate precursor was investigated under both heating conditions used by HPLC analysis at different time points of the reaction.

After cooling to <30 °C, hydrochloric acid was added and the deprotection was performed by thermal heating (90 °C, 15 min, 1 mL 2.0 M HCl) or microwave irradiation (50W, 75−85 °C, 5 min, power cycling mode, 1 mL 2.0 M HCl). Thereafter, the reaction mixture was neutralized with aqueous 6.0 M NaOH and directly applied to an isocratic semipreparative RP-HPLC for isolation of [^{18}F]**6b** (44% ACN/20 mM NH_4OAc_{aq}, 4 mL/min, Reprosil-Pur C18-AQ, 250 mm × 10 mm; 5 μm; Dr. Maisch HPLC GmbH, Germany). The collected radiotracer fraction was diluted with 40 mL of H_2O to perform final purification by sorption on a Sep-Pak C18 light cartridge (Waters, Milford, MA, USA) and successive elution with 0.75 mL of ethanol. The solvent was reduced under a gentle argon stream and the desired radiotracer formulated in sterile isotonic saline containing 10% EtOH (v/v). The identity and radiochemical purity of [^{18}F]**6b** was confirmed by radio-HPLC (gradient and isocratic mode) and radio-TLC (Alox N/UV_{254}, EE/EtOH 10/1). For radio-HPLC, a Reprosil-Pur C18-AQ column (250 mm × 4.6 mm; 5 μm; Dr. Maisch HPLC GmbH; Germany) with ACN/20 mM NH_4OAc aq as eluent mixture and a flow of 1.0 mL/min was used (gradient: eluent A 10% ACN/20 mM NH_4OAc aq; eluent B 90% ACN/20 mM NH_4OAc aq; 0−5 min 100% A, 5−10 min up to 55% B, 10−25 min 55% B, 25−30 up to 100% B, 30−40 min 100% B, 40−45 min up to 100% A, and 45−55 min 100% A; isocratic, 42% ACN/20 mM NH_4OAc_{aq}). Specific activity was determined on the base of a calibration curve carried out under isocratic HPLC conditions (42% ACN/20 mM NH_4OAc_{aq}) using chromatograms obtained at 272 nm as an appropriate maximum of UV absorbance.

In Vitro Stability and Partition Coefficient. The in vitro stability of [^{18}F]**6b** was investigated by incubation of small tracer amounts (10−15 MBq) at 40 °C in 1 mL of following solutions: (i) 0.9% aq NaCl, (ii) PBS (137 mM NaCl, 2.7 mM KCl, 10 mM Na_2HPO_4; pH = 7.4), and (iii) pig plasma samples. At various time points, aliquots were analyzed by radio-TLC and radio-HPLC.

The partition coefficient of [^{18}F]**6b** was experimentally determined for the *n*-octanol/PBS system by the shake-flask method. Aliquots of the formulated radiotracer product were diluted in the buffer (20−50 μL, 1:1000) and added to a mixture of 3.0 mL of pre-equilibrated *n*-octanol and 3.0 mL of PBS. After shaking for 20 min at room temperature, the samples were centrifuged (5000*g*, 5 min), and duplicates of samples (0.5 mL each) of the organic as well as the aqueous layers were measured in a gamma counter. Another duplicate of samples (1 mL each) of the organic layer was subjected to the same procedure until constant partition coefficient values had been obtained. All measurements were done in triplicate.

*Radiotracer Metabolism of [^{18}F]**6b** in Mice.* Blood samples of mouse were taken at 30 min after intravenous injection of 84 MBq of [^{18}F]**6b** (n = 2). Pig blood samples were taken at 2, 8, 30, and 60 min after intravenous injection of 250 MBq of [^{18}F]**6b**. Plasma was obtained by centrifugation of blood at 12000 rpm at 4 °C for 10 min. Protein precipitation was performed by addition of ice-cold ACN in a ratio of 4:1 of organic solvent to plasma. The samples were vortexed for 2 min, equilibrated on ice for 15 min, and centrifuged for 5 min at 10000 rpm. The precipitates were washed with 200 μL of solvent mixture and subjected to the same procedure. The combined supernatants (total volume between 1.0−1.5 mL) were concentrated at 65 °C under argon flow to a final volume of approximately 100 μL and analyzed by radio-TLC and analytical radio-HPLC. To determine the percentage of radioactivity in the supernatants compared to total activity, aliquots of each step as well as the precipitates were quantified by gamma counting.

4.6. In Vitro Autoradiographic Studies. Brain sections (20 μm) of flash-frozen brains of female domestic pigs (*Sus s. domestica*, 6 weeks, 12−14 kg) were cut using a cryostat, thaw-mounted onto microscope slides, and after air-drying stored at −80 °C until use. Briefly, the brain sections were allowed to thaw in air and rinsed twice in 50 mM Tris buffer, pH 7.4, to remove endogenous ligand. The sections were then incubated with the 6 nM [^{3}H]oxytocin [tyrosyl-2,6-^{3}H], 1676 GBq/mmol; PerkinElmer LAS GmbH, Rodgau, Germany) or ∼10 nM [^{18}F]**6b** in TRIS buffer (50 mM TRIS-HCl, 5 mM NaCl, 0.1% BSA pH 7.4) for 60 min at room temperature. Nonspecific binding was determined in the presence of 10 or 0.1 μM oxytocin, respectively. Displacement of [^{18}F]**6b** was also evaluated with the following ligands: 1 μM L-quisqualic acid (glutamate receptor ligand), 0.35 μM THIP ($GABA_A$ receptor ligand), 0.2 μM siramesin (σ1/2 receptor ligand), 0.08 nM SR49059 (V_{1A} receptor ligand), or 3 nM tolvaptan ($V_{1/2}$ receptor ligand). Subsequently, the sections were washed twice for 2 min in ice-cold TRIS buffer and rinsed for 5 s in ice-cold distilled H_2O. The sections were rapidly dried in a stream of cold air before being exposed to a tritium-sensitive imaging plate. Developed autoradiographs were analyzed in a phosphor imager (Fuji BAS 1800 II). The quantification was performed by using 2D-densitometric analysis (AIDA 2.31 software; raytest Isotopenmessgeräte GmbH, Germany).

4.7. In Vivo Studies in Mice. Animals for in vivo studies were obtained from the Medizinisch-Experimentelles Zentrum, Universität Leipzig. All procedures that include animals were approved by the respective State Animal Care and Use committee and conducted in accordance with the German Law for the Protection of Animals (TVV 08/13). For all in vivo studies in mice, female CD-1 mice, 10−12 weeks old, 20−25 g, were used.

*Biodistribution of [^{18}F]**6b** in Mice.* Mice received an injection of approximately 200 kBq [^{18}F]**6b** with a specific activity of 70 GBq/μmol in 200 μL of 0.9% saline into the tail vein. The animals were anesthetized for blood and urine sampling and euthanized by luxation of the cervical spine at 5 and 30 min pi (n = 2 per each time point). The organs of interest were removed and weighed, and the radioactivity was measured by gamma counting (Wallac 1470 Wizard 3″; PerkinElmer LAS GmbH, Rodgau, Germany). The percentage of injected dose per gram of wet tissue (% ID/g wet weight) was calculated.

*PET/MR Studies of [^{18}F]**6b** in Mice.* Mouse small animal PET acquisitions were obtained on a preclinical PET/MR system (nanoScan PET/MR, Mediso Medical Imaging Systems, Budapest, Hungary). Anesthesia was induced by exposing mice to 4% isoflurane in air and then maintained by reducing the ratio to 1.5% for the duration of the studies. The animal was placed in the PET scanner followed by a 15 min MR scan. The subsequent 60 min PET scan was started with the beginning of the intravenous injection of [^{18}F]**6b** (mean = 11.8 MBq; 10.4−13.1 MBq), and radioactivity concentration was measured in sequential frames of 5 min duration. Activity volumes were reconstructed with iterative reconstruction (OSEM, four iterations, six subsets) including an MR-based attenuation and scatter correction, achieving a reconstructed spatial resolution of 1.5 mm.[45] Additional experiments were similarly performed in mice preinjected with cyclosporin (50 mg/kg iv, 60 min prior to radioligand administration).

4.8. PET Study in Pig. Animal procedure was approved by the Animal Care and Use Committee of Saxony (TVV 08/13). One piglet (6 weeks old) was used in this study. Anaesthesia and surgery of the animal was performed as described previously.[56] In brief, the animal was premedicated with midazolam (1 mg·kg^{-1} im) followed by induction of anesthesia with 3% isoflurane in 70% N_2O/30% O_2. All

DOI: 10.1021/acs.jmedchem.5b01080
J. Med. Chem. 2016, 59, 1800−1817

incision sites were infiltrated with 1% lidocaine, and anesthesia was maintained throughout the surgical procedure with 1.5% isoflurane. A central venous catheter was introduced through the left external jugular vein and used for the administration of the radiotracer and drugs and for volume substitution with heparinized (50 IE·mL^{-1}) lactated Ringer's solution (2 mL·kg^{-1}·h^{-1}). An endotracheal tube was inserted by tracheotomy for artificial ventilation (Servo Ventilator 900C, Siemens-Elema, Sweden) after immobilization with pancuronium bromide (0.2 mg·kg^{-1}·h^{-1}). The artificial ventilation was adjusted to maintain normoxia and normocapnia (Radiometer ABL 500, Copenhagen, Denmark). Polyurethane catheters (Ø 0.5 mm) were advanced through the left and the right femoral arteries into the abdominal aorta to withdraw arterial blood samples for regular monitoring of blood gases and for radiotracer input function measurements. Body temperature was monitored by a rectal temperature probe and maintained at ∼38 °C by a heating pad. After completion of surgery, anesthesia was maintained with 0.5% isoflurane in 70% N_2O/30% O_2, and the animal was allowed to stabilize for 1 h before PET imaging.

PET Scanning Protocol. PET imaging was performed according to the protocol described recently.[57] In brief, animals were scanned position prone, with the head held in the aperture of a clinical tomograph (ECAT EXACT HR+, CTI/Siemens) using a custom-made head holder. For attenuation and scatter correction, transmission scans were acquired using three rotating ^{68}Ge rod sources. [^{18}F]**6b** (225 MBq; A_s, 54 GBq/μmol) was applied in 10 mL saline as a 2 min iv infusion using a syringe pump, followed by flushing with 10 mL of heparinized saline (50 IE·mL^{-1}). The emission recording started upon initiation of the injection, and dynamic emission data were acquired for a total of 120 min. Arterial blood was sampled continuously using a peristaltic pump during the first 20 min of the recording, followed by manual sampling at 25, 30, 40, 50, 60, 90, and 120 min after injection. After centrifugation, the plasma radioactivity concentration was measured using a gamma counter (1470 Wizard, PerkinElmer, Shelton, CT, USA) cross calibrated to the PET scanner. Additionally, arterial blood was sampled manually at 4, 16, 30, and 60 min pi and plasma obtained as described above to determine the fractions of nonmetabolized [^{18}F]**6b** (see below).

Quantification of PET Data. After correction for attenuation, scatter, decay, and scanner-specific dead time, images were reconstructed by filtered back projection using a 4.9 mm FWHM Hanning filter into 40 frames of increasing length. A summed PET image of a 30 min FDG scan of the same pig, performed directly after the first PET scan, was used for alignment with a T1-weighed MR image of a 6-week-old farm-bred pig as described previously.[58] The following volumes of interest (VOIs) were chosen: olfactory bulb, frontal cortex, hippocampus, striatum (defined as mean radioactivity in caudate and putamen), colliculi, and cerebellum. Radioactivity in all VOIs was calculated as the mean radioactivity concentration (Bq/mL) for the left and right sides. To generate standardized uptake values (SUVs) the VOI activities were normalized to the injected dose and corrected for animal weight.

AUTHOR INFORMATION

Corresponding Author

*E-mail: b.wenzel@hzdr.de. Phone: +49 341 2341794637.

Author Contributions

#B.W. and J.M. contributed equally to this work.

Notes

The authors declare no competing financial interest.

ACKNOWLEDGMENTS

The project was funded by Europäischer Fonds für regionale Entwicklung (EFRE). We thank Dr. Karsten Franke for providing [^{18}F]fluoride. We thank Dr. Achim Hiller, Juliane Schaller, and Tina Spalholz for their assistance in the lab. We are very grateful to Bice Chini from the Instituto di Neuroscienze, Milano, Italy, for providing the hOTR-CHO cell line.

ABBREVIATIONS USED

ACN, acetonitrile; EtOAc, ethyl acetate; PE, petroleum ether; Hünig's base, *N*,*N*-diisopropylamine; Steglich base, 4-dimethylaminopyridine; COMU, (1-cyano-2-ethoxy-2-oxoethylidenaminooxy)dimethylamino-morpholino-carbenium hexafluorophosphate; TBTU, *O*-(benzotriazol-1-yl)-*N*,*N*,*N*′,*N*′-tetramethyluronium tetrafluoroborate; HATU, 1-bis-(dimethylamino)methylene-1*H*-1,2,3-triazolo[4,5-*b*]-pyridinium-3-oxid hexafluorophosphate; EDCI, 1-ethyl-3-(3-dimethylamino-propyl) carbodiimide hydrochloride carbodiimide hydrochloride; HOBt, 1-hydroxybenzotriazole; DAST, diethylaminosulfur trifluoride; TAC, time−activity curve; VOI, volume of interest; SUV, standard uptake value; V_T, distribution volume; BP, binding potential; PSA, polar surface area; TPSA, topological polar surface area

REFERENCES

(1) Nussey, S.; Whitehead, S. The pituitary gland. In *Endocrinology: An Integrated Approach*; BIOS Scientific Publisher: Oxford, 2001; Chapter 7.

(2) Gimpl, G.; Fahrenholz, F. The oxytocin receptor system: structure, function, and regulation. *Physiol. Rev.* **2001**, *81*, 629−683.

(3) Viero, C.; Shibuya, I.; Kitamura, N.; Verkhratsky, A.; Fujihara, H.; Katoh, A.; Ueta, Y.; Zingg, H. H.; Chvatal, A.; Sykova, E.; Dayanithi, G. REVIEW: Oxytocin: Crossing the bridge between basic science and pharmacotherapy. *CNS Neurosci. Ther.* **2010**, *16*, e138−56.

(4) Loup, F.; Tribollet, E.; Dubois-Dauphin, M.; Dreifuss, J. J. Localization of high-affinity binding sites for oxytocin and vasopressin in the human brain. An autoradiographic study. *Brain Res.* **1991**, *555*, 220−32.

(5) Freeman, S. M.; Inoue, K.; Smith, A. L.; Goodman, M. M.; Young, L. J. The neuroanatomical distribution of oxytocin receptor binding and mRNA in the male rhesus macaque (Macaca mulatta). *Psychoneuroendocrinology* **2014**, *45*, 128−41.

(6) Tribollet, E.; Audigier, S.; Dubois-Dauphin, M.; Dreifuss, J. J. Gonadal steroids regulate oxytocin receptors but not vasopressin receptors in the brain of male and female rats. An autoradiographical study. *Brain Res.* **1990**, *511*, 129−40.

(7) Freund-Mercier, M. J.; Stoeckel, M. E.; Palacios, J. M.; Pazos, A.; Reichhart, J. M.; Porte, A.; Richard, P. Pharmacological characteristics and anatomical distribution of [^{3}H]oxytocin-binding sites in the Wistar rat brain studied by autoradiography. *Neuroscience* **1987**, *20*, 599−614.

(8) Freund-Mercier, M. J.; Stoeckel, M. E.; Waeber, C.; Kremarik, P.; Palacios, J. M.; Richard, P. Neurophysins, rather than Receptors, are Involved in [^{3}H]Oxytocin and [^{3}H]Vasopressin Binding Detected by Autoradiography in the Hypothalamo-Neurohypophyseal System. *J. Neuroendocrinol.* **1991**, *3*, 285−95.

(9) Neumann, I. D. Brain oxytocin: a key regulator of emotional and social behaviours in both females and males. *J. Neuroendocrinol.* **2008**, *20*, 858−65.

(10) Ross, H. E.; Young, L. J. Oxytocin and the neural mechanisms regulating social cognition and affiliative behavior. *Front. Neuroendocrinol.* **2009**, *30*, 534−47.

(11) Insel, T. R.; Young, L. J. The neurobiology of attachment. *Nat. Rev. Neurosci.* **2001**, *2*, 129−36.

(12) Macdonald, K.; Macdonald, T. M. The peptide that binds: a systematic review of oxytocin and its prosocial effects in humans. *Harv. Rev. Psychiatry* **2010**, *18*, 1−21.

(13) Zink, C. F.; Meyer-Lindenberg, A. Human neuroimaging of oxytocin and vasopressin in social cognition. *Horm. Behav.* **2012**, *61*, 400−9.

(14) Meyer-Lindenberg, A.; Domes, G.; Kirsch, P.; Heinrichs, M. Oxytocin and vasopressin in the human brain: social neuropeptides for translational medicine. *Nat. Rev. Neurosci.* **2011**, *12*, 524−38.

DOI: 10.1021/acs.jmedchem.5b01080
J. Med. Chem. 2016, 59, 1800−1817

(15) Kanat, M.; Heinrichs, M.; Domes, G. Oxytocin and the social brain: Neural mechanisms and perspectives in human research. *Brain Res.* **2014**, *1580*, 160−171.
(16) Neumann, I. D. The advantage of social living: brain neuropeptides mediate the beneficial consequences of sex and motherhood. *Front. Neuroendocrinol.* **2009**, *30*, 483−96.
(17) Goldman, M.; Marlow-O'Connor, M.; Torres, I.; Carter, C. S. Diminished plasma oxytocin in schizophrenic patients with neuroendocrine dysfunction and emotional deficits. *Schizophr. Res.* **2008**, *98*, 247−55.
(18) MacDonald, K.; MacDonald, T. M.; Brune, M.; Lamb, K.; Wilson, M. P.; Golshan, S.; Feifel, D. Oxytocin and psychotherapy: a pilot study of its physiological, behavioral and subjective effects in males with depression. *Psychoneuroendocrinology* **2013**, *38*, 2831−43.
(19) Green, J. J.; Hollander, E. Autism and oxytocin: new developments in translational approaches to therapeutics. *Neurotherapeutics* **2010**, *7*, 250−7.
(20) Green, L.; Fein, D.; Modahl, C.; Feinstein, C.; Waterhouse, L.; Morris, M. Oxytocin and autistic disorder: alterations in peptide forms. *Biol. Psychiatry* **2001**, *50*, 609−13.
(21) Smith, A. L.; Freeman, S. M.; Stehouwer, J. S.; Inoue, K.; Voll, R. J.; Young, L. J.; Goodman, M. M. Synthesis and evaluation of C-11, F-18 and I-125 small molecule radioligands for detecting oxytocin receptors. *Bioorg. Med. Chem.* **2012**, *20*, 2721−38.
(22) Smith, A. L.; Freeman, S. M.; Voll, R. J.; Young, L. J.; Goodman, M. M. Investigation of an F-18 oxytocin receptor selective ligand via PET imaging. *Bioorg. Med. Chem. Lett.* **2013**, *23*, 5415−20.
(23) Smith, A. L.; Freeman, S. M.; Voll, R. J.; Young, L. J.; Goodman, M. M. Carbon-11 N-methyl alkylation of L-368,899 and in vivo PET imaging investigations for neural oxytocin receptors. *Bioorg. Med. Chem. Lett.* **2013**, *23*, 902−6.
(24) Lemaire, W.; O'Brien, J. A.; Burno, M.; Chaudhary, A. G.; Dean, D. C.; Williams, P. D.; Freidinger, R. M.; Pettibone, D. J.; Williams, D. L., Jr. A nonpeptide oxytocin receptor antagonist radioligand highly selective for human receptors. *Eur. J. Pharmacol.* **2002**, *450*, 19−28.
(25) Williams, P. D.; Anderson, P. S.; Ball, R. G.; Bock, M. G.; Carroll, L.; Chiu, S. H. L.; Clineschmidt, B. V.; Culberson, J. C.; Erb, J. M.; Evans, B. E.; Fitzpatrick, S. L.; Freidinger, R. M.; Kaufman, M. J.; Lundell, G. F.; Murphy, J. S.; Pawluczyk, J. M.; Perlow, D. S.; Pettibone, D. J.; Pitzenberg, S. M.; Thompson, K. L.; Veber, D. F.; et al. 1-((7,7-Dimethyl-2(S)-(2(S)-amino-4-(methylsulfonyl)-butyramido)bicyclo [2.2.1]-heptan-1(S)-yl)methyl)sulfonyl)-4-(2-methylphenyl)piperaz ine (L-368,899): an orally bioavailable, nonpeptide oxytocin antagonist with potential utility for managing preterm labor. *J. Med. Chem.* **1994**, *37*, 565−571.
(26) Failli, A. A.; Shumsky, J. S.; Caggiano, T. J.; Sabatucci, P. J.; Memoli, K. A.; Trybulski, E. J.; Sanders, W. J. Novel tricyclic hydroxy carboxamides and derivatives thereof tocolytic oxytocin receptor antagonists. (Wyeth) WO 02/083680, 2002.
(27) Ring, R. H.; Malberg, J. E.; Potestio, L.; Ping, J.; Boikess, S.; Luo, B.; Schechter, L. E.; Rizzo, S.; Rahman, Z.; Rosenzweig-Lipson, S. Anxiolytic-like activity of oxytocin in male mice: behavioral and autonomic evidence, therapeutic implications. *Psychopharmacology* **2006**, *185*, 218−25.
(28) Chen, X.; Liu, Y.; Liu, D. K.; Wang, P. B. 1-(2-Nitrobenzyl)-1H-pyrrole-2-carbaldehyde. *Acta Crystallogr., Sect. E: Struct. Rep. Online* **2011**, *67*, O1473.
(29) Artico, M.; DeMartino, G.; Filacchioni, G.; Giuliano, R. Studies on substances with antitumor activity. XXXVI. Anthramycin and similar compounds. I. Synthesis of 10,11-diidro-5*H*-pyrrole-(2,1-*c*)(1,4)-benzodiazepine. *Farmaco Sci.* **1969**, *24*, 276−284.
(30) Wright, W. B.; Greenblatt, E. N.; Day, I. P.; Quinones, N. Q.; Hardy, R. A. Derivatives of 11-(1-Piperazinyl)-5h-Pyrrolo[2,1-C]-[1,4]Benzodiazepine as Central Nervous-System Agents. *J. Med. Chem.* **1980**, *23*, 462−465.
(31) Tang, P. C.; Li, X.; Li, X.; Chen, Y.; Wang, B.; Zhu, Z. Phtalazinone ketone derivative, preparation method thereof and pharmaceutical use thereof. (Jiangsu Hansoh Pharmaceutical Co., Ltd.) US 2013/0131068 A1, 2013.
(32) Cheng, Y.; Prusoff, W. H. Relationship between the inhibition constant (K1) and the concentration of inhibitor which causes 50% inhibition (I50) of an enzymatic reaction. *Biochem. Pharmacol.* **1973**, *22*, 3099−3108.
(33) Donovan, S. F.; Pescatore, M. C. Method for measuring the logarithm of the octanol-water partition coefficient by using short octadecyl-poly(vinyl alcohol) high-performance liquid chromatography columns. *J. Chromatogr. A* **2002**, *952*, 47−61.
(34) Taillardat-Bertschinger, A.; Carrupt, P. A.; Barbato, F.; Testa, B. Immobilized artificial membrane HPLC in drug research. *J. Med. Chem.* **2003**, *46*, 655−665.
(35) Waterhouse, R. N. Determination of lipophilicity and its use as a predictor of blood-brain barrier penetration of molecular imaging agents. *Mol. Imaging Biol.* **2003**, *5*, 376−89.
(36) Rankovic, Z. CNS drug design: balancing physicochemical properties for optimal brain exposure. *J. Med. Chem.* **2015**, *58*, 2584−608.
(37) van de Waterbeemd, H.; Camenisch, G.; Folkers, G.; Chretien, J. R.; Raevsky, O. A. Estimation of blood-brain barrier crossing of drugs using molecular size and shape, and H-bonding descriptors. *J. Drug Target.* **1998**, *6*, 151−65.
(38) Wils, P.; Warnery, A.; Phung-Ba, V.; Legrain, S.; Scherman, D. High lipophilicity decreases drug transport across intestinal epithelial cells. *J. Pharmacol. Exp. Ther.* **1994**, *269*, 654−658.
(39) Vallabhajosula, S. Radiolabeled Molecular Imaging Probe. In *Molecular Imaging: Radiopharmaceuticals for PET and SPECT*; Springer-Verlag: Dordrecht, Heidelberg, New York, 2009; p 141.
(40) Brust, P.; van den Hoff, J.; Steinbach, J. Development of ^{18}F-labeled radiotracers for neuroreceptor imaging with Positron Emission Tomography. *Neurosci. Bull.* **2014**, *30*, 777−811.
(41) Tavares, A. A.; Lewsey, J.; Dewar, D.; Pimlott, S. L. Radiotracer properties determined by high performance liquid chromatography: a potential tool for brain radiotracer discovery. *Nucl. Med. Biol.* **2012**, *39*, 127−35.
(42) Taillardat-Bertschinger, A.; Galland, A.; Carrupt, P. A.; Testa, B. Immobilized artificial membrane liquid chromatography: proposed guidelines for technical optimization of retention measurements. *J. Chromatogr. A* **2002**, *953*, 39−53.
(43) Vraka, C.; Nics, L.; Weiss, V.; Wagner, K.; Hacker, M.; Wadsak, W.; Mitterhauser, M. Combination of high throughput HPLC methods for rapid prediction of blood−brain barrier penetration of newly developed radiotracers. *Eur. J. Nucl. Med. Mol. Imaging* **2014**, *41*, S442.
(44) Freeman, S. M.; Walum, H.; Inoue, K.; Smith, A. L.; Goodman, M. M.; Bales, K. L.; Young, L. J. Neuroanatomical distribution of oxytocin and vasopressin 1a receptors in the socially monogamous coppery titi monkey (Callicebus cupreus). *Neuroscience* **2014**, *273*, 12−23.
(45) Kaur, N. An insight into medicinal and biological significance of privileged scaffold: 1,4-benzodiazepine. *Int. J. Pharm. Bio. Sci.* **2013**, *4*, 318−337.
(46) Freund-Mercier, M. J.; Stoeckel, M. E.; Dietl, M. M.; Palacios, J. M.; Richard, P. Quantitative autoradiographic mapping of neurohypophysial hormone binding sites in the rat forebrain and pituitary gland–I. Characterization of different types of binding sites and their distribution in the Long-Evans strain. *Neuroscience* **1988**, *26*, 261−72.
(47) Colaianni, G.; Tamma, R.; Di Benedetto, A.; Yuen, T.; Sun, L.; Zaidi, M.; Zallone, A. The oxytocin-bone axis. *J. Neuroendocrinol.* **2014**, *26*, 53−7.
(48) Demeule, M.; Wenger, R. M.; Beliveau, R. Molecular interactions of cyclosporin A with P-glycoprotein. Photolabeling with cyclosporin derivatives. *J. Biol. Chem.* **1997**, *272*, 6647−52.
(49) Syvänen, S.; Lindhe, O.; Palner, M.; Kornum, B. R.; Rahman, O.; Langstrom, B.; Knudsen, G. M.; Hammarlund-Udenaes, M. Species differences in blood-brain barrier transport of three positron emission tomography radioligands with emphasis on P-glycoprotein transport. *Drug Metab. Dispos.* **2009**, *37*, 635−43.
(50) Rötering, S.; Scheunemann, M.; Fischer, S.; Hiller, A.; Peters, D.; Deuther-Conrad, W.; Brust, P. Radiosynthesis and first evaluation

DOI: 10.1021/acs.jmedchem.5b01080
J. Med. Chem. 2016, 59, 1800−1817

in mice of [^{18}F]NS14490 for molecular imaging of alpha7 nicotinic acetylcholine receptors. *Bioorg. Med. Chem.* **2013**, *21*, 2635−42.
(51) Rötering, S.; Deuther-Conrad, W.; Cumming, P.; Donat, C. K.; Scheunemann, M.; Fischer, S.; Xiong, G.; Steinbach, J.; Peters, D.; Sabri, O.; Bucerius, J.; Brust, P. Imaging of alpha7 nicotinic acetylcholine receptors in brain and cerebral vasculature of juvenile pigs with [^{18}F]NS14490. *EJNMMI Res.* **2014**, *4*, 43.
(52) Kelder, J.; Grootenhuis, P. D.; Bayada, D. M.; Delbressine, L. P.; Ploemen, J. P. Polar molecular surface as a dominating determinant for oral absorption and brain penetration of drugs. *Pharm. Res.* **1999**, *16*, 1514−9.
(53) TPSA calculation was performed by using the free Molecular Property Calculation service of Molinspiration (molinspiration.com).
(54) Ertl, P.; Rohde, B.; Selzer, P. Fast calculation of molecular polar surface area as a sum of fragment-based contributions and its application to the prediction of drug transport properties. *J. Med. Chem.* **2000**, *43*, 3714−7.
(55) Pajouhesh, H.; Lenz, G. R. Medicinal chemical properties of successful central nervous system drugs. *NeuroRx* **2005**, *2*, 541−53.
(56) Brust, P.; Patt, J. T.; Deuther-Conrad, W.; Becker, G.; Patt, M.; Schildan, A.; Sorger, D.; Kendziorra, K.; Meyer, P.; Steinbach, J.; Sabri, O. In vivo measurement of nicotinic acetylcholine receptors with [^{18}F]norchloro-fluoro-homoepibatidine. *Synapse* **2008**, *62*, 205−18.
(57) Deuther-Conrad, W.; Fischer, S.; Hiller, A.; Becker, G.; Cumming, P.; Xiong, G.; Funke, U.; Sabri, O.; Peters, D.; Brust, P. Assessment of alpha7 nicotinic acetylcholine receptor availability in juvenile pig brain with [^{18}F]NS10743. *Eur. J. Nucl. Med. Mol. Imaging* **2011**, *38*, 1541−9.
(58) Brust, P.; Zessin, J.; Kuwabara, H.; Pawelke, B.; Kretzschmar, M.; Hinz, R.; Bergman, J.; Eskola, O.; Solin, O.; Steinbach, J.; Johannsen, B. Positron emission tomography imaging of the serotonin transporter in the pig brain using [^{11}C](+)-McN5652 and S-([^{18}F]fluoromethyl)-(+)-McN5652. *Synapse* **2003**, *47*, 143−51.

DOI: 10.1021/acs.jmedchem.5b01080
J. Med. Chem. 2016, 59, 1800−1817

4 Summary and Discussion

This thesis highlights the demand of preclinical *in vitro* studies to predict BBB penetration and interactions with the efflux transporter P-gp in early tracer development.

It was shown that high throughput methods were refined and are now routinely available for a broad range of substance classes to gain essential information about the drug properties while being cost and time efficient.

The special emphasis was placed on the lipophilicity and the predictive potential of this value concerning BBB penetration. In the **first manuscript** 121 substances were experimentally tested including the most relevant brain radiotracer. Furthermore, selected data were compared to two different methods: the traditional shake-flask method and the calculated logP value. A big variance in the results and a different potential to predict brain uptake was shown. In the letter to the editor (**manuscript two**), it was further highlighted that using a single value as the logP is inexpedient to predict the complexity of BBB penetration.

In **third manuscript** additionally, two other HPLC methods were established, measuring plasma protein binding (PPB) and the membrane coefficient (K_{IAM}) and permeability (Pm) of a drug. These values are supposed to correlate with brain uptake. Various drugs with different pharmacological characteristics (113 compounds) were experimentally tested and these molecules were split into three groups due to the ability to cross the BBB (CNS positive radiotracers, CNS negative drugs and drugs with interactions to efflux transporters). A level of significance between the groups was only reached for the experimental logP value, however showing a broad overlap among the groups. As a matter of fact, the influence of the logP strongly depends on the selected method (ClogP versus HPLC logP). Hence, prediction using solely a single parameter is intricate and interpretation of the influence of a value should always refer to the used method.

In the **fourth manuscript,** a new method to predict potential interactions of PET tracers with the most potent human efflux transporter, P-gp, is presented. Thereby, seven PET tracers (P-gp substrates and non-substrates) were evaluated in this new real-time kinetic model and the results of the substrates compared to a standard uptake assay.

4.1 Molecular Weight

The compound selection for the classification into these three drug groups was based on the molecular weight. Molecular weight is attributed to have a major impact on the BBB penetration and on the interactions with efflux transporters. Approximately 100% of large molecules do not show any brain uptake. Additionally, it is known that ~98% of small molecules do not cross the BBB. Therefore, the groups of CNS negative drugs and drugs with interactions to efflux transporters contain a certain percentage of compounds with low molecular weight. For the CNS negative drugs, the total percentage was 77% of small molecules (≤500 Da) and for compounds interacting with efflux transporters, half (50%) of the tested compounds were small molecules and 72.5% had a lower than 600 Da mass. A huge challenge is the selection of CNS non-penetrating compounds. Indeed, the selection of the CNS non-penetrating compounds were based on literature research (no brain uptake reported) or no known or no reported effect or side effects in CNS. However, the most direct information about brain exposure can be taken from imaging studies. A database covering exclusively PET and SPECT tracers (peripheral, central and efflux transporter substrates and inhibitors) would be favorable to avoid misclassification into the groups. Indeed, that would have reduced the number of tested compounds.

4.2 Lipophilicity

The lipophilicity will remain an important factor in drug development since it is known to contribute to membrane penetration, biodistribution, non-specific binding, binding to plasma proteins, on metabolism and excretion. However, it is not the sole factor predicting these pharmacokinetic properties. Within this thesis, it was shown that the logP values of the same compound derived from different methods are not comparable. Thus, interpreting the effect of logP, originating from various methods on BBB penetration is inadequate. Furthermore, it was demonstrated that the logP, evaluated by the presented HPLC method, has a significant predictive value on BBB penetration when comparing the three groups in contrast to the calculated ClogP values. Hence, the predictive power of these values on pharmacokinetic properties strongly depends on the selected method. However, there is a broad overlap of the HPLC logP values among the different groups. Thus, the establishment of an “optimum” range or threshold is therefore inexpedient.

4.3 High Performance Bioaffinity Chromatography (HPBAC)

In radiopharmaceutical sciences, HPBAC continuously gains in popularity. Since in 2012 an article was published, correlating the measured Pm and the PPB of ten radiotracers with the %ID of the whole brain. Additionally, K_{IAM} was correlated with the binding potential (BP_{ND}) of imaging studies, showing a strong correlation for this parameters and brain uptake. On the contrary, the correlation of logP measurements with the %ID showed a weaker relationship (20). However, only these ten radiotracers that serve as reference values are found in literature.

4.4 Plasma Protein Binding using HPBAC (HSA)

Besides the discussion on the effect of the logP value, there is also a long-standing debate on the influence of PPB on the tracer availability at the target area. The mathematical model of the free drug hypothesis still persists in radiopharmaceutical sciences, especially, as the free drug concentration is used for kinetic modeling approaches in PET imaging. Within this thesis, a high throughput method is presented, which is reliable for a broad range of compounds. This method strongly correlates to the gold standard ultrafiltration method, which is in accordance to literature. The results of the different examined groups did not show a significant difference in the PPB group mean values. Additionally, also here, an excessive overlapping length of the single values was found between the groups. Both findings together indicate that the PPB is not a crucial factor for the prediction of the BBB penetration at early stages of drug development and not useful for candidate selection.

4.5 Fluid Membrane Coefficient and Permeability using HPBAC (IAM)

A comparison of Pm and K_{IAM} results among the groups showed a trend of higher values in the CNS_{neg} drugs and in the $DRUG_{efflux}$ group. However, these results were not significant and overlapping in a broad range. Moreover, difficulties to interpret and compare data occur, since different methods using IAM chromatography are found, resulting in divergent K_{IAM} values. They vary in the content of organic phase (0% to

70%), the pH of aqueous phase and the number of iterations which are used to extrapolate to 100% aqueous phase. To obtain comparable and reliable results, it was necessary to adapt the method in such a way that a broad range of different compounds can be tested using the same setup.

4.6 In vitro Real-Time Assay to Predict Interactions with the Human P-gp

On the one hand, this thesis points out the challenges of PET imaging of efflux transporters and on the other hand the importance of understanding the efflux transporters and their influence on drug pharmacokinetics as well as their involvement in neurological diseases and drug resistance. Furthermore, the special challenges in imaging efflux transporters were emphasized. Thereby, it was shown that there is a high demand of new PET tracers (inhibitors and substrates) with high affinity (<5nM) and high selectivity in the absence of interfering radiometabolites. Consequently, new *in vitro* methods which reliably predict interactions with various efflux transporters by using the PET tracers directly, are of high interest. This thesis includes a new method, which measures the real-time uptake of the candidate tracers to predict interactions towards P-gp. The greatest advantage is the direct use of the PET tracer in a concentration which does not exceed the *in vivo* situation (subnanomolar range). To this end, concentration depending process differences in the outcome that occur from labeling with other radionuclides might be prevented.

5 Conclusion

Understanding the BBB is clearly the bottleneck in CNS drug development. The diverse strategies using mostly *in silico* methods are not promising. Accordingly, exceptions to these rules create new rules. According to the presented results, the fundamental weakness is the impossibility to compare logP values from different methods. Therefore, using different methods leads to inconsistent interpretations of the influence of these values.

This thesis evaluated the logP and PPB on the basis of high throughput methods and additionally generated an *in vitro* method, which can be used to predict interactions with P-gp. Three HPLC methods were presented and a high number of reference values were collected and the experimental results were discussed in respect to their influence on BBB penetration.

Overall, the results discussed in this thesis, comprise four manuscripts that were either published or are under review. Additionally, a scientific discussion was set off, after the publication of the manuscript “LogP, a yesterday’s value?”, which was also highlighted on the cover of “Nuclear Medicine and Biology”. This gave the opportunity to publish further details in a reply letter to the editor, which was also highlighted on the cover in November.

All articles were submitted to the peer-reviewed journals Nuclear Medicine and Biology (Impact factor 2.426).

Two of the manuscripts are published:

Vraka C, Nics L, Wagner KH., Hacker M, Wadsak W, Mitterhauser M. LogP, a yesterday’s value? Nucl Med Biol. 2017, Mar 20; 50:1-10

Vraka C and Mitterhauser M “Reconsider LogP!” Nucl Med Biol. 2017; 54:p42

The following authorship is in review process:

Vraka C, Mijailovic S, Fröhlich V, Wadsak W, Wagner KH, Hacker M, Mitterhauser M. Expanding LogP: Present Possibilities. Submitted, 2017 September 22nd, Journal of Nuclear Medicine and Biology, (NUCMEDBIO_2017_232).

Last manuscript was submitted on 13th November 2017:

Vraka C, Dumanic M, Racz T, Pichler F, Philippe C, Balber T, Klebermass EM, Wagner KH, Hacker M, Wadsak W, Mitterhauser M. A New Model for the Prediction of the Interaction of Radiotracers with the P-glycoprotein (P-gp) transporter (NUCMEDBIO_2017_285).

6 Outlook

A future manuscript is in progress: the data set of the three presented drug groups (cf. manuscript 3) was extended with calculated values (ClogP, PSA, RNB, HBA and HBD) derived from different software and available drug databases. The group comparison of every single parameter shall be analysed by a supervised machine learning (SML) algorithm. SML approaches provide high sensitivity and specificity over heterogeneous and independent datasets. As it is highly generic, it does not require any prior knowledge about the origin and nature of features it operates with. Hence, it calculates the weighting of the parameters based on the drug classification (preliminary data presented as poster at the ISRS, 2017 Dresden, Germany).

The most popular concept is optimizing the physicochemical properties of a CNS drugs as there is a plenty of rules, threshold and ranges available. As discussed in this thesis, this concept is ranging too short and there is a need of improved understanding of passive diffusion through the BBB. However, there are a few more ideas and concepts about drug delivery known and studied, which maybe have fallen in oblivion: prodrug systems, intracerebral application, olfactory route, Trojan-horse concepts, modulation of the BBB, inhibition of efflux transporters, delivery via endogens transporters and focusing on penetrating peptides or nanoparticles. A lot of these trails failed or are associated with serve side effects. Indeed, some of the other concepts may be interesting especially for radiopharmaceutical sciences as penetrating peptides and should be considered for future work.

Bibliography

1. Alavijeh MS, Chishty M, Qaiser MZ, Palmer AM. Drug metabolism and pharmacokinetics, the blood-brain barrier, and central nervous system drug discovery. NeuroRX. 2005 Oct;2(4):554–71.

2. Pardridge WM. The Blood-Brain Barrier: Bottleneck in Brain Drug Development. NeuroRx. 2005 Jan;2(1):3–14.

3. WHO | Mental disorders affect one in four people [Internet]. WHO. [cited 2017 Apr 6]. Available from: http://www.who.int/whr/2001/media_centre/press_release/en/

4. Welcome to BCC Live Chat [Internet]. [cited 2017 Jul 18]. Available from: https://secure.livechatinc.com/licence/7126481/open_chat.cgi?groups=0&embedded=1&newWebserv=undefined&__lc_vv=2&session_id=S1500385048.c168445e8e&server=secure.livechatinc.com#https://www.bccresearch.com/market-research/pharmaceuticals/drugs-central-nervous-system-disorders-phm068a.html

5. Lindsley CW. 2013 Statistics for Global Prescription Medications: CNS Therapeutics Maintain a Leading Position among Small Molecule Therapeutics. ACS Chem Neurosci. 2014 Apr 16;5(4):250–1.

6. Lammertsma AA. Positron emission tomography. Brain Topogr. 1992;5(2):113–7.

7. Ollinger JM, Fessler JA. Positron-emission tomography. IEEE Signal Process Mag. 1997 Jan;14(1):43–55.

8. Bailey DL, editor. Positron emission tomography: basic sciences. New York: Springer; 2005. 382 p.

9. Spence AM, Mankoff DA, Muzi M. Positron emission tomography imaging of brain tumors. Neuroimaging Clin N Am. 2003 Nov;13(4):717–39.

10. Morris ED, Endres CJ, Schmidt KC, Christian BT, Muzic Jr. RF, Fisher RE. Chapter 23 - Kinetic Modeling in Positron Emission Tomography. In: Aarsvold MNWN, editor. Emission Tomography [Internet]. San Diego: Academic Press; 2004 [cited 2015 Jul 23]. p. 499–540. Available from: http://www.sciencedirect.com/science/article/pii/B9780127444826500260

11. Innis RB, Cunningham VJ, Delforge J, Fujita M, Gjedde A, Gunn RN, et al. Consensus nomenclature for in vivo imaging of reversibly binding radioligands. J Cereb Blood Flow 38 Metab. 2007 Sep;27(9):1533–9.

12. Matthews PM, Rabiner EA, Passchier J, Gunn RN. Positron emission tomography molecular imaging for drug development: PET for drug development. Br J Clin Pharmacol. 2012 Feb;73(2):175–86.

13. Rizzo G, Veronese M, Tonietto M, Zanotti-Fregonara P, Turkheimer FE, Bertoldo A. Kinetic Modeling without Accounting for the Vascular Component Impairs the

Quantification of [^{11} C]PBR28 Brain PET Data. J Cereb Blood Flow Metab. 2014 Jun;34(6):1060–9.

14. Pike VW. PET radiotracers: crossing the blood–brain barrier and surviving metabolism. Trends Pharmacol Sci. 2009 Aug;30(8):431–40.

15. Laruelle M. Relationships between radiotracer properties and image quality in molecular imaging of the brain with positron emission tomography. Mol Imaging Biol. 2003 Dec;5(6):363–75.

16. Pardridge WM. BLOOD-BRAIN BARRIER DRUG TARGETING: THE FUTURE OF BRAIN DRUG DEVELOPMENT. Mol Interv. 2003 Mar 1;3(2):90–105.

17. Reichel A. The role of blood-brain barrier studies in the pharmaceutical industry. Curr Drug Metab. 2006 Feb;7(2):183–203.

18. Abraham MH, Acree WE, Fahr A, Liu X. Analysis of immobilized artificial membrane retention factors for both neutral and ionic species. J Chromatogr A. 2013 Jul;1298:44–9.

19. De Vrieze M, Lynen F, Chen K, Szucs R, Sandra P. Predicting drug penetration across the blood–brain barrier: comparison of micellar liquid chromatography and immobilized artificial membrane liquid chromatography. Anal Bioanal Chem. 2013 Jul;405(18):6029–41.

20. Tavares AAS, Lewsey J, Dewar D, Pimlott SL. Radiotracer properties determined by high performance liquid chromatography: a potential tool for brain radiotracer discovery. Nucl Med Biol. 2012 Jan;39(1):127–35.

21. Giaginis C, Tsantili-Kakoulidou A. Alternative measures of lipophilicity: From octanol-water partitioning to IAM retention. J Pharm Sci. 2008 Aug;97(8):2984–3004.

22. Vrakas D, Giaginis C, Tsantili-Kakoulidou A. Different retention behavior of structurally diverse basic and neutral drugs in immobilized artificial membrane and reversed-phase high performance liquid chromatography: Comparison with octanol–water partitioning. J Chromatogr A. 2006;(1116):158–64.

23. Rankovic Z. CNS Drug Design: Balancing Physicochemical Properties for Optimal Brain Exposure. J Med Chem. 2015 Mar 26;58(6):2584–608.

24. Ghose AK, Herbertz T, Hudkins RL, Dorsey BD, Mallamo JP. Knowledge-Based, Central Nervous System (CNS) Lead Selection and Lead Optimization for CNS Drug Discovery. ACS Chem Neurosci. 2012 Jan 18;3(1):50–68.

25. Banks WA. Characteristics of compounds that cross the blood-brain barrier. BMC Neurol. 2009;9(Suppl 1):S3.

26. Pardridge WM. Drug transport across the blood–brain barrier. J Cereb Blood Flow Metab. 2012 Nov;32(11):1959–72.

27. Pajouhesh H, Lenz GR. Medicinal Chemical Properties of Successful Central Nervous System Drugs. NeuroRx. 2005 Oct;2(4):541–53.

28. Lipinski CA, Lombardo F, Dominy BW, Feeney PJ. Experimental and computational approaches to estimate solubility and permeability in drug discovery and development settings. Adv Drug Deliv Rev. 1997 Jan;23(1–3):3–25.

29. Lipinski CA. Drug-like properties and the causes of poor solubility and poor permeability. J Pharmacol Toxicol Methods. 2000 Aug;44(1):235–49.

30. Lipinski CA, Lombardo F, Dominy BW, Feeney PJ. Experimental and computational approaches to estimate solubility and permeability in drug discovery and development settings. Adv Drug Deliv Rev. 2001 Mar 1;46(1–3):3–26.

31. Lipinski CA. Lead- and drug-like compounds: the rule-of-five revolution. Drug Discov Today Technol. 2004 Dec;1(4):337–41.

32. Norinder U, Haeberlein M. Computational approaches to the prediction of the blood-brain distribution. Adv Drug Deliv Rev. 2002 Mar 31;54(3):291–313.

33. Clark DE. In silico prediction of blood–brain barrier permeation. Drug Discov Today. 2003 Oktober;8(20):927–33.

34. Rankovic Z. CNS Drug Design: Balancing Physicochemical Properties for Optimal Brain Exposure. J Med Chem. 2015 Mar 26;58(6):2584–608.

35. Hitchcock SA, Pennington LD. Structure-brain exposure relationships. J Med Chem. 2006 Dec 28;49(26):7559–83.

36. Hansch C, Steward AR, Anderson SM, Bentley D. The parabolic dependence of drug action upon lipophilic character as revealed by a study of hypnotics. J Med Chem. 1968 Jan;11(1):1–11.

37. Young RC, Mitchell RC, Brown TH, Ganellin CR, Griffiths R, Jones M, et al. Development of a new physicochemical model for brain penetration and its application to the design of centrally acting H2 receptor histamine antagonists. J Med Chem. 1988 Mar;31(3):656–71.

38. van de Waterbeemd H, Camenisch G, Folkers G, Chretien JR, Raevsky OA. Estimation of blood-brain barrier crossing of drugs using molecular size and shape, and H-bonding descriptors. J Drug Target. 1998;6(2):151–65.

39. Kelder J, Grootenhuis PD, Bayada DM, Delbressine LP, Ploemen JP. Polar molecular surface as a dominating determinant for oral absorption and brain penetration of drugs. Pharm Res. 1999 Oct;16(10):1514–9.

40. Doan KMM, Humphreys JE, Webster LO, Wring SA, Shampine LJ, Serabjit-Singh CJ, et al. Passive Permeability and P-Glycoprotein-Mediated Efflux Differentiate Central Nervous System (CNS) and Non-CNS Marketed Drugs. J Pharmacol Exp Ther. 2002 Dec 1;303(3):1029–37.

41. Didziapetris R, Japertas P, Avdeef A, Petrauskas A. Classification analysis of P-glycoprotein substrate specificity. J Drug Target. 2003 Aug;11(7):391–406.

42. Leeson PD, Davis AM. Time-related differences in the physical property profiles of oral drugs. J Med Chem. 2004 Dec 2;47(25):6338–48.

43. Gleeson MP. Generation of a set of simple, interpretable ADMET rules of thumb. J Med Chem. 2008 Feb 28;51(4):817–34.

44. Waring MJ. Defining optimum lipophilicity and molecular weight ranges for drug candidates—Molecular weight dependent lower logD limits based on permeability. Bioorg Med Chem Lett. 2009 May;19(10):2844–51.

45. Wager TT, Hou X, Verhoest PR, Villalobos A. Moving beyond Rules: The Development of a Central Nervous System Multiparameter Optimization (CNS MPO) Approach To Enable Alignment of Druglike Properties. ACS Chem Neurosci. 2010 Jun 16;1(6):435–49.

46. Wager TT, Chandrasekaran RY, Hou X, Troutman MD, Verhoest PR, Villalobos A, et al. Defining Desirable Central Nervous System Drug Space through the Alignment of Molecular Properties, in Vitro ADME, and Safety Attributes. ACS Chem Neurosci. 2010 Jun 16;1(6):420–34.

47. Hitchcock SA. Structural Modifications that Alter the P-Glycoprotein Efflux Properties of Compounds. J Med Chem. 2012 Jun 14;55(11):4877–95.

48. Desai PV, Sawada GA, Watson IA, Raub TJ. Integration of in Silico and in Vitro Tools for Scaffold Optimization during Drug Discovery: Predicting P-Glycoprotein Efflux. Mol Pharm. 2013 Apr;10(4):1249–61.

49. Vraka C, Nics L, Wagner K-H, Hacker M, Wadsak W, Mitterhauser M. LogP, a yesterday's value? Nucl Med Biol. 2017 Mar 21;50:1–10.

50. Wilson AA, Jin L, Garcia A, DaSilva JN, Houle S. An admonition when measuring the lipophilicity of radiotracers using counting techniques. Appl Radiat Isot. 2001 Feb;54(2):203–8.

51. McNaught AD, Wilkinson A. IUPAC, Compendium of Chemical Terminology-Gold Book [Internet]. second edition. Oxford: Blackwell Scientific Publications; 1997. Available from: http://goldbook.iupac.org (2006)

52. Habgood MD, Begley DJ, Abbott NJ. Determinants of passive drug entry into the central nervous system. Cell Mol Neurobiol. 2000 Apr;20(2):231–53.

53. Veber DF, Johnson SR, Cheng H-Y, Smith BR, Ward KW, Kopple KD. Molecular properties that influence the oral bioavailability of drug candidates. J Med Chem. 2002 Jun 6;45(12):2615–23.

54. Ertl P, Rohde B, Selzer P. Fast calculation of molecular polar surface area as a sum of fragment-based contributions and its application to the prediction of drug transport properties. J Med Chem. 2000 Oct 5;43(20):3714–7.

55. Rankovic Z. CNS Physicochemical Property Space Shaped by a Diverse Set of Molecules with Experimentally Determined Exposure in the Mouse Brain: Miniperspective. J Med Chem. 2017 Jul 27;60(14):5943–54.

56. Valko K, Nunhuck S, Bevan C, Abraham MH, Reynolds DP. Fast gradient HPLC method to determine compounds binding to human serum albumin. Relationships with octanol/water and immobilized artificial membrane lipophilicity. J Pharm Sci. 2003;92(11):2236–2248.

57. Hollósy F, Valkó K, Hersey A, Nunhuck S, Kéri G, Bevan C. Estimation of Volume of Distribution in Humans from High Throughput HPLC-Based Measurements of Human Serum Albumin Binding and Immobilized Artificial Membrane Partitioning. J Med Chem. 2006 Nov;49(24):6958–71.

58. Smith DA, Di L, Kerns EH. The effect of plasma protein binding on in vivo efficacy: misconceptions in drug discovery. Nat Rev Drug Discov. 2010 Dec;9(12):929–39.

59. Chung TDY, Terry DB, Smith LH. In Vitro and In Vivo Assessment of ADME and PK Properties During Lead Selection and Lead Optimization – Guidelines, Benchmarks and Rules of Thumb. In: Sittampalam GS, Coussens NP, Brimacombe K, Grossman A, Arkin M, Auld D, et al., editors. Assay Guidance Manual [Internet]. Bethesda (MD): Eli Lilly & Company and the National Center for Advancing Translational Sciences; 2004 [cited 2017 Aug 22]. Available from: http://www.ncbi.nlm.nih.gov/books/NBK326710/

60. Liu X, Wright M, Hop CECA. Rational Use of Plasma Protein and Tissue Binding Data in Drug Design: Miniperspective. J Med Chem. 2014 Oct 23;57(20):8238–48.

61. Hillery AM, Lloyd AW, Swarbrick J, editors. Drug delivery and targeting for pharmacists and pharmaceutical scientists. London: Taylor & Francis; 2001. 475 p.

62. Davson H, Segal MB. Physiology of the CSF and blood-brain barriers. Boca Raton: CRC Press; 1996. 822 p.

63. Price JC, Mayberg HS, Dannals RF, Wilson AA, Ravert HT, Sadzot B, et al. Measurement of Benzodiazepine Receptor Number and Affinity in Humans Using Tracer Kinetic Modeling, Positron Emission Tomography, and [^{11} C]Flumazenil. J Cereb Blood Flow Metab. 1993 Jul;13(4):656–67.

64. Parsey RV, Slifstein M, Hwang D-R, Abi-Dargham A, Simpson N, Mawlawi O, et al. Validation and Reproducibility of Measurement of 5-HT $_{1A}$ Receptor Parameters with [*carbonyl* - ^{11} C]WAY-100635 in Humans: Comparison of Arterial and Reference Tissue Input Functions. J Cereb Blood Flow Metab. 2000 Jul;20(7):1111–33.

65. Gandelman MS, Baldwin RM, Zoghbi SS, Zea-Ponce Y, Innis RB. Evaluation of Ultrafiltration for the Free-Fraction Determination of Single Photon Emission Computed Tomography (SPECT) Radiotracers: β-CIT, IBF, and Iomazenil. J Pharm Sci. 1994 Jul;83(7):1014–9.

66. Barré J, Chamouard JM, Houin G, Tillement JP. Equilibrium dialysis, ultrafiltration, and ultracentrifugation compared for determining the plasma-protein-binding characteristics of valproic acid. Clin Chem. 1985 Jan 1;31(1):60–4.

67. Culot M, Fabulas - da Costa A, Sevin E, Szorath E, Martinsson S, Renftel M, et al. A Simple Method for Assessing Free Brain/Free Plasma Ratios Using an In Vitro Model of the Blood Brain Barrier. Deli MA, editor. PLoS ONE. 2013 Dec 3;8(12):e80634.

68. Hage DS, Anguizola J, Barnaby O, Jackson A, Yoo MJ, Papastavros E, et al. Characterization of drug interactions with serum proteins by using high-performance affinity chromatography. Curr Drug Metab. 2011 May;12(4):313–28.

69. Singh SS, Mehta J. Measurement of drug–protein binding by immobilized human serum albumin-HPLC and comparison with ultrafiltration. J Chromatogr B. 2006 Apr;834(1–2):108–16.

70. Pidgeon C, Venkataram UV. Immobilized artificial membrane chromatography: supports composed of membrane lipids. Anal Biochem. 1989 Jan;176(1):36–47.

71. Pidgeon C, Ong S, Liu H, Qiu X, Pidgeon M, Dantzig AH, et al. IAM Chromatography: An in Vitro Screen for Predicting Drug Membrane Permeability. J Med Chem. 1995;(38):590–4.

72. Ong S, Liu H, Pidgeon C. Immobilized-artificial-membrane chromatography: measurements of membrane partition coefficient and predicting drug membrane permeability. J Chromatogr A. 1996;(728):113–28.

73. Taillardat-Bertschinger A, Carrupt P-A, Barbato F, Testa B. Immobilized artificial membrane HPLC in drug research. J Med Chem. 2003 Feb 27;46(5):655–65.

74. Yang CY, Cai SJ, Liu H, Pidgeon C. Immobilized Artificial Membranes - screens for drug membrane interactions. Adv Drug Deliv Rev. 1996;(23):229–56.

75. Yoon CH. Rapid Screening of Blood-Brain Barrier Penetration of Drugs Using the Immobilized Artificial Membrane Phosphatidylcholine Column Chromatography. J Biomol Screen. 2005 Oct 18;11(1):13–20.

76. Mensch J, L LJ, Sanderson W, Melis A, Mackie C, Verreck G, et al. Application of PAMPA-models to predict BBB permeability including efflux ratio, plasma protein binding and physicochemical parameters. Int J Pharm. 2010 Aug;395(1–2):182–97.

77. Agarwal S, Jain R, Pal D, Mitra AK. Functional characterization of peptide transporters in MDCKII-MDR1 cell line as a model for oral absorption studies. Int J Pharm. 2007 Mar 6;332(1–2):147–52.

78. Vandenhaute E, Sevin E, Hallier-Vanuxeem D, Dehouck M-P, Cecchelli R. Case study: adapting in vitro blood-brain barrier models for use in early-stage drug discovery. Drug Discov Today. 2012 Apr;17(7–8):285–90.

79. Nakhlband, Ailar, Omidi, Yadollah. Barrier Functionality of Porcine and Bovine Brain Capillary Endothelial Cells. 2011 [cited 2014 Oct 28]; Available from: http://dx.doi.org/10.5681/bi.2011.021

80. Cecchelli R, Berezowski V, Lundquist S, Culot M, Renftel M, Dehouck M-P, et al. Modelling of the blood–brain barrier in drug discovery and development. Nat Rev Drug Discov. 2007 Aug;6(8):650–61.

81. Cecchelli R, Dehouck B, Descamps L, Fenart L, Buée-Scherrer V, Duhem C, et al. In vitro model for evaluating drug transport across the blood–brain barrier. Adv Drug Deliv Rev. 1999 Apr;36(2–3):165–78.

82. Dehouck MP, Méresse S, Delorme P, Fruchart JC, Cecchelli R. An easier, reproducible, and mass-production method to study the blood-brain barrier in vitro. J Neurochem. 1990 May;54(5):1798–801.

83. Weksler B, Romero IA, Couraud P-O. The hCMEC/D3 cell line as a model of the human blood brain barrier. Fluids Barriers CNS. 2013;10(1):16.

84. Abbott NJ, Rönnbäck L, Hansson E. Astrocyte–endothelial interactions at the blood–brain barrier. Nat Rev Neurosci. 2006 Jan;7(1):41–53.

85. Di L, Kerns EH, Bezar IF, PETUSKY SL, HUANG Y. DRUG DISCOVERY INTERFACE Comparison of Blood–Brain Barrier Permeability Assays: In Situ Brain Perfusion, MDR1-MDCKII and PAMPA-BBB. J Pharm Sci. 2008 Jun;98(6):1980–90.

86. Culot M, Lundquist S, Vanuxeem D, Nion S, Landry C, Delplace Y, et al. An in vitro blood-brain barrier model for high throughput (HTS) toxicological screening. Toxicol In Vitro. 2008 Apr;22(3):799–811.

87. Abbott NJ, Patabendige AAK, Dolman DEM, Yusof SR, Begley DJ. Structure and function of the blood–brain barrier. Neurobiol Dis. 2010 Jan;37(1):13–25.

88. Laruelle M, Slifstein M, Huang Y. Relationships between radiotracer properties and image quality in molecular imaging of the brain with positron emission tomography. Mol Imaging Biol MIB Off Publ Acad Mol Imaging. 2003 Dec;5(6):363–75.

89. Vogelgesang S, Warzok RW, Cascorbi I, Kunert-Keil C, Schroeder E, Kroemer HK, et al. The role of P-glycoprotein in cerebral amyloid angiopathy; implications for the early pathogenesis of Alzheimer's disease. Curr Alzheimer Res. 2004 May;1(2):121–5.

90. Luurtsema G, Molthoff CFM, Schuit RC, Windhorst AD, Lammertsma AA, Franssen EJF. Evaluation of (R)-[11C]verapamil as PET tracer of P-glycoprotein function in the blood–brain barrier: kinetics and metabolism in the rat. Nucl Med Biol. 2005 Jan;32(1):87–93.

91. Theodoulou FL, Kerr ID. ABC transporter research: going strong 40 years on. Biochem Soc Trans. 2015 Oct 1;43(5):1033–40.

92. Brinkmann U, Roots I, Eichelbaum M. Pharmacogenetics of the human drug-transporter gene MDR1: impact of polymorphisms on pharmacotherapy. Drug Discov Today. 2001 Aug 15;6(16):835–9.

93. Chen Z, Shi T, Zhang L, Zhu P, Deng M, Huang C, et al. Mammalian drug efflux transporters of the ATP binding cassette (ABC) family in multidrug resistance: A review of the past decade. Cancer Lett. 2016 Jan 1;370(1):153–64.

94. Endres CJ, Hsiao P, Chung FS, Unadkat JD. The role of transporters in drug interactions. Eur J Pharm Sci Off J Eur Fed Pharm Sci. 2006 Apr;27(5):501–17.

95. Thiebaut F, Tsuruo T, Hamada H, Gottesman MM, Pastan I, Willingham MC. Cellular localization of the multidrug-resistance gene product P-glycoprotein in normal human tissues. Proc Natl Acad Sci U S A. 1987 Nov;84(21):7735–8.

96. Cordon-Cardo C, O'Brien JP, Boccia J, Casals D, Bertino JR, Melamed MR. Expression of the multidrug resistance gene product (P-glycoprotein) in human normal and tumor tissues. J Histochem Cytochem Off J Histochem Soc. 1990 Sep;38(9):1277–87.

97. Wanek T, Mairinger S, Langer O. Radioligands targeting P-glycoprotein and other drug efflux proteins at the blood–brain barrier. J Label Compd Radiopharm. 2013 März;56(3–4):68–77.

98. Golden PL, Pollack GM. Blood-brain barrier efflux transport. J Pharm Sci. 2003 Sep;92(9):1739–53.

99. Kannan P, John C, Zoghbi SS, Halldin C, Gottesman MM, Innis RB, et al. Imaging the Function of P-Glycoprotein With Radiotracers: Pharmacokinetics and In Vivo Applications. Clin Pharmacol 38 Ther. 2009 Oct;86(4):368–77.

100. Römermann K, Wanek T, Bankstahl M, Bankstahl JP, Fedrowitz M, Müller M, et al. (R)-[11C]verapamil is selectively transported by murine and human P-glycoprotein at the blood–brain barrier, and not by MRP1 and BCRP. Nucl Med Biol. 2013 Oct;40(7):873–8.

101. Colabufo NA, Berardi F, Contino M, Niso M, Perrone R. ABC pumps and their role in active drug transport. Curr Top Med Chem. 2009;9(2):119–29.

102. Bauer M, Karch R, Zeitlinger M, Philippe C, Römermann K, Stanek J, et al. Approaching complete inhibition of P-glycoprotein at the human blood-brain barrier: an (R)-[11C]verapamil PET study. J Cereb Blood Flow Metab Off J Int Soc Cereb Blood Flow Metab. 2015 May;35(5):743–6.

103. Müllauer J, Kuntner C, Bauer M, Bankstahl JP, Müller M, Voskuyl RA, et al. Pharmacokinetic modeling of P-glycoprotein function at the rat and human blood-brain barriers studied with (R)-[11C]verapamil positron emission tomography. EJNMMI Res. 2012;2(1):58.

104. Müllauer J, Karch R, Bankstahl JP, Bankstahl M, Stanek J, Wanek T, et al. Assessment of cerebral P-glycoprotein expression and function with PET by

combined [11C]inhibitor and [11C]substrate scans in rats. Nucl Med Biol. 2013 Aug;40(6):755–63.

105. Wanek T, Kuntner C, Bankstahl JP, Bankstahl M, Stanek J, Sauberer M, et al. A comparative small-animal PET evaluation of [11C]tariquidar, [11C]elacridar and (R)-[11C]verapamil for detection of P-glycoprotein-expressing murine breast cancer. Eur J Nucl Med Mol Imaging. 2012 Jan;39(1):149–59.

106. Bauer M, Zeitlinger M, Karch R, Matzneller P, Stanek J, Jäger W, et al. Pgp-mediated interaction between (R)-[11C]verapamil and tariquidar at the human blood-brain barrier: a comparison with rat data. Clin Pharmacol Ther. 2012 Feb;91(2):227–33.

107. Weidner LD, Fung KL, Kannan P, Moen JK, Kumar JS, Mulder J, et al. Tariquidar Is an Inhibitor and Not a Substrate of Human and Mouse P-glycoprotein. Drug Metab Dispos. 2016 Jan 16;44(2):275–82.

108. Langer O. Use of PET Imaging to Evaluate Transporter-Mediated Drug-Drug Interactions. J Clin Pharmacol. 2016 Jul;56 Suppl 7:S143-156.

109. Kannan P, Pike VW, Halldin C, Langer O, Gottesman MM, Innis RB, et al. Factors that limit positron emission tomography imaging of p-glycoprotein density at the blood-brain barrier. Mol Pharm. 2013 Jun 3;10(6):2222–9.

110. Udo de Haes JI, Cremers TIFH, Bosker F-J, Postema F, Tiemersma-Wegman TD, den Boer JA. Effect of Increased Serotonin Levels on [18F]MPPF Binding in Rat Brain: Fenfluramine vs the Combination of Citalopram and Ketanserin. Neuropsychopharmacology. 2005 Sep;30(9):1624–31.

Abbreviations

AC (astrocytes)

ADME (absorption, distribution, metabolism, excretion)

AGM (astrocytes growth medium, Lonza)

α-gp or AGP (alpha-glycoprotein)

Al-OH (aluminiumhydroxide)

AM (astrocytes growth medium, ScienceCell)

AUC_{plasma} (area under the curve of concentration in plasma)

AUC_{brain} (area under the curve of concentration in brain)

Å (Angstrom)

BBB (blood brain barrier)

BBCEC (bovine brain endothelial cells)

CC-2565 (cerebral normal human astrocytes, Lonza)

ClogP (calculated Lipophilicity)

c-NHA (cerebrum normal human astrocytes, ScienCell)

CNS (central nervous system)

CT (computed tomography)

Cu_{br}(unbound concentration in brain)

Cu_{pl} (unbound concentration in plasma)

D_m (membrane diffusion coefficient of the solute)

EBM (endothelial cells growth medium)

EC (endothelialcells)

HA-c (cerebellar normal human astrocytes, ScienceCell SC-1810)

HB (Hydrogen Bond)

HBA (Hydrogen Bond Acceptor)

HBD (Hydrogen Bond Donors)

HEPES (Hepes-buffered Ringer'ssolution)

HPLC (high pressure liquid chromatography)

HSA (human serum albumin)

ID% (Injected Dose in percent)

IAM (immobilized artificial membrane chromatography)

K_1 (kinetic influx rate of a tracer from plasma to first compartment in brain, two compartment model of PET quantification)

K_m (membrane coefficient (solute distribution between the aqueous phase and the membrane) represents all possible molecular interactions between a solute and the membrane)

L (membran thickness, 30 Å for hydro carbon domain of bilayer)

logBBB (the brain-plasma ratio of the concentration of biomarker/radiotracer)

logD (distribution coefficient of the sum of concentration of all forms of substances (ionized plus un-ionized) in two immiscible phases (1-octanol and water) at equilibrium)

LogK (logarithm of the equilibrium constants)

logk' (log capacity factor of retained substance)

logP (partition coefficient of the concentration of unionized substances in two immiscible phases (1-octanol and water) at equilibrium)

MDCK (Madin-Darby canine kidney cells)

MRI magnetic resonance imaging

MW (molecular weight)

N (Nitrogen)

O (Oxygen)

OH (Hydroxide)

ODP (octadecylpoly(vinyl)alcohol)

PBS (phosphate buffered saline)

PET (positron emission tomography)

P-gp (p-glycoprotein, efflux transporter)

pKa (acid dissociation constant)

P_m (permeability)

PPB% (plasma protein binding in percent)

PSA (polare surface area)

PTFE (polytetrafluoroethylene)

RIA (radioimmunoassay)

Rt (retention time)

Rt_0 (columns death time)

Ro5 (rule of five)

Si-OH (silicic acid)

SPECT (Single-photon emission computed tomography)

SUV (*standardized uptake value, SUV=activity [Bq/ml] / injected Dose [Bq] x body weight [kg])*

TCM (Tissue Compartment Model)

TEER (transendothelial electrical resistance)

TJ (tight junction)

tol (toluene)

tri (triphenylen)

V (molar volume of drug molecule)

VD (volume of distribution)

V_m (total volume of solvent within the IAM-column, V_m=flow rate [ml/min] x columns death time [min])

V_s (volume of the IAM interphase created by the immobilized phospholipids, $Vs= W_{PhC}/\delta_{PhC}+ W_{C10}/\delta_{C10}+W_{C3}/\delta_{C3}$)

List of figures

List of tables

List of Publications- Peer reviewed articles

Nics L, Hahn A, Zeilinger M, **Vraka C**, Ungersboeck J, Haeusler D, Hartmann S, Wagner K-H, Lanzenberger R, Wadsak W, Mitterhauser M. Quantification of the radio-metabolites of the serotonin-1A receptor radioligand [carbonyl-11C]WAY-100635 in human plasma: An HPLC-assay which enables measurement of two patients in parallel. Applied Radiation and Isotopes 70 (2012) 2730–6.

Rami-Mark C, Bornatowicz B, Fink C, Otter P, Ungersboeck J, **Vraka C**, Haeusler D, Nics L, Spreitzer H, Hacker M, Mitterhauser M, Wadsak W. Synthesis, radiosynthesis and first in vitro evaluation of novel PET-tracers for the dopamine transporter: [(11)C]IPCIT and [(18)F]FE@IPCIT. Bioorg Med Chem. 2013 Dec 15;21(24):7562-9.

Neudorfer C, Shanab K, Jurik A, Schreiber V, Neudorfer C, **Vraka C**, Schirmer E, Holzer W, Ecker G, Mitterhauser M, Wadsak W, Spreitzer H. Development of potential selective and reversible pyrazoline based MAO-B inhibitors as MAO-B PET tracer precursors and reference substances for the early detection of Alzheimer's disease. Bioorg Med Chem Lett. 2014 Sep 15;24(18):4490-4495.

Rami-Mark C, Berroterán-Infante N, Philippe C, Foltin S, **Vraka C**, Hoepping A, Lanzenberger R, Hacker M, Mitterhauser M, Wadsak W. Radiosynthesis and first preclinical evaluation of the novel norepinephrine transporter pet-ligand [(11)C]ME@HAPTHI. EJNMMI Res. 2015 Dec;5(1):113.

Wenzel B, Mollitor J, Deuther-Conrad W, Dukic-Stefanovic S, Kranz M, **Vraka C**, Teodoro R, Günther R, Donat C, Ludwig F-A, Fischer S, Smits R, Wadsak W, Mitterhauser M, Steinbach J, Hoepping A, Brust P. On the development of a novel non-peptidic ^{18}F-labeled radiotracer for in vivo imaging of oxytocin receptors with positron emission tomography. J Med Chem. 2016 Mar 10;59(5):1800-17.

Vraka C, Nics L, Wagner KH., Hacker M, Wadsak W, Mitterhauser M. LogP, a yesterday's value? Nucl Med Biol. 2017, Mar 20; 50:1-10

Vraka C and Mitterhauser M "Reconsider LogP!" Nucl Med Biol. 2017; 54:p42

Vraka C, Dumanic M, Racz T, Pichler F, Philippe C, Balber T, Klebermass EM, Wagner KH, Hacker M, Wadsak W, Mitterhauser M. A New Model for the Prediction of the Interaction of Radiotracers with the P-glycoprotein (P-gp) transporter. Submitted, 2017 November 13th, Journal of Nuclear Medicine and Biology (NUCMEDBIO_2017_285).

Vraka C, Mijailovic S, Fröhlich V, Wadsak W, Wagner KH, Hacker M, Mitterhauser M. Expanding LogP: Present Possibilities. Submitted, 2017 September 22nd, Journal of Nuclear Medicine and Biology, (NUCMEDBIO_2017_232).

Hahn A, Gryglewski G, Nics L, Rischka L, Ganger S, Sigurdardottir H, **Vraka C**, Silberbauer L, Vanicek T, Kautzky A, Wadsak W, Mitterhauser M, Hartenbach M, Hacker M, Kasper S, Lanzenberger R. Task-relevant brain networks identified with simultaneous PET/MR imaging of metabolism and connectivity. Brain Structure and Function 2017. Epub xxx [2016, IF: 4.698]; in press

Published abstracts in congress special editions

Vraka C, Nics L, Hendl M, Hacker M, Wadsak W, Mitterhauser M. Immobilized Arificial Membrane (IAM) Chromatography- A preclinical Tool to Predict the Blood Brain Barrier Penetration?. Oral Presentation, "Radioactive Isotopes in Molecular Imaging", 31st International Austrian Winter Symposium (Former Gastein Meeting), 22-25 January 2014, Zell am See, Austria. Nuklearmedizin 2013; 52:205-257.

Vraka C, Nics L, Hendl M, Hacker M, Wadsak W, Mitterhauser M. Die Lipophilie (logP) Bestimmung- eine geeignete Methode zur Vorhersage der Bluthirnschranken Penetration? Oral Presentation, 52. Jahrestagung der Deutschen Gesellschaft für Nuklearmedizin, 26 - 29 März 2014 in Hannover, Deutschland. Nuklearmedizin 2014;53:1-18.

Vraka C, Nics L, Weiss V, Wagner K-H, Hacker M, Wadsak W, et al. Combination of High Throughput HPLC Methods for Rapid Prediction of Blood Brain Barrier Penetration

of Newly Developed Radiotracers. Poster Presentation, EANM'14 Congress, Gothenburg, Sweden. Eur J Nucl Med Mol Imaging. 2014;(41):442.

Vraka C, Nics L, Wadsak W, Wagner K-H, Hacker M, Mitterhauser M. Vergesst logP! Der Mythos von der Blut-Hirn-Schranke und der Lipophilie. Oral Presentation, 53. Jahrestagung der Deutschen Gesellschaft für Nuklearmedizin, 22. – 25. April 2015 in Hannover, Deutschland. Nuklearmedizin 2015;54:A67.

Vraka C, Racz T, Philippe C, Rami-Mark C, Wagner KH, Wadsak W, Mitterhauser M. First-Real-Time Kinetic in vitro Method for Rapid Prediction of P-glycoprotein Interactions of Newly Developed Radioligands. Oral Presentation (OP115), Annual Congress of the European Associatiob of Nuclear Medicine, October 15-19, 2016 Barcelona, Spain. Eur J Nucl Med Mol Imaging. 2016; 43 (Suppl 1): S38.

Vraka C, Papp L, Mijailovic S, Nics L, Wadsak W, Hacker M, Mitterhauser M. Prediction of Blood Brain Barrier Penetration of newly developed radiotracer using machine-learning software. 22nd International Symposium on Radiopharmaceutical Sciences, poster presentation (P216). J Label Compd Radiopharm 2017:60 (Suppl.1):S380.